

This item was submitted to [Loughborough's Research Repository](#) by the author.
Items in Figshare are protected by copyright, with all rights reserved, unless otherwise indicated.

Energy-saving retrofits for residential buildings in the hot summer and cold winter zone in China

PLEASE CITE THE PUBLISHED VERSION

PUBLISHER

Loughborough University

LICENCE

CC BY-NC-ND 4.0

REPOSITORY RECORD

Tsang, Christopher. 2020. "Energy-saving Retrofits for Residential Buildings in the Hot Summer and Cold Winter Zone in China". Loughborough University. <https://doi.org/10.26174/thesis.lboro.12937004.v1>.

**Energy Saving Retrofits for Residential
Buildings in the Hot Summer and Cold
Winter Zone in China**

Christopher Tsang

Doctoral Thesis Submitted in Partial
Fulfilment of the Requirements for the Degree of
Doctor of Philosophy of Loughborough University

September 2020

© Christopher Tsang, 2020

Abstract

Urban areas in the Hot Summer and Cold Winter (HSCW) zone in China are home to 8% of the world's population. Existing residential buildings in the HSCW zone in China are cold in winter and overheat in summer, due to a lack of adequate building fabric and central space heating in response to current legislation. As living standards increase, the number of residential buildings with installed air conditioning (AC) systems is also growing, which leads to a sharp increase in energy consumption. Building retrofit plays a vital role in reducing energy consumption and carbon dioxide emissions while increasing occupants' thermal comfort. This study aims to develop retrofit measures for urban residential buildings and quantify the potential annual space-conditioning energy savings with regards to kWh at a city scale in the HSCW zone in China.

A typical urban multi-storey residential building in Chongqing, a city in the HSCW zone of China, was used to develop a dynamic thermal model (DTM), following a systematic review to characterise building parameters. Then, a single flat was calibrated using indoor air temperature measured over one week. Afterwards, energy and thermal comfort performance was evaluated before and after energy saving retrofits using the calibrated DTM of the single flat, and twelve different flats location with regards to the building. To represent typical residential users, three types of households with different AC operating schedules were developed: high, medium, and low. After that, an optimum combination of retrofit measures able to reduce energy consumption and thermal discomfort of the typical building was selected for each of the seven retrofit measures accordingly: external wall insulation, roof insulation, double-glazed windows, air infiltration control, additional window overhang, enclosed communal staircase, and energy-efficient AC. Finally, a DTM of the typical building was created at nine levels of computational detail. The most computationally efficient DTM was then identified to devise twelve residential building archetypes, to quantify the energy reduction due to energy saving retrofits at a city scale for 321 residential buildings in Chongqing.

The results showed that a substantial amount of annual space-conditioning energy is required to maintain comfortable conditions for existing residential buildings in the HSCW zone. Despite a high energy consumption for comfort was theoretically required, results predicted that energy used was only 9.2 to 18.8 kWh/m², depended on the use that was made of the AC system. As the predicted mean indoor air temperature in winter was 14°C and in summer was 29°C due to the occupants' adaption to the environment. Not surprisingly, retrofitting these buildings was not cost-efficient, with a payback period of 56 years, when adaptive behaviour was considered. Yet, thermal comfort was improved significantly in winter and at the same time summertime overheating was prevented under the proposed retrofit measures. To evaluate large-scale residential energy saving retrofits, DTM with different level of computational detail were created, the most suitable DTM was used to wider applicability of outputs of the typical building; results showed that it reduced simulation time by 70% and achieved a 5% prediction difference of energy demand when compared to the case study building (DTM with the greatest level of computational detail).

The devised residential building archetypes predicted an annual 73% to 76% reduction for heating, 39% to 45% reduction for cooling, and 50% to 57% reduction for total energy consumption. At a city-scale for 321 residential buildings with built area of 4.07 million m², 17 TWh of annual space-conditioning energy can be reduced if the proposed retrofit measures are employed. More importantly, the potential long-term energy savings do outweigh the cost, given the Chinese government pursuit of net-zero emissions by 2050.

Acknowledgements

I am very thankful to my principal supervisor Dr Efi Spentzou, who has always been available to provide support, guidance, and encouragement throughout my research journey.

I am sincerely grateful to my second supervisor, Prof Kevin Lomas for believing in me and offer me the opportunity to study this PhD, as well as provide valuable help, guidance and critical appraisal throughout my studies.

I would also like to express my sincere gratitude to my third supervisor Dr Candy He, for her technical advice, as well as support on writing my first conference publication. I would also like to thank Dr Simon Taylor for his help during the earlier stage of the work. Thanks to Dr Christina Hopfe, my internal assessor, for her keen advice, along with referring me to this PhD project. Special thanks to Prof Alan Short, director of the project “Low carbon climate responsive Heating and Cooling of cities (LoHCool)”, to arrange site visits to China, and meetings with other project partners, which lay the foundation of this PhD. I would like to express my thanks to the external examiner Dr Giridharan Renganathan and my internal examiner Dr David Allinson, for their constructive feedback and valuable discussions.

I do like to thank everyone in the hub in Loughborough for creating such a great environment to work in. I would also like to thank all the friends I meet in the UK, as well as friends back home, to provide constant source of support.

Sincere thanks to my parents to provide support, both financially and mentally, throughout my studies. Finally, I would like to thank my partner Tyra for a constant source of support, energy and motivation.

Table of contents

Abstract.....	i
Acknowledgements.....	iii
Table of contents	iv
List of Figures	xi
List of Tables	xxi
List of Nomenclatures	xxv
List of Abbreviations	xxv
Chapter 1 : Introduction.....	1
1.1 Background.....	1
1.2 Overview of the LoHCool project and significance of research.....	5
1.3 Aim and Objectives	7
1.4 Contribution of research.....	7
1.5 Outline of the thesis	10
Chapter 2 : Literature review	11
2.1 Introduction	11
2.2 The Hot Summer and Cold Winter zone: Characteristics.....	12
2.2.1 Geographic characteristics.....	12
2.2.2 Climatic characteristics.....	12
2.2.3 Characteristics of existing residential buildings	17
2.2.4 Summary of existing codes and regulations.....	19
2.3 Building energy consumption in the HSCW zone	20
2.3.1 Sources of building energy consumption.....	20
2.3.2 Trends of building energy consumption.....	21
2.3.3 Performance of heating and cooling systems.....	23

2.3.4 Electricity generation method and carbon intensity	25
2.4 Indoor thermal comfort.....	26
2.4.1 Importance of indoor thermal comfort	26
2.4.2 Thermal comfort approaches	27
2.4.3 Factors affecting indoor thermal comfort.....	27
2.4.4 Adaptive thermal comfort models.....	30
2.5 Methodological review of performance evaluation tools for energy saving retrofits.....	34
2.5.1 Steady-state energy performance evaluation tools	34
2.5.2 Dynamic thermal simulation	35
2.5.3 Model calibration techniques in building energy modelling	38
2.5.4 Location of flat in an apartment building.....	41
2.5.5 Optimisation of energy saving retrofits	42
2.5.6 Level of detail of building energy models	43
2.5.7 City-scale model.....	45
2.6 Characterisation of the building parameters for urban residential buildings in the HSCW zone.....	49
2.6.1 Introduction	49
2.6.2 Geometrical parameters.....	50
2.6.2.1 Floor area	50
2.6.2.2 Floor to ceiling height	51
2.6.2.3 Number of storeys	51
2.6.2.4 Number of flats per floor	52
2.6.2.5 Window to wall ratio.....	52
2.6.3 Building fabric parameters	55
2.6.3.1 Thermo-physical parameters of materials	55
2.6.3.2 External wall construction parameters.....	55
2.6.3.3 Roof construction.....	57

2.6.3.4 Internal floor and wall construction	58
2.6.3.5 Window parameters.....	60
2.6.3.6 Air infiltration rate.....	61
2.6.4 Occupant parameters.....	63
2.6.4.1 The significance of occupant parameters on predicted energy consumption	63
2.6.4.2 Measured energy consumption.....	66
2.6.4.3 Heating and cooling COP	67
2.6.4.4 Heating and cooling set-point	68
2.6.4.5 Heating and cooling schedule.....	70
2.6.5 Internal heat gain.....	75
2.6.6 Window opening.....	77
2.7 Building retrofit measures for urban residential buildings in the HSCW zone	81
2.7.1 The significance of identifying building retrofit measures for building energy modelling.....	81
2.7.2 External wall insulation.....	81
2.7.3 Roof insulation	83
2.7.4 Air infiltration control.....	84
2.7.5 Double-glazed windows	86
2.7.6 Shading devices	87
2.7.7 Energy-efficient air conditioners	89
2.8 Discussion	90
Chapter 3 : Research Methodology.....	95
3.1 Introduction	95
3.2 Research design outline	96
3.3 Selection of a typical residential building in the HSCW zone	100

3.3.1 Characteristics of the urban residential building stock in the HSCW zone	100
3.3.2 Selection of a case study building	102
3.4 Development of a dynamic thermal model.....	105
3.4.1 Selection of a dynamic thermal modelling tool	105
3.4.2 Development of a dynamic thermal model for the case study flat	106
3.4.3 Development of a dynamic thermal model for the case study building	108
3.4.4 Justification of building parameters used in the dynamic thermal model	110
3.5 Selection of retrofit measures	120
3.6 Development of retrofit measures.....	127
3.7 Metered annual electricity consumption: Secondary data.....	135
3.8 Summary	138
Chapter 4 : Calibration of a dynamic thermal model for building fabric parameters in a case study flat	139
4.1 Introduction.....	139
4.2 Development of a steady-state model	140
4.3 Comparison of predicted energy demand using single-zone steady-state and dynamic thermal models.....	147
4.4 Sensitivity analysis of building fabric parameters	148
4.4.1 Development of uncertainty bands for building fabric parameters	148
4.4.2 Predicted sensitivities of building fabric parameters using a steady-state model	150
4.4.3 Predicted sensitivities of building fabric parameters using a dynamic thermal model	151
4.5 Indoor air measured conditions of the case study flat.....	153

4.5.1 Measurement set-up	153
4.5.2 Analysis of measured indoor air temperature	157
4.5.3 Analysis of measured indoor relative humidity	159
4.5.4 Analysis of measured indoor air velocity	161
4.6 Development of a customised weather file	162
4.6.1 Weather file construction	162
4.6.2 Analysis of the weather data collected	163
4.7 Calibration of a dynamic thermal model for a case study flat	166
4.8 Limitations of calibration performed	173
4.9 Discussion	174
Chapter 5 : Energy saving retrofits for a case study building	177
5.1 Introduction	177
5.2 Energy and thermal comfort performance of a case study flat: Pre-retrofit conditions.....	178
5.2.1 Predicted energy performance	178
5.2.2 Predicted thermal comfort performance	180
5.3 Energy and thermal comfort performance of different flat locations: Pre-retrofit conditions	183
5.3.1 Predicted energy consumption	183
5.3.2 Predicted thermal comfort performance	187
5.4 Energy and thermal comfort performance of the whole case study building: Pre-retrofit conditions	189
5.4.1 Predicted energy consumption	189
5.4.2 Predicted thermal comfort	190
5.5 Selection of an optimum combination of retrofit measures in reducing energy and thermal discomfort for a case study building.....	191
5.6 Predicted energy and thermal discomfort reduction for the selected retrofit measures for the case study building	198

5.6.1 Predicted retrofit performance in the case study flat	198
5.6.2 Predicted retrofit performance for different flat positions in the building.....	202
5.6.3 Predicted retrofit measures for the whole case study building ...	207
5.7 Retrofit cost	210
5.8 Discussion	213
Chapter 6 : Large scale residential energy saving retrofits	219
6.1 Introduction.....	219
6.2 Calculating building level energy consumption	220
6.3 Development of the LoD required for energy modelling of the case study building	223
6.4 LoD selection for a city-scale study	228
6.5 Development of building archetypes for city-scale study	235
6.5.1 Parameter 1: Number of bedrooms.....	235
6.5.2 Parameter 2: Building height.....	240
6.5.3 Parameter 3: Energy users	241
6.5.4 Summary of building archetypes selected.....	242
6.6 Residential building archetypes energy saving retrofits	244
6.7 City-scale energy saving retrofits contribution	249
6.8 Discussion	252
Chapter 7 : Conclusions.....	255
7.1 Introduction.....	255
7.2 Key findings	255
7.3 Impact of work	257
7.3.1 Academia	257
7.3.2 Government	258
7.3.3 Industry	259
7.3.4 Society	259

7.4 Limitations and recommendations for future work	259
References	261
APPENDICES	A-1
Appendix A: Steady-state model.....	A-2
Appendix B: Calculation of vertical solar radiation	A-5
Appendix C: City scale geometrical parameters	A-7

List of Figures

Figure 1-1: Five climate zones for building design in China, with the studied Hot Summer and Cold Winter zone, highlighted in blue (adapted from Gou et al. 2015)	2
Figure 1-2: Simplified correlation of indoor and outdoor temperature in north China (with central space heating) and south China (without central space heating) (adapted from Li et al., 2014)	3
Figure 2-1: Map of China. Circles indicate the cities of Chongqing and Hangzhou (Source: http://www.china-mike.com/china-travel-tips/tourist-maps/china-provinces-map).....	13
Figure 2-2: East Asia map of Köppen climate classification (Köppen climate classification, 2016).....	14
Figure 2-3: Average annual sum of global horizontal irradiation in China (SolarGIS, 2015).	16
Figure 2-4: Climate characteristics (dry-bulb temperature, relative humidity, global horizontal radiation, and wind speed) for Chongqing and Hangzhou.	17
Figure 2-5: China's urbanisation rate from 1990 to 2017 (NBS, 2018).....	18
Figure 2-6: New urban residential building completed each year (NBS, 2018).	18
Figure 2-7: a) Height, b) structure and c) floor area of buildings in Chongqing municipality and Zhejiang province (NBS, 2010).....	19
Figure 2-8: Distribution of China's urban residential building energy consumption (adapted from TUBERC 2018).....	21
Figure 2-9: Trend of building energy consumption from 1996 to 2011 in China (THUBERC, 2013).	22
Figure 2-10: Residential energy metrics considering a) final energy use per household and b) final energy use per capita for selected countries (IEA, 2015b).....	22
Figure 2-11: Heating energy consumption of urban residential buildings in the HSCW zone (Hu et al., 2016).....	24
Figure 2-12: Measured electricity use for different cooling system and devices in Beijing (Li, 2007).	24

Figure 2-13: Energy generation methods in China from 1990-2006 (adapted from NBS, 2017).....	26
Figure 2-14: Acceptability of thermal environment among all conditions (Jing et al., 2012).	28
Figure 2-15: Box-plot of wind velocity versus comfort sensation vote (Kang et al., 2013).	28
Figure 2-16: Correlation between garment insulation and indoor temperature in Chongqing, where shaded diamonds correspond to male samples and unshaded diamonds correspond to female occupants (Yoshino et al., 2006).	29
Figure 2-17: Acceptable operative temperature ranges for naturally conditioned spaces (ASHRAE, 2010).....	30
Figure 2-18: Change in comfort temperature with monthly mean outdoor temperature (Nicol and Humphreys, 2002).....	31
Figure 2-19: Daily neutral temperature with outdoor daily running mean air temperature (Liu et al., 2017).	31
Figure 2-20: Linear regression of mean outdoor temperature and thermo-neutral temperature (Li et al., 2011).	32
Figure 2-21: Range of the indoor operative temperature of the thermal environment in free-running buildings in the hot summer and cold winter zone, 1 – the category I; 2 – the category II (Li et al., 2014).	33
Figure 2-22: Heat flow rates within a building (CIBSE, 2015).....	34
Figure 2-23: Measured versus predicted energy consumption for 121 commercial buildings in the US (Turner and Frankel, 2008).	38
Figure 2-24: Typical residential buildings built before 2001 with a) one stair one household point building, b) one stair two household plank building, c) one stair four household plank building.....	47
Figure 2-25: Temperature variation of a household using air conditioner in a representative day in winter (Guo et al., 2015).....	64
Figure 2-26: Measured electricity consumption for residential flats in the HSCW zone (adapted from Ouyang et al., 2009; 2011).	66
Figure 2-27: Percentage distributions of different set points of air conditioners in summer (left) and winter (right) (adapted from S. Chen et al. 2015).....	69

Figure 2-28: Surveys and measurement of heating set-point temperature (Zhe Wang et al., 2015b).....	69
Figure 2-29: Mean usage hours per day of air conditioners in winter and summer (adapted from S. Chen et al., 2015).	70
Figure 2-30: Hourly use of space heaters in a representative day in winter (adapted from Chen et al., 2011)	72
Figure 2-31: Hourly use of space heaters in a representative day in winter (adapted from Yoshino et al., 2006)	72
Figure 2-32: Hourly use of space heaters in a representative day in winter (adapted from Hu et al., 2013)	72
Figure 2-33: Hourly use of air conditioners for cooling in a representative weekday in summer (adapted from Chen et al., 2010).....	73
Figure 2-34: Hourly use of air conditioners for cooling in a representative day in summer (adapted from Yoshino et al., 2006)	73
Figure 2-35: Hourly use of air conditioners for cooling in a representative weekday in summer (adapted from Hu et al., 2013).....	74
Figure 2-36: Occupant behaviour in air conditioner usage. Left – above 55 years of age, right – 55 years of age or under (adapted from Chen et al., 2013)	74
Figure 2-37: Comparison of window opening proportion in South Korea, UK and Europe (Jeong et al., 2016).....	78
Figure 2-38: Proportion of windows opened with outside temperature (Liu et al., 2017)	78
Figure 2-39: Histogram of open-window duration per day in winter for conditions under which occupants opened windows in the HSCW zone (red lines are fitted curves with log-normal or normal distribution) (J. Liu et al., 2018)	79
Figure 2-40: Air infiltration rate in northern and southern China (boxes present the 25 th and 75 th percentiles; whiskers present the 5 th and 95 th percentiles) (J. Liu et al., 2018)	86
Figure 3-1: Schematic illustrating the outline of the thesis.	99
Figure 3-2: GoogleMap view of the Yuzhong District, Chongqing, with the selected representative area highlighted in a black box.....	101

Figure 3-3: GoogleMap view of the Shangcheng District, Hangzhou, with the selected representative area highlighted in a black box.	101
Figure 3-4: Floor plan of the second floor of the case study building, showing the location of entrance staircase (green), three staircases in the outdoor communal corridor (red), twelve flats in each floor (blue) and the case study flat (orange).....	103
Figure 3-5: Aerial view showing the selected building (circled) and the surrounding buildings in Chongqing.	103
Figure 3-6: Front view of the case study building (left) and inside view of the case study flat (right) (Photograph by author, 2015).	104
Figure 3-7 a) Shops at ground floor level, with entrance staircase to the flats highlighted with a black box, b) view to front from entrance staircase, c) view from the outdoor communal corridor and staircases of the case study building (Photograph by author, 2015).....	104
Figure 3-8: Floor plan of the case study flat.	105
Figure 3-9: Plan view for the modelled case study flat in DesignBuilder. ...	106
Figure 3-10: Axonometric view of the modelled case study flat in DesignBuilder with area and orientation of the windows modelled.	107
Figure 3-11: Plan view for the re-modelled case study flat in DesignBuilder considering windowsill.....	108
Figure 3-12: 3D representation of the studied building in the DTM software showing the location of studied flats facing front.	109
Figure 3-13: 3D representation of the studied building in the DTM software showing the location of studied flats facing rear.	109
Figure 3-14: Window dividers and frames modelled for the flat, with divider and frame both 0.05m.	112
Figure 3-15: AC operating hours for the three energy users developed which represent households in the HSCW zone, where the blue-shaded area represents living room occupied hours and the green-shaded area represents bedroom occupied hours.	115
Figure 3-16: Operating schedule of cooling in summer (blue), heating in winter (red), daily occupancy (green) and lighting (yellow) for living room and bedroom.	117

Figure 3-17: Sensitivity coefficient for selected retrofit measures using steady state model.....	125
Figure 3-18, continued : Correlation between heating and cooling energy consumption for a,b) U-value of external wall, c,d) U-value of window, e,f) internal heat capacity coefficient, g,h) external shading factor, i,j) g-value of external wall, k,l) air infiltration rate, m,n) g-value of glazing, o) heating COP, p) cooling COP and q,r) U-value of roof.	127
Figure 3-19: Location of proposed additional window overhang installed in the case study flat, where h refers to the overhang length.....	131
Figure 3-20: DTM of the case study building, a) before enclosed communal staircase, b) after enclosed communal staircase in axonometric view	132
Figure 4-1: Monthly quasi-steady-state calculation spreadsheet (BSI, 2008).	141
Figure 4-2: Vertical solar radiation in London collected from CIBSE guide J.	145
Figure 4-3: Vertical solar radiation in London predicted from horizontal-vertical translation method.....	145
Figure 4-4: Monthly outdoor temperature in Chongqing and London.	146
Figure 4-5: Vertical solar radiation in Chongqing predicted from horizontal-vertical translation method.	146
Figure 4-6: Comparison of predicted monthly heating and cooling energy demand with a single-zone steady-state model and dynamic thermal model for the case study flat.	148
Figure 4-7: Bar chart representation of sensitivity of building fabric parameters using steady-state model. Blue bar represents the percentage change of energy demand due to a decrease in input parameter value (low band). Red bar represents the percentage change of energy demand due to an increase in input parameter value (high band).....	151
Figure 4-8: Bar chart representation of sensitivity of building fabric parameters using dynamic thermal model. Blue bar represents the percentage change of energy demand due to a decrease in input parameter value (low band). Red bar represents the percentage change of energy demand due to an increase in input parameter value (high band).....	152

Figure 4-9: View of living room and location of sensors (source: Yao, 2017).	154
Figure 4-10: Plan view of the sensors' locations in the living room, in coordinates for x,y,z in meters from internal corner B (original source: Yao, 2017).	154
Figure 4-11: Location of the thermocouples used to measure external wall temperature for two configurations, with red boxes showing thermocouples and blue boxes showing fire hydrant (source: Yao, 2017).....	155
Figure 4-12: Naming of the thermocouples used to measure external wall temperature with dimensions for two configurations (original source: Yao, 2017).	156
Figure 4-13: Location of the clamp meter to measure AC electricity consumption (source: Yao, 2017).....	156
Figure 4-14: Measured indoor room temperature for different sensors.	157
Figure 4-15: Measured outdoor wall temperature for different sensors.	158
Figure 4-16: Measured indoor wall temperature for different sensors.	158
Figure 4-17: Comparison between measured indoor air temperature, indoor wall temperature, outdoor wall temperature, and outdoor air temperature.	159
Figure 4-18: Measured indoor relative humidity for different sensors.....	160
Figure 4-19: Comparison between measured indoor and outdoor relative humidity.....	160
Figure 4-20: Measured indoor air velocity for different sensors.....	161
Figure 4-21: Comparison between indoor air velocity and outdoor wind speed.	161
Figure 4-22: Interface of Elements (a customise weather editing tool).....	163
Figure 4-23: a) Cumulative percentage of wind speed, b) cumulative percentage of gust speed, c) wind direction for the measurement period. .	164
Figure 4-24: Outdoor air temperature and relative humidity for the measurement period.	165
Figure 4-25: Weather conditions for the measurement period (Thorsen, 2019).	165
Figure 4-26: Moisture content of outdoor air for the measurement period..	165
Figure 4-27: Prediction of diffuse and beam radiation from global horizontal solar radiation.....	166

Figure 4-28: Comparison between measured and simulated temperature without pre-validation period.	167
Figure 4-29: Comparison between measured and simulated temperature with pre-validation period.....	168
Figure 4-30: Comparison between online source and measured data during the measurement period.	168
Figure 4-31: Comparison between measured and base case indoor air temperature for the selected pre-validation period.	170
Figure 4-32: Variation of indoor temperature for three walls' U-values.	171
Figure 4-33: Variation of indoor temperature for three windows' U-value and g-value.	172
Figure 4-34: Variation of indoor temperature when air infiltration is changed.	173
Figure 5-1: Predicted monthly energy consumption for different energy users in case study flat.	180
Figure 5-2: Predicted monthly indoor air temperature without AC.....	181
Figure 5-3: Predicted monthly indoor air temperature with medium energy users.	182
Figure 5-4: Energy consumption for different flat locations for three energy users.	184
Figure 5-5: Percentage change in energy consumption for different energy users when compare to flat MCF	185
Figure 5-6: Percentage change in energy consumption when compared to flat MCF.	186
Figure 5-7: Percentage change in energy consumption when compared to flat MCR.....	187
Figure 5-8: Discomfort hours (DH) increase for different flat locations when compared to flat MCF.....	188
Figure 5-9: Discomfort hours (DH) increase for different flat locations when compared to flat MCR.	189
Figure 5-10: Energy consumption and discomfort hours reduction for external wall insulation (flat MCF).....	192
Figure 5-11: Energy consumption and discomfort hours reduction for roof insulation (flat TCF).....	193

Figure 5-12: Energy consumption and discomfort hours reduction for double-glazed windows (flat MCF).	194
Figure 5-13: Energy consumption and discomfort hours reduction for reducing air infiltration rate (flat MCF).	195
Figure 5-14: Energy consumption and discomfort hours reduction for additional overhang (flat MCF).	196
Figure 5-15: Energy consumption and discomfort hours reduction for enclosed communal staircase (flat MCF).	197
Figure 5-16: Energy consumption and discomfort hours reduction for energy-efficient AC (flat MCF).	197
Figure 5-17: Percentage of heating, cooling and total energy reduction after retrofit with medium energy users.	199
Figure 5-18: Percentage of energy reduction after retrofit with low, medium, and high energy users.	200
Figure 5-19: Absolute value of energy reduction after retrofit for case study flat with low, medium, and high energy users.	200
Figure 5-20: Comparison between indoor air temperature before and after retrofit and outdoor air temperature.	201
Figure 5-21: Thermal discomfort hours for winter, summer and annual reduction after retrofit.	202
Figure 5-22: Total energy consumption when seven retrofit measures were employed for different flat locations for three energy users.	203
Figure 5-23: Percentage of heating, cooling and total energy consumption after retrofit with medium energy users for flat MCR.	204
Figure 5-24: Percentage of heating, cooling and total energy consumption after retrofit with medium energy users for flat TCF.	205
Figure 5-25: Thermal discomfort hours reduction for winter, summer, and annual reduction after retrofit for flat MCR.	206
Figure 5-26: Thermal discomfort hours reduction for winter, summer, and annual reduction after retrofit for flat TCF.	206
Figure 5-27: Percentage of energy reduction after retrofit for the whole case study building with low, medium and high energy users.	207
Figure 5-28: Absolute value of energy reduction after retrofit for the whole case study building with low, medium and high energy users.	208

Figure 5-29: Variation of heating, cooling, and total energy consumption after retrofit with medium energy users for different housing units, with black dots representing the entire case study building.	209
Figure 5-30: Variation of thermal discomfort hours reduction for winter, summer, and annual reduction after retrofit for different housing units, with black dots representing the entire case study building.	210
Figure 6-1: 3D representation of the studied building in the DTM software showing the location of selected flats for building scale simulation.	221
Figure 6-2: DTM of the case study flat with a plan view, including wall thickness.	224
Figure 6-3: DTM of the case study building for LoD3, showing an axonometric view of the building (left) and plan view of a flat (right).	225
Figure 6-4: DTM of the case study flat showing window frames for LoD2 (left) and LoD3 (right).	225
Figure 6-5: DTM of the case study building combining unoccupied thermal zones (LoD5), showing an axonometric view of the flat (left) and plan view of the flat (right).	226
Figure 6-6: 3D representation of the studied building in the DTM software showing the excluded adjacent block.	226
Figure 6-7: DTM of the case study building combining unoccupied thermal zones (LoD5), showing an axonometric view of the flat (left) and plan view of the flat (right).	227
Figure 6-8: DTM of the case study building with whole floor model, showing a) axonometric view of the building and b) plan view of the flat	228
Figure 6-9: Annual building level heating energy demand, the percentage difference of building level energy consumption for LoD2 to LoD9 compared with LoD1 (P_{LoDi}), and the percentage difference of building level energy consumption for LoD2 to LoD9 compared respective with the previous LoD (S_{LoDi}).	230
Figure 6-10: Annual building level cooling energy demand, the percentage difference of building level energy consumption for LoD2 to LoD9 compared with LoD1 (P_{LoDi}), and the percentage difference of building level energy consumption for LoD2 to LoD9 compared respective with the previous LoD (S_{LoDi}).	232

Figure 6-11: Annual building level total energy demand, the percentage difference of building level energy consumption for LoD2 to LoD9 compared with LoD1 (P_{LoDi}), and the percentage difference of building level energy consumption for LoD2 to LoD9 compared respective with the previous LoD (S_{LoDi}).....	233
Figure 6-12: Absolute percentage difference and simulation time for various LoDs, the percentage difference of building level energy consumption for LoD2 to LoD9 compared with LoD1 (P_{LoDi}), and the percentage difference of building level energy consumption for LoD2 to LoD9 compared respective with the previous LoD (S_{LoDi}).....	234
Figure 6-13: Typical floor plans for residential buildings in the HSCW zone as found in study a) Yu et al. (2009b), b) Yu et al. (2008), c) Short et al. (2018), d) W. Yu et al. (2015), e) Ichinose et al. (2017), f) Short et al. (2019), g) Short et al. (2019), h) Meng et al. (2019), i) Yao (2012) and j) Yao (2012).....	238
Figure 6-14: Axonometric view of flats with different number of bedrooms.	240
Figure 6-15: Dynamic thermal models with different number of stories (one-bedroom flat).	241
Figure 6-16: Parametric tree of the selected building archetypes.....	242
Figure 6-17: Dynamic thermal model for the selected twelve building archetypes in city-scale study.....	243
Figure 6-18: Predicted energy consumption for twelve residential archetypes with three energy users, with the blue box refer to the range of metered energy consumption from literature (7.7 to 17 kWh/m ²).	245
Figure 6-19: Predicted energy consumption in kWh per flat for twelve residential archetypes with three energy users, with the blue box refer to the range which exceed threshold suggested by Chinese regulation (>930 kWh/household).	246
Figure 6-20: Predicted energy consumption in kWh per flat and total energy reduction post-retrofit for twelve residential archetypes with three energy users.	247
Figure 6-21: Correlation of a) number of storeys, b) number of bedrooms (quantified by floor area of flat) and c) energy users (quantified by averaged heating and cooling AC operating hours, in living room and bedroom combined), versus total energy consumption pre-retrofit in kWh/m ²	248

Figure 6-22: Correlation of a) number of storeys, b) number of bedrooms (quantified by floor area of flat) and c) energy users (quantified by averaged heating and cooling AC operating hours, in living room and bedroom combined) versus percentage of energy reduction after retrofit.	248
Figure 6-23: Space heating and cooling energy consumption pre-retrofit and post-retrofit in the representative area for three energy users.	251
Figure 6-24: Carbon dioxide emissions pre-retrofit and post-retrofit in the representative area for three energy users.	252

List of Tables

Table 2-1: Outdoor temperature characteristics of climate zones in China (adapted from MOHURD, 1993).....	13
Table 2-2: Overview of cities/climates investigated in building performance and/or energy studies in literature.	15
Table 2-3: Summary of climate information of cities in the HSCW zone (adapted from Li et al. 2011).	16
Table 2-4: Design codes and regulations in China for residential buildings.	20
Table 2-5: Case studies of heating system used (adapted from Guo et al., 2014).....	23
Table 2-6: Comparison of carbon intensity for China, UK and US in 2013 (International Energy Agency, 2015).....	26
Table 2-7: Criteria of built thermal environment in the HSWW zone (Zhang, 2015).....	29
Table 2-8: Temperature ranges for three categories of indoor environment (CEN, 2007).	30
Table 2-9: Assessment category for indoor thermal environments in free-running buildings (Li et al., 2014).	33
Table 2-10: Summary of dynamic thermal simulation used as found previous studies.....	37
Table 2-11: Acceptance criteria used for calibration of building energy models.	39
Table 2-12: Calibration levels based on the building information available (adapted from Reddy, 2006).	40

Table 2-13: Level of development for BEM parameters during building design (AIA and AGC of America, 2019).	44
Table 2-14: Typical residential buildings built before 2001 characterised (X. Li et al., 2018).	48
Table 2-15: Assumption of floor area as found in previous studies.	50
Table 2-16: Assumption of floor to ceiling height as found in previous studies.	51
Table 2-17: Assumption of the number of storeys as found in previous studies.	52
Table 2-18: Distribution of the number of flats per floor as found previous studies.	52
Table 2-19: Window to wall ratio from the survey (adapted from Yao 2012).53	
Table 2-20: Assumption of window to wall ratio in residential buildings in literature.	54
Table 2-21: Typical thermo-physical parameters of commonly use construction materials in residential buildings.....	55
Table 2-22: Typical external wall construction as found previous studies. ...	57
Table 2-23: Typical roof construction as found in previous studies.	58
Table 2-24: Typical internal floor construction as found in previous studies.	59
Table 2-25: Typical internal wall construction as found in previous studies.	59
Table 2-26: Typical building fabric parameters of window as found in previous studies.....	61
Table 2-27: Assumption of air infiltration rate as found in previous studies..	63
Table 2-28: Predicted energy consumption for residential buildings.	66
Table 2-29: Measured heating, cooling and total energy consumption for residential buildings.....	67
Table 2-30: Heating and cooling COP as found previous studies.	68
Table 2-31: Measured mean heating and cooling AC operating hours as found previous studies.	71
Table 2-32: Documented internal heat gains as found previous studies	77
Table 2-33: Documented air ventilation rate as found previous studies	80
Table 2-34: Common building fabric parameters of insulating material.....	82
Table 2-35: Construction of external wall with insulation as found in previous studies.....	83

Table 2-36: Construction of roof with insulation as found in previous studies	84
Table 2-37: Documented air infiltration rate for retrofitted or new buildings as found in previous studies	86
Table 2-38: Window parameters for retrofitted or new buildings as found in previous studies	88
Table 2-39: Energy efficiency rating for heating and cooling COP of air conditioner from Chinese standard	89
Table 2-40: Energy efficiency rating for SCOP and SEER for air conditioners from EU commission (EU commission, 2019).....	90
Table 2-41: Assumption of AC heating and cooling COP as found in previous studies.....	90
Table 3-1: Building fabric parameters of external wall (Liu et al., 2015; MOHURD, 2010).....	113
Table 3-2: Building fabric parameters of internal wall and internal floor (Gou et al., 2018; MOUHRD, 2010).	113
Table 3-3: Building fabric parameters of roof (Xiaotong Wang et al., 2015; MOUHRD, 2010).....	113
Table 3-4: Frequency of wind speed annually in number of hours when windows are opened	119
Table 3-5: Summary of modelling assumptions of the case study building.	119
Table 3-6: Selection of retrofit measures from 26 commonly used strategies using three selection criteria (measures identified in the following sources (Gao et al., 2014; Ge et al., 2018; Gou et al., 2018; Liu et al., 2015; Ouyang et al., 2011, 2009; Pan et al., 2018; Xi Wang et al., 2015; Xiaotong Wang et al., 2015; Yao and Xu, 2010; Yu et al., 2008; Zhao et al., 2015)	122
Table 3-7: Ten retrofit measures tested	123
Table 3-8: Summary of selected seven practical retrofit measures.....	134
Table 3-9: Heating and cooling electricity (energy) consumption collected from electricity meters from various households in residential buildings.	136
Table 3-10: Monthly and annual average outdoor air temperature for year 2000, 2005, 2010, 2015, 2019 and TMY weather data used in DesignBuilder	138
Table 4-1: Input parameters used for the steady-state model.....	143
Table 4-2: Uncertainty bands for building fabric parameters.....	149

Table 4-3: Technical specification of measuring instruments (source: Yao, 2017).....	153
Table 4-4: MBE and CvRMSE for different options of adjustment when compared to simulated temperature.....	169
Table 4-5: Building fabric parameters used in model calibration	171
Table 5-1: Annual energy consumption for three energy users and monitoring studies.....	179
Table 5-2: Exposed roof/wall to floor area ratio for twelve types of flats in the case study building.....	183
Table 5-3: Annual energy consumption for three energy users of the case study flat and building.	190
Table 5-4: Selection of optimum combination of retrofit measures.....	198
Table 5-5: Payback period for low, medium, and high energy users, with a product life of 30 years for building fabric retrofit and 12 years for energy-efficient AC.....	213
Table 6-1: Predicted building level energy consumption in kWh/m ² for the four options.....	222
Table 6-2: Window to wall ratio of the main facade for the case study flat.	224
Table 6-3: Floor area of different zones for typical residential buildings as found previous studies.	236
Table 6-4: Mean value of floor area for different zones according to Table 6-3 for typical residential buildings.....	236
Table 6-5: Floor area of thermal zones assumed in flats with different bedrooms.	239
Table 6-6: Window to wall ratio of flats with different number of bedrooms.	240
Table 6-7: Mean built area per floor for four types of residential buildings in the representative area.	250
Table 6-8: Total built area for twelve archetypes in the representative area.	250

List of Nomenclatures

g-value	Total Solar Energy Transmittance
N30°E	30° from north towards east
S30°W	30° from south towards west
tce	Tonne of coal equivalent
U-value	Thermal transmittance

List of Abbreviations

AC	Air Conditioning
ACH	Air Changes per Hour
aPMV	Adaptive Predicted Mean Vote
ASHRAE	American Society of Heating, Refrigerating and Air-Conditioning Engineers
CIBSE	Chartered Institution of Building Services Engineers
COP	Coefficient of Performance
CvRMSE	Coefficient of Variation of Root Mean Square Error
DTM	Dynamic Thermal Model
EPS	Expanded polystyrene foam
HSCW	Hot Summer and Cold Winter
HSWW	Hot Summer Warm Winter
IEA	International Energy Agency
LoD	Level of Detail
LoHCool	Low Carbon Climate-Responsive Heating and Cooling of Cities – EPSRC funded project (EP/N009797/1)
MBE	Mean Bias Error
MCF	Middle floor flat on the Centre facing Front
MCR	Middle floor flat on the Centre facing Rear
MLF	Middle floor flat on the Left facing Front
MLR	Middle floor flat on the Left facing Rear
MOHURD	Ministry of Housing and Urban-Rural Development
MRF	Middle floor flat on the Right facing Front
MRR	Middle floor flat on the Right facing Rear

NBS	National Bureau of Statistics of China
PMV	Predicted Mean Vote
PPD	Predicted Percentage of Dissatisfied
RH	Relative Humidity
RMB	Chinese Yuen (dollar)
SBS	Sick building syndrome
TCF	Top floor flat on the Centre facing Front
TCR	Top floor flat on the Centre facing Rear
THUBERC	Tsinghua University of Building Energy Research Centre
TLF	Top floor flat on the Left facing Front
TLR	Top floor flat on the Left facing Rear
TRF	Top floor flat on the Right facing Front
TRR	Top floor flat on the Right facing Rear
uPVC	unplasticised Poly Vinyl Chloride
USD	United States Dollar
VRF	Variable Refrigerant Flow
WWR	Window to Wall Ratio
XPS	Extruded polystyrene foam

Chapter 1 : Introduction

1.1 Background

The world's building sector accounts for around one-third of the global energy consumption and carbon dioxide emissions (International Energy Agency [IEA], 2015a). China is the second largest economy in the world contributing up to 20% of the global energy consumption (Lawrence Berkeley National Laboratory, 2016), reaching 4.36 billion tce (tonne of coal equivalent) in 2016, a threefold increase compared to the 2001 levels. Additionally, China's building sector comprise 20% of the country's energy consumption (Tsinghua University of Building Energy Research Centre [THUBERC], 2017). China is also the largest consumer of coal, constituting 50% of the global coal consumption (Dudley, 2018) and 69.6% (National Bureau of Statistics of China [NBS], 2017) of all the energy consumption in China in 2016. Building energy consumption reductions can lead to coal reductions and thus significantly reduce carbon dioxide generation. However, as China is undergoing rapid urbanisation, the number of buildings and their building energy consumption are expected to rise in the future.

Five climate zones were developed for energy characterisation of buildings in the country (Figure 1-1). The Hot Summer and Cold Winter (HSCW) zone of China contains 40% of China's population and is responsible for 45% of the country's building energy consumption (Gui et al., 2018; NBS, 2017; L. Xu et al., 2013). The climate in this zone has a considerable variation; in winter, the average temperature can drop to 0-10°C, and in summer, the average temperature can reach up to 25-30°C (Li et al., 2011). The existing urban domestic building stock in the HSCW zone covers around 3.4 billion m² with 550 million citizens, among which 300 million live in urban areas (NBS, 2017); this makes 8% of the world's population. Nevertheless, according to China's design regulation for the HSCW zone, central space heating is not required

(Ministry of Housing Urban and Rural Development [MOHURD], 1993). Central space heating is provided to households in the cold and severe cold zones (defined by the central government), whereas the household occupants in the HSCW zone do not benefit from central space heating as this zone lies below the heating line (Guo et al., 2015).



Figure 1-1: Five climate zones for building design in China, with the studied Hot Summer and Cold Winter zone, highlighted in blue (adapted from Gou et al. 2015)

The newly enforced construction codes and regulations aim to reduce the building energy consumption in the HSCW zone by providing guidelines on the required building fabric and passive design (MOHURD, 2001). Nonetheless, many urban residential buildings were constructed before the implementation of building regulations, and hence often have poor building fabric thermal parameters (L. Xu et al., 2013).

In winter, indoor air temperatures of urban residential buildings in the HSCW zone can drop to 5 to 15°C, which is much lower than urban residential buildings with central space heating in northern China (severe cold and cold zone), where the outdoor temperature can drop to -20 to 0°C, but the indoor air temperature averages 20 to 25°C (Li et al., 2014). In summer, buildings in the HSCW zone can be overheated, with indoor air temperature rising to 25-35°C (Li et al., 2014; Figure 1-2).

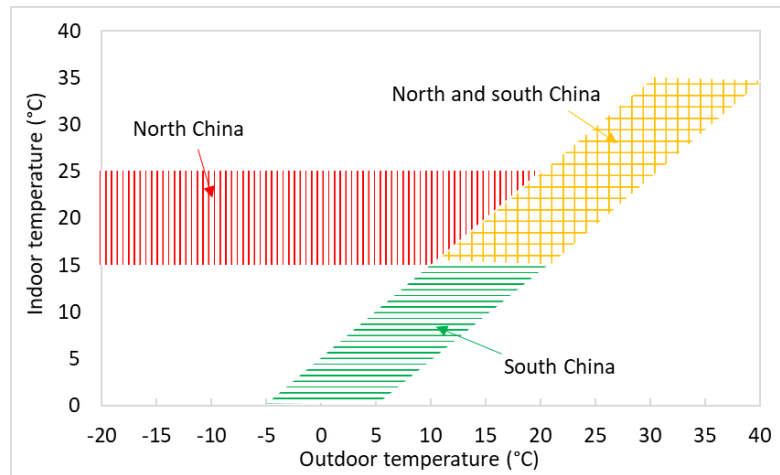


Figure 1-2: Simplified correlation of indoor and outdoor temperature in north China (with central space heating) and south China (without central space heating) (adapted from Li et al., 2014)

To battle the low uncomfortable indoor temperatures in the HSCW zone during winter, air conditioners with low efficiency are used (75% of households) for heating, typically combined with electric heaters (Wu et al., 2017). Over the summer period, around 60% to 80% of occupants operate AC, either combined with electric fans and/or with openable windows to minimise energy consumption and to keep cool (Yoshino et al., 2006). Both space heating and space cooling energy used in the HSCW zone has shown an eight fold increase from 2001 to 2015 (THUBERC, 2017).

To improve comfort in winter, installing central space heating would not be cost-effective and would likely result in a sharp increase (i.e., ten times increase) in heating energy consumption (Hu et al., 2016; MOHURD, 2010a), as the heating season is short, and the winter is not markedly cold in the HSCW zone compared to northern China. To improve comfort in summer, installing central cooling or variable refrigerant flow (VRF) systems will likely result in a sharp increase in cooling energy consumption (a five to ten times increase; Du et al., 2015). In addition, the cooling season is shorter in the HSCW zone than in the Hot Summer and Warm Winter (HSWW) zone, which makes the potential installation of central cooling or VRF systems even less cost-efficient (MOHURD, 1993).

The retrofit of residential buildings built in the 1980s, in accordance with the government’s policies (MOHURD, 2013a), is a common practice in China’s cold and severe cold zones. These policies focus on the building envelope (e.g.

insulation, windows) and the replacement of heating networks (MOHURD, 2013a). Approximately 750 million m² of residential buildings had already been retrofitted by 2014, while the entire residential building stock (1200 million m²) is planned to be retrofitted by 2020 (MOHURD, 2017). The policy regarding the retrofitting of urban residential buildings in the HSCW zone was introduced in the *12th Five-Year Energy Development Plan (2010-2015)*; State Council of the People's Republic of China [State Council], 2012). A total of 70 million m² of urban residential buildings were retrofitted in the HSCW zone between 2010-2015 (MOHURD, 2017). This exceeded the planned retrofit rate of 50 million m². However, the required retrofit of the total built-up area is estimated to be 3.4 billion (3400 million) m². Therefore, only 2% of the urban residential building stock was retrofitted between 2010-2015.

A mandatory building regulation “*Design standard for energy efficiency of residential buildings in Hot Summer and Cold Winter zone*” was issued in 2001 (MOHURD, 2001), and revised in 2010 (MOHURD, 2010a). It was intended to provide guidelines for the design of new residential buildings in the HSCW zone (such as U-values limits for external walls, roofs, and windows). “*Retrofit guidelines for existing residential buildings in Hot Summer and Cold Winter (HSCW) zone*” was also issued in 2012, to provide guidelines for energy saving retrofit measures (such as energy saved for external wall insulation, new windows, etc.; MOUHRD, 2012a). Yet, both the existing regulations and guidelines fail to consider households with different AC operating schedules and the variation of building designs at a city scale. The energy saving of some retrofit measures, such as air infiltration control, additional window overhang, and energy-efficient AC, are not quantified.

The future usage of AC for residential buildings is likely to increase as living standards improve. This is likely to lead to a sharp increase in energy consumption and a significant impact on greenhouse gas emissions (IEA, 2015a; Zhang et al., 2010). This could be minimised by developing innovative retrofit solutions in the HSCW zone, including building fabric retrofits and energy-efficient AC. Large-scale retrofits could result in improved thermal comfort for many millions of people and reduce future energy consumption.

1.2 Overview of the LoHCool project and significance of research

This thesis forms part of the Low Carbon Climate-Responsive Heating and Cooling of Cities (LoHCool) project, a collaboration between the Chongqing University and Zhejiang University in China, the University of Reading, led by the University of Cambridge. It is funded by the UK Engineering and Physical Sciences Research Council (EPSRC; EP/N009797/1), it started on 1st October 2015 and ended on 31st March 2019. The project is multi-disciplinary and involves engineers, building scientists, atmospheric scientists, architects, and behavioural researchers. The aim of the LoHCool project is to develop a holistic approach to achieving carbon dioxide reductions associated with providing space heating and cooling, whilst satisfying rising aspirations towards the thermal environment. There are several objectives to address this aim. The aim which relates to this study is “to invent and catalogue climate-responsive, performance-improving re-engineering and refurbishment solutions for heating and cooling”.

Dynamic thermal simulation is the primary method of this thesis. Collaboration with the LoHCool research team is required for obtaining input data, these include:

- Building parameters in representative areas selected in two major cities (Chongqing and Hangzhou) in the HSCW zone;
- Selection of a representative urban residential building with information of architectural characteristics;
- Measured data of internal air parameters for a selected case study flat.

Research conducted as part of the LoHCool project has focused on these areas in residential buildings in the HSCW zone, data of which has been shared and used, these include:

- A parametric analysis of a case study building to evaluate climate-sensitive passive design solutions to reduce energy demand and improve indoor thermal conditions (Yao et al., 2018);

- Developing building archetypes using clustering analysis of satellite images for a representative area (Yuzhong District) in Chongqing to predict the aggregated energy consumption for the residential buildings requiring retrofit (X. Li et al., 2018);
- Identify reoccurring residential buildings using correlation and cluster analysis, to offer guidance for designing proper retrofit strategies from a representative area (Shangcheng District) in Hangzhou (Gui et al., 2018);
- Develop an innovative windcatcher and exhaust-stack natural ventilation system to improve comfort and reduce summer cooling loads for a case study building (Short et al., 2018).

However, none of the above studies aimed to quantify energy saving retrofits for a whole case study building, evaluate the accuracy of reducing level of details of DTM, or provide design guidance by predicting energy saving retrofits in city-scale; all of which are achieved in this thesis.

This research and the LoHCool project both aim to develop retrofit measures for residential buildings in the HSCW zone to achieve energy reduction whilst satisfying rising aspirations towards the thermal environment. LoHCool selected four case study residential building from the city of Chongqing and Hangzhou, this research use one of the building in Chongqing. Moreover, LoHCool sampled 206 residential building in Hangzhou and 334 residential building in Chongqing, where building parameters collected in Chongqing was used in this thesis. Difference of this research with LoHCool project was this research discuss that in the absence of established data base on building fabric and other parameters, the energy consumption could be modelled with good accuracy in a complex urban environments in the context of HSCW zone. Subsequently, the findings in this research can be useful for moving towards a HSCW zone specific energy benchmarking exercise.

1.3 Aim and Objectives

The aim of this study is to develop retrofit measures for urban residential buildings and quantify the potential energy reductions at a city scale in the HSCW climate zone in China.

The research aim will be achieved through the following objectives:

1. Characterise the urban residential building stock, identify building parameters in the HSCW zone, and select a typical building, in order to develop a dynamic thermal model (DTM) representative of the urban residential buildings in the HSCW zone;
2. Increase the reliability of model predictions by creating a verified DTM of a single flat using measured data, and predict sensitivity of energy demand to alternative building fabric options;
3. Quantify the energy savings performance of practical retrofit measures, and select an optimum combination able to reduce energy consumption and occupants' thermal discomfort of the single flat and the building;
4. Ensure wider applicability of outputs by creating a DTM with reduced levels of modelling detail using the typical building, and evaluate potential energy reductions on a larger scale;
5. Evaluate the feasibility of the selected retrofit measures at a city scale with regards to energy reductions for a range of building designs, using the DTM with reduced levels of modelling detail.

1.4 Contribution of research

Many residential buildings were constructed prior to the implementation of building regulations (in 2001), and thus often lack adequate building fabric. As living standards increase, the use of AC for residential buildings in the HSCW zone increases, and leads to a sharp increase in energy consumption and greenhouse gas emissions. Many studies have evaluated energy saving retrofits for residential buildings in the HSCW zone by selecting a typical building to develop a DTM and subsequently generalising outputs to similar buildings (Yao et al., 2018; Yu et al., 2008). In the UK, defining building fabric

parameters of buildings when creating simulation models typically derive from regulations of the era, because building regulation has been enforced from as far back as 1965 (HM Government, 1965). However, in China, the vast majority of the existing residential buildings were built before the enforcement of building regulations, in which case building fabric parameters of simulation models are reliant on author's knowledge, resulting in substantial variation of selected building fabric parameters across existing studies. For instance, one study assumed U-values of external walls to be 3.67 W/m²K (Yu et al., 2008), while another study assumed U-value of external walls to be 1.97 W/m²K (Yao et al., 2018) for a similar building design/construction, resulting in a considerable variation of predicted energy consumptions and consequently energy saving retrofits. Occupant behaviour, particularly in relation to energy consumption, is a significant factor in the overall building energy performance, yet most studies have evaluated a single type of energy user (L. Xu et al., 2013; Yu et al., 2008). The literature showed radically different AC operating hours across households (Chen et al., 2015), which caused significant variations of energy consumption. Accordingly, for the purpose of this research, a representative area in Chongqing was selected, with 95% of the residential buildings in the area built prior to the implementation of building regulations. Subsequently, the case study building selected is typical in the representative area.

Furthermore, a limited number of studies have considered calibrating the indoor temperature prediction in DTM, which may lead to model prediction discrepancies with measured data (P. Xu et al., 2013) and thus, less reliable predictions of energy saving retrofits. Model calibration prior to DTM can improve the reliability of predictions when evaluating energy saving retrofits. According to the literature, different indicators can be used to evaluate the calibrated DTM model; energy consumption and indoor air temperature are the most common ones (Nguyen and Reiter, 2012; P. Xu et al., 2013). A sensitivity analysis was performed using a monthly quasi-steady-state model (herby "steady-state model"), prescribed from ISO 13790:2008 and developed using excel spreadsheets by Taylor (2016), to inform the model calibration process.

Many studies have quantified energy saving retrofits for residential buildings in the HSCW zone (Xiaotong Wang et al., 2015; Yu et al., 2008; Zhao et al., 2015). They showed that improving the external wall insulation by 10 mm of extruded polystyrene (XPS) and the roof insulation by 40 mm XPS can lead to 6% and 7% energy reductions respectively for a typical urban residential building in the HSCW zone (Ouyang et al., 2009). Similarly, replacing single-glazed windows with double-glazed windows with low emissivity surface leads to an 8% energy reduction for a typical urban residential building in the HSCW zone (Yu et al., 2008). However, these studies failed to identify the optimum retrofit measure from the perspective of both energy consumption and thermal comfort performance for each type of retrofit measure. Also, many studies evaluated retrofit measures on a single residential flat (Gong et al., 2012; Zhao et al., 2015) to reduce simulation time; however, the energy demand would vary for different housing units (Yao, 2012). The above limitations are addressed in Objective 3, by quantifying the energy consumption and thermal comfort performance of seven types of retrofit measures considering households with different AC operating hours and different flats in the building.

When developing DTMs of a case study building, most studies use simplified box models (Gong et al., 2012) or study middle floor flats with one zone in a building (Yao et al., 2018) to reduce simulation time. Limited studies modelled residential flats in the HSCW zone with two or more zones (Yu et al., 2008), which renders the predictions less reliable. Also, few studies have developed DTMs using high levels of architectural detail, as it requires a substantial amount of data to implement a detailed model (Taylor et al., 2013). However, one study reported that DTMs with a lower level of detail impacted on modelling accuracy by a significant degree for houses in the UK (Taylor et al., 2013). Thus, Objective 4 is to identify the most suitable level of information required in the development of building archetypes for the representative area.

Urban building energy models are often used to analyse energy performance of building stock, which requires data including building types, floor area, year of construction, and building height (Reinhart and Cerezo Davila, 2016). The case study building represents buildings with similar number of storeys and number of bedrooms (one-bedroom). However, throughout the representative

area, the buildings have a different number of storeys and flats with a varying number of bedrooms. Building archetypes can be used to present the general characteristics of the urban residential building stock, to quantify the potential energy reduction for the representative area, addressing Objective 5 and also the research aim.

This study sets out to address all the above limitations by completing the five objectives to achieve the research aim. Results from this study address the LoHCool project aim by providing strategies to retrofit residential buildings.

1.5 Outline of the thesis

The thesis starts with an overview of the background, aim, and objectives, and contribution to knowledge of this research (Chapter 1). It then proceeds with a comprehensive literature review (Chapter 2), which covers characteristics of the HSCW zone, the existing building energy consumption, thermal comfort conditions, methods to assess building performance, methods to characterise building parameters, and strategies to develop retrofit measures. The research methodologies developed to address the aim and objectives are further discussed in Chapter 3. Results and analysis of the computational work conducted are addressed in Chapters 4 to 6. Chapter 7 summarises the conclusion and possible directions of further research based on the results of this study.

Chapter 2 : Literature review

2.1 Introduction

This research starts with a thorough literature review in the context of the HSCW zone, which covers a wide range of topics.

Section 2.2 presents the characteristics of the HSCW zone, including the geographic and climatic characteristics of the HSCW zone, the constructional features in existing residential buildings, and a summary of existing codes and regulations.

Section 2.3 presents the contribution of carbon dioxide (CO₂) emissions by coal-fuelled heating and cooling systems in existing residential buildings. This includes a review of the sources and trends of building energy consumption, the performance of heating and cooling systems, electricity generation methods, and carbon intensity in existing residential buildings.

Section 2.4 presents the factors affecting indoor thermal comfort (air temperature, relative humidity, wind speed and garment insulation value) and adaptive thermal comfort models, specifically for existing residential buildings in the HSCW zone.

Section 2.5 presents a review of the methodological approach of performance evaluation tools for energy saving retrofits. This incorporates a review on steady-state energy performance evaluation tools, dynamic thermal simulation, model calibration and validation, sensitivity and uncertainty analysis, optimisation of energy saving retrofits, level of detail in building energy modelling, and city-scale model.

Section 2.6 presents an in-depth analysis of existing building parameters, which derived from literature data from modelling predictions, measurements and meter readings of existing residential buildings in the HSCW zone.

Section 2.7 presents recent studies that explored building retrofit measures in existing residential buildings. There are a significant number of potential retrofit measures that could be suitable in the context of Chinese domestic multi-storey buildings. It is therefore essential to review recent studies that investigated practical retrofit measures which could be applied in existing residential buildings. This is achieved in this thesis by an extensive literature review which examines building retrofit measures in existing residential buildings.

2.2 The Hot Summer and Cold Winter zone: Characteristics

2.2.1 Geographic characteristics

China covers 9.6 million km² of land with a coastline of 18,000 km. It is divided into 22 provinces, five autonomous regions, four central government-controlled municipalities, and two special autonomous regions. Two cities located in the Hot Summer and Cold Winter (HSCW) zone are the focus of this study. Chongqing (29° 33' N / 106° 33' E) is in southwest China; it is a central government-controlled municipality. It has a population of 33 million, and with a terrain of 82400 km², it is located upstream of the Yangtze River. The city area in Chongqing is surrounded by the Yangtze River and Jialing River and has 10 million residents. Zhejiang province (31° 0' N / 121° 24' E) is located in the east side of China along the coastline. Hangzhou (30° 15' N / 120° 10' E) is the province capital of Zhejiang province with a 7.12 million population (Figure 2-1).

2.2.2 Climatic characteristics

The five climate zones in China are defined according to the mean temperatures of the coldest month (January) and the hottest month (July) (Table 2-1; MOHURD, 1993). According to Köppen climate classification, HSCW zone belongs to the “Cwa” category, with a humid subtropical climate (Figure 2-2).

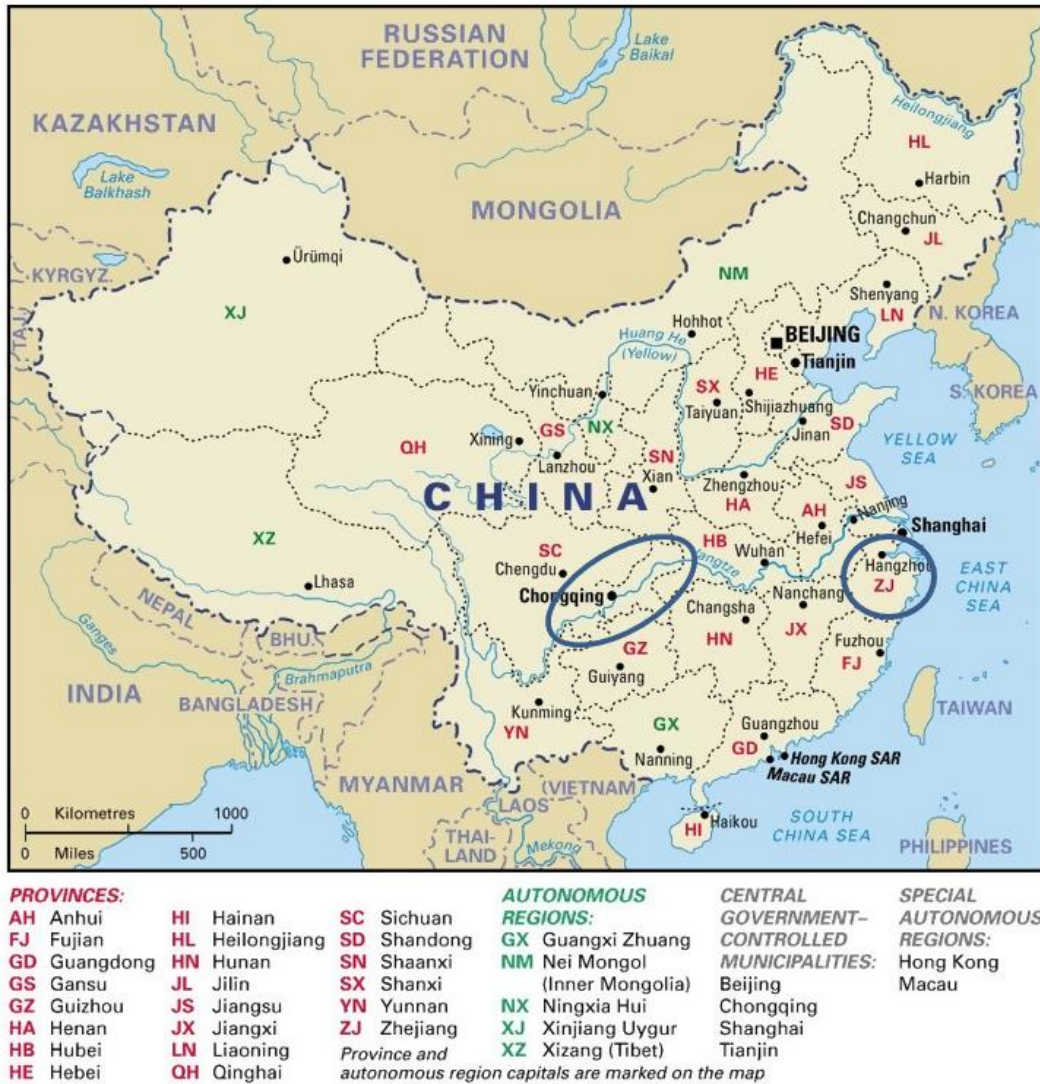


Figure 2-1: Map of China. Circles indicate the cities of Chongqing and Hangzhou (Source: <http://www.china-mike.com/china-travel-tips/tourist-maps/china-provinces-map>).

Table 2-1: Outdoor temperature characteristics of climate zones in China (adapted from MOHURD, 1993).

Climate zone	Outdoor temperature $\leq 5^{\circ}\text{C}$ (days)	Outdoor temperature $\geq 25^{\circ}\text{C}$ (days)	Mean outdoor temperature in January ($^{\circ}\text{C}$)	Mean outdoor temperature in July ($^{\circ}\text{C}$)
Severe Cold	≥ 145	0 days	≤ -10	≤ 25
Cold	90 to 145	≤ 80	-10 to 0	18 to 28
Hot Summer and Cold Winter	0 to 90	40 to 110	0 to 10	25 to 30
Hot Summer and Warm Winter	0	100 to 200	>10	25 to 29
Mild	0 to 90	0	0 to 13	18 to 25

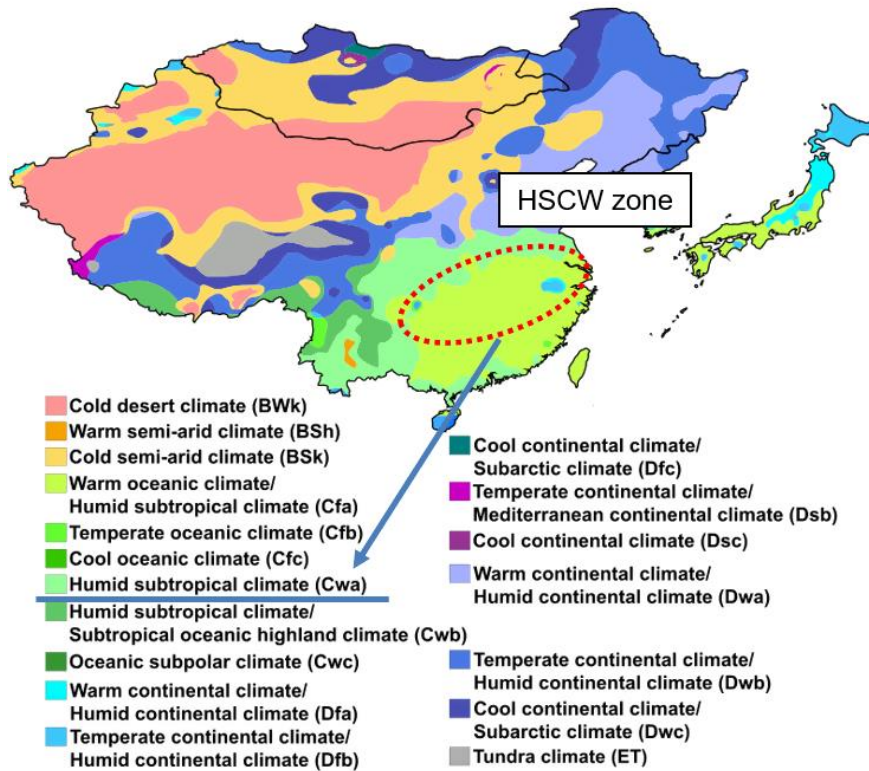


Figure 2-2: East Asia map of Köppen climate classification (Köppen climate classification, 2016).

Within the HSCW zone, six major cities (Shanghai, Hangzhou, Changsha, Wuhan, Chongqing, and Chengdu) are frequently investigated in the literature (Table 2-2). Shanghai and Chongqing are central government-controlled municipalities; Hangzhou, Changsha, Wuhan, and Chengdu are the provincial capitals of Zhejiang, Hunan, Hubei, and Sichuan province respectively (Figure 2-1). These cities are characterised by the wet cold winters and very hot and humid summers (Li et al., 2011). In winter, Chongqing has the highest mean temperature of the coldest month (6.3°C) among the six cities (Table 2-3). The mean temperature of the coldest month is the lowest in Wuhan, with a temperature of 3.3°C lower than Chongqing. In summer, Changsha has the highest mean temperature of the hottest month (29.3°C), and Chengdu has the lowest mean temperature of the hottest month (27.6°C) among the six cities. Relative humidity of these six cities in the HSCW zone is 75 to 85% throughout the year. Cities in the HSCW zone often experience extreme temperatures. In winter, there are 67 days in Hangzhou and 62 days in Shanghai in which the temperature falls below 5°C (Li et al., 2011). In summer, there are 25 days in Chongqing and 22 days in Hangzhou with air temperatures exceeding 35°C (Li et al., 2011) (Table 2-3).

Therefore, the six cities in the HSCW zone can be categorised into two groups: cities with colder winters (Hangzhou, Shanghai, Changsha, and Wuhan) and cities with milder winters (Chongqing and Chengdu).

The average global horizontal solar radiation is 1500 kWh/m² across China, with a significant variation from 800 to 2300 kWh/m² (Muneer et al., 2012). In Chongqing with latitude of 29.3°N, the average global horizontal solar radiation is 1000 kWh/m², which is the lowest in China and the intensity is similar to the UK with a latitude of 51.5°N (Muneer et al., 2012). Hangzhou is located at 30°N, where the average global horizontal solar radiation is 1200 kWh/m², 20% higher than Chongqing (Figure 2-3).

Table 2-2: Overview of cities/climates investigated in building performance and/or energy studies in literature.

Chongqing	Chengdu	Hangzhou	Changsha	Shanghai	Wuhan	Others	Reference
		✓					(Ouyang et al., 2009)
		✓					(Ouyang et al., 2011)
			✓				(Yu et al., 2008)
		✓					(Xiaotong Wang et al., 2015)
				✓			(Chen et al., 2009)
✓							(L. Xu et al., 2013)
✓			✓	✓			(Yao et al., 2018)
✓							(X. Li et al., 2018)
	✓		✓	✓		Shaoguan	(Yu et al., 2013)
✓							(Zhao et al., 2015)
	✓		✓	✓		Shaoguan	(Yu et al., 2011)
	✓		✓	✓	✓		(Gong et al., 2012)
				✓			(Pan et al., 2018)
✓				✓	✓		(Yang et al., 2015)
						Yichang	(Xi Wang et al., 2015)
✓				✓	✓		(Gao et al., 2014)
						Ningbo	(Yao and Xu, 2010)
✓	✓		✓	✓	✓		(Ichinose et al., 2017)
		✓	✓			Nanjing	(Fu et al., 2017)
✓		✓		✓	✓		(Xiong et al., 2018)
		✓					(Short et al., 2018)
				✓			(Chen and Yang, 2018)
	✓						(Feng et al., 2016)
✓	✓			✓	✓	Nanjing	(Hu et al., 2016)
				✓			(Peng et al., 2012)
✓				✓			(Ma et al., 2015)
✓							(W. Yu et al., 2015)
		✓					(Yao, 2012)
				✓			(Gou et al., 2018)

Table 2-3: Summary of climate information of cities in the HSCW zone (adapted from Li et al. 2011).

City	Mean temperature of the coldest month (°C)	No. of days which daily average temperature <5°C	Mean temperature of the hottest month (°C)	No. of days which daily average temperature >35 °C
Chongqing	6.3	0	28.6	25
Chengdu	5.4	0	27.6	4
Hangzhou	3.7	67	28.6	22
Shanghai	3.5	62	28.2	16
Changsha	4.6	45	29.3	30
Wuhan	3.0	67	28.8	23

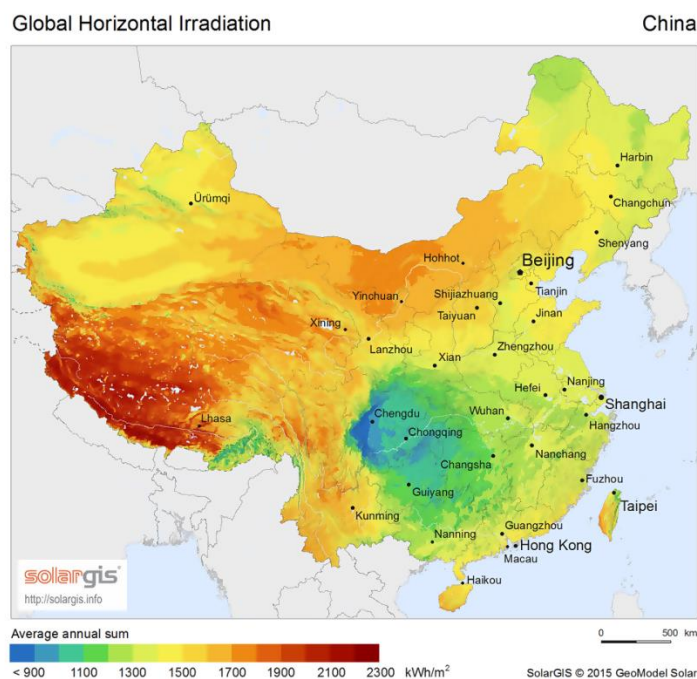


Figure 2-3: Average annual sum of global horizontal irradiation in China (SolarGIS, 2015).

Both Chongqing and Hangzhou experience high humidity (65-90%) throughout the year; relative humidity in Chongqing is higher than Hangzhou in winter. Chongqing experiences less solar radiation than Hangzhou in winter; but in July and August, they receive a similar amount of solar radiation. Both cities experience even wind speed patterns throughout the year (1-3m/s), with wind speed in Hangzhou 0.5m/s higher than Chongqing throughout the year (Figure 2-4).

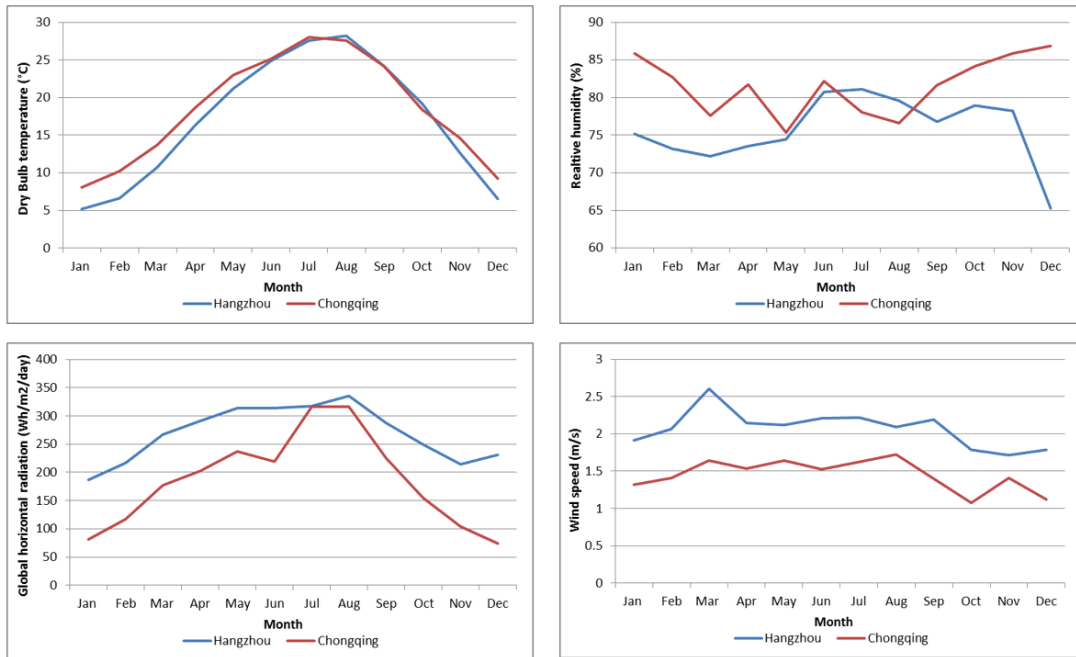


Figure 2-4: Climate characteristics (dry-bulb temperature, relative humidity, global horizontal radiation, and wind speed) for Chongqing and Hangzhou.

2.2.3 Characteristics of existing residential buildings

China's latest Statistical Yearbook, published in 2018, reported rapid urbanisation over the past 20 years from 26% in 1990 to 58.5% in 2017. This is an average annual rate increase of around 1.4% and it is expected to increase further in the future (Figure 2-5). According to the 13th Five-Year Plan (2016-2020), the anticipated urbanisation rate in 2020 is expected to be 60% (Central Compilation & Translation Press, 2016). Currently, China's total floor area of buildings is approximately 58.1 billion m², of which urban residential floor area consists of 23.1 billion m², rural residential floor area is 23.3 billion m², public, and commercial floor area is 11.7 billion m².

In order to cope with the rapid urbanisation rate, many urban residential buildings were built in the past 20 years. The number of new urban residential buildings in 2015 is 10.04 million m² (Figure 2-6). The floor space per capita has doubled in the past 20 years, and it is expected to increase in the future (Berkelmans and Wang, 2012).

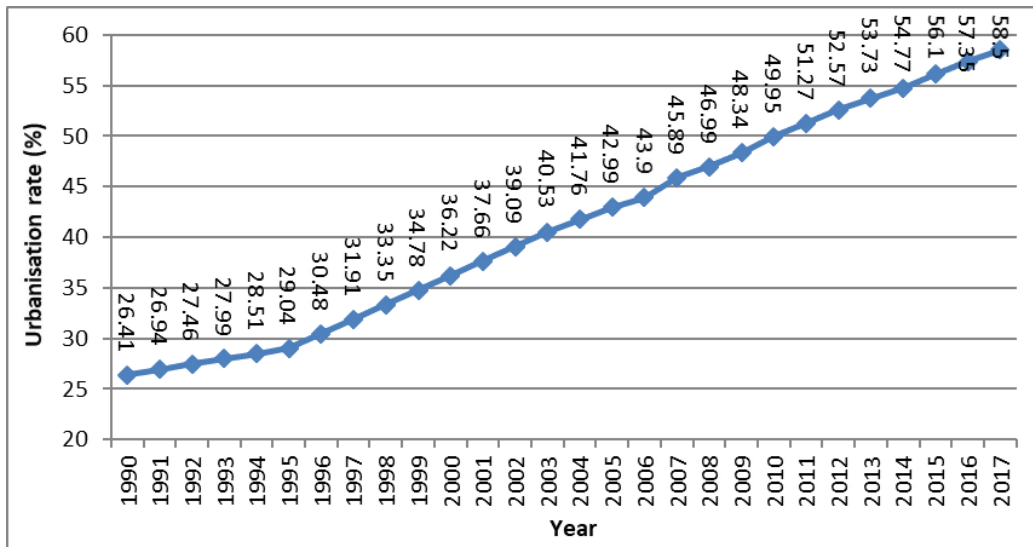


Figure 2-5: China's urbanisation rate from 1990 to 2017 (NBS, 2018).

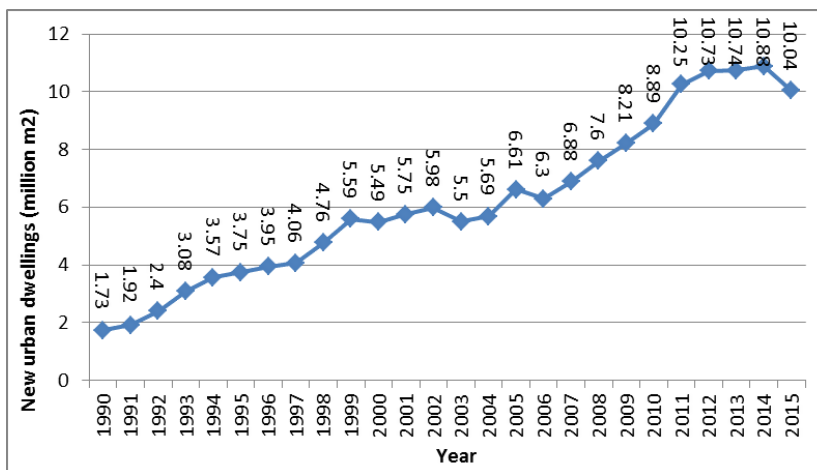


Figure 2-6: New urban residential building completed each year (NBS, 2018).

A population census of China is issued every 10 years from National Bureau of Statistics (NBS); the latest census was published in 2010. The census provides information on height, structure and built-up area of residential buildings in China and in each province (NBS, 2010).

In Chongqing (municipality), over 80% of the buildings are higher than four storeys and 60% for Zhejiang (province). For Chongqing, 30% of the residential buildings are between 7-9 storey and 30% are over 10 storeys high (Figure 2-7a). Over 90% of residential buildings in Chongqing and Zhejiang are reinforced, either with concrete or mixed structure (reinforced concrete and brick) (Figure 2-7b). About 50% of residential buildings in Chongqing and Zhejiang were built before 2000 (Figure 2-7c).

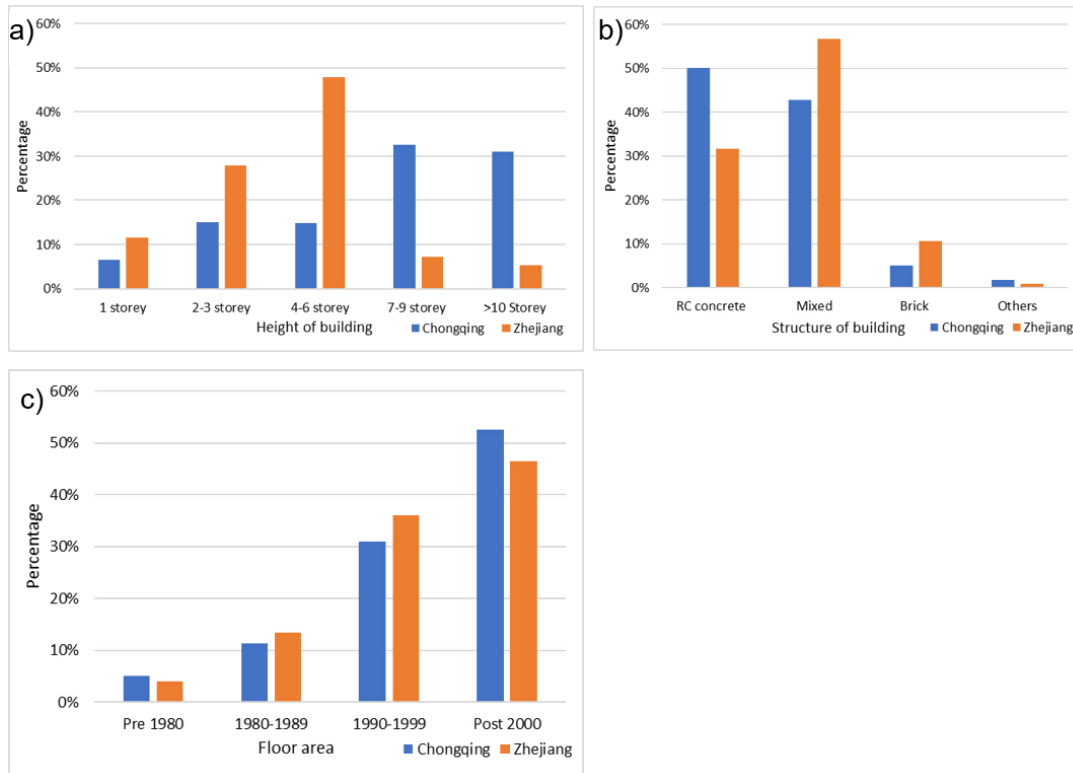


Figure 2-7: a) Height, b) structure and c) floor area of buildings in Chongqing municipality and Zhejiang province (NBS, 2010).

2.2.4 Summary of existing codes and regulations

The Ministry of Housing and Urban-Rural Development (MOHURD) develops and coordinates the national building energy codes in China. In particular, the 12th Energy Development Five-Year Plan addresses several major challenges to China’s development from 2010 to 2015, including resource constraints, energy security, and environmental quality. Implementation of mandatory standards for new construction, green building demonstration and development, and renovation of existing building stocks have been planned (Central Compilation & Translation Press, 2011).

Before 1995, there were no design standards governing the construction of buildings. Between 1995 and 2001, the first design standard was introduced (MOHURD, 1995); however, regulations were focused on cold and severe cold regions (North China). Mandatory design standards were enforced for buildings in HSCW zone (MOHURD, 2001) in 2001, and they were updated in 2010 (MOHURD, 2010a). In 2010, standards were developed for different provinces within the HSCW zone (MOHURD, 2010b; Table 2-4). These design

standards list several mandatory design conditions for newly built urban residential buildings, which are discussed in detail in Section 2.6.

Table 2-4: Design codes and regulations in China for residential buildings.

Standard code	Name of standard	Notes
JGJ 26-95	Energy conservation design standard for civil buildings (residential buildings with central heating systems).	First design standard introduced in China (focus on cold and severe cold region).
JGJ 134-2001	Design standard for energy efficiency of residential buildings in hot summer and cold winter zone.	Mandatory design standard implemented for newly built residential buildings in the HSCW zone.
JGJ 134-2010	Design standard for energy efficiency of residential buildings in hot summer and cold winter zone.	Update base on JGJ 134-2001 for the HSCW zone, aim to reduce energy use by 50% compared to 1980s level.
DBJ 50-071-2010	Design standard for energy efficiency 65% of residential building in Chongqing.	Aim to reduce energy use by 65% compared to 1980s level in Chongqing municipality.

2.3 Building energy consumption in the HSCW zone

2.3.1 Sources of building energy consumption

The total building energy consumption was 896 Mtce in 2018, accounting for 20% of China's total energy consumption. China's building energy consumption can be divided into four categories, which are discussed as follows (THUBERC, 2018):

- Central space heating: 21% of total building energy consumption, only residential buildings in northern China have access to central space heating.
- Public and commercial buildings: 31% of total building energy consumption.
- Urban residential buildings: 23% of total building energy consumption; includes energy consumption in urban residential buildings but excludes central space heating in northern China. In this sub-sector, space heating in the HSCW zone accounts for 9% of urban residential building energy consumption, where space cooling accounts for 12%.
- Rural residential building: 25% of total building energy consumption.

Urban household building energy consumption in the HSCW zone involves space heating, space cooling, lighting, equipment (e.g. TV, refrigerator, computer, washing machine), water heating, and cooking (Figure 2-8). Over half of the households use piped gas as the dominant fuel for cooking, and gas boilers are commonly used (50%) for water heating in the HSCW zone (THUBERC, 2017).

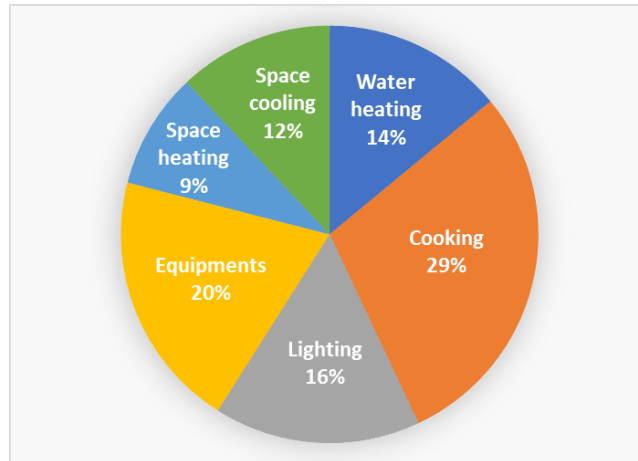


Figure 2-8: Distribution of China's urban residential building energy consumption (adapted from TUBERC 2018).

2.3.2 Trends of building energy consumption

Building energy consumption for heating in the HSCW zone has increased by a magnitude of ten from 1996 to 2001, while the energy consumption for cooling also increased by a magnitude of ten and other household electricity consumption (e.g. lighting and equipment) has increased by a magnitude of five (Figure 2-9; Building Energy Research Center of Tsinghua University, 2013). Another study further validates the dramatic trend of increasing building energy consumption by showing urban residential energy consumption in Shanghai (a major city in the HSCW zone) has risen tenfold from 55 kWh in 1980 to 574 kWh in 2005 (Chen et al., 2009).

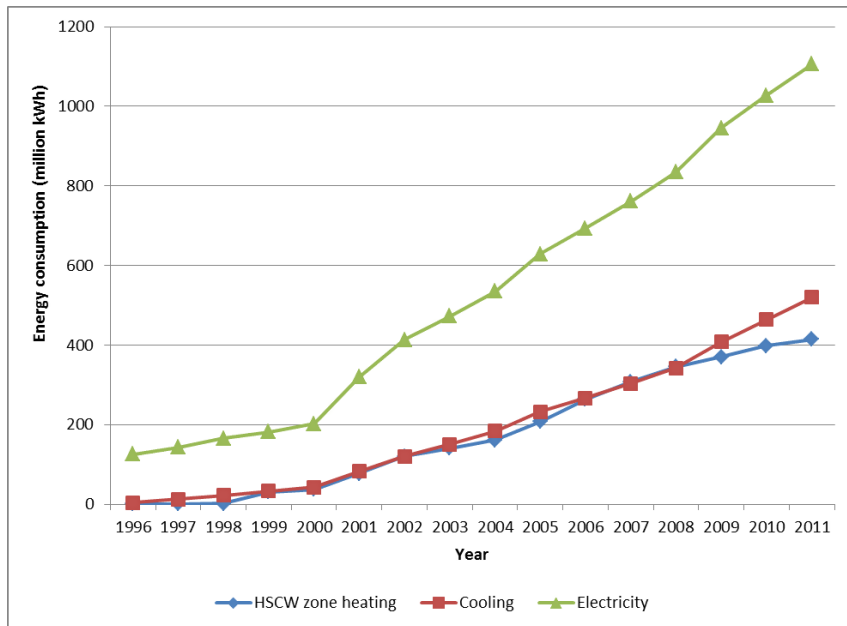


Figure 2-9: Trend of building energy consumption from 1996 to 2011 in China (THUBERC, 2013).

Despite the rapid energy consumption increase, residential energy consumption per household in urban China is about half of that in Western countries (e.g. USA, Germany; Figure 2-10a), in the case of per capita value, the consumption is even less (one fourth of energy; International Energy Agency, 2015a; Zhang et al., 2010; Figure 2-10b). It is interesting to note that Figure 2-9 includes buildings in northern China with central space heating, this shows that the difference between residential buildings in the HSCW zone and those in developed countries is even more substantial. The considerable variation is due to cultural factors, such as occupants using less air conditioner (a phenomenon which will be discussed in detail later in this review).

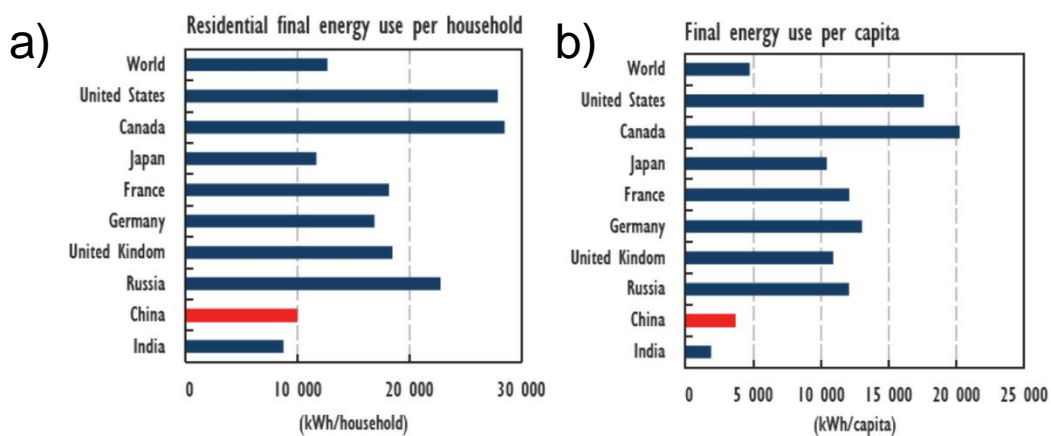


Figure 2-10: Residential energy metrics considering a) final energy use per household and b) final energy use per capita for selected countries (IEA, 2015b).

2.3.3 Performance of heating and cooling systems

Guo et al., (2015) conducted a survey study in five urban residential buildings located in the HSCW zone to evaluate the heating energy consumption of different heating systems (i.e., electric heater, split air conditioners, VRF system, gas boiler, and central heating). Results showed that split air conditioners and electric heaters had the lowest heating energy consumption (Table 2-5). Flats equipped with central heating and gas boilers experienced similar indoor temperatures than those using split air conditioners and electric heaters. However, the energy consumption was ten times higher when central heating or gas boilers were used, due to the inability of occupants to control the central heating and gas boiler systems manually. Variable refrigerant flow (VRF) systems were predicted to be more efficient with regards to occupants' comfort and energy consumed relative to central heating or gas boilers, due to the fact that occupants can control the system manually. The electricity price and energy consumption are the lowest for split air conditioners and electric heating (almost ten times cheaper than central heating; Table 2-5).

Table 2-5: Case studies of heating system used (adapted from Guo et al., 2014).

Type of system	Central heating	VRF	Gas boilers	Split air conditioner	Electric heater
Building location	Wuhan	Wuhan	Shanghai	Shanghai	Nanjing
Building construction year	~2010	2009	2000	2000	1990
Energy consumption (kWh/m ²)	95.8	31.9	83.3	9.4	1.7
Electricity price (RMB/m ²)	25.5	6.38	21.7	2.4	0.9
Indoor temperature (°C)	>18	>25	15-17	15-17	14-17
Operating schedule	Full	Part	Full	Part	Part

The primary heating energy consumption in the HSCW zone is increasing; due to more people using VRF, gas boilers, central heating systems, and ground source heat pumps (Figure 2-11; Hu et al., 2016); these heating systems consume more energy than split air conditioners and electric heaters. A study showed that the percentage of households using district heating and gas boilers has increased from 5% in 2012 to 25% in 2014 (Guo et al., 2015). However, usage of air source heat pumps is still widespread (more than 50% of occupants) due to their relatively high efficiency and reasonable price (Guo et al., 2015).

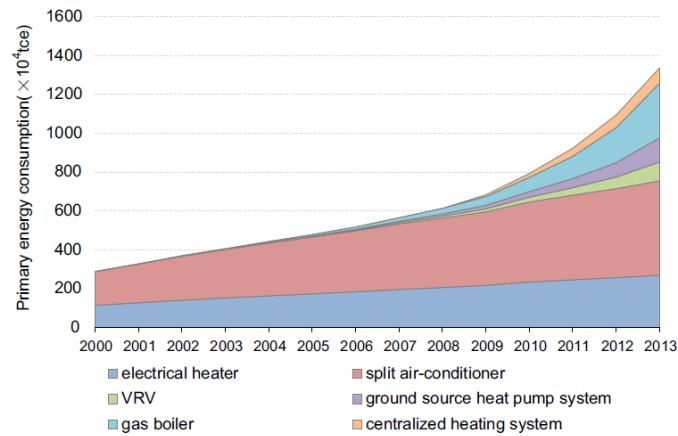


Figure 2-11: Heating energy consumption of urban residential buildings in the HSCW zone (Hu et al., 2016).

Li (2007) performed a monitoring study in urban residential buildings located in Beijing to evaluate the cooling energy consumption of different cooling systems (split air conditioners, VRF systems, and central cooling). Beijing is located in the cold zone, but the average temperature in summer is 26.7°C, that is similar to cities in the HSCW zone (average temperature of 25 to 30°C; Li, 2007). Results indicated that cooling energy consumption ranged from 1 to 14 kWh/(m².a) for split air conditioners (Li, 2007). The cooling energy consumption for VRF systems was 5 to 10 kWh/m² and central air conditioners was 20 kWh/m² per year, much higher than the average consumption of split type air conditioners (Figure 2-12). Similar to heating energy consumption, occupants cannot manually control central conditioners, and thus they are operated for the whole cooling season, leading to high energy consumption (Li, 2007).

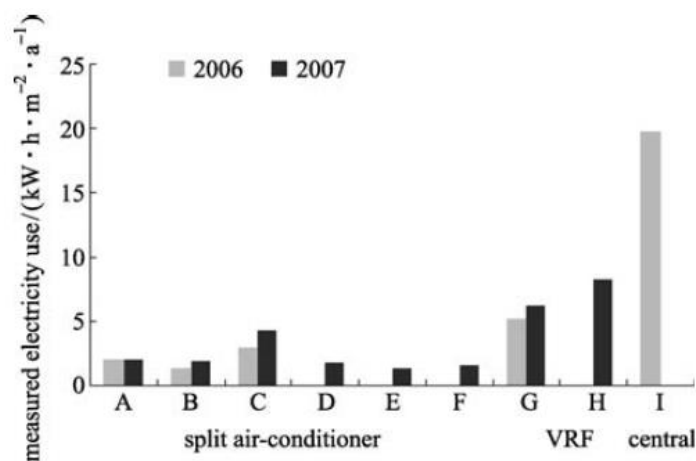


Figure 2-12: Measured electricity use for different cooling system and devices in Beijing (Li, 2007).

Yoshino et al. (2006) investigated the rate of usage regarding air conditioners, fans, and window opening in summer by surveys in cities located in the HSCW zone (Chongqing, Changsha, and Shanghai). Results showed that 60 to 80% of occupants have AC installed and half of them combined electric fans with AC to save energy. Others combined electric fans and open windows to keep cool. The study also reflected that air conditioners are not frequently used in the HSCW zone even though they were installed in the flats.

The above showed that although new heating and cooling technologies (VRF systems, central heating, central cooling, gas boiler, and ground source heat pump) can provide desired thermal comfort conditions, the energy consumption is higher than split air conditioners (two to four times higher). This will lead to a sharp increase in energy consumption if split air conditioners are replaced by new heating and cooling technologies.

2.3.4 Electricity generation method and carbon intensity

The total energy consumption in China reached 4.36 billion tce (tonne of coal equivalent) in 2016 (Figure 2-13). Coal consumption peaked at 2013 with 2.81 billion tce and decreased to 2.7 billion tce in 2016 (NBS, 2017). In 2016, coal (62%), oil (18%) and natural gas (6%) were the main generation methods of electricity, with 13% generated by other sources such as solar energy (NBS, 2017). In December 2016, the Energy Supply and Consumption Revolution Strategy (2016-2030) was announced as part of a national policy in China. The policy aims to cap the total energy consumption at 5.0 billion tce by 2020 and 6.0 billion tce by 2030 (NDRRC, 2016).

The concentration of CO₂ in the atmosphere has increased significantly by 40% from the mid-1800s to 2014, and the average growth in the last ten years is around 2ppm/year (International Energy Agency, 2015). The indicator of CO₂ emissions per kWh is commonly used to account for the energy consumption of different countries. The carbon intensity in China is higher than that of developed countries such as the UK and US, considering energy use in all sectors (Table 2-6).

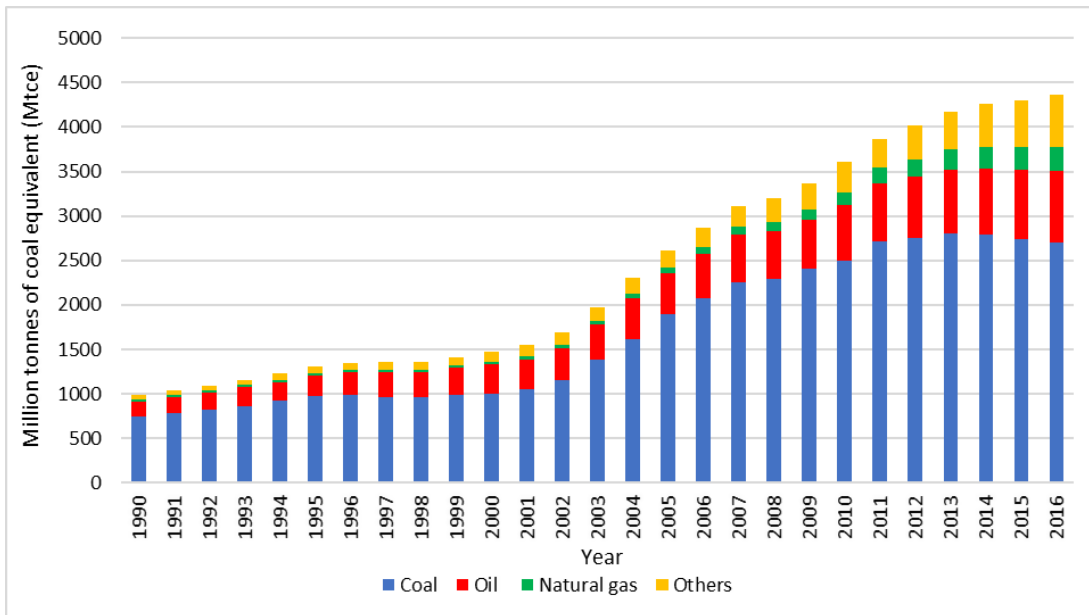


Figure 2-13: Energy generation methods in China from 1990-2006 (adapted from NBS, 2017).

Table 2-6: Comparison of carbon intensity for China, UK and US in 2013 (International Energy Agency, 2015).

	Million tons of CO ₂	TWh of electricity	kgCO ₂ /kWh
China	8977.1	5436.6	1.65
UK	448.7	356.3	1.26
US	5119.7	4286.9	1.19

2.4 Indoor thermal comfort

2.4.1 Importance of indoor thermal comfort

Vulnerable groups, such as the very young and very old are sensitive to very high or low indoor temperatures (Ormandy and Ezratty, 2012). Sick building syndrome (SBS) is a phenomenon affecting building occupants who experience health and comfort problems (Sarafis et al., 2010). Common symptoms of SBS include mucous membrane and skin irritation, non-specific hypersensitive reactions, and odour and taste sensations (Wang et al., 2008). Moreover, Chen and Chang, (2012) showed that productivity of occupants in office buildings reduced due to low humidity, low temperature, and high ventilation rate indoors compare to outdoors, and occupants experience SBS symptoms. Thus, it is essential to have comfortable temperatures indoors for residential buildings to prevent SBS.

2.4.2 Thermal comfort approaches

There are two different approaches to assess thermal comfort, the heat-balance approach (Fanger's thermal comfort equation) and the adaptive approach. Fanger's thermal comfort equation is commonly used to describe thermal comfort conditions and includes six evaluation factors: metabolic rate, clothing insulation, air temperature, radiant temperature, air velocity, and relative humidity. It can be assessed by two indices, Predicted Mean Vote (PMV) and Predicted Percent Dissatisfied (PPD). PMV is a thermal scale running from Cold (-3) to Hot (+3), and PPD is measured with a scale from 0% to 100% indicating the percentage of dissatisfied people (ASHRAE, 2010).

Adaptive comfort is based on the idea that outdoor climate will influence indoor comfort as humans can adapt to different temperatures during different times of the year. In general, an adaptive thermal comfort model can be established in different climates for the respective comfortable indoor and outdoor temperature, as shown in equation 2-1 (ASHRAE, 2010).

$$T_n = a + bT_{out} \quad (2-1)$$

where T_{out} is the mean outdoor temperature, and T_n is neutral temperature

2.4.3 Factors affecting indoor thermal comfort

A study using surveys found that the thermal neutral temperature, where residents feel comfortable, was 27.6°C in summer and 17.5°C in winter (Li et al., 2011). As the suggested cooling set-point temperature of 26°C in Chinese design standard (MOHURD, 2010a) is lower than the thermal neutral temperature of 27.6°C, the percentage of people dissatisfied will be higher, and energy will be unnecessarily used for such recommended cooling set-point.

Relative humidity in Chongqing ranges between 70 to 90% throughout the year, but the comfort conditions for humans regarding relative humidity lies between 25 to 60% (Li et al., 2011). In hot environments, the vaporisation on the surface of human skin is slower when humidity is high, hence it hinders the rate of heat reduction, which makes the person feels hotter. In a cold environment, the

vaporisation on the surface of human skin can create a feeling of cold and wet, which makes the person feel colder (Zhang et al., 2015). Moreover, Jing et al., (2012) performed an experiment in an environmental chamber in Chongqing predicted that approximately 80% of the occupants were uncomfortable in indoor temperatures exceeding 30°C and relative humidity of 80%, but the acceptance increased when relative humidity decreased to 60% (Figure 2-14).

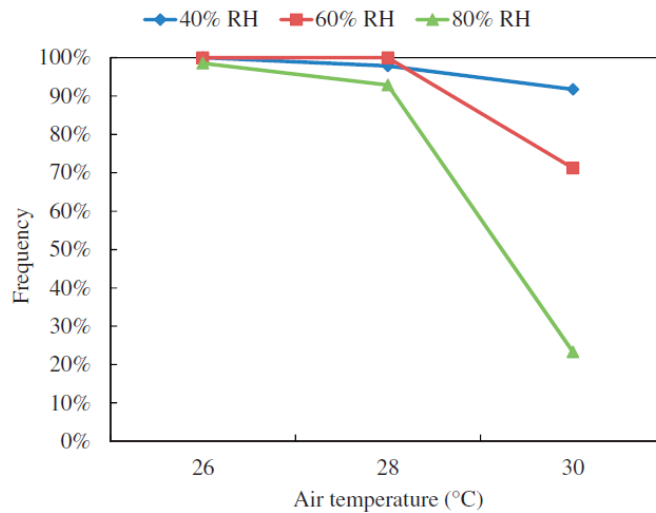


Figure 2-14: Acceptability of thermal environment among all conditions (Jing et al., 2012).

Wind speed is also an essential factor affecting indoor thermal comfort. It has been found that occupants feel thermal discomfort when air velocity is above 1.2 m/s, and the peak of thermal comfort is around 0.41 m/s in naturally ventilated buildings (Figure 2-15; Kang et al., 2013).

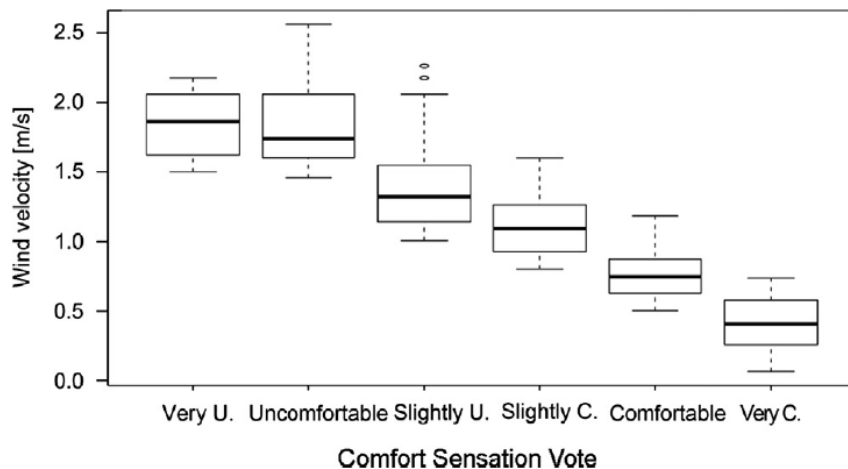


Figure 2-15: Box-plot of wind velocity versus comfort sensation vote (Kang et al., 2013).

A thermal comfort study was carried out in residential buildings in Guangzhou, with a monthly mean of 28.4°C and 82% relative humidity in July, similar to the HSCW zone (25-30°C). The study suggested design criteria with an acceptable range of 80% occupant satisfaction in the thermal environment, as shown in Table 2-7 (Zhang, 2015).

Table 2-7: Criteria of built thermal environment in the HSWW zone (Zhang, 2015).

Actions	Acceptable range of indoor air temperature	Requirements
Open windows and doors	18.0-28.5°C	Indoor airspeed reaches 0.3m/s
Use electric fans	≥29.5°C	Indoor airspeed reaches 0.9m/s
Use split air conditioners	Operate when ≥29.5°C	Air conditioners setting conditions, DB: 24-28°C and RH: 50-70%
Improve indoor humidity and radiation conditions	Upper limit for indoor air temperature to be acceptable or turn on air conditioners can be further raised by 1°C	

Garment insulation value (I_{clo}) is commonly used to quantify the amount of clothing a person wears, where the I_{clo} ranges from 0.5-1.5 throughout the winter and summer (ASHRAE, 2010). In particular, occupants in Chongqing wear more clothes when it is cold, with the distinct difference of very high insulation value (e.g. wear a jacket indoors) in winter for some occupants ($I_{clo} = 1.5$); whereas in summer they wear light clothes ($I_{clo} = 0.5$) such as T-shirts (Figure 2-16; Yoshino et al., 2006).

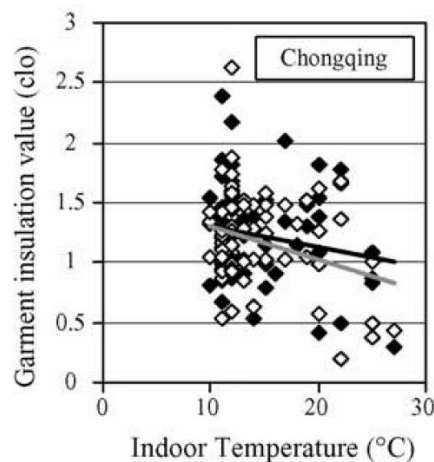


Figure 2-16: Correlation between garment insulation and indoor temperature in Chongqing, where shaded diamonds correspond to male samples and unshaded diamonds correspond to female occupants (Yoshino et al., 2006).

2.4.4 Adaptive thermal comfort models

Recommendations of an acceptable indoor air temperature range are provided by British Standard for naturally ventilated residential buildings (Table 2-8; EN 15251, 2007), and an operative temperature range is recommended by ASHRAE standard for naturally ventilated buildings (Figure 2-17; ASHRAE, 2010). These are international standards which are commonly used in the literature to assess thermal comfort performance (Porritt et al., 2012; Silva et al., 2016).

Table 2-8: Temperature ranges for three categories of indoor environment (CEN, 2007).

Type of building or space	Category	Temperature range for heating (°C) Clothing ~ 1clo	Temperature range for cooling (°C) Clothing ~ 0.5clo
Residential buildings, living spaces (e.g. bedroom and living rooms)	I	21.0-25.0	23.5-25.5
	II	20.0-25.0	23.0-26.0
	III	18.0-25.0	22.0-27.0
Residential buildings, other spaces (e.g. kitchens and storages)	I	18.0-25.0	/
	II	16.0-25.0	/
	III	14.0-25.0	/

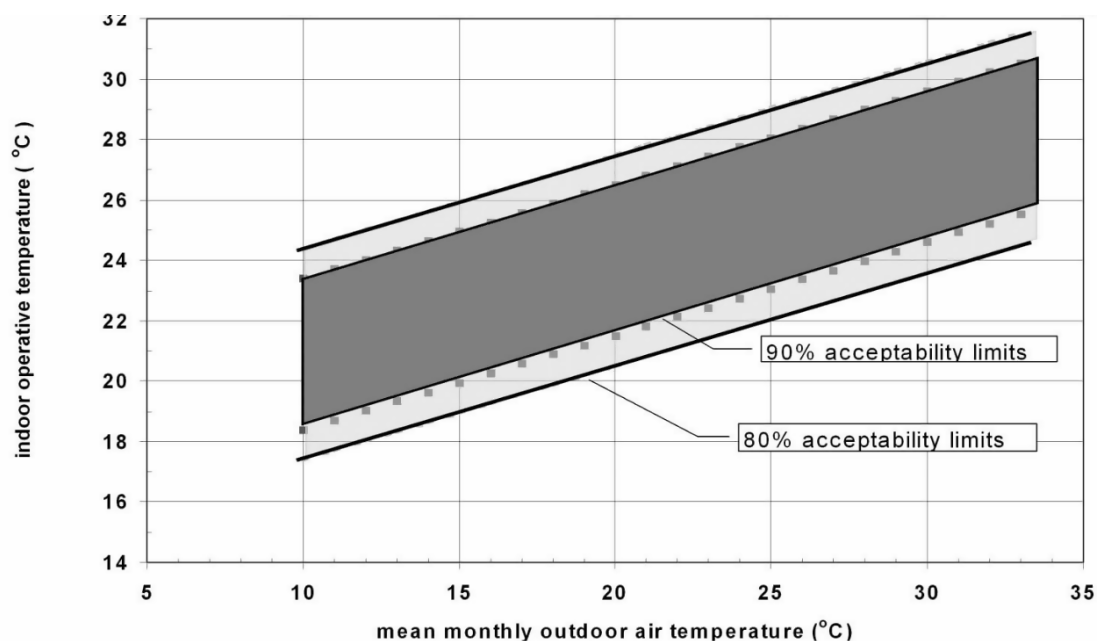


Figure 2-17: Acceptable operative temperature ranges for naturally conditioned spaces (ASHRAE, 2010).

A correlational analysis of neutral temperature and mean outdoor temperature found a correlation of $T_c = 13.5 + 0.54T_o$ for naturally ventilated buildings, where T_o is the monthly mean of outdoor air temperature and T_c is comfort temperature, and the relationship was linear. However, the correlation for

heated or cooled buildings was less linear, which suggested that the indoor temperature was more directly governed by the custom of the occupants for heated and cooled buildings (Figure 2-18; Nicol and Humphreys, 2002).

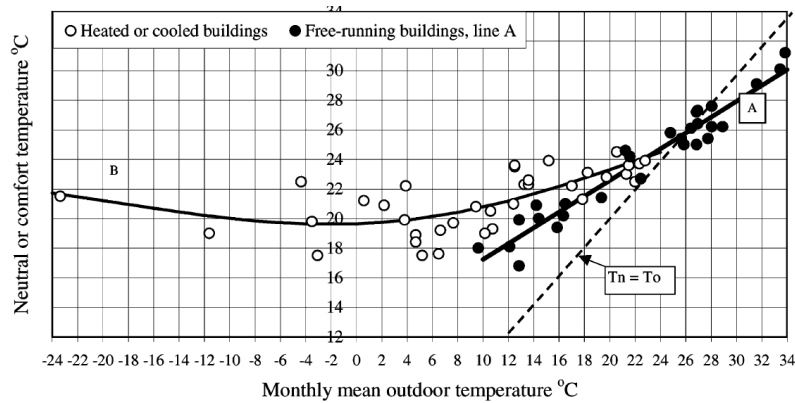


Figure 2-18: Change in comfort temperature with monthly mean outdoor temperature (Nicol and Humphreys, 2002).

Several studies have developed adaptive thermal comfort models in the context of the HSCW zone. As an example, Liu et al., (2017) plotted a regression equation for each of the four seasons to correlate neutral temperature and running mean air temperature, using survey data collected throughout the year (Figure 2-19). The correlation for the whole year was found to be $T_n = 0.709T_{out} + 8.25$ ($R^2 = 0.87$). Additionally, Li et al., (2011) plotted a linear regression equation for outdoor temperature against neutral temperature (Figure 2-20), and the relation was found to be $T_n = 0.294T_{out} + 14.989$ ($R = 0.7426$).

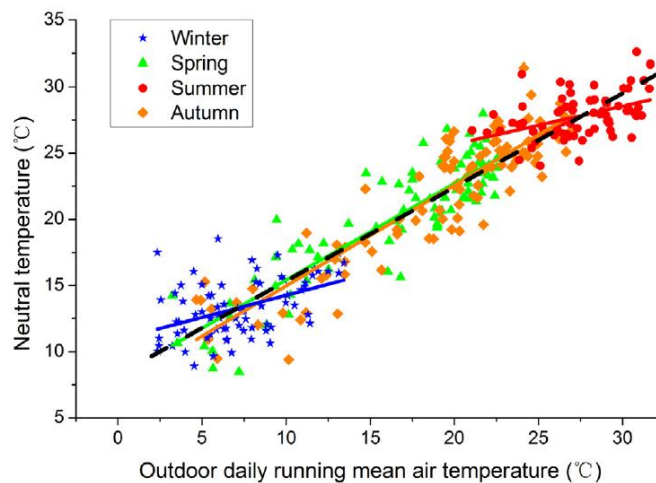


Figure 2-19: Daily neutral temperature with outdoor daily running mean air temperature (Liu et al., 2017).

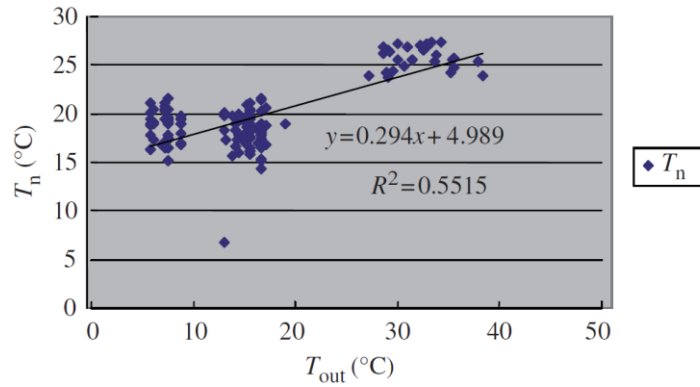


Figure 2-20: Linear regression of mean outdoor temperature and thermo-neutral temperature (Li et al., 2011).

Field studies have shown that the predicted PMV is greater than the actual PMV in the summer and less than the actual PMV in the winter (Yao et al., 2009). Thus, equation 2-2 was developed to calculate the aPMV, derived from PMV.

$$aPMV = \frac{PMV}{1 + \lambda PMV} \quad (2-2)$$

Where λ is the adaptive coefficient, which has a positive value when in warm conditions and a negative value when in cold conditions.

The value of the adaptive coefficient can be found based on field studies by taking into account the local climate, culture, and social background. A field study was conducted in Chongqing to derive the adaptive coefficient in the HSCW zone. Results found that $\lambda = 0.21$ when $PMV \geq 0$ and $\lambda = -0.49$ when $PMV < 0$ can be used for the aPMV calculation in the HSCW zone (Li et al., 2014).

The thermal comfort condition can be categorised in three ways, with the aPMV value calculated using equation 2-2 (Table 2-9). Then, a graph was plotted with indoor operative temperature against operative temperature for the three categories (category I: 90% satisfactory and category II: 75% satisfactory), with the respective linear regression equations developed (Figure 2-21; Li et al., 2014).

Table 2-9: Assessment category for indoor thermal environments in free-running buildings (Li et al., 2014).

Category	Represents	Assessment index
I	90% satisfactory	$-0.5 \leq \text{aPMV} \leq 0.5$
II	75% satisfactory	$-1 \leq \text{aPMV} < -0.5$ or $0.5 < \text{aPMV} \leq 1$
III	Unacceptable	$\text{aPMV} < -1$ or $\text{aPMV} > 1$

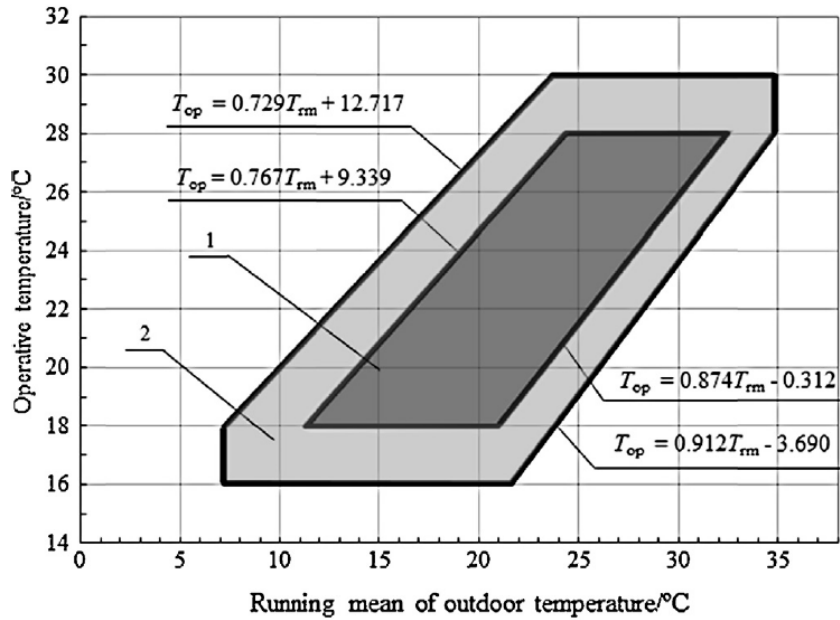


Figure 2-21: Range of the indoor operative temperature of the thermal environment in free-running buildings in the hot summer and cold winter zone, 1 – the category I; 2 – the category II (Li et al., 2014).

2.5 Methodological review of performance evaluation tools for energy saving retrofits

2.5.1 Steady-state energy performance evaluation tools

Building energy models predict the energy demand by calculating the heat flow rates within a building, for a set calculation period (annual, monthly, or hourly). The heating load is the heat required to compensate for the difference between total heat transmission and total heat gain; the cooling load is the heat required to be removed from the difference between total heat gain and total heat transmission (Figure 2-22). Simplified steady-state models can be developed by setting the calculation period to monthly; examples are heating and cooling degree days method, and quasi-steady-state model.

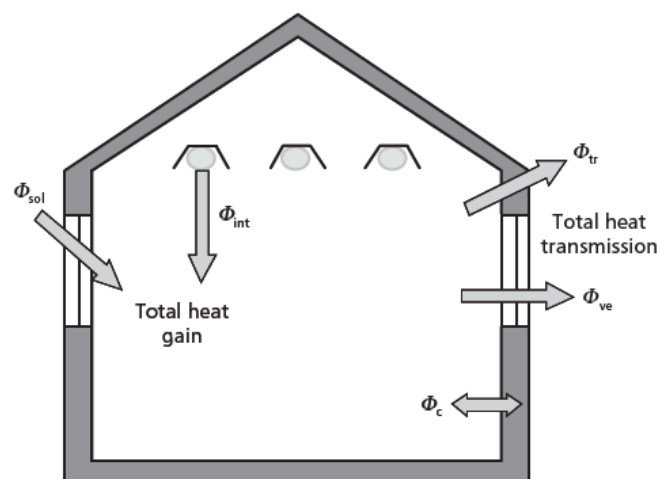


Figure 2-22: Heat flow rates within a building (CIBSE, 2015).

Quasi-steady-state methods involve calculating the heat balance for one month and taking dynamic effects into account by an empirically determined gain and loss utilisation factor. ISO 13790 provided a fully prescribed monthly quasi-steady-state calculation method which is commonly used in the literature (Bruno et al., 2016; Corrado and Mechri, 2009; Jokisalo and Kurnitski, 2007; Kokogiannakis et al., 2008).

The steady-state model can be an effective way to predict the energy demand of a building. It has short simulation time, is easy to use, and takes dynamic parameters into concern to increase prediction accuracy (Kokogiannakis et al.,

2008). However, it has a limited ability to predict hourly outputs (energy demand) and other essential building performance indicators such as temperature.

Surprisingly, to date no existing studies have used a steady-state model to predict monthly and annual energy demand in the context of the HSCW zone. This may be due to Chinese design standard recommending a dynamic thermal modelling tool (DOE-2) to predict energy demand in a flat. In addition, the steady-state model prescribed by ISO 13790 standard was aimed at European countries, which have different climatic conditions compared to the HSCW zone. The simple implementation of the steady-state model is beneficial for building engineers, house owners, and house buyers, as they can use this tool to predict building energy demand. Consequently, methods to apply the steady-state model prescribed by ISO 13790 in the context of the HSCW zone are discussed in this thesis. Nevertheless, dynamic thermal simulation is the primary method used in this thesis because the prediction of hourly outputs is crucial to assess thermal comfort performance.

2.5.2 Dynamic thermal simulation

Building energy programs based on dynamic methods are increasingly popular nowadays, as they allow visualisation of the building's energy consumption. Over the past 50 years, hundreds of building energy programs have been developed (Crawley et al., 2006). The reason is that whole building energy simulation is a useful way to predict key building performance indicators such as energy consumption, energy demand, temperature, humidity, and cost, after the impact of external inputs (i.e., weather, occupancy, construction parameters, heating, and cooling characteristics). Simulations can be performed through detailed heat balance calculations at discrete intervals based on physical parameters of the building and mechanical systems, as well as dynamic external inputs.

DOE-2 is a building energy analysis program which aims to perform whole-building energy simulation with actual weather conditions to predict hourly energy use and energy cost of a building. It has been used for more than 25

years to analyse retrofit options, building design, and test building energy standards around the world (Crawley et al., 2005; Curtis et al., 1984).

eQUEST is an easy to use building energy analysis tool, which provides high-quality results by combining an energy efficiency measure (EEM) wizard, a building creation wizard, and a graphical result display module with an enhanced DOE-2 derived dynamic thermal simulation program (Crawley et al., 2005).

DesignBuilder is a dynamic thermal simulation program based on EnergyPlus with better visualisation function, with a CAD interface, templates, and wizards. Examples of typical uses for DesignBuilder are to evaluate design options on building energy consumption, HVAC equipment sizes, and daylighting analysis (DesignBuilder, 2019).

DeST (Designer's Simulation Toolkits) allows detailed analysis of building thermal process and HVAC system performance. It was developed by Tsinghua University in China in the early 1980s and has been widely used in China. It has different modules to evaluate weather data, natural ventilation, additional window overhang, lighting, and CAD interface (Yan et al., 2008).

EnergyPlus is a modular, structured code based on the most popular features and capabilities of BLAST and DOE-2. It is a simulation engine with input and output of text files. Loads calculated by a heat balance engine at a 15 minute default interval are passed to the building systems simulation module to carry out dynamic thermal simulation (Crawley et al., 2005).

Other dynamic thermal simulation programs includes WUFI Plus, developed by the Fraunhofer Institute for Building Physics in Germany. It is a holistic building energy calculation program, which allows transient assessment of the interaction between building equipment, building utility, building envelope, and exterior climate (Lengsfeld and Holm, 2007). THERB is a dynamic thermal simulation program which is the official software approved by the Japanese government and applied widely in Japan. It can estimate indoor temperature, humidity, and heating/cooling loads for the whole building (Ozaki and Tsujimaru, 2005).

In the context of the HSCW zone, previous research has used various dynamic thermal simulation tools to predict energy consumption for residential buildings in the HSCW zone, with most common tools being: DOE-2; eQUEST; DesignBuilder; DeST; and EnergyPlus. An outline of previous studies, focusing on modelling residential buildings in the HSCW zone, revealed that DeST and EnergyPlus is the most popular dynamic thermal simulation software, followed by eQUEST, DOE-2 and the least popular being DesignBuilder (Table 2-10).

Table 2-10: Summary of dynamic thermal simulation used as found previous studies.

DesignBuilder	EnergyPlus	DOE-2	eQUEST	DeST	Others	Reference
		✓				(Ouyang et al., 2009)
		✓				(Ouyang et al., 2011)
			✓			(Yu et al., 2008)
		✓				(Xiaotong Wang et al., 2015)
			✓			(L. Xu et al., 2013)
	✓					(Yao et al., 2018)
	✓					(X. Li et al., 2018)
			✓			(Yu et al., 2013)
					WUFI Plus	(Zhao et al., 2015)
			✓			(Yu et al., 2011)
					THERB	(Gong et al., 2012)
				✓		(Pan et al., 2018)
				✓		(Yang et al., 2015)
✓						(Xi Wang et al., 2015)
✓						(Gao et al., 2014)
		✓				(Yao and Xu, 2010)
			✓			(Ichinose et al., 2017)
✓						(Fu et al., 2017)
	✓					(Xiong et al., 2018)
	✓					(Short et al., 2018)
	✓					(Chen and Yang, 2018)
				✓		(Feng et al., 2016)
				✓		(Hu et al., 2016)
				✓		(Peng et al., 2012)
				✓		(Ma et al., 2015)
	✓					(W. Yu et al., 2015)
				✓		(Yao, 2012)
	✓					(Gou et al., 2018)

2.5.3 Model calibration techniques in building energy modelling

Various input parameters (e.g. building, climatic, and computational parameters) are required in building simulation models to accurately predict desired outputs (e.g. energy demand and indoor temperature). Yet, the accuracy of the building energy model depends on the accuracy of the input parameters. Limitation of building energy modelling tools leads to a potentially massive difference between simulated and measured building energy performance. For instance, energy consumption for 121 commercial Leadership in Energy and Environmental Design (LEED) buildings in the US was recorded. These buildings achieve a good LEED rating with regard to the predicted performance of the building. In reality, some buildings with a good LEED rating consume more energy than the code baseline (Figure 2-23). To solve the problem, calibration which aims to understand the actual performance of the building can be performed to achieve more accurate and reliable results.

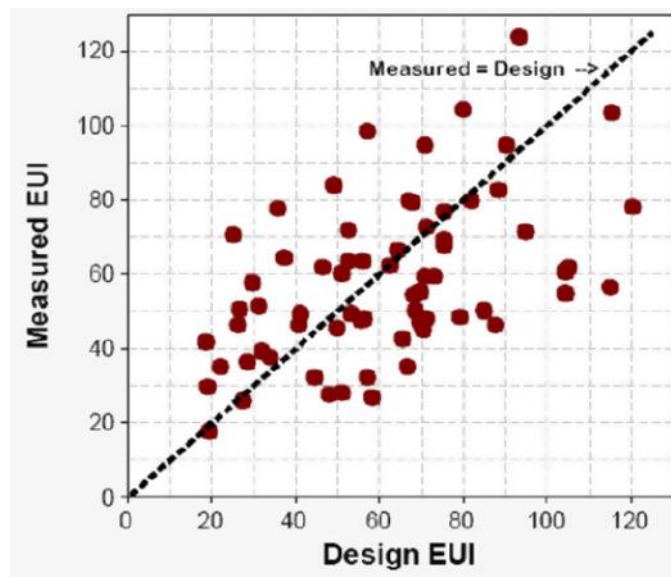


Figure 2-23: Measured versus predicted energy consumption for 121 commercial buildings in the US (Turner and Frankel, 2008).

Statistical indices of Mean Bias Error (MBE), listed in equation 2-3, is an indicator of the overall bias in the model. It captures the mean difference between measured and predicted hourly indoor air temperatures. Nonetheless, MBE suffers from a cancellation effect, where over-estimations are cancelled out by under-estimations when summed. As a consequence, the Coefficient of

Variation of Root Mean Square Error $Cv(RMSE)$, calculated by equation 2-4, is used to address the cancellation effect. $CvRMSE$ is an indicator which determines how well a model fits the data by capturing offsetting error between measured and simulated data (Coakley et al., 2014). ASHRAE Guideline 14, International Performance Measurement and Verification Protocol (IPMVP) and Federal Energy Management Program (FEMP) in the US provided guidance of the acceptance criteria for calibration of building energy models (Table 2-11).

$$MBE(\%) = \frac{\sum_{i=1}^{N_p} (m_i - s_i)}{\sum_{i=1}^{N_p} (m_i)} \quad (2-3)$$

$$CvRMSE(\%) = \frac{\sqrt{\left(\sum_{i=1}^{N_p} (m_i - s_i)^2 / N_p\right)}}{\bar{m}} \quad (2-4)$$

where m_i and s_i are the respective measured and simulated data points for each model instance 'i' and N_p is the number of data points at interval 'p' (i.e., $N_{monthly}=12$, $N_{hourly}=8760$) and \bar{m} is the average of the measured data points.

Table 2-11: Acceptance criteria used for calibration of building energy models.

Standard/guideline	Monthly criteria (%)		Hourly criteria (%)	
	MBE	CVRMSE	MBE	CVRMSE
ASHRAE Guideline 14	5	15	10	30
IPMVP	20	-	5	20
FEMP	5	15	10	30

The methodology for calibration depends on the availability of building input data, and it can be divided into five levels (Table 2-12) as follows:

- Utility bills: To provide an electric utility with a breakdown of baseline, cooling, and heating energy use, this is achieved by gathering monthly utility bills for an entire year from households.
- As-built data: Understand the layout and zoning of a building by collecting floor plan drawings.
- Site visit or inspection: Visit the existing building to define occupant parameters in the building, namely lighting power densities, equipment quantities and number of occupants.

- Short-term monitoring: Measure critical end-uses data for a short period of time (e.g. measure the AC operating hours in winter for a representative day).
- Long-term monitoring: Measure hourly data (e.g. indoor air temperature and energy consumption) for a week, a month, a season, or even a year in the building.

Table 2-12: Calibration levels based on the building information available (adapted from Reddy, 2006).

Calibration levels	Building input data available				
	Utility bills	As-built data	Site visit or inspection	Short-term monitoring	Long-term monitoring
Level 1	✓	×	×	×	×
Level 2	✓	✓	×	×	×
Level 3	✓	✓	✓	×	×
Level 4	✓	✓	✓	✓	×
Level 5	✓	✓	✓	✓	✓

Sensitivity analysis prior to calibration can be used to identify critical parameters for detail investigation (Coakley et al., 2014). This is performed by varying an input parameter, then the corresponding change in the output parameter is a direct measure of the effect of the change made by that single input parameter (Lomas and Eppel, 1992).

Calibration of dynamic thermal models is commonly performed in the building energy research community (Beizaee, 2016; Bou-saada and Haberl, 1995; Coakley, 2014; Georgiou et al., 2013; Marini et al., 2014; Mustafaraj et al., 2014; P. Xu et al., 2013; Yoon et al., 2003). For example, an office building was calibrated by introducing twelve iterations, each with a specific change to input parameters to make the energy model match measured data. These changes involved adjusting the value of some input parameter, adding extra functions to the energy model, changing the schedules (e.g. occupancy, heating, and cooling), and changing the set-point temperatures (Bou-saada and Haberl, 1995), in order to achieve the desired MBE and CvRMSE value. Another study collected on-site as-built data, BEMS record, and monitoring data for one week. The model was calibrated using evidence-based model development. It was then extrapolated to the whole year to compare the measured (monthly utility bills) and simulated building energy consumption.

Results confirmed that the extrapolated data was accurate (Mustafaraj et al., 2014).

Nevertheless, there is a lack of calibration of dynamic thermal models in the context of the HSCW zone. Many researchers performed detailed measurements of building input data, which will be discussed in Section 2.6.4, but only a few studies linked measured data with building energy models. Short et al., (2018) measured indoor air temperature for one week in January and one week in August, and also compared with the dynamic thermal model developed in EnergyPlus. The study showed that the model predicts indoor air temperature with reasonable accuracy; however, the authors did not evaluate which input parameters had the potential to improve the indoor air temperature predictions and subsequently adjust the base case model to generate a refined model. This would have resulted in a better match between the simulated and measured indoor air temperature, leading to more reliable predictions of energy saving retrofits.

2.5.4 Location of flat in an apartment building

The location of the flat in an apartment building affects the predicted energy consumption in a dynamic thermal model, as many key factors depend on the location of flat in an apartment building, including the flat orientation, and whether the external wall, roof, or both are exposed to the outdoor environment.

In the context of the HSCW zone, few researchers add the factor of flat location within an apartment building to the predicted energy consumption. Specifically, Yao (2012) compared the predicted energy demand of a middle floor flat in the centre, with two middle floor flats on the corner (one external wall with free access to the external environment), in a newly built residential building in Hangzhou, and found a 15% prediction difference of energy reduction. Meanwhile, Short et al. (2018) compared the predicted energy demand of eight middle floor flats, facing different orientations, in a residential building located in the HSCW zone which requires retrofit, and found a 30% prediction difference of energy reduction for north and south facing flats. Additionally, Yu et al. (2008) compared the predicted energy demand of individual thermal zones (with different zone orientation) in a middle floor building, and found a

10% prediction difference of energy reduction. Yet, none of the studies evaluated the effect of top floor flats to building energy demand. In the cold zone in China, Ling et al. (2015) evaluated the effect of flat location (including top and bottom flats) on heating energy consumption in several cities in the cold zone for newly built apartment buildings. The climate in the cold zone (-10 to 0°C) in winter is slightly lower than that in the HSCW zone (0 to 10°C). Results showed that heating energy consumption in a top-floor flat was significantly larger (30%) than a middle-floor flat.

Considering evaluation of thermal comfort conditions in different flat locations, Yao (2012) and Yu et al. (2008) failed to predict the thermal comfort performance due to location of flat in an apartment building, whereas Short et al., (2018) presented the predicted indoor air temperature for a month in January and August, but did not appraise the thermal comfort performance annually.

2.5.5 Optimisation of energy saving retrofits

Optimisation is a technique of maximising or minimising specific objective functions under constraints. The objective functions are formulated to present the decision criteria (Kolokotsa et al., 2009). Decision criteria that are commonly used on retrofit decisions are energy savings, CO₂ reduction, comfort improvement, and retrofit cost. One or more of them could be chosen in order to optimise retrofit strategies. A careful combination of technologies is required in order to avoid the use of multiple measures that produce the same results and therefore have no additional positive impact, yet increase the cost of energy saving retrofits (Hestnes and Kofoed, 2002).

In the context of the HSCW zone, previous researchers have evaluated energy saving retrofits for residential buildings (Xiaotong Wang et al., 2015; Yu et al., 2008; Zhao et al., 2015). For instance, Ouyang et al. (2009) predicted that improving the external wall insulation by 10mm of extruded polystyrene (XPS) and the roof insulation by 40mm of XPS can lead to energy reductions of 6% and 7% respectively for a typical urban residential building in the HSCW zone. Likewise, Yu et al. (2008) predicted an 8% energy reduction when replacing single glazed windows with double glazed windows with low emissivity surface

leads for a typical urban residential building in the HSCW zone. However, these studies did not consider the effect of retrofit on improving thermal comfort. Yao et al. (2018) considered the effect of six passive measures on reducing energy consumption and improving thermal comfort. Results showed a 50% reduction of energy consumption and 2112 comfort hours in a year for the optimum combination of retrofit measures; however this study also had some limitations. To begin with, Yao et al. (2018) considered construction age as one type of passive measure, however properties built in the same time varied in factors such as external wall, windows, air infiltration, and AC efficiency. The effect of changing one of these four parameters was not considered. Besides, the thermal comfort hours were calculated for the whole year, but not the occupied hours. Additionally, the study did not quantify the effect of a reduction in heating and cooling comfort hours due to individual retrofit measures.

2.5.6 Level of detail of building energy models

Level of detail (LoD) of building energy models was developed to study the implications of the level of information on the building energy models and design of buildings. There are various definitions of LoD to discuss the level of information required in a design process (Abualdenien and Borrmann, 2019; Biljecki et al., 2016; Gerrish et al., 2017), in which the levels reflect the shortage of suitable data at one end of the scale and the effort involved in implementing detailed building energy models at the other (Taylor et al., 2013). For example, the level of development (LOD) definitions provided by the American Institute of Architects (AIA) and the Associated General Contractors (AGC) of America, (2019) provided the basis for defining information extent and maturity throughout the design, to which information from building energy modelling is applied (Table 2-13). Another study defined four LoDs: LoD1 to be a box model; LoD2 with roof and wall; LoD3 an architecturally detailed model with windows and doors; and LoD4 including indoor features (Kolbe, 2009). Furthermore, a study summarised the information required for building energy modelling as building location, geometry, usable spaces in the building, building parameters, and occupancy schedules (Gerrish et al., 2017).

Table 2-13: Level of development for BEM parameters during building design (AIA and AGC of America, 2019).

Design stage	Level of Development
Early concept design	LOD100 – elements represented in model symbolically (no geometric information)
Late concept design	LOD200 – elements in model represented graphically as generic system with geometrics indicated
Early detailed design	LOD300 – elements represent specific systems with defined location with parametric information included
Late detailed design	LOD350 – element interfaces with other systems included
Construction	LOD400 – fabrication and operation information stored within/alongside element
In use	LOD500 – all information regarding installed elements is included ready for use by Facilities Manager

Using the LoD can ensure the evaluation of information required to achieve accurate predictions in building energy modelling, and identification of the inputs that can be neglected and still achieve reasonable accuracy. However, there are limited studies which evaluate the effect in energy demand predicted by building energy models with different levels of detail. By doing so, design features that do not improve the accuracy of outputs of building energy models are identified, which can be excluded to achieve reasonably accurate results. For example, one study found that DTM with a lower LoD (equivalent to LOD100 in Table 2-13) impacted on modelling accuracy by a significant degree (20% difference in heating energy demand) for houses in the UK, when compare to DTM with the highest level of detail (equivalent to LOD500 in Table 2-13; Taylor et al., 2013). Another study evaluated the impact of four LoDs based on Kolbe (2009), to evaluate the change in heating demand for apartment buildings in Germany (Monien et al., 2017), the prediction difference was 10% for heating energy consumption. Furthermore, Purdy and Beausoleil-Morrison (2001) found a vast heating load difference (7.5%) for multi-zone and single-zone thermal models for Canadian housing stock. In fact, many studies modelled a residential flat as a single-zone model to evaluate energy saving retrofits in the HSCW zone (Gong et al., 2012; Gou et al., 2018), i.e., the living room, bedroom, and auxiliary area have the same AC operating schedule and internal heat gains. One reason for this is the ratio of living room, bedroom, and auxiliary area was unknown to the building modeller, thus the case study flat was modelled as a single zone. Moreover, Xiong et al., (2019) and Yao et

al., (2018) further simplified the modelling details by modelled an entire middle floor with a single thermal zone model.

However, the studies discussed above did not consider the predicted cooling energy demand for different LoD, because coincidentally cooling was not required in the countries investigated (Monien et al., 2017; Purdy and Beausoleil-Morrison, 2001; Taylor et al., 2013).

2.5.7 City-scale model

To estimate the energy consumption in a city, top-down or bottom-up modelling approaches can be employed (Swan and Ugursal, 2009). The top-down approach uses regression to find the relationship between building stock energy consumption and top-level variables, including macroeconomic indicators, energy price, and climate. Top-down models can provide estimates of what would happen if more buildings of a particular type were to be built or converted into another type. However, such models necessarily extrapolate from the status quo and are hence less suitable when an analysis focuses on a specific neighbourhood (Reinhart and Cerezo Davila, 2016). The bottom-up approach determines the energy consumption of every building within a representative area in order to calculate the stock energy consumption. Therefore, the bottom-up approach can be useful to evaluate the impact of energy saving retrofits in a whole city, or area (Li et al., 2019). Within the bottom-up approach, the statistical approach tries to find the relationship between the building energy consumption and building feature using historical energy consumption dataset. While these quantities can be measured for a small group of existing buildings, such detailed data collection efforts become impractical for larger urban areas. Another approach is the archetype approach, which abstracts a building stock into building archetypes that represent a group of buildings with similar parameters. It has been classified as a white-box based approach utilising a detailed thermal physics simulation (Tardioli et al., 2015). This approach has been extensively used in the context of national or regional city-scale models to understand the aggregated impact of energy conservation measures and determine building energy end-use distribution. This archetype modelling approach has been applied in the UK

(Firth et al., 2010); across multiple European countries (Ballarini et al., 2014); in Italy (Ballarini et al., 2017); in Greece (Dascalaki et al., 2011); in Austria (Nageler et al., 2017); in the USA (Sokol et al., 2017); and in Japan (Shimoda et al., 2004).

The generation of archetypes requires two steps. Firstly, the building stock is segmented; it involves dividing into groups according to building shape, age, use, climate, and systems. Then, the building parameters (including construction parameters, usage patterns, and building systems) are characterised (Reinhart and Cerezo Davila, 2016).

Comparison of the aggregated annual measured versus predicted energy consumption of multiple buildings in a city-scale is vital to increase the reliability of energy saving retrofits. For example, Shimoda et al. (2004) predicted that the total energy consumption of a residential sector in Osaka City, Japan was 32018 TJ/year, 18% smaller than the value reported in the energy handbook for the residential sector in Japan, in which data were sourced from surveys. Dall'o' et al. (2012) predicted the annual energy consumption for heating was 92055 MWh in Carugate, Italy, 10% smaller than data measured by the gas distributor. Heiple and Sailor (2008) predicted the annual energy consumption with geospatial modelling techniques in Houston, United States. Results showed a 10% difference when compared to a survey performed through state county and city government by the Federal Geographic Data Committee.

Considering the context in the HSCW zone, a study performed as part of the LoHCool project identified reoccurring residential building designs in a representative area in Hangzhou (Gui et al., 2018). Gui et al. (2018) characterised residential buildings into "point-type" and "plank-type" buildings. Point-type buildings are less than 30 m in length along the longer side of the building, and the aspect ratio (ratio of the longer side of the building divided by the shorter side of the building) is smaller than two. Plank-type buildings mean either the length of the longer side of the building is smaller than 30 m and the aspect ratio is larger than two, or the length of the longer side of the building is larger than 30m. The study showed that 83% of residential buildings built

before 2001 are plank-type buildings and 17% of them are point-type buildings. Figure 2-24 showed the typical geometrical parameters of point-type and plank-type buildings identified from the study.

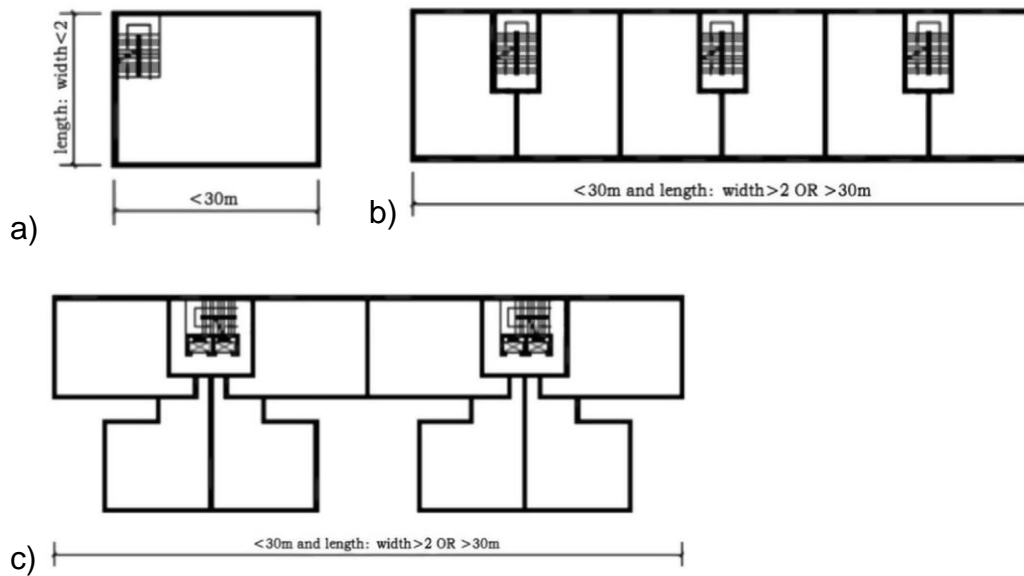


Figure 2-24: Typical residential buildings built before 2001 with a) one stair one household point building, b) one stair two household plank building, c) one stair four household plank building.

Another study performed during the LoHCool project developed archetypes for residential buildings in a representative area in Chongqing (X. Li et al., 2018). Results showed that out of the three archetypes identified, two of them (archetypes 1 and 2) can be identified as plank-type buildings and archetype 3 can be identified as a point-type building from the classification of Gui et al. (2018) (Table 2-14). Interestingly, results showed that point type buildings have a more considerable building height (78m) than plank-type buildings (24m) (Table 2-14). A possible explanation for the numerous point-type buildings in Chongqing is that there are more residential buildings with high building height in Chongqing; this was reflected in Figure 2-7 discussed in Section 2.2.3, where about 30% of residential buildings are over ten-storeys high in Chongqing but only 5% of them in Hangzhou. Therefore, it is more representative to characterise building designs by building height rather than by the building shape.

Table 2-14: Typical residential buildings built before 2001 characterised (X. Li et al., 2018).

Archetype	Aspect ratio	Length of longer side of building	Building height	Percentage in the building stock	Representative building shape
1	1.56	>30m	24m	48%	
2	3.19	>30m	24m	18%	
3	1.16	<30m	78m	34%	

The above studies characterise the typical building shape for residential buildings in the HSCW zone. However, the floor area of individual flats, and also the partitioning of zones (e.g. living room and bedroom) were not considered. Another study published by LoHCool modelled five typical residential flats in the HSCW zone which have different floor areas. However, this study was performed in flat scale, and thus the building shape and height was not considered (Li et al., 2019). Furthermore, the study stated that the selection method was by “referencing actual extant floor plan design drawings collected from across the Chongqing urban residential estate market”, and there was no apparent justification of the function of the usable spaces (living room, bedroom, kitchen, and toilet) within the flat. Hence, a literature review is required to characterise geometrical parameters for residential buildings in the HSCW zone to identify the crucial parameters to model at a city scale.

2.6 Characterisation of the building parameters for urban residential buildings in the HSCW zone

2.6.1 Introduction

A systematic literature review was conducted involving studies on modelling residential buildings in the HSCW zone. A summary table was developed for each building property to summarise values as found in these studies. Building parameters can be sub-divided into geometrical (Section 2.6.2), building fabric (Section 2.6.3), and occupant (Section 2.6.4) parameters.

Geometrical parameter contained: built area of individual flats, number of storeys, number of flats per floor, window to wall ratio, and floor to ceiling height. The explanation is that there are residential buildings with varying built forms throughout the HSCW zone, causing the need for multiple dynamic thermal models, bringing about respective predictions.

Building fabric parameters included: thermophysical parameters of external walls, roofs, internal floors, internal walls and windows, along with air infiltration rate. The reason being that the vast majority of existing residential buildings were built before the enforcement of building regulations in the HSCW zone, in which building fabric parameters of simulation models were reliant on authors' knowledge, resulting in a variety of selected building fabric parameters across existing studies.

Occupant parameters encompass: heating and cooling set-point, heating and cooling air conditioning (AC) operating schedule, heating and cooling coefficient of performance, internal heat gains, and window opening rate. Delivering a review of survey studies covers a large sample of household residents in the HSCW zone, thereby serving as quantification of the relevant occupant parameters; hence making the model predictions more robust. To enhance the validity of model predictions, the comparison of the predicted energy consumption with energy meter readings from existing households is vital. By reviewing studies which collect energy meter reading from household residents, the information from a variety of data sources is evaluated and thus provides a potent tool to study the results.

2.6.2 Geometrical parameters

2.6.2.1 Floor area

From Chinese national statistics, the average living area for one flat is 79m² for Chongqing and 78.6m² for Zhejiang (NBS, 2017). However, the floor area of flats modelled using DTM in the literature varied from 50 to 132m² (Table 2-15). For example, one study modelled a one-bedroom flat with a floor area of 50m² (Short et al., 2018), another study with a floor area of 132 m² per flat (a flat with three bedrooms, two reception rooms, one kitchen, and two toilets; Ichinose et al., 2017). Another study conducting a city-scale prediction of energy demand for residential buildings used the following categories of floor areas: <50m²; 50-90m²; 90-130m²; 130-170m²; 170-210m²; 210-250m²; >250m² (Hu et al., 2016). Further, a study performed 300 surveys in Hangzhou and found the mean floor area was 105m² with a standard deviation of 45m². The study also showed that the measured heating and cooling energy consumption is significantly correlated with floor area ($p < .01$) (Chen et al., 2013). Therefore, it is important to consider flats with different floor areas in a city-scale model.

Table 2-15: Assumption of floor area as found in previous studies.

Floor area (m ²)	Reference
50	(Short et al., 2018)
52.7	(Ouyang et al., 2011)
76.5	(Yao et al., 2018)
80	(Ma et al., 2015; Pan et al., 2018; Yu et al., 2013)
85	(Yao, 2012)
86	(Yang et al., 2015)
88.5	(Xiaotong Wang et al., 2015)
88.75	(Ouyang et al., 2009)
90	(Gou et al., 2018; W. Yu et al., 2015)
95.4	(Xiong et al., 2018)
96	(Gao et al., 2014)
99.3	(Yu et al., 2008)
100	(Yao and Xu, 2010; Zhao et al., 2015)
109	(Feng et al., 2016)
123.8	(L. Xu et al., 2013)
130	(Fu et al., 2017)
132	(Ichinose et al., 2017)

2.6.2.2 Floor to ceiling height

Floor to ceiling height varied between 2.7 to 3 m in the cases studied in the literature (Table 2-16), with a large percentage of flats having the floor to ceiling height of 3 m, without providing justification in most studies, with Short et al., (2018) selecting floor to ceiling height value of 2.7 m based on floor plan. A study showed that increasing floor to ceiling height from 3.3 to 3.7 m lead to a 10% increase in heating energy consumption in office buildings in the UK (Duran, 2018), due to the increase of the external wall surface and volume to be heated. This shows the importance of identifying the floor to ceiling height accurately from the floor plan.

Table 2-16: Assumption of floor to ceiling height as found in previous studies.

Floor to ceiling height (m)	Reference	No. of cases
2.7	(Chen and Yang, 2018; Short et al., 2018)	2
2.8	(Ma et al., 2015; Yao, 2012; Yao and Xu, 2010; W. Yu et al., 2015)	4
3	(Fu et al., 2017; Gao et al., 2014; Gong et al., 2012; Gou et al., 2018; Ichinose et al., 2017; Xi Wang et al., 2015; Xiong et al., 2018; Yang et al., 2015; Yu et al., 2013, 2008; Zhao et al., 2015)	11

2.6.2.3 Number of storeys

Number of storeys vary from 3 to 23 (Table 2-17), 80% of buildings examined were lower than ten storeys, with the exception of one high rise residential building being 23 storeys (Short et al., 2018). This fact is reflected in Section 2.2.3, where residential buildings having four to nine storeys account for 50% of the residential building stock in Chongqing and Zhejiang. Although these studies presented in Table 2-17 provide the number of storeys of the case study building investigated, it is common for studies to model the flat located on the middle floor to provide more generalisable results. However, studies have shown that flats located on the top floor in residential buildings have higher energy consumption than flats on lower floors (Ling et al., 2015). This shows the importance of modelling both the flat located on the middle floor and the top floor, to predict reliable results for the whole building.

Table 2-17: Assumption of the number of storeys as found in previous studies.

No. of storeys (-)	Reference
1 to 3	(Feng et al., 2016; Fu et al., 2017; Gou et al., 2018; W. Yu et al., 2015)
4 to 6	(Ma et al., 2015; Ouyang et al., 2011; Pan et al., 2018; Xi Wang et al., 2015; Xiaotong Wang et al., 2015; Yang et al., 2015; Yao and Xu, 2010; Yu et al., 2008)
7 to 9	(Ichinose et al., 2017; Ouyang et al., 2009; Xiong et al., 2018; Yao et al., 2018)
>10	(Short et al., 2018; L. Xu et al., 2013; Yao, 2012; Yu et al., 2013)

2.6.2.4 Number of flats per floor

The number of flats evaluated per floor varies from two to eight in the literature (Table 2-18). The most common combination is four flats on one floor; the rationale of having four flats per floor is validated by actual floor plans from existing buildings used in the studies. The largest number of flats is eight flats per floor (Short et al., 2018). It is essential to determine the number of flats per floor when evaluating building energy performance, as the flat location (e.g. centre or corner flat located on middle floor) in buildings affects the resulted energy consumption (Ling et al., 2015; Short et al., 2018; Yao, 2012).

Table 2-18: Distribution of the number of flats per floor as found previous studies.

Number of flats on one floor (-)	Reference	Number of cases
2	(Feng et al., 2016; Fu et al., 2017; Ma et al., 2015; W. Yu et al., 2015)	4
4	(Gao et al., 2014; Gou et al., 2018; Meng et al., 2019; Ouyang et al., 2009; Pan et al., 2018; Xiaotong Wang et al., 2015; Xiong et al., 2018; Yang et al., 2015; Yao et al., 2018; Yu et al., 2008, 2013)	11
6	(Ichinose et al., 2017; Ouyang et al., 2011; Yao, 2012; Yao and Xu, 2010)	5
8 or more	(Short et al., 2019, 2018)	3

2.6.2.5 Window to wall ratio

During the LoHCool project, X. Li et al. (2018) performed surveys and collected window to wall ratio (WWR) for residential buildings in the representative area in Yuzhong district. Out of 321 pre-retrofit residential buildings, 18% of them had a WWR of 0.2, 66% of them had a WWR of 0.3 and 16% of them had a

WWR of 0.4. Moreover, Yao (2012) performed a survey for 78 new built residential buildings with various heights, with the results shown in Table 2-19.

Table 2-19: Window to wall ratio from the survey (adapted from Yao 2012).

Building storey	No. of samples	WWR south	WWR north	WWR east	WWR west
6-8	53	0.37	0.27	0.13	0.14
9-20	17	0.4	0.25	0.17	0.16
>20	8	0.44	0.35	0.23	0.22

The Chinese design standard defines a WWR of 0.4 for north-facing, 0.35 for south and west-facing and 0.45 for east-facing windows (MOUHRD, 2010). During the LoHCool project Chen et al. (2017) performed a survey for 253 pre-retrofit residential buildings in Hangzhou. Less than 10% of these buildings exceed the WWR limit according to Chinese design standard issued in 2010.

Many studies have investigated the effect of WWR on building energy consumption. For WWRs varying from 0.2 to 0.5 with intervals of 0.05, results showed a WWR of 0.5 consumed 8% more cooling energy consumption and 2% more heating energy consumption for north-oriented windows compare to WWR of 0.2, where south-oriented windows consumed 10% more cooling energy consumption and 2% less heating energy consumption (Yu et al., 2008). Another study varied WWR from 0.1 to 0.9 with intervals of 0.1 for new built residential buildings. In this case, a WWR of 0.5 consumed 50% more cooling energy consumption for north and south oriented windows, with 10% less heating energy consumption for south-oriented windows and 5% more heating energy consumption for north-oriented windows (Yang et al., 2015). Gong et al. (2012) found that with varied WWRs of 0.15, 0.3, 0.45, and 0.6, total energy consumption was within 10% for newly built residential buildings. The difference may be because different case study buildings and inputs were used.

WWR varied significantly throughout buildings examined in the literature (Table 2-20). As an example, Xi Wang et al., (2015) assumed an equal WWR of 30% in all orientations, whereas other studies assumed 30% WWR for south, east, and west orientation, and 20% WWR for north orientation (Xiong et al., 2018; Yao et al., 2018). From Section 2.6.1, 80% of the pre-retrofit buildings are plank-type. A number of studies suggested a north-south orientated built

form was often practised for plank-type buildings, these are derived from actual floor plans so these assumptions reflect reality (Ma et al., 2015; Ouyang et al., 2009; L. Xu et al., 2013; Yao, 2012; Yu et al., 2015; Zhao et al., 2015). Considering the WWR of the building as a whole, these studies suggested a large south oriented window (WWR from 0.35 to 0.5), slightly smaller north-oriented window (WWR from 0.18 to 0.27) and smallest east/west oriented window (WWR from 0.04 to 0.15). Identifying the WWR accurately is vital because Gou et al. (2018) showed that WWR in all directions (north, south, east, and west) are the second to fifth most influential parameters for energy demand among 37 design parameters for a residential building in Shanghai. In particular, north and south WWRs are more sensitive than east and west WWR to energy demand (Gou et al., 2018).

This showed that there is a considerable variation in the WWR assumed in the literature. This section concludes that the typical WWR of residential buildings is large (0.2 to 0.4) for south/north orientation, and small (0.04 to 0.15) for east/west orientation in building scale.

Table 2-20: Assumption of window to wall ratio in residential buildings in literature.

WWR south	WWR north	WWR east	WWR west	Reference
0.15	0.15	0.15	0.15	(Gong et al., 2012)
0.25	0.25	0.25	0.25	(Yu et al., 2013)
0.3	0.2	0.3	0.3	(Yao et al., 2018)
0.3	0.2	0.3	0.3	(Xiong et al., 2018)
0.3	0.27	0.22	0.22	(Gao et al., 2014)
0.3	0.3	0.3	0.3	(Yu et al., 2008)
0.3	0.3	0.3	0.3	(Ichinose et al., 2017)
0.3	0.3	0.3	0.3	(Xi Wang et al., 2015)
0.35	0.23	0.12	0.12	(Ouyang et al., 2009)
0.35	0.26	0.35	0.35	(Yao and Xu, 2010)
0.38	0.27	0.15	0.15	(Yao, 2012)
0.4	0.4	0.4	0.4	(Chen and Yang, 2018)
0.4	0.3	0.15	0.15	(Ma et al., 2015)
0.4	0.18	0.03	0.03	(Zhao et al., 2015)
0.45	0.4	0.3	0.3	(L. Xu et al., 2013)
0.5	0.45	0.3	0.3	(Yang et al., 2015)
0.5	0.2	0.04	0.04	(W. Yu et al., 2015)
0.5	0.35	0.25	0.25	(Gou et al., 2018)

2.6.3 Building fabric parameters

2.6.3.1 Thermo-physical parameters of materials

When modelling residential buildings, Ichinose et al. (2017), Ouyang et al. (2009b), and Yu et al. (2008) did not specify clearly the thermo-physical parameters (i.e., conductivity, specific heat, and density) of the materials used for external walls, internal walls, floors, and roofs. CIBSE Guide A and a Chinese design standard issued in 2010 (MOHURD, 2010b) provide thermo-physical parameters of commonly used construction materials, which can be used as a reference to model residential buildings (Table 2-21). The conductivity, density, and specific heat of materials affect the U-value and internal heat capacity of the investigated building fabric. U-value (W/m^2K) is calculated by dividing the conductivity by thickness of the investigated building fabric. Internal heat capacity (J/m^2K) is calculated by dividing the specific heat by density, then multiplying the thickness of the investigated building fabric.

Table 2-21: Typical thermo-physical parameters of commonly use construction materials in residential buildings.

Component	Conductivity (W/mK)		Density (kg/m ³)		Specific heat (J/kgK)	
	CIBSE	Chinese standard	CIBSE	Chinese standard	CIBSE	Chinese standard
Cement	0.72	/ *	1860	/	840	/
Cement mortar	0.93	0.93	1900	1800	840	1050
Lime plaster	0.8	/	1600	/	840	
Lime mortar	0.7	0.81	1600	1600	840	1050
Brick	0.72	1.1	1920	1900	840	1050
Reinforced concrete	2.3	1.74	2300	2500	1000	920
Lime cement mortar	/	0.87	/	1700	/	1050
Lime plaster mortar	/	0.76	/	1500	/	1050

* '/' refers to not provided

2.6.3.2 External wall construction parameters

The external wall building fabric parameters have been estimated in various combinations and thicknesses throughout the literature, ranging from 1.96 to 3.67 W/m^2K in 17 studies found (Table 2-22). Three studies do not provide construction details and only provided u-values. One study considered four layers of construction (Yu et al., 2009a), and all other studies considered three layers of construction. All studies considered 20mm plaster, mortar, or cement

for the inside and outside layer; the thermophysical parameters of these materials are different according to Table 2-21. The predicted thickness of the middle layer ranged from 190-240mm, with one study suggesting 300 mm reinforced concrete (Short et al., 2018). Type of constructions in the middle layer are predicted to be reinforced concrete for two studies (U-value = 3.67 W/m²K), and brick for other studies (U-value = 1.96 to 2.23 W/m²K). Therefore, from the evidence above, the most plausible construction characteristics of external walls will have three layers of construction, with 20 mm cement/plaster/mortar for the inside and outside layer, and 160-240 mm brick or reinforced concrete for the middle layer.

A brick-concrete structure is typical for urban residential buildings built in the 1990s. As Chen et al. (2010) showed, 80% of the investigated urban residential buildings in a city in the HSCW zone (Changsha) have brick-concrete structure. The 2010 census data in Chongqing suggested that 50% of the residential building had a reinforced concrete structure, 43% had a brick-concrete structure, and 7% had a brick structure. A survey conducted in the HSCW zone suggests there are 37.8% brick-concrete construction and 61.9% reinforced concrete construction (Li et al., 2018), including newly built residential buildings. According to the literature, the mean U-value for the external wall construction is 2.22 W/m²K.

Table 2-22: Typical external wall construction as found previous studies.

Construction details (list from inner layer to outer layer)	U-value of external wall (W/m ² K)	Reference
240mm Brick	/	(Yoshino et al., 2006)
20mm cement plaster + 240mm red brick + 20mm lime plaster	/	(Liu et al., 2015)
20mm mixed mortar + 300mm reinforced concrete + 20mm cement mortar	/	(Short et al., 2018)
20mm cement mortar + 240mm brick + 20mm lime cement mortar	1.96	(L. Xu et al., 2013)
Solid clay bricks	1.97	(Yao et al., 2018)
Not mentioned	1.97	(X. Li et al., 2018)
Plastered 240mm bricks	2.0	(Cai et al., 2013)
Not mentioned	2.0	(McNeil et al., 2016)
Rendering outside + 240mm brick wall + rendering inside	2.03	(Chen et al., 2009)
20mm cement mortar + 190mm hollow brick + 20mm lime mortar	2.041	(Yu et al., 2009b)
Not mentioned	2.189	(Ouyang et al., 2011)
20mm cement mortar + 240mm solid clay brick + 20mm cement & lime mix mortar	2.21	(Xiaotong Wang et al., 2015)
Not mentioned	2.355	(Ouyang et al., 2009)
20mm mortar + 240mm concrete + 20mm mortar	2.96	(Hogan et al., 2001)
20mm cement + 200mm reinforced concrete layer + 20mm sand plaster	3.67	(Yu et al., 2008)

2.6.3.3 Roof construction

The literature suggests typical roof u-values of residential buildings lie between 1.5 and 3.969 W/m²K (Table 2-23). Only three existing studies provide exact construction details. The total roof thickness for the case with a U-value of 1.38 W/m²K is 310 mm, where the total roof thickness for the other two cases are 186 mm and 202 mm, which is 100 mm thinner and thus lead to a massive difference in the predicted U-value of roof. One study performed optimum insulation roof thickness in residential buildings; the thickness of the roof was assumed to be 170 mm without insulation (Yu et al., 2011). Two studies which provide construction details assume a 150 mm reinforced concrete layer, and both suggested a high U-value (Xiaotong Wang et al., 2015; Yu et al., 2008). It is strange that the four studies which assumed U-value of roof to have U-values between 1.5 and 1.67 W/m²K yet they did not provide any construction details; it is assumed that these values arrived from authors' knowledge.

Table 2-23: Typical roof construction as found in previous studies.

Construction details (list from inner layer to outer layer)	U-value of roof (W/m ² K)	Reference
30mm concrete + roof membrane + 20mm cement sand + 120mm concrete + cement stucco	/	(Yu et al., 2011)
Not mentioned	1.5	(McNeil et al., 2016)
Not mentioned	1.62	(Yao et al., 2018)
Not mentioned	1.62	(X. Li et al., 2018)
Not mentioned	1.663	(L. Xu et al., 2013)
10mm built up roof with medium colour paint + building paper felt + 160mm reinforced concrete layer + 16mm gypsum layer	2.74	(Yu et al., 2008)
20mm cement mortar + 2mm waterproof material APP + 20mm cement mortar + 150mm reinforced concrete + 10mm cement & lime mix mortar	3.31	(Xiaotong Wang et al., 2015)
Not mentioned	3.969	(Ouyang et al., 2009)
Not mentioned	3.969	(Ouyang et al., 2011)

2.6.3.4 Internal floor and wall construction

Typically, studies focus on a single flat or zone when performing building energy simulations, rather than the whole building which would provide more reliable energy consumption predictions. Typical parameters of internal floor and wall construction found in the literature are presented in Table 2-24 and Table 2-25, respectively. Only three studies specify internal floor construction for pre-retrofit residential buildings, they are 0.2 m cast concrete with a U-value of 2.237 W/m²K (Xi Wang et al., 2015), or with 0.1 m reinforced concrete with a U-value of 4.35 W/m²K (Xiaotong Wang et al., 2015).

Some studies were found which specify indoor floor construction for newly built buildings, where an XPS board (Gou et al., 2018) or polystyrene insulation layer (Ichinose et al., 2017; Yu et al., 2009a) is included. However, all three studies suggested a 120 mm middle layer, indicating Xiaotong Wang et al. (2015) provide a typical internal floor construction with a U-value of 4.35 W/m²K. Two studies suggested a 20 mm cement mortar layer on both sides (Gou et al., 2018; Short et al., 2018) and one study suggested a 10 mm cement mortar layer on both sides (Xiaotong Wang et al., 2015).

Table 2-24: Typical internal floor construction as found in previous studies.

Construction details (list from inner layer to outer layer)	U-value of internal floor (W/m ² K)	Reference
20mm cement mortar + 120mm reinforced concrete + 20mm cement mortar	/	(Gou et al., 2018)
120mm concrete	/	(Yu et al., 2009a)
120mm concrete	/	(Ichinose et al., 2017)
200m cast concrete	2.237	(Xi Wang et al., 2015)
10mm cement mortar + 100mm reinforced concrete + 10mm cement & lime mix mortar	4.35	(Xiaotong Wang et al., 2015)
20mm cement mortar + 200mm reinforced concrete + 20mm cement mortar	/	(Short et al., 2018)

The internal wall building fabric parameters have been estimated in various combinations and thicknesses throughout the literature, ranging from 0.785 to 2.061 W/m²K in six studies found (Table 2-25). Many studies assume the thickness of brick to be around 200 mm (Ichinose et al., 2017; Xi Wang et al., 2015; Xiaotong Wang et al., 2015; Yu et al., 2009a), which has similar thickness with a typical external wall construction (Table 2-25). However, the actual construction of the internal wall is often thinner than the external wall to reduce cost and increase the floor area in the flat. Therefore Gou et al., (2018) present a more realistic representation of the internal wall with construction “0.02 m cement mortar + 0.03 XPS board + 0.12 m reinforced concrete + 0.02 m cement mortar”. However, similar to internal floor construction, XPS boards are installed for new buildings for insulation. The internal walls for existing buildings will have similar construction but without the XPS board.

Table 2-25: Typical internal wall construction as found in previous studies.

Construction details (list from inner layer to outer layer)	U-value of internal wall (W/m ² K)	Reference
20mm plaster + 200mm brick + 20mm plaster	2.061	(Xi Wang et al., 2015)
20m cement mortar + 120m reinforced concrete + 20mm cement mortar	/	(Gou et al., 2018)
190mm air brick with plaster on both sides	2.0	(Yu et al., 2009a)
20mm cement & lime mix mortar + 240mm solid clay brick + 20mm cement & lime mix mortar	1.78	(Xiaotong Wang et al., 2015)
Plaster + 190mm porous brick + plaster	2.0	(Ichinose et al., 2017)
Reinforced concrete and covered on both sides by a cement layer	1.33	(Xiong et al., 2018)
20mm wood floor + 20mm cement mortar + 200mm reinforced concrete + 20mm cement mortar	/	(Short et al., 2018)

2.6.3.5 Window parameters

All existing studies in buildings in the HSCW zone to the author knowledge have reported typical window construction to be single-glazed. A study that performed more than 6000 surveys in the HSCW zone showed that 81.2% of buildings have a single-glazed window, with the remaining having double-glazed windows which are newly built buildings (B. Li et al., 2018). Table 2-26 shows the 15 variations of U-value and g-value of windows found in the literature, ranging from 4.70 to 6.65 W/m²K, 13 of them include construction details. Window thicknesses vary according to studies, and five studies suggested the windows have 3 mm thickness, with U-values ranging from 5.5 to 6.17 W/m²K and g-value ranging from 0.86 to 0.95 (Su and Zhang, 2010; Yu et al., 2013, 2009a, 2008). Two studies suggested the windows have 5 mm thickness, with U-value 4.7 W/m²K and g-value ranges from 0.7 to 0.75, with the values lower than window with 3 mm thickness.

For window frames, aluminium (Ouyang et al., 2009; Short et al., 2018; Yu et al., 2008), plastic (Ouyang et al., 2011; Xiaotong Wang et al., 2015), and steel (Cai et al., 2013; Hogan et al., 2001; Ouyang et al., 2011; L. Xu et al., 2013) frames are conventional. One study performed 200 surveys in Shanghai (a major city in the HSCW zone) and showed that 30% of occupants use aluminium alloy window frames, 20% use plastic steel, and 50% use iron (Chen et al., 2009). The mean U-value and g-value of windows calculated from studies in Table 2-17 are 5.93 W/m²K and 0.88.

Table 2-26: Typical building fabric parameters of window as found in previous studies.

Construction details	U-value of window (W/m ² K)	g-value of glazing (-)	Reference
Not mentioned	/	0.7	(Zhao et al., 2015)
Singled-glazing, aluminium frame, sliding-type windows	/	/	(Short et al., 2018)
5mm single-glazing, plastic steel frame	4.70	0.70	(Ouyang et al., 2011)
5mm single-glazing windows, plastic frame	4.70	0.75	(Xiaotong Wang et al., 2015)
3mm single-glazing	5.5	0.87	(Yu et al., 2013)
Single-glazing	5.74	0.82	(Yao et al., 2018)
Not mentioned	5.74	0.85	(X. Li et al., 2018)
3mm single-glazing, aluminium frame	5.85	0.87	(Yu et al., 2008)
3mm single-glazing	5.85	0.87	(Yu et al., 2009a)
3mm single glazing	6.17	/	(Su and Zhang, 2010)
5mm single glazing, aluminium frame	6.25	0.80	(Ouyang et al., 2009)
Not mentioned	6.4	0.95	(McNeil et al., 2016)
Single glazed	6.40	/	(Lang, 2004)
Single glazing, steel frame	6.5	0.95	(Cai et al., 2013)
Single glazing, steel frame	6.554	0.87	(L. Xu et al., 2013)
Single glazing, steel frame	6.65	0.87	(Hogan et al., 2001)

2.6.3.6 Air infiltration rate

Improving air tightness can minimise heat loss due to ventilation and subsequently reduce energy consumption (Everett, 2007), but there are limited studies to quantify air infiltration rate for existing residential buildings in the HSCW zone. Chen et al. (2012) performed air leakage tests in northern China, and results identified a number of building fabric problems that affect energy consumption: windows could not remain firmly closed and the smoke exhaust ventilator in the kitchen is connected by a big hole to the vertical smoke chimney, which increases the chance of air leakages. Results from the blower door test of an existing residential building with similar building fabric parameters (i.e., single-glazed windows, no external wall insulation) in northern China within the HSCW zone, predicted that the air change rate at pressure difference of 50 Pa (air change per hour when the pressure difference between inside and outside is 50 Pa) was 16.7 ach⁻¹ (Chen et al., 2012). The prevailing air infiltration rate is defined as air change per hour under normal pressure during regular operation; a reference pressure of 4 Pa is commonly used to represent natural conditions (Sherman and Grimsrud, 1980).

Therefore, the equivalent air infiltration rate with a pressure difference of 4 Pa is 0.98 ach⁻¹. Ji and Duanmu (2017) also performed the blower door test on ten detached houses built before implementation of energy efficiency codes in Northern China, which also have similar building fabric parameters as residential buildings in the HSCW zone. Results showed that the air change rate at pressure difference of 50 Pa has a mean value of 1.42 ach⁻¹. The typical air leakage places are the reserved holes in the outer wall that were not well filled after construction, the frames of windows and doors that were not fitted correctly, deformed draught seals, and the check valves at the inlets of the discharge flue and exhaust airway in the house.

Despite a number of studies which performed the blower door test to predict the air infiltration rate in Northern China, no study performed the test in the HSCW zone. Thus, typical air infiltration rates are summarised in Table 2-27 as identified in the literature, and the value ranged from 0.44 to 2 ach⁻¹. These studies performed energy modelling for existing residential buildings in the HSCW zone. Many of them assumed existing residential buildings in the HSCW zone have poor air infiltration performance with 1 ach⁻¹ (Yu et al., 2009a) or abysmal air infiltration performance with 2 ach⁻¹ (McNeil et al., 2016). However, the studies listed in Table 2-27 mix ventilation rate and infiltration rate as one input, which lead to potential under-estimates of the total air change rate. These studies do not specify clearly whether air change rate means air infiltration rate or air infiltration and ventilation rate combined, and define the input as air change rate. To put it into context, two studies assumed air infiltration rate to be 2 ach⁻¹ (McNeil et al., 2016; Yao et al., 2018); four studies assumed air change rate to be 1 ach⁻¹ (Xiaotong Wang et al., 2015; Yu et al., 2008) or 2 ach⁻¹ (Li et al., 2019; X. Li et al., 2018); and two studies assumed air exchange rate due to ventilation and infiltration to be 1 ach⁻¹ (Yu et al., 2013, 2009a).

Further, Zhao et al. (2015) assumed different air infiltration rates in the flat, with an air change rate of 1.0 ach⁻¹ in the perimeter and 0.4 ach⁻¹ in the corner of the building. Zhao et al. (2015) also varied air infiltration rate from 0 to 2 ach⁻¹ for residential buildings to find the percentage change of energy consumption; the base case infiltration rate is 0.44 ach⁻¹ for living area and 0.6 ach⁻¹ for

staircase. Zhao et al. (2015) assumed the ventilation rate to be 1 ach⁻¹, making the base case of air change rate due to ventilation and infiltration to be 1.44 ach⁻¹.

Table 2-27: Assumption of air infiltration rate as found in previous studies.

Details	Airtightness (ach ⁻¹)	Reference
Air change rate (1.0 ach ⁻¹ in the perimeter zone and 0.4 ach ⁻¹ in the corner of the building)	1.0	(Yu et al., 2008)
Air change rate	1.0	(Xiaotong Wang et al., 2015)
Air exchange rate due to ventilation and infiltration	1.0	(Yu et al., 2009a)
Air exchange rate due to ventilation and infiltration	1.0	(Yu et al., 2013)
Air infiltration rate	2.0	(Yao et al., 2018)
Air change rate	2.0	(X. Li et al., 2018)
Air infiltration rate	2.0	(McNeil et al., 2016)
Air change rate	2.0	(Li et al., 2019)

2.6.4 Occupant parameters

2.6.4.1 The significance of occupant parameters on predicted energy consumption

Occupant behaviour, particularly in relation to energy consumption, is a significant factor in the overall building energy performance. S. Chen et al. (2015) showed that different households have radically different AC operating hours and set-point temperatures, which causes significant variation in energy consumption.

The Chinese design standard suggested a heating set-point temperature of 18°C and cooling set-point temperature of 26°C (MOHURD, 2010a), and many researchers use this assumption (X. Li et al., 2018; Ouyang et al., 2009; Pan et al., 2018; Xiaotong Wang et al., 2015; L. Xu et al., 2013; Yao et al., 2018; Yu et al., 2013, 2009a, 2008). However, Section 2.4.4 showed occupants in the HSCW zone have adaptive behaviour. Therefore, studies reduced the heating set-point and increased the cooling set-point to capture the HSCW zone thermal comfort criteria model. For example, Short et al. (2018) predicted heating and cooling energy consumption on the application of local thermal comfort criteria (16.3–28.1°C), referenced from Li et al. (2011). Zhao et al. (2015) assumed heating-set-point to be 15 °C and cooling set-point to be 29 °C,

referenced from Ye et al. (2006) which suggested the acceptable temperature range in Shanghai's naturally ventilated buildings is between 14.7°C and 29.8 °C.

The Chinese design standard did not provide a value of typical AC operating schedule when modelling residential buildings in the HSCW zone (MOHURD, 2010a). Ouyang et al. (2009b) modelled a typical building in the HSCW zone, assuming continuous 24 hours AC operation. The predicted heating and cooling energy consumption was 90 kWh/m², but the actual measured heating and cooling energy consumption in the same building was 12.3 kWh/m², a seven-fold difference. Further, Guo et al. (2015) measured indoor air temperature in different rooms of a household using air conditioners in a typical day in winter. Results showed that indoor air temperature peaked at 22°C in bedroom 3 at 9:00, 18°C in the living room at 21:00 and 20°C in bedroom 3 at 23:00. Indoor air temperature rose gradually in one hour (8:00-9:00) from 15 to 22°C and dropped gradually in over hours (9:00-12:00) from 22 to 17°C (Figure 2-25). Therefore, Guo et al. (2015) showed an intermittent behaviour of AC operation throughout a day, and Ouyang et al. (2009b) showed the importance of developing an AC operating schedule on the reliability of predicted energy consumption.

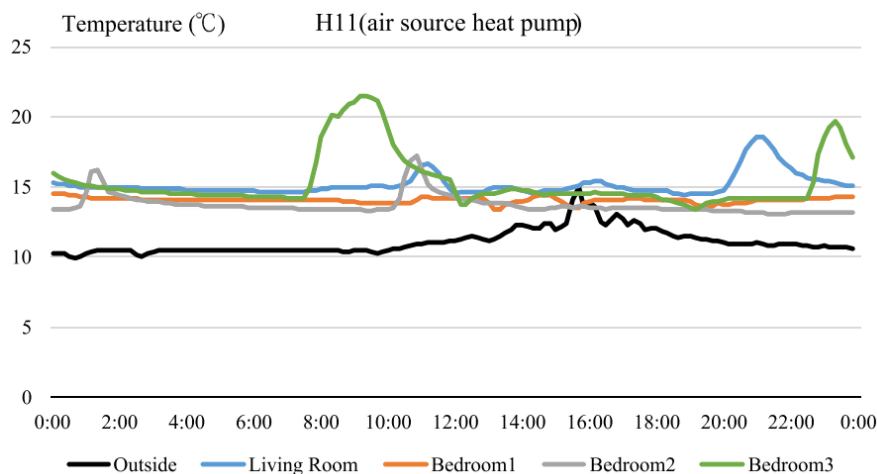


Figure 2-25: Temperature variation of a household using air conditioner in a representative day in winter (Guo et al., 2015).

The studies listed in Table 2-28 attempted to develop a heating/cooling AC operating schedule to model the intermittent behaviour. For example, L. Xu et

al. (2013) assumed 13 hours (18:00–8:00) AC operation on weekdays and 24 hours on weekends for both heating and cooling. Yao et al. (2018) assumed the AC operating schedule for cooling was longer than heating, with an AC operating schedule for cooling assumed to be available 24 hours on weekends and 14 hours (18:00-8:00) on weekdays when occupants are supposed to be at home after work. An AC operating schedule for heating was assumed to be available for 16 hours (7:00-23:00) on weekends and for 5 hours (18:00-23:00) on weekdays. X. Li et al. (2018) referenced Hu et al. (2016), and assumed heating was available for one hour in the morning (7:00-8:00) and four hours before sleep (18:00-22:00), while cooling was available for 15 hours, that is, always available except during working hours (17:00-8:00). Li et al. (2019) argued that accordingly to Zhe Wang et al. (2015b), activity areas (living room) and bedrooms are heated and cooled, and auxiliary areas (i.e., toilet, storage room, and kitchen) usually are not heated or cooled. Results from Zhe Wang et al. (2015b) also showed that the majority (90%) of HSCW residents turn the heating off before sleep, but cooling was operated when sleeping. Accordingly, Li et al. (2019) assumed an AC operating schedule for heating and cooling in activity areas to be available for 5 hours (17:00-22:00). In the bedroom, the heating AC operating schedule was assumed to be available for 2 hours (22:00-24:00), and cooling for 10 hours (22:00-8:00).

Although a heating/cooling AC operating schedule was developed to model the intermittent behaviour, there was a significant variation in the predicted heating and cooling energy consumption (Table 2-28). The variation of heating energy consumption can be up to three times different (5.8 to 19 kWh/m²), where cooling energy consumption has a 20% variation (19.1 to 25 kWh/m²).

There is also a considerable variation in the ratio of heating and cooling energy consumption. For example, Ouyang et al. (2009b) predicted a heating to cooling ratio of 70/30, but Short et al. (2018) and Yao et al. (2018) predicted a heating to cooling ratio to be the opposite (20/80), while others suggest a 40/60 or 50/50 ratio (Li et al., 2019; X. Li et al., 2018; L. Xu et al., 2013). The reason for this variation may be due to the widespread assumptions of building parameters in the models developed, which leads to inconsistent conclusions and outputs.

Table 2-28: Predicted energy consumption for residential buildings.

Heating energy consumption (kWh/m ²)	Cooling energy consumption (kWh/m ²)	Total energy consumption (kWh/m ²)	Heating to cooling ratio	Reference
19	25	44	40/60	(L. Xu et al., 2013)
6.0	23.6	29.6	20/80	(Yao et al., 2018)
18.2	19.5	37.7	50/50	(X. Li et al., 2018)
12	20.3	32.3	40/60	(Li et al., 2019)
5.8	19.1	24.9	20/80	(Short et al., 2018)

2.6.4.2 Measured energy consumption

Ouyang et al. (2011, 2009) collected monthly energy consumption (including heating, cooling, lighting, and equipment energy consumption) from energy meters, and thus, heating and cooling energy consumption needed to be deduced. In April and October, the measured energy consumption was the lowest, because no heating and cooling was used. This was defined as baseload (sum of lighting and equipment energy consumption), the baseloads were assumed to be the same in one year. Heating energy consumption from November to March was calculated by subtracting the measured electricity by baseload. Cooling energy consumption from May to September was calculated by subtracting the measured electricity by baseload (Figure 2-26). This method was used by many researchers in China to estimate the space heating and cooling energy consumption from energy (electricity) meters for residential buildings in the HSCW zone (Chen et al., 2013, 2009, 2008; Gu et al., 2013; Hu et al., 2013; Ouyang et al., 2011, 2009).

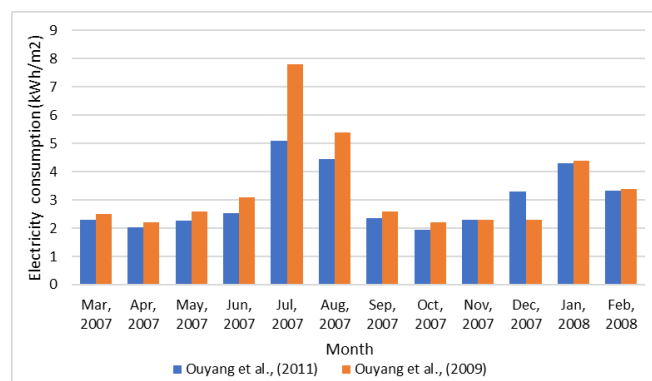


Figure 2-26: Measured electricity consumption for residential flats in the HSCW zone (adapted from Ouyang et al., 2009; 2011).

The annual energy consumption for the residential building was 26.4 kWh/m² with a heating and cooling energy consumption of 13.97 kWh/m², accounting

for 53% of annual energy consumption (Ouyang et al., 2011). Another residential building consumed 36.3 kWh/m² of energy annually, with an estimated heating and cooling energy consumption of 12.28 kWh/m², accounting for 34% of annual energy consumption (Ouyang et al., 2009).

Using the same method as Ouyang et al. (2011, 2009), Table 2-29 lists twelve studies which predict the heating and cooling energy consumption from energy meters. Most of the studies presented in Table 2-29 included a number of households; thus, only the mean value is shown here. Results show that the total energy consumption is around 7.7 to 17 kWh/m², which is much lower (halved) than the predicted energy consumption for the studies summarised in Table 2-28. The heating energy consumption varied from 2.2 to 7.4 kWh/m² and cooling energy consumption varied from 6.5 to 10.32 kWh/m². The heating to cooling ratio varies from around 20/80 (Chen et al., 2009), 30/70 (Hu et al., 2013), to 40/60 (Ouyang et al., 2009).

Table 2-29: Measured heating, cooling and total energy consumption for residential buildings.

Heating energy consumption (kWh/m ²)	Cooling energy consumption (kWh/m ²)	Total energy consumption (kWh/m ²)	Reference
2.9	/	/	(Chen et al., 2011)
/	2.69	/	(Chen et al., 2010)
2.2	9.32	11.52	(Chen et al., 2009)
3.65	10.32	13.97	(Ouyang et al., 2011)
5.51	6.77	12.28	(Ouyang et al., 2009)
7.42	9.5	16.92	(Gu et al., 2013)
/	/	7.67	(Chen et al., 2013)
4.30	8.27	12.57	(Hu et al., 2013)
9.4	/	/	(Hu et al., 2016)
3.99	6.83	10.82	(Chen et al., 2008)
3.6	/	/	(Guo et al., 2015)
/	/	9.8	(BERC, 2018)

2.6.4.3 Heating and cooling COP

The Chinese design standard suggests a heating COP of 1.9 and cooling COP of 2.3 (MOHURD, 2010a). Table 2-30 shows that ten out of 12 publications assumed heating and cooling COP according to Chinese design standard. Two studies suggested that some households use electric heaters instead of air conditioners for heating, with a heating COP of 1 (X. Li et al., 2018; Yao et al., 2018). One study suggested that cooling COP is 2.2 instead of 2.3 (Ge et

al., 2018), and one study assumed heating COP of 2.5 and cooling COP of 2.8, much higher than the Chinese design standard suggested (Yu et al., 2008).

Table 2-30: Heating and cooling COP as found previous studies.

Heating COP (-)	Cooling COP (-)	Reference
1.9	2.3	(Ge et al., 2018; X. Li et al., 2018; Liu et al., 2015; Xiaotong Wang et al., 2015; L. Xu et al., 2013; Yao et al., 2018; Yu et al., 2013, 2011, 2009a; Zhao et al., 2015)
1.0	2.2	(X. Li et al., 2018; Yao et al., 2018)
1.9	2.2	(Ge et al., 2018)
2.5	2.8	(Yu et al., 2008)

2.6.4.4 Heating and cooling set-point

Chen et al. (2013), S. Chen et al. (2015), and Zhe Wang et al. (2015b) performed surveys to identify the heating and cooling set-point that occupants choose to set for air conditioners. S. Chen et al. (2015) showed that 56% of the occupants use a heating set-point of 22-24°C and 49% use a cooling set-point of 24-26°C (Figure 2-27). A residential building was further selected by S. Chen et al. (2015) to perform a yearlong monitoring in order to provide more reliable results. Results showed that the heating set-point temperature was between 20-23°C and the cooling set-point temperature was between 25-28°C (Chen et al., 2015). Chen et al. (2013) performed 300 surveys in Hangzhou; results showed that the mean heating set-point temperature was 22.1°C (standard deviation of 2.1°C) and the cooling set-point temperature was 26.6°C (standard deviation of 2.1°C). Zhe Wang et al. (2015b) performed surveys and field measurements for residential buildings in the HSCW zone. Results showed that 60% of occupants select a heating set-point of 16 to 20°C for air conditioners (Figure 2-28). These results concluded that the heating set-point occupants chose to set for air conditioners was higher than 18°C (the recommended heating set-point from the Chinese design standard). The cooling set-point occupants chose to set for air conditioners was lower than 26°C (the recommended cooling set-point from the Chinese design standard).

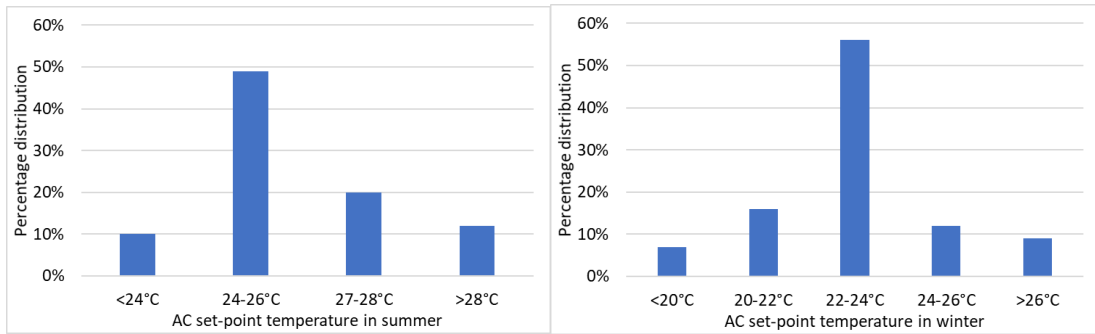


Figure 2-27: Percentage distributions of different set points of air conditioners in summer (left) and winter (right) (adapted from S. Chen et al. 2015)

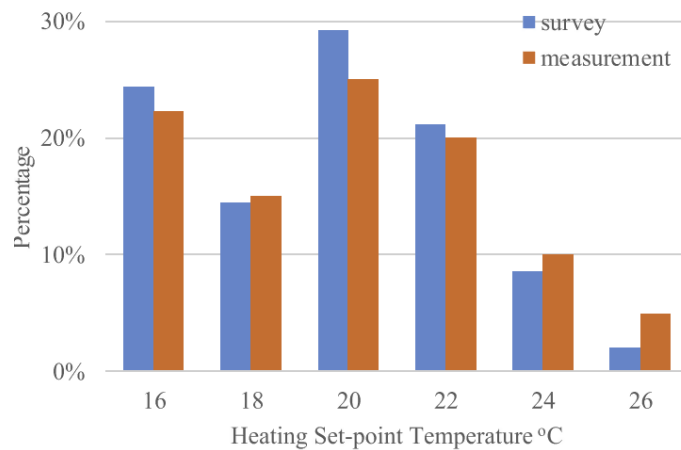


Figure 2-28: Surveys and measurement of heating set-point temperature (Zhe Wang et al., 2015b).

However, Lin et al. (2016) performed an on-site measurement for residential buildings and found that the average measured temperature when heating was operated was 13.5-15.1°C in the living room and 12.7-15.5°C in the bedroom, much lower than the heating set-point that occupants choose to set for air conditioners, where the maximum indoor air temperature during heating was 20.6°C on average in the living room and 21.1°C for the bedroom. This may be due to the shoddy building fabric conditions and high air infiltration rate of existing residential buildings as discussed in previous Sections. Further, Zhe Wang et al. (2015a) developed an energy model and recommended a heating temperature set-point of 17-18°C, according to the fact that residents accept a lower temperature (16.5°C) in winter due to adaptive behaviour as discussed in Section 2.4.

The above studies indicate that despite the occupants setting the heating set-point temperature to a high value (e.g. 25°C), the actual temperature in the zone of existing residential buildings will be much lower than the set-point

temperature, which potentially leads to uncomfortable temperatures despite the higher electricity cost paid.

2.6.4.5 Heating and cooling schedule

S. Chen et al. (2015) performed a survey and found that the usage hours per day of air conditioners in winter and summer can vary from 1 to 12 hours (Figure 2-29). A residential building was further selected by S. Chen et al., (2015) to perform a yearlong monitoring; results showed that the average AC operating schedule is 4.8 hours in winter and 6.4 hours in summer. Chen et al. (2013) performed surveys in Hangzhou and showed that the mean hours of heating usage is 4.4 hours with a standard deviation of 2.4 hours, and mean hours of cooling usage is 9.6 hours with a standard deviation of 4.2 hours.

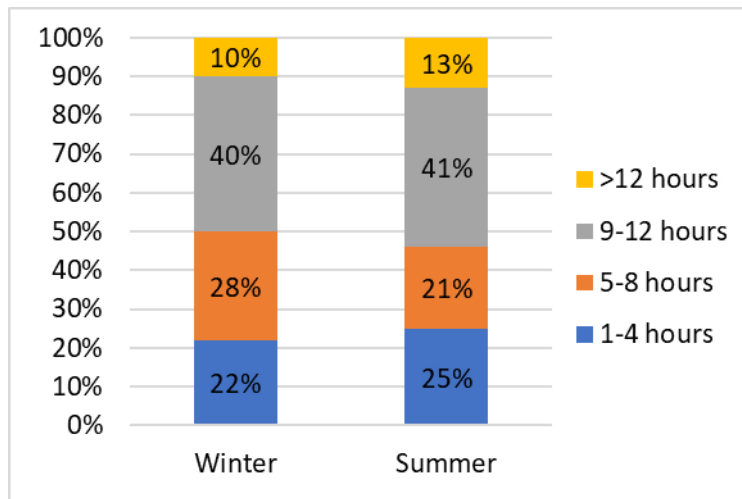


Figure 2-29: Mean usage hours per day of air conditioners in winter and summer (adapted from S. Chen et al., 2015).

The studies listed in Table 2-31 performed a survey for residential buildings in the HSCW zone to find out the heating and cooling AC operating hours. Most of the studies presented in Table 2-31 included a number of households; thus, the mean value is shown here only. The average AC operating hours from the twelve studies reported in Table 2-31 was 5.05 hours in winter and 8.92 hours in summer.

Table 2-31: Measured mean heating and cooling AC operating hours as found previous studies.

Average AC operating hours in winter (hours)	Average AC operating hours in summer (hours)	Reference
7.27	/	(Chen et al., 2011)
/	9	(Chen et al., 2010)
6.5	6.5	(Chen et al., 2015)
4.8	6.4	(Chen et al., 2015)
4.4	9.6	(Chen et al., 2013)
3.71	10.47	(Hu et al., 2013)
2.5	8.8	(Chen et al., 2008)
6.36	11.66	(Yoshino et al., 2006)
3.15	/	(Yoshino et al., 2004)
3.3	/	(Lin et al., 2016)
7.5	/	(Zhe Wang et al., 2015b)
6.0	/	(Guo et al., 2015)

The literature summarised findings in Table 2-31 show AC operating hours; however, not the operating schedule. A few studies have been performed to quantify the percentage of operation hourly for a typical day. Chen et al. (2011) surveyed the hourly use of space air conditioners for flats in two cities (Changsha and Chongqing) in the HSCW zone. Results showed that most households operate heating in the evening between 18:00 to 23:00 (over 50% probability of operation) and in the afternoon between 11:00 to 13:00 (with over 30% probability of operation for Changsha and over 10% for Chongqing; Figure 2-30). The reason for more extended operation in the city of Changsha may due to the average temperature in winter being lower than in Chongqing, so occupants operate space AC more often. A similar study was performed by Yoshino et al. (2006) which also measured the hourly use of space air conditioners for flats in two cities, and arrived at similar results to Chen et al. (2011), which further validates the argument as discussed (Figure 2-31). Another study performed by Hu et al. (2013) showed that most households operate heating in the evening between 18:00 to 22:00 (over 75% probability of operation), especially in Chongqing with a percentage higher than 90% (Figure 2-32).

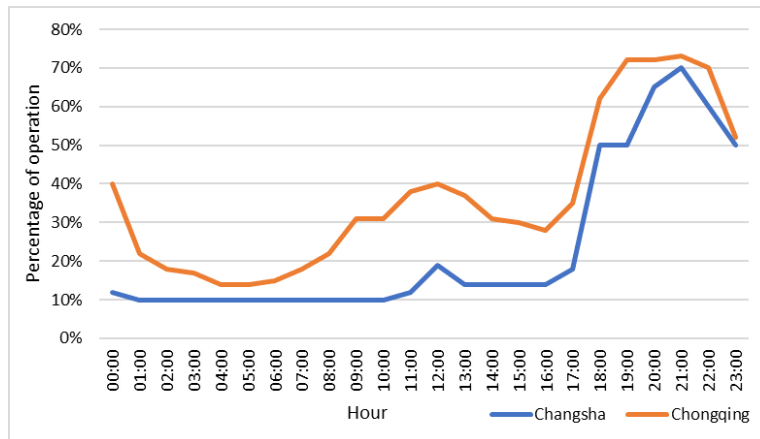


Figure 2-30: Hourly use of space heaters in a representative day in winter (adapted from Chen et al., 2011)

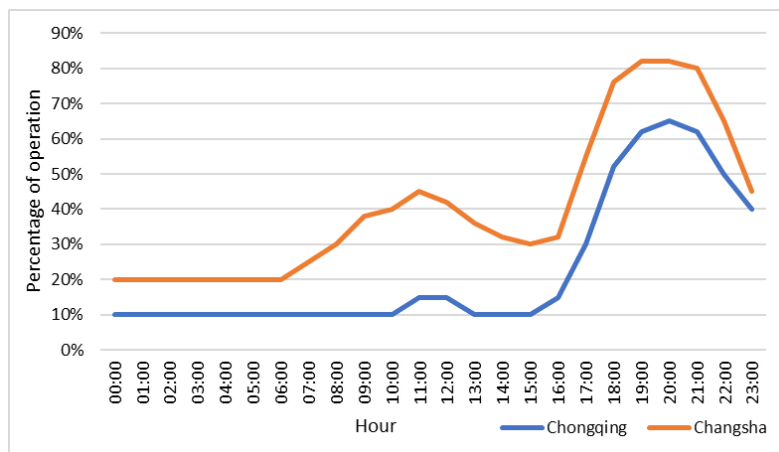


Figure 2-31: Hourly use of space heaters in a representative day in winter (adapted from Yoshino et al., 2006)

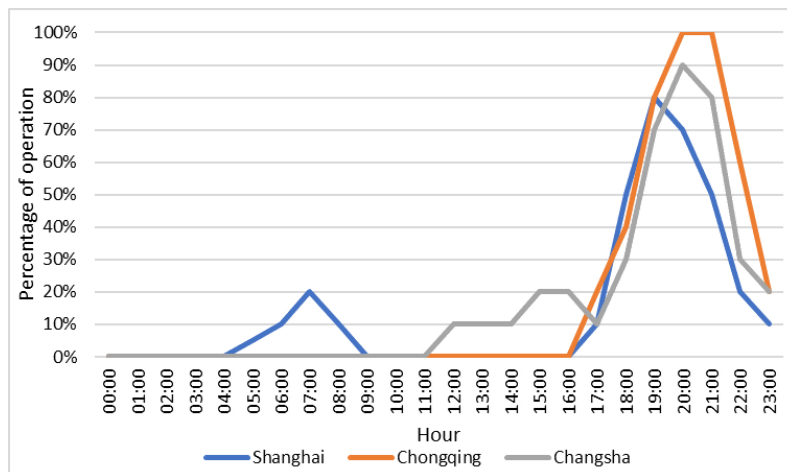


Figure 2-32: Hourly use of space heaters in a representative day in winter (adapted from Hu et al., 2013)

For operation during the summer, Chen et al. (2010) measured the hourly use of room air conditioners in Shanghai and Changsha within the HSCW zone.

Results showed that the percentage of operation of air conditioners is higher in summer than winter. The percentage of operation is above 60% for both cities from 12:00 to 14:00, and the percentage of operation is above 70% from 18:00 to 23:00. The percentage of operation from 0:00 to 6:00 gradually drops from 60% to 10%, which indicates that only bedroom air conditioners operate at night, as Figure 2-33 only shows the percentage of operation for the whole flat. Similarly, Yoshino et al. (2006) and Hu et al. (2013) also measured the hourly use of room air conditioners for flats in Changsha, Shanghai, and Chongqing, and reported similar results to Chen et al. (2011), which further validates the argument as discussed (Figure 2-34 and Figure 2-35).

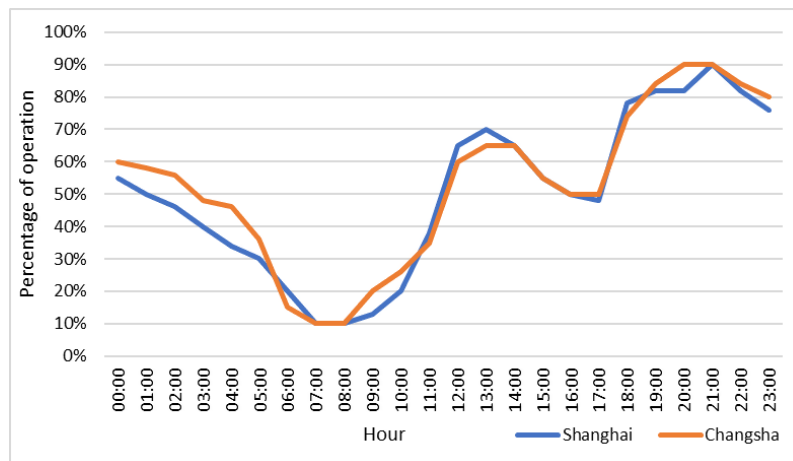


Figure 2-33: Hourly use of air conditioners for cooling in a representative weekday in summer (adapted from Chen et al., 2010)

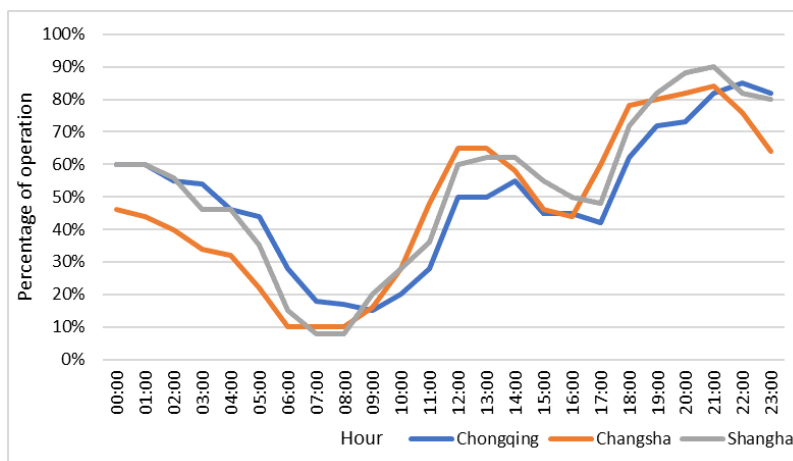


Figure 2-34: Hourly use of air conditioners for cooling in a representative day in summer (adapted from Yoshino et al., 2006)

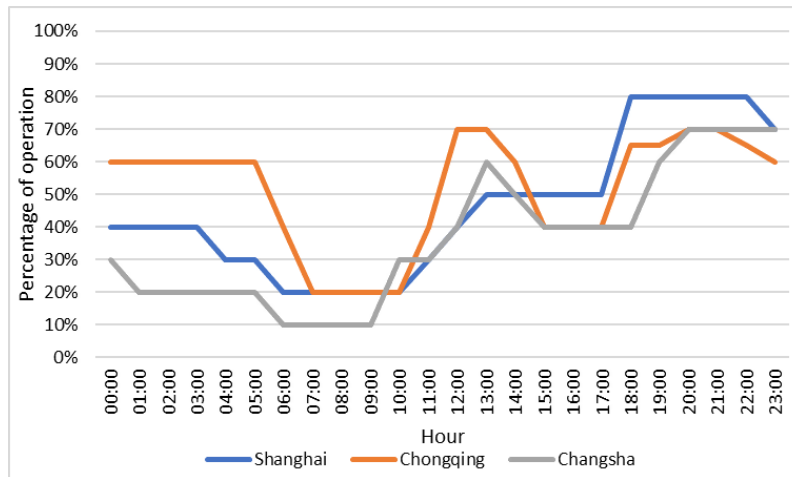


Figure 2-35: Hourly use of air conditioners for cooling in a representative weekday in summer (adapted from Hu et al., 2013)

AC operating hours were also found to be correlated with the age of occupants. Older occupants often use much less air conditioner, which leads to lower energy use. Chen et al. (2013) performed surveys in the HSCW zone; results showed that only 26.4% of occupants above 55 years of age operate air conditioners during sleep, compared to 58.5% of occupants below 55 years of age (Figure 2-36). Another study showed that 73% of residents in the HSCW zone choose to turn off heating when they go to bed (Zhe Wang et al., 2015b).

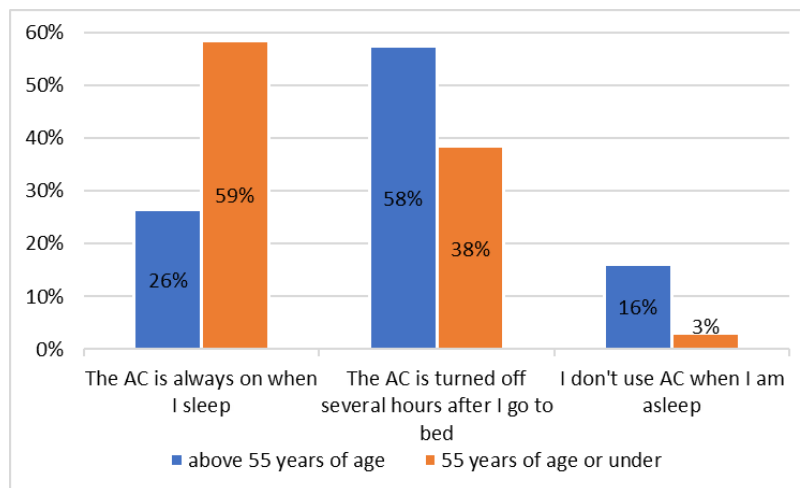


Figure 2-36: Occupant behaviour in air conditioner usage. Left – above 55 years of age, right – 55 years of age or under (adapted from Chen et al., 2013)

2.6.5 Internal heat gain

Internal heat gain consists of lighting, occupant, and equipment heat gain. The studies listed in Table 2-32 showed an extensive range of documented internal heat gain in modelling studies, ranging between 0 to 28.5 W/m² for residential buildings in the HSCW zone.

Standards for lighting design of buildings issued by the Chinese government in 2013, with a mandatory intensity of 6 W/m² for residential buildings, but suggest the intensity can be reduced to 5 W/m² as an energy saving measure (MOHURD, 2013b). Thus when evaluating building energy performance, many studies assume lighting heat gain to be 5 W/m² (Gao et al., 2014; Yang et al., 2015) or 6 W/m² (X. Li et al., 2018; Yao et al., 2018). However, the documented lighting heat gain in modelling studies ranges between 0 to 10 W/m² for residential buildings in the HSCW zone (Table 2-32). Four studies assume the lighting heat gain to have very low value of 0.59 W/m² (Ichinose et al., 2017; Yao and Xu, 2010; Yu et al., 2013, 2009a). A study claimed the reason to select this value is the assumption that lighting heat gain to be 0.0141 kWh/m² per day (Yu et al., 2009a). The Chinese design standard suggested internal heat gain to be 4.3 W/m² as a design parameter, where some studies assume all heat gains (lighting + occupant + equipment) to be 4.3 W/m² (Gou et al., 2018). This leads to lack of clarity in many studies that fails to explain the breakdown of this value (Fu et al., 2017; Zhao et al., 2015). Yu et al. (2008) defined different lighting gains in different zones, assuming 10 W/m² in bedrooms, with 10% (1 W/m²) when sleeping, 10 W/m² in the living room, 15 W/m² in the dining room, 8 W/m² in the bathroom, and 20 W/m² in the corridor for lighting heat gains. The lighting heat gain for the flat studied by Yu et al. (2008) was equivalent to 0.352 kWh/m² per day, 25 fold when compared to the assumption of 0.0141 kWh/m² per day (Ichinose et al., 2017; Yao and Xu, 2010; Yu et al., 2013, 2009a).

Occupant heat gain is a difficult parameter to predict, as the number of occupants varies significantly for each residential flat. According to Chinese national statistics, the average number of people living in one residential flat nationally is 2.62, equivalent to 30 m²/people or 0.033 people/m² (NBS, 2017).

Two studies used this assumption and assumed an occupant density of 0.033 people/m² (L. Xu et al., 2013; Yao et al., 2018). Metabolic rate per person is 123W in the living room (light office work/standing/walking), with a factor of 0.9 (Men = 1.0, women = 0.85, children = 0.75), the assumed heat emission is 111W (ASHRAE, 2018). Thus, the occupant heat gain with an occupant density of 0.033 people/m² is 3.7 W/m². Further, Gao et al. (2014) provided a higher assumption for occupants of 0.1 people/m² in the bedroom, kitchen, toilet, and corridor (three times higher than the national average), and 0.15 person/m² in lounge (five times higher than the national average). The occupant density was 0.12 person/m² for the flat investigated by Gao et al. (2014), equivalent to 13.3 W/m² by assuming heat emission per occupant of 111W. Ichinose et al. (2017) assumed 8.36 m²/person in the living room, 0.93 m²/person in the corridor, 9.29 m²/person in the bedroom, 5.57 m²/person in the kitchen and toilet). The average occupant density was 0.13 person/m² for the flat investigated by Ichinose et al. (2017), equivalent to 14.4 W/m² by assuming heat emission per occupant is 111W.

Equipment heat gain includes computer, television, and kitchen equipment, which can be predicted from finding the corresponding heat emission from the ASHRAE handbook. Yu et al. (2008) defined different heat gains for equipment as 3.2W/m² in the living room, 3.2 W/m² in the bedroom (20% of the value when sleeping), and a higher value of 10.8 W/m² in dining room due to the presence of kitchen equipment. Gao et al. (2014) also provided a realistic estimation of equipment loads, with 3.5 W/m² in the bedroom, 4 W/m² in the living room, 30 W/m² in the kitchen, 1.5 W/m² in the toilet, and 2 W/m² in the corridor. Yang et al. (2015) provided a high estimate of the equipment load of 12.7 W/m² (3 times higher than design standard) in the living room and 9.3 W/m² (2 times higher than design standard) in the bedroom (Table 2-32).

Most studies assume the lighting gain to have the same schedule as the occupancy schedule (Gou et al., 2018; L. Xu et al., 2013; Yao et al., 2018), i.e., lighting operates as long as there is an occupant. For example, L. Xu et al. (2013) one study assumed that the operating schedule was 13 hours (18:00-8:00) on weekdays and 24 hours on weekends, for lighting, other internal gains, occupancy, and AC. A common practice for studies is to assume the same

schedule for all the zones (living room, bedroom, kitchen, etc.) in a residential flat.

Table 2-32: Documented internal heat gains as found previous studies

Details	Light. gains (W/m ²)	Occu. gains (W/m ²)	Equip. gains (W/m ²)	Total gain (W/m ²)	Reference
Assume there is no internal gains	/	/	/	0	(Gong et al., 2012)
Total internal heat gain is 4.3 W/m ²	/	/	/	4.3	(Fu et al., 2017; Gou et al., 2018; Zhao et al., 2015)
Combined occupant and equipment heat gains is 4.3 W/m ²	0.59	4.3		4.89	(Yao and Xu, 2010; Yu et al., 2013, 2009a)
Specified lighting and Occupant heat gain	5.5	3.7	0	9.2	(L. Xu et al., 2013)
Combined occupant and equipment heat gains is 4.3 W/m ²	6	4.3		10.3	(X. Li et al., 2018)
Occupant heat gain provided in each thermal zone	0.59	5.6	4.3	10.49	(Ichinose et al., 2017)
Occupant and equipment heat gains	6	3.7	4.3	14	(Yao et al., 2018)
Combine lighting, occupant and equipment's	/	/	/	16.7	(Short et al., 2018)
Occupant and equipment heat gain provided in each thermal zone	5	4.2	10	19.2	(Yang et al., 2015)
Lighting, occupant and equipment heat gain provided in each thermal zone	14.5	5.6	4.6	20.2	(Yu et al., 2008)
Lighting, occupant and equipment heat gain provided in each thermal zone	5	13.3	5	28.5	(Gao et al., 2014)

2.6.6 Window opening

Window opening is the most common and preferable natural ventilation method (Barlow and Fiala, 2007), and its operation can vary (Figure 2-37). Jeong et al. (2016) showed that the proportion of windows opened was the lowest in winter and highest in summer, for the UK, Europe, and South Korea (Figure 2-37). In the HSCW zone, Hu et al. (2016) performed surveys for urban residential buildings and found that 55% of households open windows frequently and 45% of households open windows rarely in winter. Another study showed that the proportion of windows open during summer could be

over 90%, while the proportion of windows open increases for increasing ambient temperatures (Liu et al., 2017). Interestingly, Liu et al. (2017) also showed that 50% of the windows are opened when the outdoor temperature drops to 10°C, due to the lack of mechanical ventilation, which can further lead to potential heating energy wasted in winter (Figure 2-38). Further, Liu et al. (2018) monitored 16 flats in the HSCW zone in a winter season. Results showed that the probability of occupants opening windows was 83%, with a median opening hour of 394 mins (6.6 hours) in winter. Surprisingly, it is possible that occupants opened windows for the whole day (1400 minutes or 24 hours) (Figure 2-39).

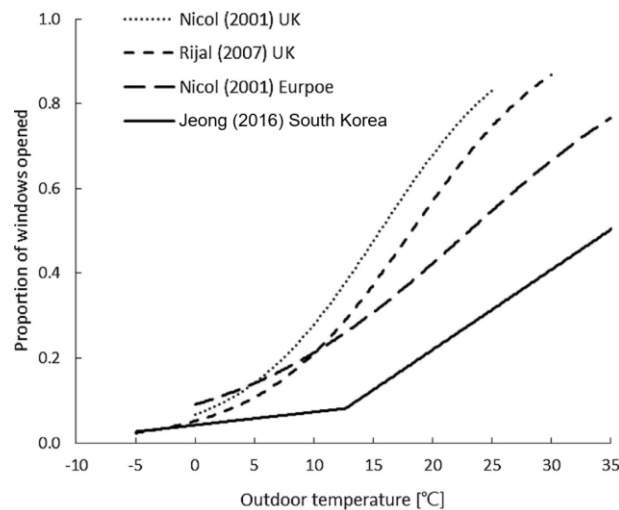


Figure 2-37: Comparison of window opening proportion in South Korea, UK and Europe (Jeong et al., 2016)

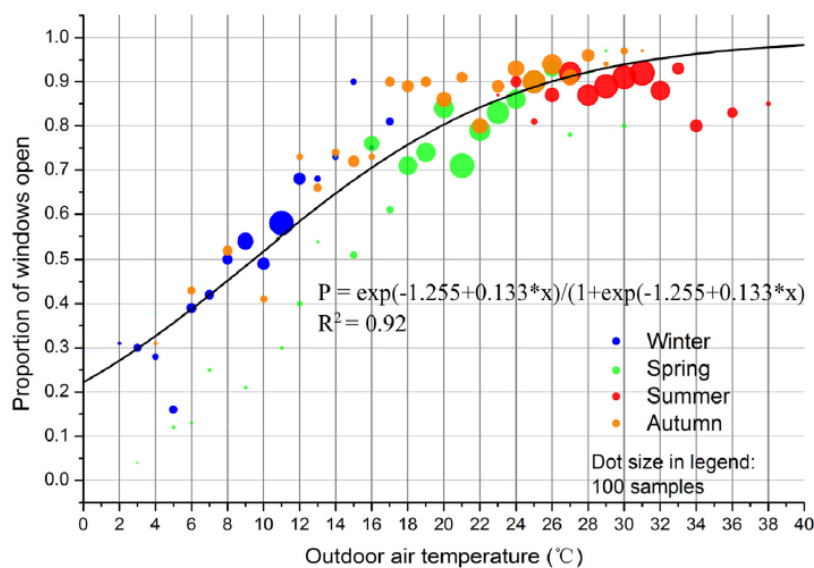


Figure 2-38: Proportion of windows opened with outside temperature (Liu et al., 2017)

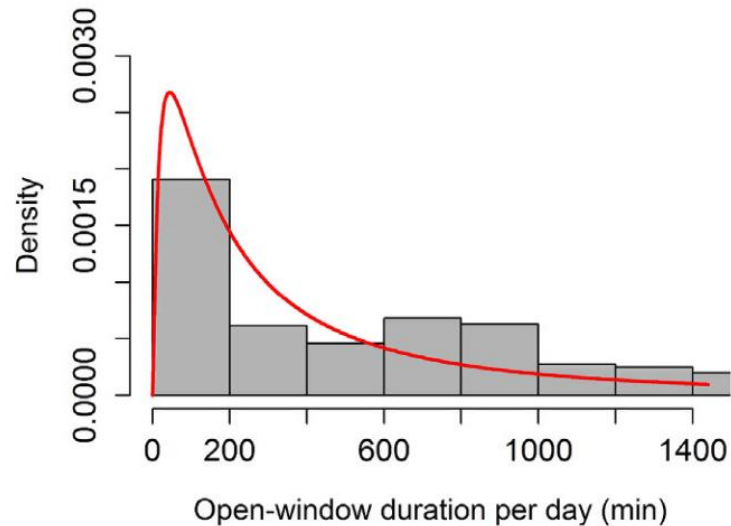


Figure 2-39: Histogram of open-window duration per day in winter for conditions under which occupants opened windows in the HSCW zone (red lines are fitted curves with log-normal or normal distribution) (J. Liu et al., 2018)

The metric air ventilation rate was used to quantify the window opening when modelling residential buildings in the HSCW zone. Recall from Section 2.6.3.6, studies listed in Table 2-27 mix ventilation rate and infiltration rate as one input, which lead to a potential under-estimate of total air change rate. These studies do not specify clearly whether air change rate means air infiltration rate or air infiltration and ventilation rate combined. Similarly, some studies listed in Table 2-33 mix ventilation rate and infiltration rate as one input (air change rate). To put it into context, four studies (Xiaotong Wang et al., 2015; Yao and Xu, 2010; Yu et al., 2013, 2009a) documented an air change rate of 1 ach^{-1} , two studies (Li et al., 2019; X. Li et al., 2018) documented an air change rate of 1 ach^{-1} (Table 2-33), where two studies (Ichinose et al., 2017; Zhao et al., 2015) documented an air ventilation rate of 1 ach^{-1} . Chinese ventilation standard defines a minimum ventilation rate for residential buildings of 0.45 to 0.75 ach^{-1} , depending on the floor area of the flat (MOHURD, 2012b). However, as most of the existing residential buildings have a poor air infiltration rate of over 1.0 ach^{-1} (Section 2.6.3.6), the design standard will be easily achieved even when windows are closed.

As it is common to open windows in summer for ventilation, Yao et al. (2018) and Fu et al. (2017) evaluated the feasibility of natural ventilation via windows in summer, to improve thermal comfort conditions. Yao et al. (2018) varied

natural ventilation rates of 1, 3, and 5 ach⁻¹, and found that a natural ventilation rate of 5 ach⁻¹ reduces the average indoor temperature in summer. Fu et al. (2017) also varied natural ventilation rates from 0 to 5 ach⁻¹ and found that 5 ach⁻¹ can save 6.3% of cooling energy. Short et al. (2018) found that an average flow rate of 0.15 m³/s (equivalent to 4 ach⁻¹) can be achieved by opening windows, for a residential building in the HSCW zone.

Table 2-33: Documented air ventilation rate as found previous studies

Details	Ventilation rate (ach ⁻¹)	Reference
Air change rate, air exchange rate due to ventilation and infiltration	1	(Xiaotong Wang et al., 2015; Yao and Xu, 2010; Yu et al., 2013, 2009a)
Air change rate	2	(Li et al., 2019; X. Li et al., 2018)
Ventilation rate	0.5	(Gong et al., 2012)
Ventilation rate	1	(Ichinose et al., 2017; Zhao et al., 2015)
Reference from minimum fresh air required (30m ³ /h/person)	0.4	(Xi Wang et al., 2015)
Natural ventilation rate (Outdoor temperature is between 18 °C to 26 °C, and wind speed is less than 20 m/s)	1, 3, 5	(Yao et al., 2018)
Outdoor temperature is lower than the indoor temperature in summer	0 to 5	(Fu et al., 2017)

2.7 Building retrofit measures for urban residential buildings in the HSCW zone

2.7.1 The significance of identifying building retrofit measures for building energy modelling

Section 1.4 showed that studies failed to identify the optimum retrofit measures from the perspective of both energy consumption and thermal comfort performance for each type of retrofit measure. Therefore, an extensive literature review was conducted on journal publications which studied building retrofit measures for residential buildings in the HSCW zone. A summary table was developed for each of the seven practical building retrofit measures, to summarise the range of values documented. The results of which will feed into the development of retrofit measures that will facilitate the research aim and Objective 3.

Retrofit will involve the application of passive strategies that reduce heat losses (i.e. adding external wall insulation, replacing windows with lower U-value and improve air tightness) with the assistance of split air conditioners to improve thermal comfort conditions in winter. However, these strategies may lead to overheating in summer, which increases the cooling load of the air conditioner. Thus, passive strategies which reduce heat gain (i.e. reducing g-value of window and installing overhangs) will also apply. In addition to building fabric retrofit, improving energy efficiency of split air conditioners is another useful measure (Wu et al., 2017). Subsequently, seven practical retrofit measures will be discussed in this section: external wall insulation, roof insulation, double-glazed windows, air infiltration control, external overhang, enclosed communal staircase, and energy-efficient air conditioners.

2.7.2 External wall insulation

Adding insulation to an external wall is commonly used to minimise heat loss due to convection (Liu et al., 2015). Common insulation materials are XPS and expanded polystyrene (EPS). These materials have very low conductivity and density (Table 2-34). Gou et al., (2018) evaluated the thickness of the optimum insulation in Shanghai (a major city in the HSCW zone) and suggested that

XPS is more expensive than EPS; however, the insulating performance is better for XPS (optimum thickness = 100mm, south-facing) than EPS (optimum thickness = 150mm, south-facing). The study concluded that EPS is the most economical insulation material according to life cycle cost analysis for different orientations of flats in various cities in the HSCW zone. EPS is more environmentally friendly as it contains 15% recycled content and no Hydrofluorocarbons (HFCs) (ACH foam technologies, 2013). Also, EPS is less affected by moisture content than XPS and has a higher rate of permeability, which expels moisture faster, making it suitable for the HSCW zone climate, given the high humidity throughout the year (ACH foam technologies, 2013) (Table 2-34).

Table 2-34: Common building fabric parameters of insulating material

Component	Conductivity (W/mK)	Density (kg/m ³)	Specific heat (J/kgK)	Reference
XPS	0.036	35	1380	(CIBSE, 2015)
XPS	0.042	30	1380	(MOHURD, 2010b)
EPS	0.05	25	1380	(CIBSE, 2015)
EPS	0.03	30-40	1380	(MOHURD, 2010b)

The U-value of external walls for residential buildings in the HSCW zone varied from 0.765 to 1.5 W/m²K with insulation. Yu et al. (2008) suggested that external wall insulation is more common than cavity wall insulation in the HSCW zone. Seven studies applied external EPS insulation, with insulation thickness varying from 20-30 mm, where a thickness of 20 mm (Gao et al., 2014; Xi Wang et al., 2015; Yao and Xu, 2010; Zhao et al., 2015) and 30 mm (Ge et al., 2018; Pan et al., 2018) are typical. Yu et al. (2008) applied 25 mm to 100 mm external EPS insulation, and found that 25 mm external EPS insulation saved 10% energy and 100 mm external EPS insulation saved 15% energy. Four studies applied external XPS insulation, with insulation thickness varying from 10-30 mm, where a thickness of 10 mm (Ouyang et al., 2009; Xiaotong Wang et al., 2015), 15mm (Ouyang et al., 2011) and 30 mm (Gou et al., 2018) are standard. Further, Liu et al. (2015) used a coupled heat and moisture transfer model to predict heating and cooling energy demand, and determine the optimum insulation thickness of external walls by comparing the energy demand and cost. Results showed that the optimum thickness of XPS ranges from 53 to 69 mm and optimum thickness of EPS ranges from 81 to

105 mm. Others (Ichinose et al., 2017; Yang et al., 2015) use insulation materials other than EPS and XPS. For example, 150 mm porous concrete (Yang et al., 2015) and 50 mm thermal insulation mortar (Ichinose et al., 2017) has been used; however these materials are used to construct new buildings in these studies (Table 2-35).

Table 2-35: Construction of external wall with insulation as found in previous studies

U-value of external wall (W/m ² K)	Insulation material	Reference
0.765	30mm XPS	(Gou et al., 2018)
0.8	30mm EPS	(Ge et al., 2018)
0.8	30mm EPS	(Pan et al., 2018)
0.8	EPS	(Xiong et al., 2018)
0.83	EPS	(Yao et al., 2018)
0.9	Not mentioned	(McNeil et al., 2016)
0.946	20mm EPS	(Xi Wang et al., 2015)
0.97	20mm EPS	(Zhao et al., 2015)
0.987	Use 150mm porous concrete, no insulation	(Yang et al., 2015)
1.0	20mm EPS	(Gao et al., 2014)
1.0	Not mentioned	(Zhe Wang et al., 2015a)
1.01	Not mentioned	(Zhe Wang et al., 2015b)
1.11	100mm EPS	(Yu et al., 2008)
1.2	15mm XPS	(Ouyang et al., 2011)
1.296	10mm XPS	(Ouyang et al., 2009)
1.34	10mm XPS	(Xiaotong Wang et al., 2015)
1.35	20mm EPS	(Yao and Xu, 2010)
1.48	50mm thermal insulation mortar	(Ichinose et al., 2017)
1.5	Polystyrene board	(Fu et al., 2017)

2.7.3 Roof insulation

The U-value of roof for residential buildings in the HSCW zone varied from 0.5 to 1.5 W/m²K with insulation. The variation of U-values of roof used in the literature is more important than that of external wall, with a larger thickness of insulation applied. Two studies applied external EPS insulation, with an insulation thickness of 30 mm (Xi Wang et al., 2015) and 50 mm (Ge et al., 2018). Five studies applied external XPS insulation, with insulation thicknesses of 20 mm (Xiaotong Wang et al., 2015), 25 mm (Yao and Xu, 2010), 40 mm (Ouyang et al., 2011, 2009) and 45 mm (Gou et al., 2018) (Table 2-36). Three studies used insulation material other than XPS and EPS, for example, 120 mm aerated concrete foam (Gao et al., 2014) and 50 mm foam glass (Ichinose et al., 2017); however, these materials were used to construct

new buildings in these studies similar to the case of external wall insulation. Further, the optimum insulation thickness of a typical roof was found to range between 65 mm to 187 mm for residential buildings in the HSCW zone using life cycle cost analysis (Yu et al., 2011).

Table 2-36: Construction of roof with insulation as found in previous studies

U-value of roof (W/m ² K)	Insulation material	Reference
0.5	50mm EPS	(Ge et al., 2018)
0.565	45mm XPS	(Gou et al., 2018)
0.65	Not mentioned	(McNeil et al., 2016)
0.672	40mm XPS	(Ouyang et al., 2009)
0.672	40mm XPS	(Ouyang et al., 2011)
0.743	30mm EPS	(Xi Wang et al., 2015)
0.812	Use porous concrete, no insulation	(Yang et al., 2015)
0.95	25mm XPS	(Yao and Xu, 2010)
0.96	No insulation, use 50mm foam glass	(Ichinose et al., 2017)
1.0	Polystyrene board	(Fu et al., 2017)
1.10	Not mentioned	(Zhe Wang et al., 2015b)
1.12	20mm XPS	(Xiaotong Wang et al., 2015)
1.2	EPS	(Yao et al., 2018)
1.5	No insulation, use 120mm aerated concrete foam	(Gao et al., 2014)

2.7.4 Air infiltration control

Increased air infiltration rate can reduce building energy consumption, because Gou et al. (2018) performed a sensitivity analysis for a residential building in Shanghai, which found that the air tightness (modelled as air mass flow coefficient considering cracks around the opening), is the most sensitive parameter among 37 passive design variables for building energy demand.

Documented air infiltration rate varied from 0.44 to 1 ach⁻¹ for newly built residential buildings (Table 2-37). Chinese ventilation standard defines a minimum ventilation rate for a residential building of 0.45 to 0.75 ach⁻¹ depending on the floor area of the flat (MOHURD, 2012b), indicating an air infiltration rate of 0.45 ach⁻¹ satisfied the standard even when windows were closed. Zhe Wang et al. (2015b) assumed an air infiltration rate of 0.7 ach⁻¹ for newly built residential buildings in the HSCW zone. Zhe Wang et al. (2015a) and Pan et al. (2018) assumed an air change rate (include air infiltration and ventilation rate) of 1.0 ach⁻¹ for newly built residential buildings. Further, Fu et

al. (2017) showed that health problems occur for air infiltration rates below 0.5 ach⁻¹, which would require mechanical ventilation, resulting in electricity use for mechanical ventilation which is larger than the energy reduction by air infiltration control.

Liu et al. (2018) measured 59 flats to determine the air infiltration rate using CO₂ decay method, both newly built and pre-retrofit urban residential buildings were included. Before measurement, CO₂ was injected into rooms with closed windows and doors until the concentration was higher than 2500 ppm. A fan was operated in each room to ensure a uniform CO₂ concentration. After that, the CO₂ concentration was continuously measured at one minute intervals. The infiltration rate can be calculated from equation 2-5.

$$V_i = \frac{\ln(C_1 - C_0) - \ln(C_t - C_0)}{t} \quad (2-5)$$

Where V_i is the air infiltration rate in ach⁻¹, C_1 is the initial CO₂ concentration in ppm, C_t is the final CO₂ concentration in ppm, C_0 is the outdoor CO₂ concentration in ppm, and t is the duration of the measurement in an hour.

Liu et al. (2018) grouped southern China (HSCW zone, hot summer and warm winter zone and mild zone) into one category. Results showed that air infiltration rate varied throughout the year, the median rates in spring (0.38 ach⁻¹), summer (0.42 ach⁻¹), autumn (0.32 ach⁻¹), and winter (0.31 ach⁻¹) were different (Figure 2-40). From Figure 2-40, the median air infiltration rate annually was about 0.35 ach⁻¹, with a lower quartile of 0.25 ach⁻¹ and a higher quartile of 0.5 ach⁻¹. The air infiltration rate in northern China is higher because flats in Southern China do not have indoor heating systems, resulting in only a small difference between indoor and outdoor temperatures, and thus a lower air infiltration rate measured (J. Liu et al., 2018).

Table 2-37: Documented air infiltration rate for retrofitted or new buildings as found in previous studies

Air infiltration rate (ach ⁻¹)	Reference
0.44	(Zhao et al., 2015)
0.6	(McNeil et al., 2016)
0.7	(Zhe Wang et al., 2015b)
1.0	(Gao et al., 2014; Li et al., 2019; Yao et al., 2018)
0.5	(Fu et al., 2017)

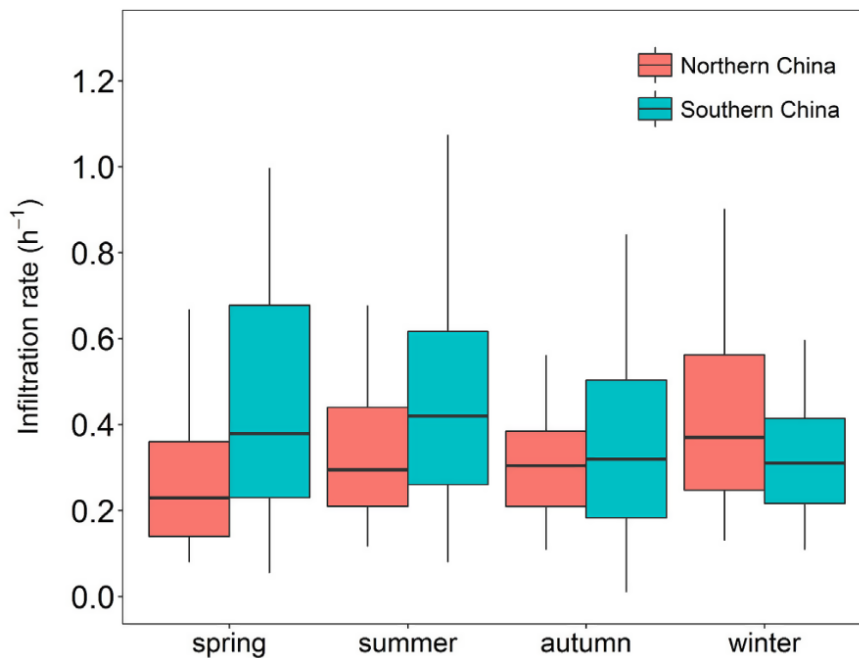


Figure 2-40: Air infiltration rate in northern and southern China (boxes present the 25th and 75th percentiles; whiskers present the 5th and 95th percentiles) (J. Liu et al., 2018)

2.7.5 Double-glazed windows

Window parameters reported in the literature in China have significant variations, with u-values ranging from 1.6 to 4.0 W/m²K and g-values of glazing ranging from 0.34 to 0.84. A metric to measure the transmittance of solar radiation, g-value of 1.0 represents full transmittance, and 0 represents no solar energy transmittance. Double glazed windows consist of three layers: the outer layer is a glass exposed to the outside, the middle layer is a cavity filled with air for insulation and the inner layer is a glass exposed to inside. The thickness of glass can vary from 8 mm (Ge et al., 2018) to 6 mm (Xi Wang et al., 2015; Yang et al., 2015). Manufacturers' catalogues provide 5, 6, 8, 10, and 12 mm glass for the outer and inner layers (Chongqing Cost, 2018).

For a fixed window percentage on the facade (30%), the heating energy consumption can be reduced by up to 16% when replacing single glazing with double glazing. However, the reduction of cooling energy is much lower (5.6%) when replacing single glazing with double glazing equipped with solar control (Ouyang et al., 2009). Low-e glass helps to retain more heat in winter reducing heating costs and reflects heat in summer reducing cooling costs. A study comparing the energy saving between double glazed window with and without low-e glass found that for fixed window percentage facade (30%), the energy consumption can be reduced by up to 4% when replacing single glazing with double glazing, a further 4% reduction is achieved by adding low-e glass (Yu et al., 2008; Table 2-38)

Plastic (uPVC), aluminium, and aluminium with thermal bridge-cut-off are commonly used for window frames. Plastic windows can degrade over the years, requiring replacement after 20 to 30 years; aluminium window frames have a longer replacement rate of 45 years. However, aluminium is a highly conductive material, which makes it thermally inefficient (the U-value of windows will be higher for aluminium frames compare to plastic frames). Recently, aluminium window frames feature thermal bridge-cut-off, which prevents heat from being conducted from outside. Despite the improved performance of aluminium frames, aluminium with thermal bridge-cut-off window frames cost RMB 550 per m², and thus cost more than plastic windows with RMB 310 per m². A cost-benefit analysis was performed for a typical residential building in Hangzhou (a major city in the HSCW zone); the study found plastic window frames with double glazing are the most cost-efficient when retrofitting windows (Xiaotong Wang et al., 2015).

2.7.6 Shading devices

Fixed shading devices can be placed outside or inside the windows in buildings in order to decrease cooling load, the most common being overhangs for residential buildings (Kirimtat et al., 2016). A study in Seoul with an average dry-bulb temperature in hottest month of 25.7 °C, which is similar to the climate in the HSCW zone, predicted that an overhang of length 0.63 m leads to a cooling load reduction of 20% and a reduction of a further 18% when a longer

overhang of 1.53 m is used (Kim et al., 2012). Moveable shading devices can be controlled by occupants to permit winter sun and block direct summer sun. Roller shades and Venetian blinds are commonly used for residential buildings. A study was performed to predict energy reduction when roller shades are installed for a residential building in the HSCW zone on the south-facing façade (Yao, 2014). The study found that the movable solar shades resulted in a 30.87% reduction in building energy demand, and a 21% improvement of indoor thermal comfort in summer. However, these studies do not account for the effect on heating energy consumption. Yu et al. (2008) found that a horizontal shading (overhang) of 1.5 m can decrease cooling electricity consumption by 4%, but that led to an increase of 2% heating electricity consumption. An interesting fact to note is about 60-70% of the windows in Chongqing have fixed overhangs mainly for rainwater protection (Hogan et al., 2001).

Table 2-38: Window parameters for retrofitted or new buildings as found in previous studies

U-value of window (W/m ² K)	g-value of glazing (-)	Notes	Reference
1.6	0.3	Double glazed window, performed parametric study	(Pan et al., 2018)
2.1	0.426	Double glazed windows, 6mm (low-e)/9A/6mm	(Yang et al., 2015)
2.2	0.4	UK standard L1A/L2A	(L. Xu et al., 2013)
2.6	/	Double glazing, 8mm glass/12AA/8mm glass	(Ge et al., 2018)
2.67	0.34	Double-glazed windows	(Yao et al., 2018)
2.67	0.34	Double glazed clear pane with PVC frame	(Xiong et al., 2018)
2.69	0.42	Double glazing windows	(Yu et al., 2008)
2.8	0.4	/	(McNeil et al., 2016)
2.8	0.496	/	(Zhao et al., 2015)
2.85	0.7	Plastic double windows	(Ouyang et al., 2009)
2.85	0.7	Aluminium double windows	(Ouyang et al., 2011)
3.0	0.4	/	(Zhe Wang et al., 2015b)
3.0	/	/	(Zhe Wang et al., 2015a)
3.157	0.7	uPVC window frame, 6mm (low-e)/13A/6mm	(Xi Wang et al., 2015)
3.16	0.76	Double glazed window with plastic frame	(Xiaotong Wang et al., 2015)
3.6	0.84	Double glazed window	(Yao and Xu, 2010)
4.0	/	China regulation	(Gao et al., 2014)
4.0	0.75	Double layer hollow glass	(Fu et al., 2017)

2.7.7 Energy-efficient air conditioners

Air source space heat pumps are commonly used by residents in the HSCW zone for heating and cooling. Chinese standards regulating the efficiency of heat pumps were issued in 2013 (MOHURD, 2013c); cooling was selected from another Chinese standard to govern the efficiency of room air conditioners (MOHURD, 2010c). Energy efficiency ratings were divided into 5. The minimum COP for heating is 3.1 (grade 5) and cooling is 3.2 (grade 3) according to the guideline (Table 2-39).

Prior to 2010, the minimum COP standards were 2.6 in 2004 (MOUHRD, 2004), 2.4 in 2000 (MOUHRD, 2000), and 2.3 in 1989 (MOUHRD, 1989). However, there was no regulation before 2013 to govern the efficiency (COP) of heating in air conditioners. The Chinese design standard suggests assuming heating COP = 1.9 (MOHURD, 2010a). Some households use electric heaters instead of electric heat pumps for heating; these electric heaters often assume to have COP = 1 (Yao et al., 2018).

In comparison to regulations in other countries, e.g. the EU commission has regulations governing energy efficiency ratings for air conditioners. For split type air conditioners, the rating is based on SEER and SCOP. Seasonal Energy Efficiency Rating (SEER) and Seasonal Coefficient of Performance (SCOP) give an indication of how efficiently a heat pump or room air conditioner operates over an entire cooling or heating season. The latest regulation governing energy efficiency ratings for air conditioners from the EU commission use the metric SCOP and SEER (Table 2-40) (EU commission, 2019). However, before 2013, air conditioners were rated according to EER (i.e., cooling COP). In Europe, the limiting cooling COP is 2.2 (Grade G), and highest cooling COP is 3.2 (Grade A).

Table 2-39: Energy efficiency rating for heating and cooling COP of air conditioner from Chinese standard

Energy efficiency rating	Heating COP (W/W)	Cooling COP (W/W)
1	3.9	3.6
2	3.7	3.4
3	3.5	3.2
4	3.3	/
5	3.1	/

Table 2-40: Energy efficiency rating for SCOP and SEER for air conditioners from EU commission (EU commission, 2019)

Energy efficiency rating	SCOP	SEER
A+++	≥5.1	≥8.5
A++	4.6	6.1
A+	4	5.6
A	3.4	5.1
B	3.1	4.6
C	2.8	4.1
D	2.5	3.6
E	2.2	3.1
F	1.9	2.6

The literature reported twelve studies with the assumption of air conditioning heating and cooling COP for new buildings. Six studies (Fu et al., 2017; Ichinose et al., 2017; Zhe Wang et al., 2015b; Yang et al., 2015; Yao and Xu, 2010; Yao et al., 2018) assumed the heating COP to be 1.9 and cooling COP to be 2.3, which implies the COP of AC does not change for new buildings. Cooling COP of 2.3 is equivalent to an F grade of energy efficiency rating defined by the EU commission back in 2002 (EU commission, 2002) (Table 2-41).

Table 2-41: Assumption of AC heating and cooling COP as found in previous studies

Heating COP (-)	Cooling COP (-)	Reference
1.9	2.3	(Fu et al., 2017; Ichinose et al., 2017; Zhe Wang et al., 2015b; Yang et al., 2015; Yao and Xu, 2010; Yao et al., 2018)
2.5	2.8	(Yu et al., 2008)
2.7	3.0	(Ge et al., 2018)
2.7	2.7	(Lee and Chen, 2008)
2.8	2.8	(L. Xu et al., 2013)
3.1	3.1	(Gong et al., 2012)
3.5	3.3	(Gao et al., 2014)

2.8 Discussion

This chapter presented studies that cover information to aid the development of a dynamic thermal model, in order to evaluate energy saving retrofits. This includes comprehensive documentation of existing work by others regarding building performance modelling, survey, and measurement studies for residential buildings in the HSCW zone.

Background information for residential buildings in the HSCW zone, i.e., the geographic, climatic, and constructional features was provided (Section 2.2). Studies showed that the landmass of the HSCW zone covers 25% (2.4 million km²) of that in China, the size is ten times larger than that of the UK. The massive landmass, therefore, contributes to the small variation of climatic features in different cities in the HSCW zone. For instance, the two cities of interest in this thesis (Chongqing and Hangzhou) have similar summer temperatures, whereas Hangzhou has colder winters than Chongqing. This small variation of climatic conditions leads to a potential prediction discrepancy of energy consumption in buildings. The critical message to convey in this thesis is the significance of energy saving retrofits for existing residential buildings in the HSCW zone, where an enormous amount of residential buildings (built area of 3.4 billion m²) are built prior to the implementation of the building regulations enforced in 2001, and hence often lack adequate building fabric.

The findings from studies on commonly used heating and cooling systems for households in the HSCW zone, revealed that their usage of gas boilers and VRF systems, has increased in recent years. Nevertheless, the prevalent heating and cooling system for the majority (95%) of households is the air conditioner, often with low energy efficiency. Interestingly, the energy consumption of households using energy-intensive heating and cooling systems is ten times higher than those using air conditioners.

Residents living in the HSCW zone can tolerate lower temperatures in winter and higher temperatures in summer, which shows adaptation (Section 2.4). This reflects the fact that the heating and cooling energy consumption could have been a lot more if the occupants were not adapting, as the residents would have used more AC. Therefore, it is clear that the occupants' adaptive behaviour needs to be considered when creating a dynamic thermal model.

The review of methodological approaches justified the methods that will be used to address the aim and objectives in this thesis (Section 2.5):

- Steady-state and dynamic thermal models are frequently used to predict building energy consumption. Dynamic thermal model can provide key

building performance evaluation metrics such as temperature and humidity, for small time intervals for an entire year.

- Calibration of dynamic thermal models produces more reliable predictions, and was commonly performed in various countries for residential buildings. Nonetheless, the lack of model calibration for existing residential buildings in the context of HSCW zone was evident in the literature, which caused a discrepancy in predicted energy consumption, confirmed by studies reviewed in Section 2.6.4.
- Previous researchers focused primarily on the evaluation of energy consumption, for individual retrofit measures they had appraised the energy saving aspect instead of the thermal comfort improvement aspect. As for the combination of all retrofit measures, they had evaluated both the energy reduction and thermal comfort improvement aspects. Nevertheless, the evaluation of both energy reduction and thermal comfort improvement for individual retrofit measure was lacking, which has been performed in this study.
- There is a lack of definition of the level of computational detail when modelling residential building archetypes for a city-scale study in the context of the HSCW zone, and thus, the predictions were less illustrative of energy consumption in a city. More notably, the definition of the level of computational detail was investigated in the more developed countries in North America and Western Europe. Yet, these studies concentrated on heating energy demand, rather than cooling energy demand, owing to the temperate climatic conditions of these investigated countries, heating was the predominant building energy consumption.
- Previous studies developed building archetypes based on the building shape or the built area of individual flats. Notwithstanding, the thorough documentation of existing studies in building parameters in Section 2.6 led to a discovery of the most vital geometrical parameters: building height, built area of individual flats, along with the AC operation hours. Conversely, none of the existing studies had considered all the above-mentioned factors when developing residential building archetypes, thereby failing to represent the majority of city-scale residential buildings in the computational simulation process.

The in-depth analysis of the documented literature suggested that some of the model assumptions in building modelling studies were unrealistic in practice, which would have undermined the accuracy of model predictions. The identification of each of the most representative building parameters can aid the development of the dynamic thermal model in Chapter 3. This method can be applied to developing countries where government data is scarce so that more reliable predictions can be made from the new, improved building energy model.

Previous researchers claimed that the potential for energy reduction was significant since idealistic retrofit measures were evaluated exclusively. However, these impractical retrofit measures not only induced a steep implementation cost but also imposed new problems. For instance, a reduction of air infiltration rate to 0 ach^{-1} was proposed by Zhao et al. (2015), however, health problems occur when air infiltration rates are below 0.5 ach^{-1} , and mechanical ventilation would be required, which potentially increases energy consumption. Consequently, Section 2.7 reviewed previous research on various types of practical retrofit measures and identified a selection of feasible measures, which assisted the amelioration of retrofit measures in this thesis in Chapter 3. This study has illustrated the representative findings of HSCW households.

This comprehensive literature review has shown the unique characteristics of residential buildings in the HSCW zone and the importance of retrofitting these buildings to reduce greenhouse gas emissions in the future. It provides sound reasoning to perform detailed research on modelling where the methods, reviewed in Section 2.5, are then subsequently described in Chapter 3, in order to address the aims of this study.

Chapter 3 : Research Methodology

3.1 Introduction

Researchers have defined three categories of research methods: the quantitative; qualitative; and the mixed methods research (Fellows and Liu, 2008). Quantitative research involves testing objective theories, where the relationships between variables are examined. Data can be measured by statistical, mathematical, or computational techniques and analysed by the researcher (Creswell, 2009). In this study, the primary research method will be quantitative, as the aim of the research can be tested by computational techniques.

This chapter consists of four main sections. Section 3.2 presents an overview of the methods used to achieve the aim and objectives in this thesis, developed from the methodological review in Section 2.5.

Section 3.3 presents the link of this thesis with the LoHCool project, where geometrical parameters of 321 residential buildings, built before the implementation of building regulations, were collected in a representative area in Chongqing. Following that, a typical building, which is one of the residential buildings in the representative area, was selected as a case study. A floor plan with detail architectural characteristics was collected for the case study building, so as to develop a dynamic thermal model.

Section 3.4 presents the development of a dynamic thermal model using the floor plan of the case study building, with 96 flats. One of the flats, which is a middle floor flat located in the centre, was selected as a case study. Additionally, other flat locations in the case study building were modelled. After that, building parameters were justified in accordance with the characterisation of the urban residential building stock in Section 2.6 and were subsequently inputted to the dynamic thermal model.

Section 3.5 presents the development of a selection of options for each retrofit measure. The selection of options was justified based on the literature review performed in Section 2.7, on the identification of feasible retrofit measures.

Section 3.6 presents the criteria to compare the outputs (annual energy consumption) using the dynamic thermal model described in Section 3.4 with secondary data, such as annual energy consumption from utility bills; these studies were reviewed in section 2.6.4.

3.2 Research design outline

To address the gaps in the literature, quantitative methods were developed and interconnected to address the five research objectives developed, based on the methodological review carried out in Section 2.5. A summary of the research design outline is presented in Figure 3-1.

To meet Objective two, a steady-state model prescribed by ISO 13790:2008 was developed using excel spreadsheets, developed initially by Taylor (2016) to predict energy demand for houses in the UK. Thus, some input parameters (monthly outdoor temperature, vertical solar radiation, and building parameters of the case study flat) needed to be adjusted accordingly to fit into the context of the HSCW zone. As an example, vertical solar radiation was collected from CIBSE guide in the UK, but there were no published data available in the context of the HSCW zone. Therefore, a model initially developed by Jack (2015) was used to calculate the solar radiation on vertical surfaces from horizontal solar radiation (Duffie and Beckman, 2013; Jack, 2015), where horizontal solar radiation was collected from weather files. Following this, a sensitivity analysis was performed to predict the sensitivity of energy demand to various building fabrics, the results of which informed the selection of building fabric parameters for calibration. Thereafter, monitoring data for a short, unoccupied period (1-week) in the case study flat was acquired through the LoHCool research team. The measurements included hourly indoor air temperature; levels of indoor relative humidity; indoor air velocity; indoor carbon dioxide concentration; outside and inside external wall temperatures. Real time hourly weather data (e.g. outdoor air temperature, outdoor relative

humidity, global horizontal radiation) near the case study building were also measured. These data were used to develop customised weather data for model calibration. Consequently, indoor air temperature in the case study flat was predicted using the dynamic thermal model developed in Section 3.4, and compared with the measured indoor air temperature. After that, three-building parameters (external wall construction, window construction, and air infiltration rate) were identified as those which could have potentially influenced the discrepancies observed between the predicted and measured indoor air temperature. These parameters were altered, with a range referenced from the characterisation of building fabric parameters, to examine if it improved the accuracy of indoor air temperature predictions.

To meet objective three, the annual heating and cooling energy consumption, as well as the summer and winter thermal discomfort hours for the case study flat were predicted, using the calibrated dynamic thermal model in Chapter 4. To improve the reliability of results, the predictions were compared with secondary data (e.g. annual energy consumption from utility bills and measured indoor air temperature); the development of the evaluation criteria will be discussed in Section 3.6. Afterwards, the analysis performed in the case study flat was repeated in twelve other flat locations in the case study building, and the results were compared with the case study flat. Subsequently, heating and cooling energy consumption reduction, combined with the summer and winter thermal discomfort hours reduction, were predicted for the selected options for each retrofit measure. An optimum option for each retrofit measure was selected based on the ability to reduce energy consumption and thermal discomfort hours. Then, a combination of the optimum retrofit measures was applied to other flat locations in the case study building, to compare the effectiveness of individual retrofit measures with the case study flat. Furthermore, the energy reduction due to the combination of all the retrofit measures was evaluated considering the whole case study building. In addition, a cost-benefit analysis of the proposed energy saving retrofits was conducted, based on the calculation of material cost and benefits over the life cycle.

To meet Objective 4 and 5, the evaluation of twelve flats with different locations in the case study building in Chapter 5 was essential since Chapter 5 aims to compare the energy saving retrofits due to location of flats. Nonetheless, this chapter intended to evaluate energy saving retrofits on a building scale. Therefore, the feasibility of reducing the number of locations of flats modelled was investigated, based on the reduction in computational time and the prediction difference in building energy consumption. After that, nine variants with decreasing Level of computational Detail (LoD) were designed by creating nine dynamic thermal models, to assess the impact of modelling detail on predicted heating and cooling energy demand. The most computationally efficient model was selected (Objective 4), in other words, the variant which achieved the most significant reduction in computational time, but also delivered accurate predictions when compared to the model with the highest modelling detail. After this, the selected model in Objective 4 was applied to develop building archetypes to represent a large population of residential buildings in the HSCW zone. With regards to the literature review performed in Section 2.6.2, building height and built area of individual flats are the essential geometrical parameters which potentially affect building energy consumption within a city. Hence, twelve building archetypes were created to represent a range of building designs in a city. The energy reductions when combining all the retrofit measures (identified in Chapter 5) were predicted and compared between the twelve archetypes. Finally, an illustrative example using the representative area in Chongqing was presented, in which the aggregated energy reduction from the combination of all retrofit measures was predicted at a city scale, to address the aim of this thesis.

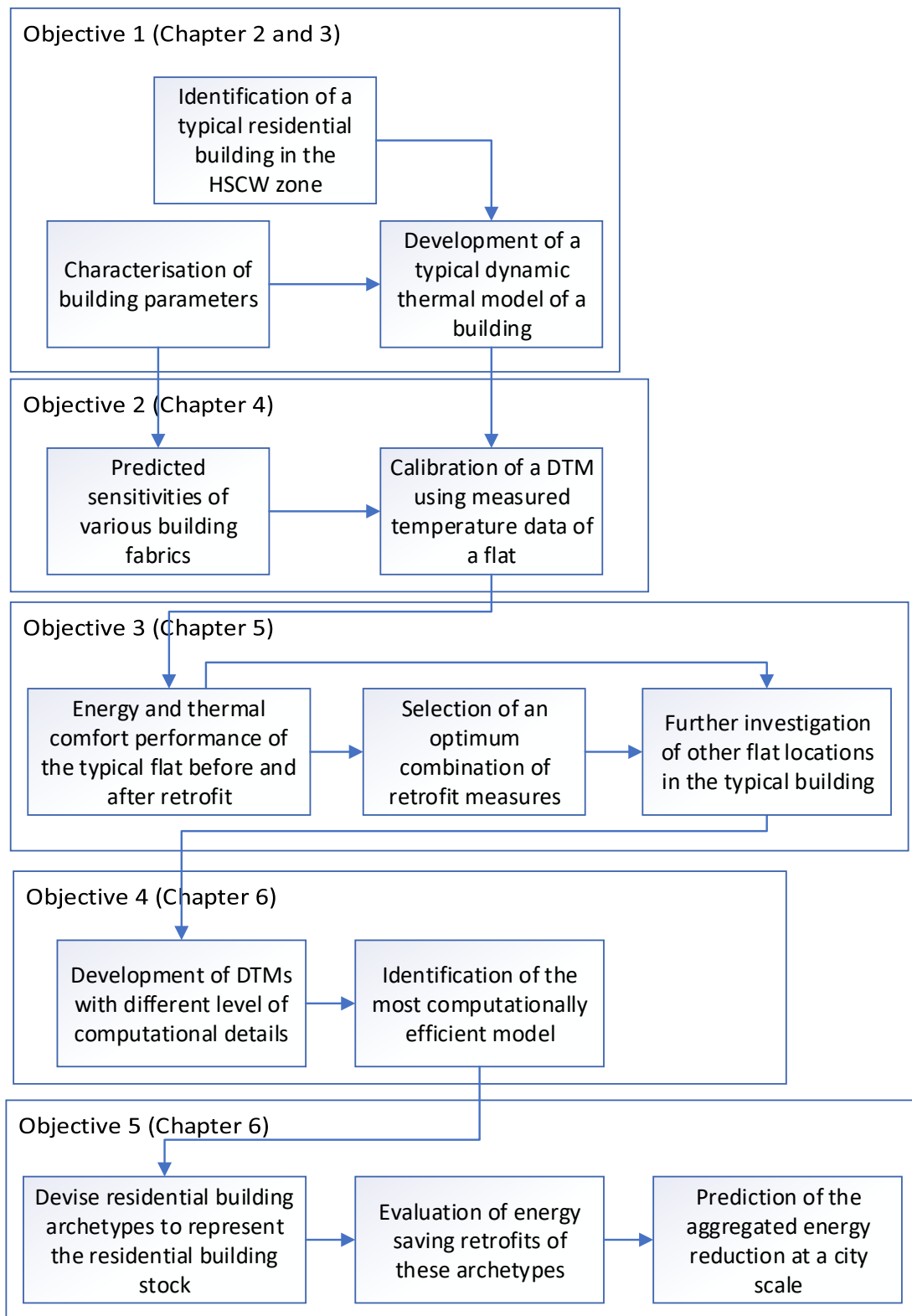


Figure 3-1: Schematic illustrating the outline of the thesis.

3.3 Selection of a typical residential building in the HSCW zone

3.3.1 Characteristics of the urban residential building stock in the HSCW zone

A site visit was performed in November 2015 to Chongqing and Hangzhou with the LoHCool research team. Chongqing and Hangzhou were selected because they represent different micro-climates in the HSCW zone (Section 2.2.2). Chongqing has a mean temperature of coldest month of 6.3°C, where Hangzhou has slightly colder winters than Chongqing (mean temperature of coldest month = 3.7°C). In Chongqing, the Yuzhong district, with a population of 649,500 people in 2015, was selected (Chongqing Municipal Bureau of Statistics, 2017). A representative area within the district with an area of 3.4 km² (accounting for 17% of the total land area of the Yuzhong district), was selected for the purpose of this research (Figure 3-2). There are 575 buildings within the area, and 334 of them are residential buildings. 95% of the residential buildings, with an estimated built-up area of 9,679,167 m², were built before the release of the first building regulations in 2001 (MOHURD, 2001). These buildings had poor building fabric conditions and required retrofit.

Similarly, in Hangzhou, the Shangcheng district, which had a population of 345,000 people in 2018, was selected (Zhejiang Bureau of Statistics, 2018). A representative area within the district which has an area of 1.5 km² was selected for the purpose of this research (Figure 3-3). There are 526 buildings within the area, and 304 of them are residential buildings. 94% of the residential buildings were built before the release of the first building regulation in 2001 (MOHURD, 2001) with an estimated built-up area of 1,150,000 m², and thus required retrofit.

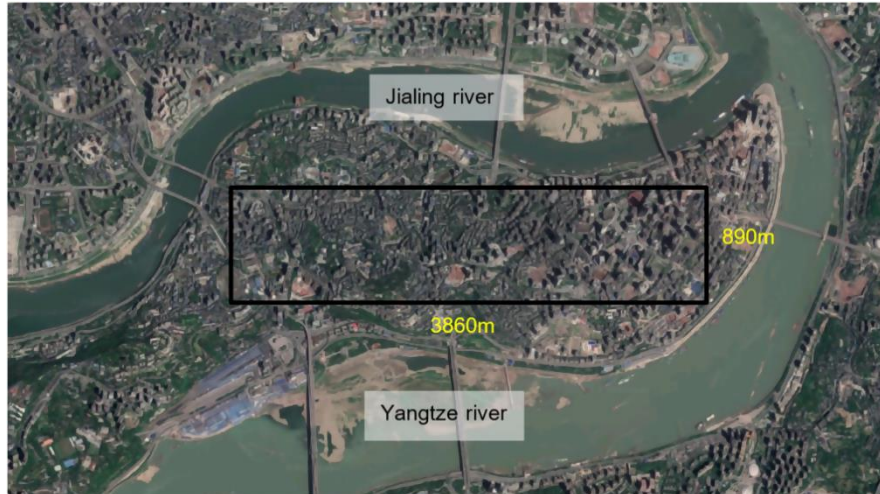


Figure 3-2: GoogleMap view of the Yuzhong District, Chongqing, with the selected representative area highlighted in a black box.



Figure 3-3: GoogleMap view of the Shangcheng District, Hangzhou, with the selected representative area highlighted in a black box.

According to the Code for Design of Civil Buildings in China (MOHURD, 2005), the urban residential building stock in the representative area can be classified into four types with regards to the number of floors as follows:

- Low-rise building with one to three floors (22% of the representative area in Chongqing and 17% in Hangzhou);
- Multi-storey building with four to six floors (15% of the representative area in Chongqing and 63% in Hangzhou);
- Middle high-rise building with seven to nine floors (33% of the representative area in Chongqing and 18% in Hangzhou);
- High-rise building with ten or more floors (31% of the representative area in Chongqing and 2% in Hangzhou).

For the representative area in Chongqing, 50% of the residential buildings have building surface area to volume ratio (building surface area divided by the building enclosed volume) from 0.15 to 0.25, and 64% of the buildings have aspect ratio (longer side width of the building divided by the width of the shorter side) from 1 to 2. For the representative area in Hangzhou, 56% of the residential buildings have building surface area to volume ratio from 0.25 to 0.3, and 83% of the buildings have an aspect ratio larger than 2. Owing to the fact that the representative area in Chongqing captured a wider variety of buildings regarding building height when compared to the representative area in Hangzhou, Chongqing was selected as the focus of this thesis.

3.3.2 Selection of a case study building

A typical residential building in Chongqing was selected as a case study building for the purpose of this research. The case study building selected was one of the 321 residential buildings requiring retrofit in the representative area in Yuzhong district (Figure 3-2). The case study building had a building surface area to volume ratio of 0.188 and aspect ratio of 2.31, these are typical values in the selected representative areas, and thus the case study building can be classified as a typical building in the HSCW zone.

The selected case study building was a ten-storey residential-commercial complex, with 12 flats per floor (96 flats in total) and was constructed in 1996; hence it required retrofit (Figure 3-4 and Figure 3-5). The ground and the first floor were for commercial use. The second to tenth floors were for residential use. The building was used as accommodation for Chongqing University staff and students. Figure 3-5 shows the floor plan for flats in the second floor, with six flats (flat 201 to 206) facing 30° from north to the direction of east (N30°E) defined as front-facing, and six flats (flat 207 to 212) facing 30° from south to the direction of west (S30°W), defined as rear-facing. There were two entrance staircases to access the residential part of the building from shops at ground floor level (Figure 3-4, Figure 3-7a, b) to the outdoor communal corridor in the second floor (Figure 3-4, Figure 3-7c). Through this outdoor communal corridor, there were three staircases. Staircase 1 had access to flats 301, 302, 307, 308 and subsequent flats on the fourth to tenth floors. Staircase 2 had access to

flats 303, 304, 309, 310 and subsequent flats on the fourth to tenth floors. Staircase 3 had access to flats 305, 306, 311, 312 and subsequent flats on the fourth to tenth floors (Figure 3-4, Figure 3-7c).

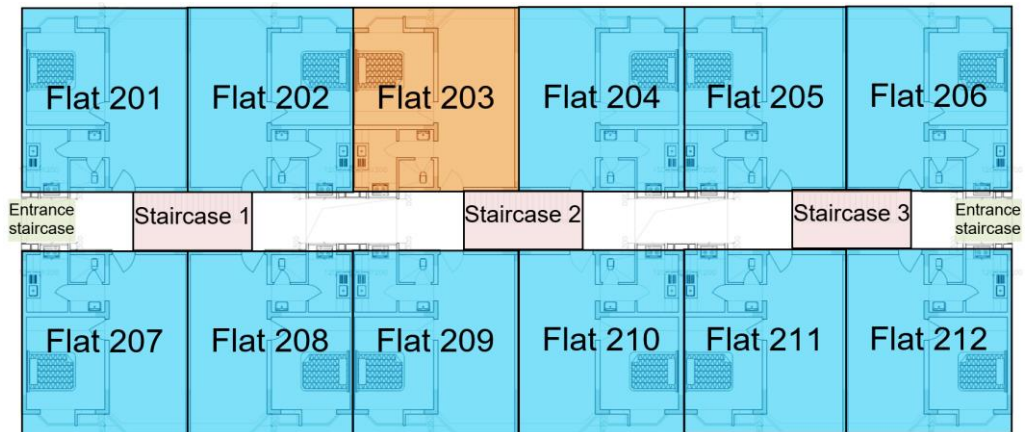


Figure 3-4: Floor plan of the second floor of the case study building, showing the location of entrance staircase (green), three staircases in the outdoor communal corridor (red), twelve flats in each floor (blue) and the case study flat (orange).

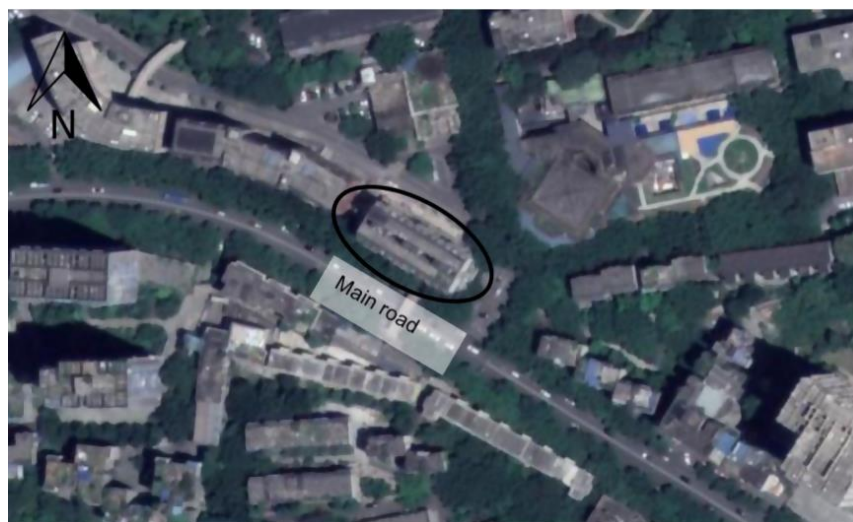


Figure 3-5: Aerial view showing the selected building (circled) and the surrounding buildings in Chongqing.

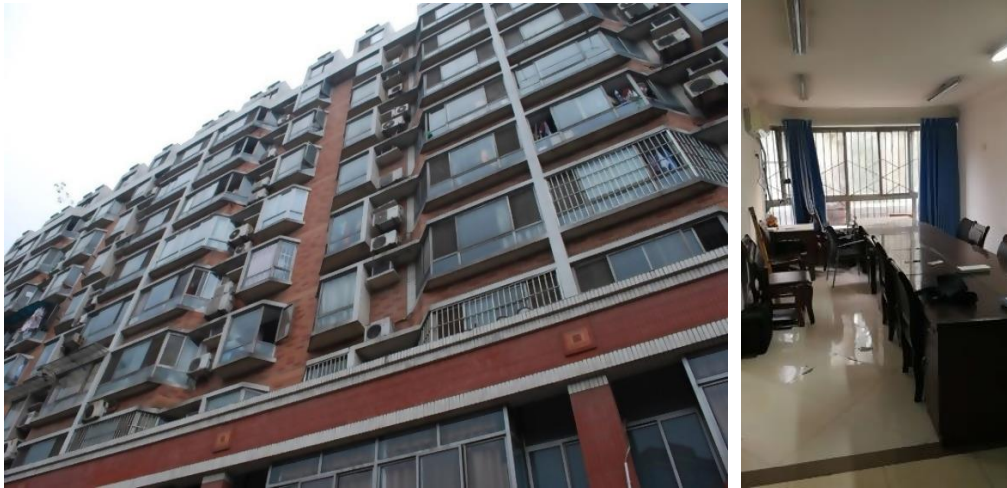


Figure 3-6: Front view of the case study building (left) and inside view of the case study flat (right) (Photograph by author, 2015).

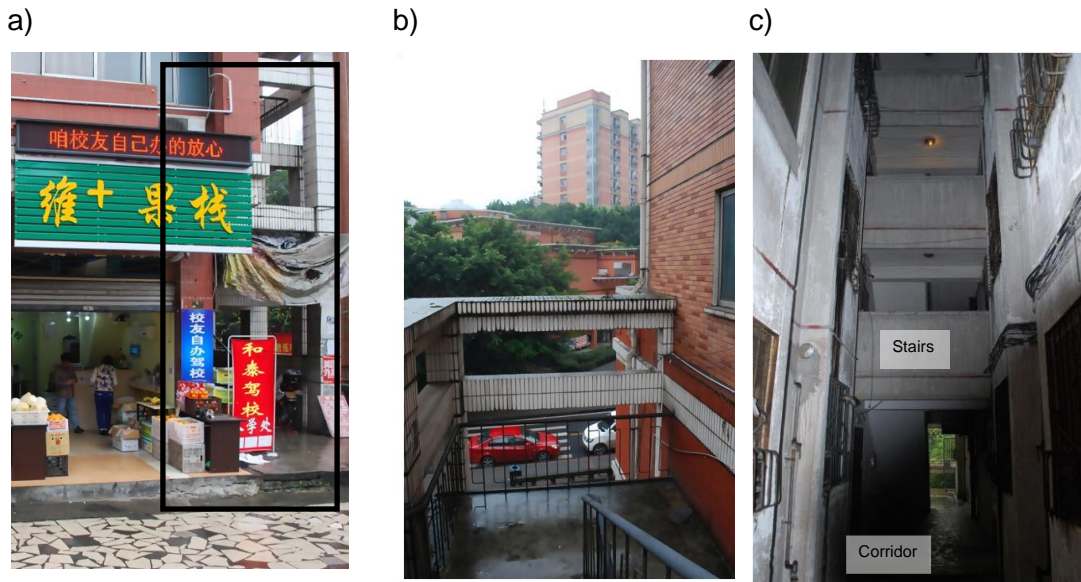


Figure 3-7 a) Shops at ground floor level, with entrance staircase to the flats highlighted with a black box, b) view to front from entrance staircase, c) view from the outdoor communal corridor and staircases of the case study building (Photograph by author, 2015).

Each flat consisted of a living room, bedroom, kitchen, and wetroom, with a floor area of 54.1m² (Figure 3-9). A flat which was used as a meeting room for University staff (Flat 203, shown in Figure 3-4) was selected as a case study flat (Figure 3-6). The flat was located on the second floor, with one external wall (oriented N30°E) exposed to external conditions, and another external wall (oriented S30°W) exposed to the outdoor communal corridor. Moreover, the two internal walls connecting to other flats (one to Flat 202 and the other to Flat 204) were considered to be adiabatic. This type of flat comprises more than half (58%) of flats located in the case study building, and hence justifies the selection as a typical flat. The methods to investigate the effect of flat

location in the case study building will be further discussed in Section 3.4.3. Each flat in the case study building had a floor area of 54.1m², volume of 131.3m³, and floor to ceiling height of 2.4m. They can be subsequently divided into five thermal zones, namely the living room (floor area of 26.34m²), bedroom (13.48m²), kitchen (4.73 m²), corridor (1.56 m²), and wetroom (1.44 m²) (Figure 3-8).

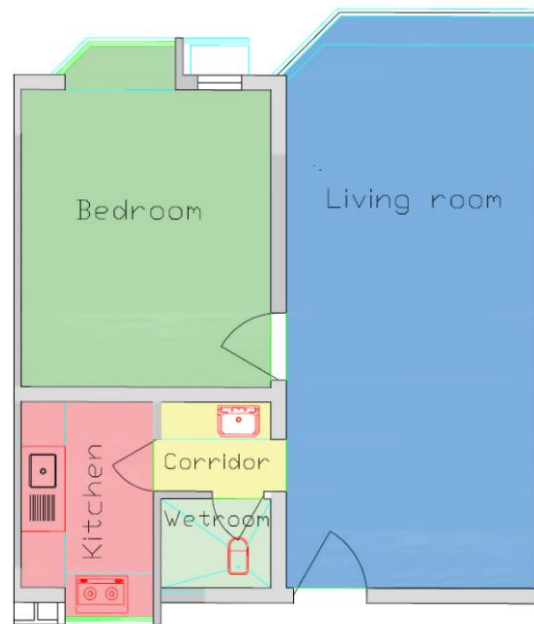


Figure 3-8: Floor plan of the case study flat.

3.4 Development of a dynamic thermal model

3.4.1 Selection of a dynamic thermal modelling tool

Dynamic thermal modelling can provide an overview of building performance for a typical year with accuracy, which is essential when assessing retrofit performance (Cook and Short, 2009). There are many widely used dynamic thermal simulation tools (e.g. EnergyPlus, TRNSYS, IES<VE> and DesignBuilder) in the literature (Crawley et al., 2006). EnergyPlus is chosen in this research because the heat balance simulation used is coupled with building system simulation, which results in more accurate space temperature predictions (Crawley et al., 2001). DesignBuilder is based on EnergyPlus for dynamic thermal simulation and has a more user-friendly interface, providing options for result visualisation and offers built-in template and datasets to

make the modelling process more accurate. The recent version v6.1.2.009 was used for DesignBuilder, and v8.9 was used for EnergyPlus.

3.4.2 Development of a dynamic thermal model for the case study flat

A dynamic thermal model with five thermal zones was developed for the case study flat (Figure 3-9), according to the exact dimensions of the floor plan described in Figure 3-8. The bedroom and living room were heated and cooled; on the other hand, other zones in the flat (kitchen, wetroom, and corridor) were not heated and cooled. All the thermal zones were separated by internal walls and doors (Figure 3-10).

The area and location of windows, external doors, and internal doors were modelled based on the floor plan of the case study flat. Internal partitions were modelled to separate the thermal zones, virtual partition was modelled to separate corridor and living room, as the corridor was not heated and cooled, whereas the living room was (Figure 3-10). Virtual partition acts as a partition between two zones which exists purely to sub-divide the space and has no corresponding wall in the actual building (DesignBuilder, 2018).

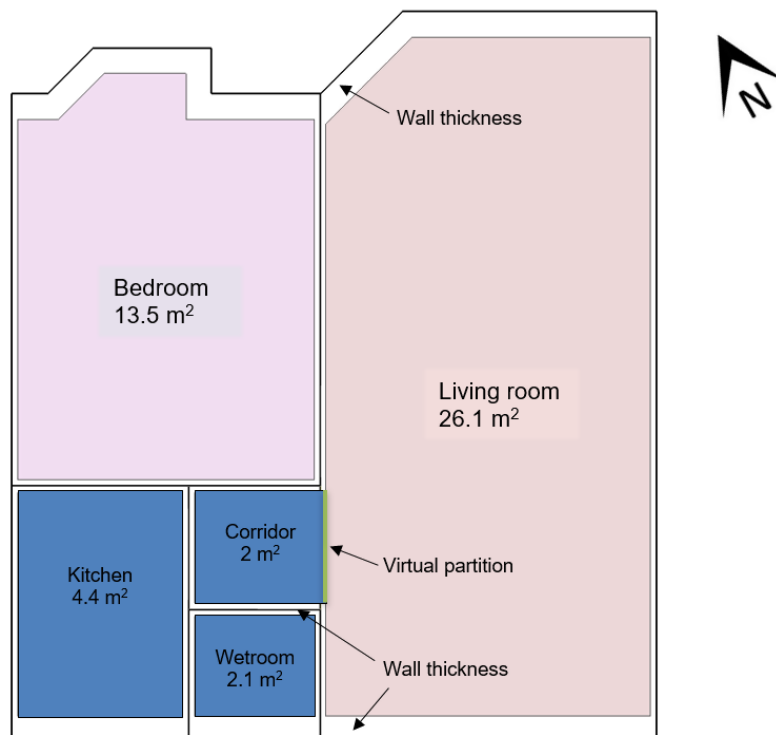


Figure 3-9: Plan view for the modelled case study flat in DesignBuilder.

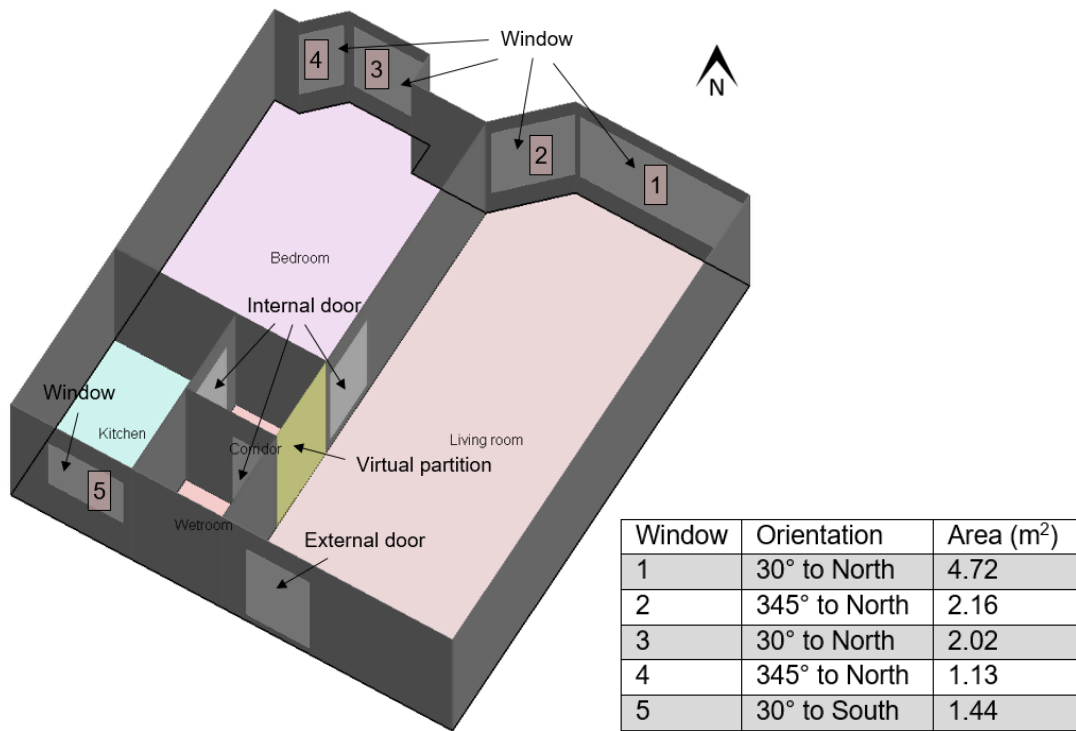


Figure 3-10: Axonometric view of the modelled case study flat in DesignBuilder with area and orientation of the windows modelled.

The simulated flat has a floor area of 49.3m², floor to ceiling height of 2.4m, volume of 118.3m³, and window to wall ratio of 43.8% for the main facade (windows 1 to 4 shown in Figure 3-10). The floor to floor height of the flat is 2.8m, and the floor to ceiling height is 2.4m with respect to the floor plan. The combined thickness of the internal floor and ceiling voids were 0.4m. Interestingly, the floor to floor height was frequently used in previous studies as an input for dynamic thermal simulation (Ma et al., 2015; Yao, 2012; W. Yu et al., 2015), as reviewed in Section 2.6.2.2, which potentially led to unreliable predictions. Thus, a floor to ceiling height of 2.4m is used for the purpose of this study. Note that the total floor area of the simulated flat (including internal and external walls) is 54.1m², but the lettable space is only 47.1 m², with a 13% reduction of floor area. Intriguingly, previous researchers often used flats' total floor area as an input for dynamic thermal simulation (Yao et al., 2018), which overpredicts the floor area of the flat modelled. Furthermore, in the case study flat, windowsill covers 2.2m² of floor area where heat exchange takes place. Hence, the windowsill needs to be included as part of the simulation floor area in the dynamic thermal model. As a result, by considering the lettable space

and windowsill, the simulated floor area of the flat increased from 47.1 m² to 49.3m² (Figure 3-11).

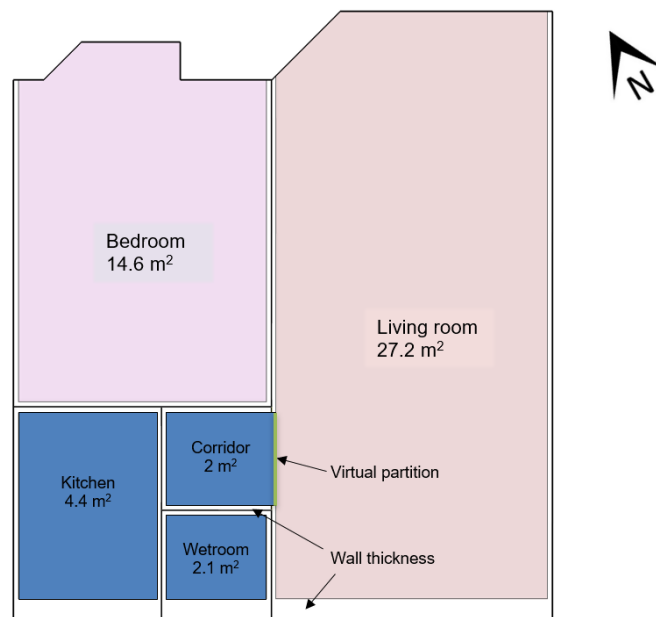


Figure 3-11: Plan view for the re-modelled case study flat in DesignBuilder considering windowsill.

3.4.3 Development of a dynamic thermal model for the case study building

To evaluate the effect of the flat location within the case study building on energy consumption, twelve types of flats were selected to be modelled out of 96 flats in the building. The six selected flats facing front were: a Middle floor flat on the Left facing Front [MLF]; a Middle floor flat on the Centre facing Front [MCF]; a Middle floor flat on the Right-facing Front [MRF]; a Top floor flat on the Left facing Front [TLF]; a Top floor flat on the Centre facing Front [TCF]; and a Top floor flat on the Right facing Front [TRF] (Figure 3-12). The six selected flats facing rear are: a Middle floor flat on the Left facing Rear [MLR]; a Middle floor flat on the Centre facing Rear [MCR]; a Middle floor flat on the Right facing Rear [MRR]; a Top floor flat on the Left facing Rear [TLR]; a Top floor flat on the Centre facing Rear [TCR]; a Top floor flat on the Right facing Rear [TRR] (Figure 3-13). The key flat of interest is the MCF. Other flats on the ground and first floor of the building were modelled as adiabatic blocks to simulate the effect of shading. The adiabatic block was assumed to have

conductivity of 0.38 W/mK, the specific heat of 1000 J/kgK and density of 1200 kg/m³.

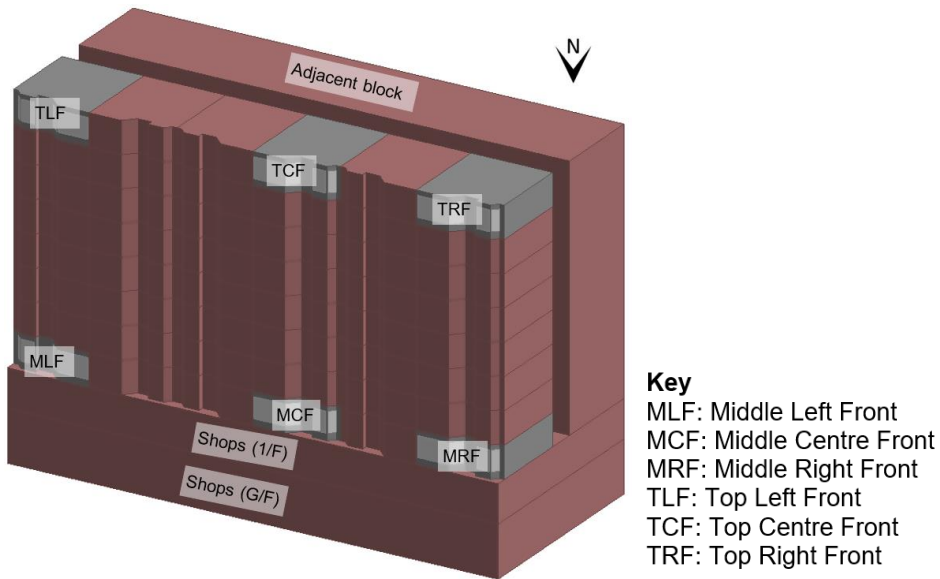


Figure 3-12: 3D representation of the studied building in the DTM software showing the location of studied flats facing front.

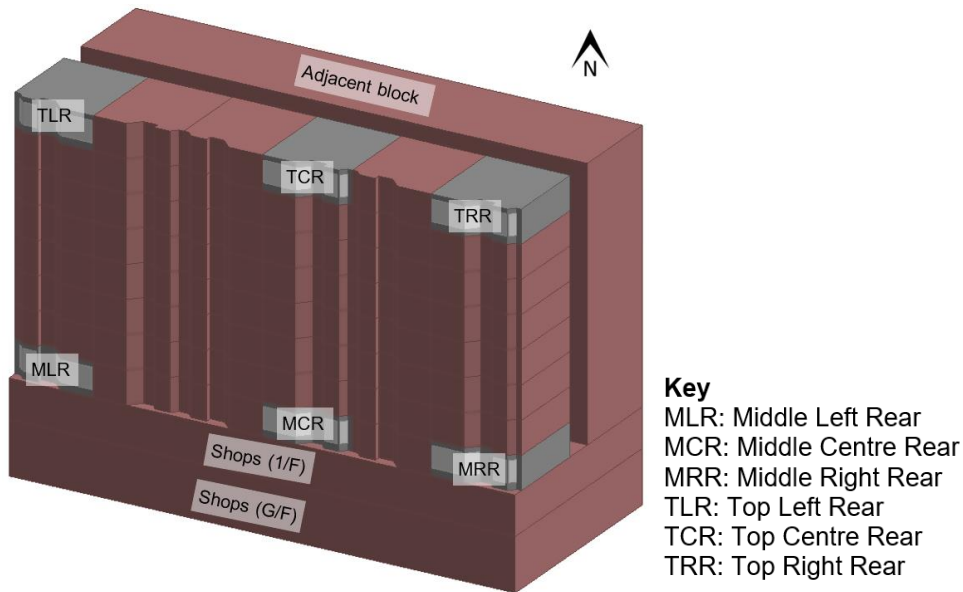


Figure 3-13: 3D representation of the studied building in the DTM software showing the location of studied flats facing rear.

3.4.4 Justification of building parameters used in the dynamic thermal model

Due to lack of construction information on the case-study building, the building parameters were defined empirically using information from other studies, referenced from Section 2.6, as well as information collected from the site visit. A summary of the selected building parameters is listed in (Table 3-5).

For the external wall construction, Section 2.6.3.2 reviewed that a brick or reinforced concrete layer for the middle layer are possible. Results indicated that eight modelling studies assumed brick construction as the middle layer (Cai et al., 2013; Chen et al., 2009; Liu et al., 2015; Xiaotong Wang et al., 2015; L. Xu et al., 2013; Yao et al., 2018; Yoshino et al., 2006; Yu et al., 2009b), whilst only two modelling studies assumed reinforced concrete construction (Short et al., 2018; Yu et al., 2008). Combined with the fact that Chen et al. (2010) reported that 80% of residential buildings in the HSCW zone built before implementation of building regulations had brick construction as the middle layer; it is evident to justify the assumption of brick construction as the middle layer. Liu et al. (2015) assumed the external walls have three layers: 0.02m cement mortar; a 0.24m lime-sand brick; and another 0.02m lime mortar layer interior finish. Lime mortar is used for the inner layer for aesthetics, as it has a white colour finish, and cement mortar is used for the outdoor layer as it has a grey colour finish. The thermo-physical parameters of the external wall construction of the case-study building were determined via the Chinese design standard (MOUHRD, 2010a) for three layers and a U-value of 2.3 W/m²K (Table 3-1).

Gao et al. (2014) assumed three layers for the internal walls and internal floors construction: 0.02m cement mortar, a 0.12m reinforced concrete layer, and another 0.02m cement mortar layer interior finish. For the case study building, the internal walls' and internal floors' construction was defined accordingly; the U-value of the internal wall was 2.83 W/m²K and the U-value of internal floors was 2.75 W/m²K (Table 3-2).

Concerning roof construction, Xiaotong Wang et al. (2015) assumed five layers for the roof construction: 0.02m cement mortar layer, a 2mm waterproof material layer, another 0.02m cement mortar layer, and a 0.15m reinforced concrete layer with 0.01m cement mortar layer interior finish. For the case-study building, the roof construction was defined accordingly, but with lime mortar for interior finish, roof construction had five layers and a total roof U-value of 3.45 W/m²K (Table 3-3).

With regards to window construction, single-glazed windows are assumed for residential buildings built before the implementation of building regulations (Ouyang et al., 2009; L. Xu et al., 2013; Yu et al., 2008). However, the window frames' material affects the thermal performance of windows, with over 80% of households in residential buildings containing steel or aluminium frames that are considered to have high conductivity (Ouyang et al., 2009b and Chen et al., 2009). Additionally, aluminium frames were observed during the site visit in the case study flat. Therefore, for the case-study building, the window construction was defined accordingly, with a U-value of the window of 5.8 W/m²K and g-value of the window of 0.87. The window was made of 3 mm single clear glazing with an aluminium frame with a thickness of 0.05m, conductivity of 160 W/mK, the specific heat of 880 J/kgK, and density of 2800 kg/m². In the living room, the area of windows was 6.88m², the area of window frames was 0.73m², and the window frame ratio was 10.6%. In the bedroom, the area of windows was 3.14m², the area of window frames was 0.52m², and the window frame ratio was 16.6%. In the kitchen, the area of the window was 1.44m², the area of window frames was 0.23m², and the window frame ratio was 16%. The percentage of window frames was 10% of the whole window (Figure 3-14).

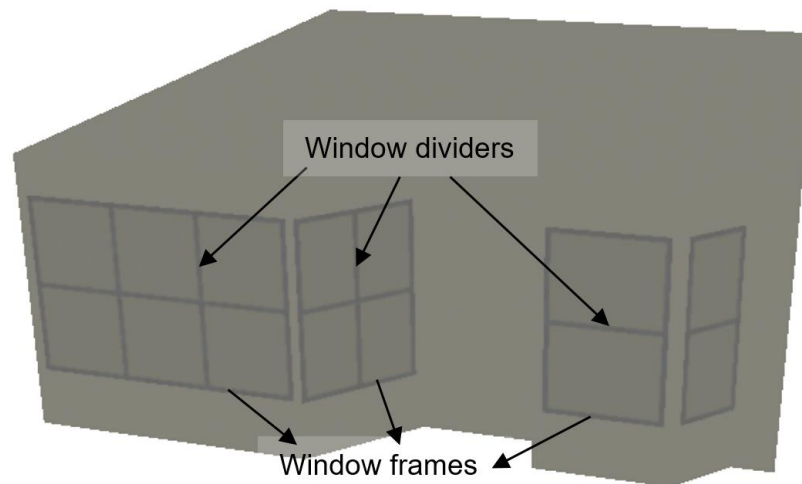


Figure 3-14: Window dividers and frames modelled for the flat, with divider and frame both 0.05m.

Air infiltration rate is a highly uncertain parameter, and the literature showed that residential buildings in the HSCW zone have either abysmal air infiltration performance with 2ach^{-1} (McNeil et al., 2016) or poor air infiltration performance with 1ach^{-1} (Yu et al., 2013, 2008). Accordingly, the air infiltration rate is assumed to be 1.5ach^{-1} , also, the air infiltration rate will be verified using measured data in Section 4.7.

As reported by the Chinese design standard (MOUHRD, 2010), heating COP is documented to be 1.9, and cooling COP is documented to be 2.3. This assumption was used by many researchers (Ge et al., 2018; X. Li et al., 2018; Liu et al., 2015; Xiaotong Wang et al., 2015; L. Xu et al., 2013; Yao et al., 2018; Yu et al., 2013, 2011, 2009a; Zhao et al., 2015), as reviewed in Section 2.6.4.3. Compellingly, 47% of households in China use split type air conditioner with a rated cooling capacity of below 4500W (H. Yu et al., 2015), the lowest energy efficiency grade of this type of air conditioner has a cooling COP of 2.6, based on Chinese energy efficiency standard for air conditioners (MOUHRD 2004). As air conditioners have an average life of 12 years (H. Yu et al., 2015), air conditioners used in current households in 2019 should comply with the standards set in 2004. In addition, split-type air conditioners often have a heating COP lower than cooling COP (Pulido-Arcas et al., 2016), where the ratio of heating COP to cooling COP is 83% from the Chinese design standard (MOHURD, 2010a). Thus, a heating COP of 2.2 and a cooling COP of 2.6 was assumed (Table 3-5).

Table 3-1: Building fabric parameters of external wall (Liu et al., 2015; MOHURD, 2010).

Layer	Component	Conductivity (W/mK)	Specific heat (J/kgK)	Density (kg/m ³)	Thickness (mm)
Outer	Cement mortar	0.93	1050	1800	20
Middle	Lime-sand brick	1.1	1050	1900	240
Inner	Lime mortar	0.81	1050	1600	20

Table 3-2: Building fabric parameters of internal wall and internal floor (Gou et al., 2018; MOUHRD, 2010).

Layer	Component	Conductivity (W/mK)	Specific heat (J/kgK)	Density (kg/m ³)	Thickness (mm)
Outer	Lime mortar	0.81	1050	1600	10
Middle	Reinforced concrete	1.74	920	2500	120
Inner	Lime mortar	0.81	1050	1600	10

Table 3-3: Building fabric parameters of roof (Xiaotong Wang et al., 2015; MOUHRD, 2010).

Layer	Component	Conductivity (W/mK)	Specific heat (J/kgK)	Density (kg/m ³)	Thickness (mm)
Outer	Cement mortar	0.93	1050	1800	20
Middle	Waterproof material	0.23	1620	1050	2
Middle	Cement mortar	0.93	1050	1800	20
Middle	Reinforced concrete	1.74	920	2500	150
Inner	Lime mortar	0.81	1050	1600	10

A heating set-point temperature of 18°C and cooling set-point temperature of 26°C are recommended in Chinese design standard (MOHURD, 2010a), and many researchers used these assumptions (X. Li et al., 2018; Ouyang et al., 2009; Pan et al., 2018; Xiaotong Wang et al., 2015; L. Xu et al., 2013; Yao et al., 2018; Yu et al., 2013, 2009a, 2008) as reported in Section 2.6.4.4. Yet, Section 2.4.4 reported that the acceptable temperature range of occupants in the HSCW zone was lower in winter and higher in summer, meaning the predicted energy consumption from previous studies could have been higher. Consequently, studies attempted to consider the acceptable temperature range of occupants by adjusting the heating set-point and cooling set-point (Short et al., 2018; Zhao et al., 2015). As an example, Short et al. (2018) assumed a heating set-point of 16.3°C and cooling set-point of 28.1°C based on the HSCW zone thermal comfort criteria developed by Li et al. (2011). The current study expands upon by reviewing a number of HSCW zone thermal comfort criteria in Section 2.4 (B. Li et al., 2018; Li et al., 2014, 2011; Liu et al., 2017; Yao et al., 2009). The most representative study was selected, where a

comprehensive survey with 6,000 samples in the HSCW zone was performed. Results showed that 90% of people felt satisfied (aPMV between -0.5 to +0.5) when indoor air temperature was 17.7°C in winter; in summer, 90% of people felt satisfied (aPMV between -0.5 to +0.5) when indoor air temperature was 27.9°C (B. Li et al., 2018), under the condition of a relative humidity of 70%. Therefore, a heating set-point temperature of 17.7°C and cooling set-point temperature of 27.9°C were selected for this research.

Chen et al. (2010) performed surveys to collect occupancy patterns. Results showed that the daily living room occupancy is 2 hours (in the afternoon for lunch) and 6 hours (in the evening after work). The daily bedroom occupancy is 7 hours (in midnight when sleeping), with a total daily occupancy of 15 hours. For the case-study building, the occupancy patterns were defined accordingly (Figure 3-16).

Three energy users were developed to represent the vast differences between energy usage by different types of occupants. Many studies (Li et al., 2019; W. Yu et al., 2015) assumed that AC systems operate during occupied hours when developing dynamic thermal models; however, other researchers reported survey data that suggested AC operating hours are less than the occupied hours (Chen et al., 2013, 2015; Yoshino et al., 2006). The typical AC operating hours are defined as medium energy user; low energy users simulate occupants who use less energy (with shorter AC operating hours); high energy users simulate occupants who use more energy (with longer AC operating hours). Previous researchers attempted to develop heating and cooling AC operating schedules to model the intermittent behaviour (Li et al., 2019; X. Li et al., 2018; Short et al., 2018; L. Xu et al., 2013; Yao et al., 2018). Nevertheless, the predicted energy consumption of these studies doubled the energy consumption collected from electricity meter readings (Chen et al., 2013, 2009, 2008; Gu et al., 2013; Hu et al., 2013; Ouyang et al., 2011, 2009) (see Section 2.6.4.2). This may be due to the over-estimation of the assumed AC operating hours of these modelling studies. Therefore, this study developed an approach by summarising previous research. Section 2.6.4.2 reported four studies which quantified the percentage of AC operation hourly for a typical day using surveys (Chen et al., 2011, 2010; Hu et al., 2013;

Yoshino et al., 2006); results were averaged (with a total of eight data points) and plotted in Figure 3-15.

The selection of AC heating and cooling operating hours are referenced in Figure 3-15; if the operating ratio is higher than 50%, then AC is operated for medium energy users. As an example, at 0:00, the operating ratio was 53% in summer and 20% in winter, thus cooling was operated from 0:00-1:00 but heating was not operated. As for medium energy users, in summer, the AC operating hours in the living room were 6 hours (over 50% operation ratio from 17:00-23:00) and 3 hours in the bedroom (over 50% operation ratio from 23:00-2:00). In winter, AC operating hours in the living room were 5 hours (over 50% operation ratio from 18:00-23:00) and 0 hours in the bedroom (operation ratio lower than 50% throughout the occupied period, 23:00-6:00). The same selection method is subsequently applied to low energy users (operation ratio over 65%) and high energy users (operation ratio over 20%) for this study.

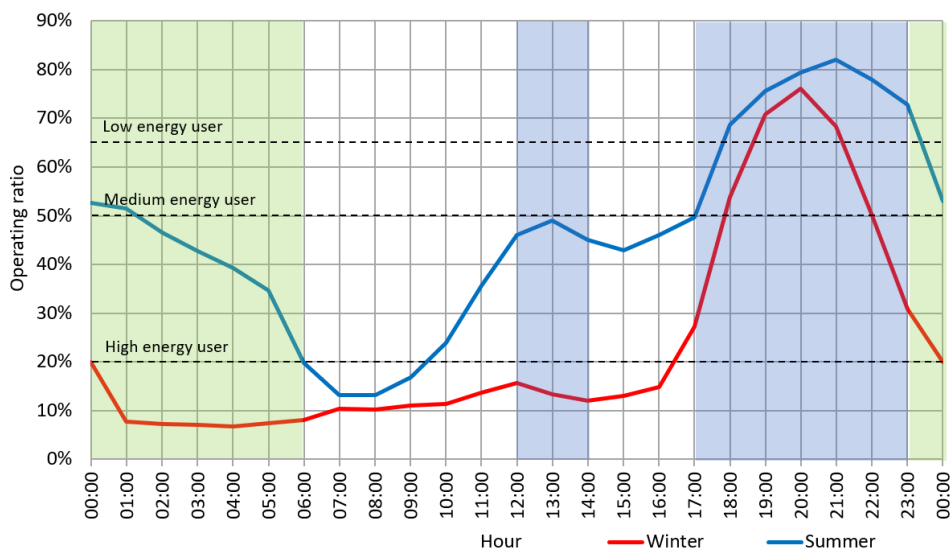


Figure 3-15: AC operating hours for the three energy users developed which represent households in the HSCW zone, where the blue-shaded area represents living room occupied hours and the green-shaded area represents bedroom occupied hours.

Considering low energy users, during the summer, the AC operating hours in the living room were 5 hours (over 65% operation ratio from 18:00-23:00) and 1 hour in the bedroom (over 65% operation ratio from 23:00-0:00). In winter, AC operating hours in the living room were 3 hours (over 65% operation ratio from 19:00-22:00) and 0 hours in the bedroom (operation ratio lower than 65% throughout the occupied period, 23:00-6:00). Regarding high energy users, in

summer, the AC operating hours in the living room were 8 hours (over 20% operation ratio from 12:00-14:00 and 17:00-23:00) and 7 hours in the bedroom (over 20% operation ratio from 23:00-6:00). In winter, AC operating hours in the living room were 6 hours (over 20% operation ratio from 17:00-23:00) and 2 hours in the bedroom (over 20% operation ratio from 23:00-0:00)

Internal heat gains are defined for the living spaces and consist of lighting gains, equipment gains, and people gains (6.6 W/m^2); their schedule has been defined according to Figure 3-16. Lighting gains is 6 W/m^2 with regards to Chinese lighting standard (MOHURD, 2013b). Equipment gains (e.g. Television, computer) is 4.3 W/m^2 based on Chinese design standard (MOHURD, 2010a). Metabolic rate per person is 90W in the bedroom and 123W in the living room (light office work/standing/walking), with a factor of 0.9 (Men = 1.0, women = 0.85, children = 0.75; ASHRAE, 2018). Regarding the average living area for one person being 29.3m^2 in Chongqing (NBS, 2017), two occupants were assumed in each flat, with heat gains of 6.6 W/m^2 . The red bar in Figure 3-16 shows the daily occupancy in the living room and bedroom. Lights are assumed to operate in the evening (17:00-23:00) and for one hour (23:00-24:00) before the occupants sleep in the bedroom (Figure 3-16, yellow bar). Equipment is assumed to have the same schedule as lighting (Figure 3-16). For other thermal zones, it is assumed that the kitchen was occupied between 18:00-19:00 for cooking, with internal heat gains assumed to be 10.8 W/m^2 according to Yu et al. (2008).

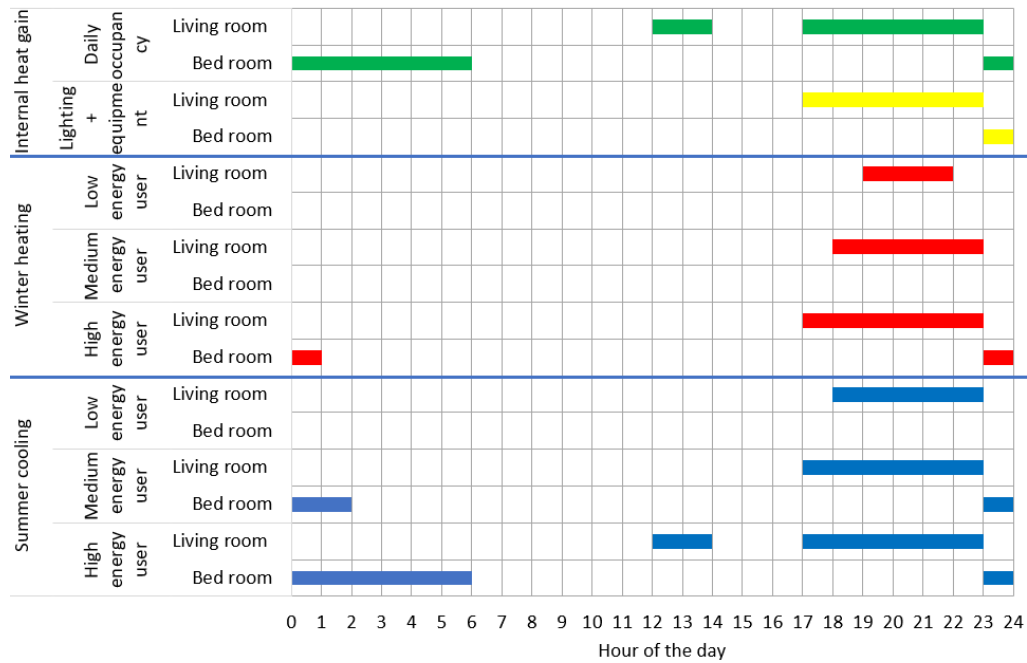


Figure 3-16: Operating schedule of cooling in summer (blue), heating in winter (red), daily occupancy (green) and lighting (yellow) for living room and bedroom.

During AC operation, the windows are assumed to be closed, and the selection is based on a survey study which reported that 82% of the occupants close the windows when they operate space heating and cooling (Hu et al., 2017). When AC is not operated, previous research found that 80% of households in the HSCW zone have windows opened when the outdoor temperature is over 17°C (Liu et al., 2018). Therefore, windows are opened when the outdoor temperature is above 17°C and windows are closed when outdoor temperature is below 17°C for the case study building. With regards to the ventilation rate during window operation, previous researchers assumed a ventilation rate of 0.5 to 1 ach⁻¹ (Gong et al., 2012; Ichinose et al., 2017; Zhao et al., 2015), but the selection in these studies lack a detailed justification. This study calculated the ventilation rate using equations from CIBSE, and the results are inputted to DesignBuilder using scheduled natural ventilation.

CIBSE guide A (CIBSE, 2015) suggested that the assumption that ventilation openings can be represented by orifice flow equations (equation 3-1), enables estimates to be made of ventilation rates using standard formulae for simple building layouts. For the case study flat, sliding windows are installed in the living room and bedroom on the main façade. Thus, standard formulae for estimating airflow rates for simple building layouts (openings on one side only)

was used, also, this study assumes only airflow rate due to wind alone is accounted. Subsequently, equation 3-2 was used to calculate the ventilation rates, the wind speed was determined by the average value of the hourly wind speed when windows are opened annually (Table 3-4). The area of the window in the living room is 6.88m² and bedroom is 3.14m². The maximum openable percentage for the living room is 38%, and the bedroom is 27% based on the floor plan drawings. Thus, the maximum openable area is 2.63 m² for living room and 0.84 m² for the bedroom. Using equation 3-2 (CIBSE, 2015) and 3-3, the air ventilation rate for the living room is 3.2 ach⁻¹ and bedroom is 1.9 ach⁻¹.

$$Q = C_d A \left(\frac{2\Delta p}{\rho} \right)^{1/2} \quad (3-1)$$

$$Q = 0.025 \times A \times u \quad (3-2)$$

$$n = \frac{3600Q}{V} \quad (3-3)$$

Where Q is the volumetric flow rate through the opening (m³/s), C_d is the discharge coefficient, A is the area of the opening (m²), u is the wind velocity, V is the volume of the flat (m³), Δp is the pressure difference across the opening (Pa), ρ is the density of air (kg/m³), and n is the air ventilation rate.

Scheduled natural ventilation was used to model air flows in this study, where a design air infiltration rate for each zone was input directly in air change rate per hour. The air flow is switched off if the zone air temperature falls below the ventilation setpoint temperature. Another option to model air flow through a building is to establish an Air Flow Network, which calculates the ventilation rate through the windows as a function of the pressure difference, using wind and stack pressure effects. Therefore, limitation of scheduled natural ventilation is the ventilation rate was calculated according to assumptions, i.e., equation 3-2 and 3-3.

Table 3-4: Frequency of wind speed annually in number of hours when windows are opened

Wind speed (m/s)	Frequency	Frequency (%)
0	990	26.5%
1	819	21.9%
2	1454	38.9%
3	372	9.9%
4	89	2.4%
5	6	0.2%
6	0	0.0%
7	10	0.3%

Table 3-5: Summary of modelling assumptions of the case study building.

Parameter	Value
U-value of external wall	2.3 W/m ² K
U-value of roof	3.45 W/m ² K
U-value of window	5.8 W/m ² K
g-value of window	0.87
U-value of door	2.82 W/m ² K
U-value of internal wall	2.83 W/m ² K
U-value of internal floor	2.75 W/m ² K
Air infiltration rate	1.5 ach ⁻¹
Overhang length	0 m
Heating COP	2.2
Cooling COP	2.6
Heating set-point	17.7°C
Cooling set-point	27.9°C
Heating AC operating hours (medium energy users)	5 hours (living room)
Cooling AC operating hours (medium energy users)	6 hours (living room), 3 hours (bedroom)
Lighting heat gain	6 W/m ²
Equipment heat gain	4.3 W/m ²
Occupant heat gain	6.6 W/m ²
Ventilation rate in summer	3.2 ach ⁻¹ (living room), 1.9 ach ⁻¹ (bedroom)

3.5 Selection of retrofit measures

There are many retrofit measures that can be applied to residential buildings, and are discussed in detail in Chapter 2: Literature review, Table 3-5 listed 26 possible retrofit measures that are commonly applied to residential buildings (Li et al., 2019; Ouyang et al., 2011, 2009; Short et al., 2018; Yao et al., 2018; Yu et al., 2008). Three criteria (no occupant control or automation, space heating and cooling energy saving, and feasibility to apply) were created for the purpose of this thesis, the retrofit measure will be selected if all the three requirements are fulfilled.

The first criterion was no occupant control or automation, where this research aims to select retrofit measures that do not require occupant control or installation of automated device in order to achieve energy savings. Therefore, six of the retrofit measures in Table 3-5 were discounted, the reasons are listed as follows:

- Installation of curtains (RM 12) reduce solar heat gain from windows in summer, and subsequently reduce space cooling energy; however, it is not investigated in this thesis as the occupants need to close the curtains during summertime to achieve energy savings.
- Installation of deployable shading, internal window blinds and external window shutters (RM 10, 11 and 21) require occupant control to achieve energy savings, thus, these retrofit measures are not selected in this thesis similar to the case above (installation of curtains).
- AC system control (RM 22) involve automate the operation of air conditioners, which can potentially reduce the AC operating hours of occupants; however, it is not investigated in this thesis as it involve installation of automated device to achieve energy savings.
- Installation of smart meters (RM 23) can potentially reduce energy consumption by adjust occupant behaviour; however, it is not investigated in this thesis as it involves occupant control to achieve energy savings.

The second criterion was to select retrofit measures that can achieve space heating and cooling energy saving. Hence, three of the retrofit measures in Table 3-6 were discounted, the reasons are listed as follows:

- Installation of central heating and cooling system (RM 14 and 15) will increase energy consumption by almost ten folded as reported in literature in Section 2.3.3, although it can improve thermal comfort significantly.
- Energy efficient lighting and appliances (RM 25), such as LED lighting, can reduce electricity consumption; but this measure is not considered in this thesis as it does not reduce space heating or cooling energy.

The final criterion was the feasibility to apply the retrofit measure in the context of urban residential buildings in the HSCW zone, using the case study building as an example. As a result, six retrofit measures were discounted, the reasons are listed as follows:

- The case study building is an eight storey residential building with 96 flats, installation of solar PV panels (RM 8) on the roof cannot provide enough electricity for all the 96 flats.
- Secondary glazing (RM 9) is discounted, as from the site visit, windows of the case study building are leaky and cracking, along with severe damp issues in the flats. Using double-glazed window can reduce air infiltration rate, improve damp issues, and reduce heat loss, where secondary glazing can only reduce heat loss.
- The case study building (a typical building in the HSCW zone), is a residential-commercial complex, with shops at the ground floor; thus, installation of ground floor insulation (RM 16) will not lead to energy savings of the flats.
- According to Yu et al., (2008), the energy saved by installation external wall, cavity wall and internal wall insulation are similar. However, it is difficult to apply cavity wall insulation (RM 18) to multi-storey buildings higher than 25mm; moreover, from the site visit, the flats have severe damp issues, the effects of internal wall insulation (RM 19) can be ruined. Thus, external wall insulation is selected in the HSCW zone.
- Similar to installation of solar PV panels (RM 8), installation of ground source heat pump (RM 24) cannot provide enough electricity for all the 96 flats.

As a result, the retrofit measures that fulfil the three criteria are external wall insulation, external wall insulation, roof insulation, double-glazed windows, air infiltration control, additional window overhang, enclosed communal staircase, energy-efficient AC, alternate thermal mass of building and change colour of external wall.

Table 3-6: Selection of retrofit measures from 26 commonly used strategies using three selection criteria (measures identified in the following sources (Gao et al., 2014; Ge et al., 2018; Gou et al., 2018; Liu et al., 2015; Ouyang et al., 2011, 2009; Pan et al., 2018; Xi Wang et al., 2015; Xiaotong Wang et al., 2015; Yao and Xu, 2010; Yu et al., 2008; Zhao et al., 2015))

Retrofit measures	Description	Non operable	energy saving	Feasibility to apply
1	External wall insulation	✓	✓	✓
2	Roof insulation	✓	✓	✓
3	Double-glazed windows	✓	✓	✓
4	Air infiltration control	✓	✓	✓
5	Additional window overhang	✓	✓	✓
6	Enclosed communal staircase	✓	✓	✓
7	Energy-efficient AC	✓	✓	✓
8	Solar PV panels	✓	✓	×
9	Secondary glazing	✓	✓	×
10	Deployable shading	×	✓	✓
11	Internal window blinds	×	✓	✓
12	Window curtain	×	✓	✓
13	Nigh time ventilation	×	✓	✓
14	Central heating system	✓	×	✓
15	Central cooling system (VRF)	✓	×	✓
16	Ground floor insulation	✓	✓	×
17	Wind catchers	✓	✓	×
18	Alternate thermal mass of building	✓	✓	✓
19	Internal wall insulation	✓	✓	×
20	Cavity wall insulation	✓	✓	×
21	External window shutters	×	✓	✓
22	AC system control	×	✓	✓
23	Install smart meter in flats	×	✓	✓
24	Ground source heat pump	✓	✓	×
25	Energy efficient lighting and appliances	✓	×	✓
26	External wall paint	✓	✓	✓

A monthly quasi-steady-state (steady state) model prescribed by ISO 13790:2008 was developed using excel spreadsheets, developed initially by Taylor (2016) to predict energy demand for houses in the UK. Details of development of the steady state model are further described in Section 4.2, the focus of this section is to use the steady state model to test which retrofit measures are sensitive to energy demand. For this preliminary test, flat MCF (oriented N30°E) and flat MCR (oriented S30°W) were tested, along with flat TCF to test the sensitivity of roof insulation.

Apply light colour paint to the surface of the external wall and roof, absorption coefficient for solar radiation changed from 0.6 to 0.4, leading to the reduction of g-value for opaque building elements in ISO 13790 from 0.012 to 0.008.

Table 3-7: Ten retrofit measures tested

Retrofit measure	Changes
External wall insulation	Reduce U-value of external wall from 2.3 to 1.0 W/m ² K
Roof insulation	Reduce U-value of roof from 3.45 to 1.5 W/m ² K
Double-glazed windows	Reduce U-value of window from 5.8 to 2.8 W/m ² K, and g-value of window from 0.87 to 0.47
Air infiltration control	Reduce air infiltration rate from 1.5 to 0.5 ach ⁻¹
Additional window overhang	Reduce external shading factor from 1 to 0.75
Enclosed communal staircase	Assume the external wall and window facing the outdoor communal corridor to be adiabatic
Energy-efficient AC	Increase heating COP from 2.2 to 3.1, cooling COP From 2.6 to 3.6
Alternate thermal mass of building	Change the internal heat capacity coefficient from 165 (medium weight) to 80 (light weight)
Change colour of external wall	Change absorption coefficient for solar radiation changed from 0.6 to 0.4

Local sensitivity analysis was used to evaluate the sensitivities of building fabric parameters from equation 3-4 (Lam and Hui, 1996).

$$SC = \frac{\Delta OP / (OP_B)}{\Delta IP / (IP_B)} \quad (\text{EQ 3-4})$$

where SC is the sensitivity coefficient; ΔIP , ΔOP are the changes in input and output; IP_B is the base case of input; and OP_B is the base case of the corresponding output.

The case study flat (flat MCF) with medium energy users, oriented N30°W, was used to test the sensitivity of the nine retrofit measures from Table 3-7

expect roof insulation. Note that roof insulation is only relevant to the top floor flats; accordingly, flat TCF was used to test the sensitivity of roof insulation. For flat MCF, the predicted base case heating energy consumption was 6.1 kWh/m² and cooling energy consumption was 14.0 kWh/m².

Predicted heating and cooling energy consumption are presented in Figure 3-18, all the results have $R^2 > 0.95$, which means the correlation are linear and the results from local sensitivity analysis are valid (Figure 3-18).

Enclosed communal staircase, assume the external wall facing the communal corridor adiabatic. Heating energy reduced by 20% and cooling energy reduced by 5.9%, and hence it is sensitive.

Sensitivity coefficient provides a measure on the importance of different building fabric parameters for heating, cooling and total energy consumption (Figure 3-17). Predicted sensitives of U-value of external wall, U-value of window, U-value of roof and air infiltration rate shows similar characteristics. Using U-value of external wall as an example, heating sensitivity index is positive, which means when U-value of external wall increases, heating energy consumption increases; cooling sensitivity index for U-value of external wall is close to zero, which means when U-value of external wall changes, cooling energy consumption remains constant. However, total sensitivity index for U-value of external wall is positive, which means when U-value of external wall increases, total energy consumption increases. Heating sensitivity index for external shading factor is negative, which means when external shading factor increases, heating energy consumption decreases; cooling sensitivity index for external shading factor is positive, which means when external shading factor increases, cooling energy consumption increases. However, total sensitivity index for external shading factor is positive, which means when external shading factor increases, total energy consumption decreases. Note that g-value of glazing shows similar characteristics with external shading factor. Both heating and cooling COP show a negative sensitivity index of -0.8, which means when heating COP increases, heating energy consumption decreases. Heating and cooling sensitivity index for internal heat capacity coefficient and g-value of external wall are insignificant (<0.05), which means these two retrofit

measures are not sensitive to energy consumption, and thus are discounted in this thesis. Therefore, seven retrofit measures are investigated in this thesis: external wall insulation, roof insulation, double-glazed windows, air infiltration control, additional window overhang, enclosed communal staircase, and energy-efficient AC.

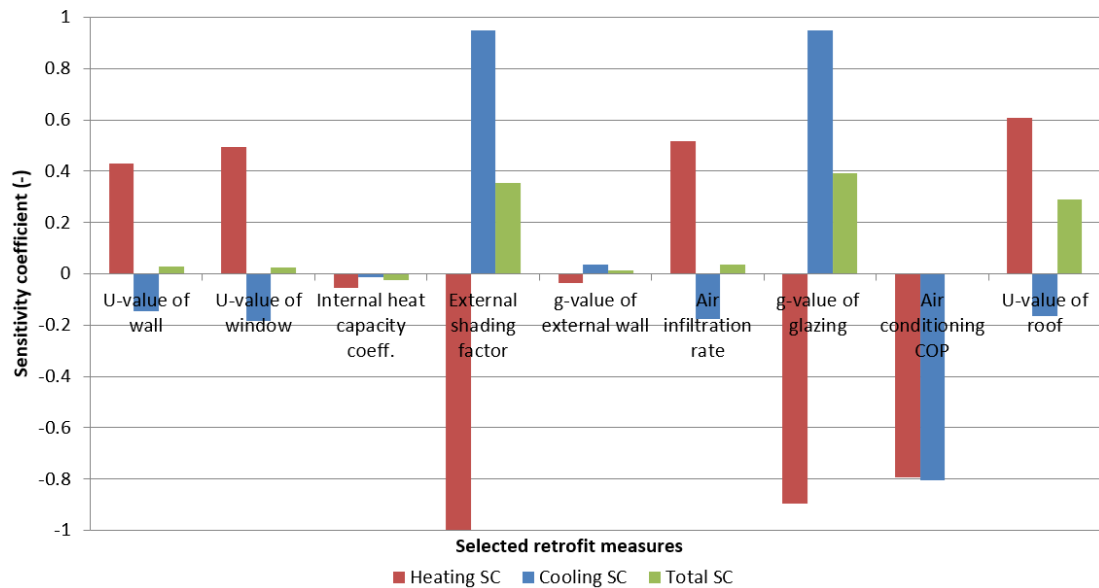


Figure 3-17: Sensitivity coefficient for selected retrofit measures using steady state model

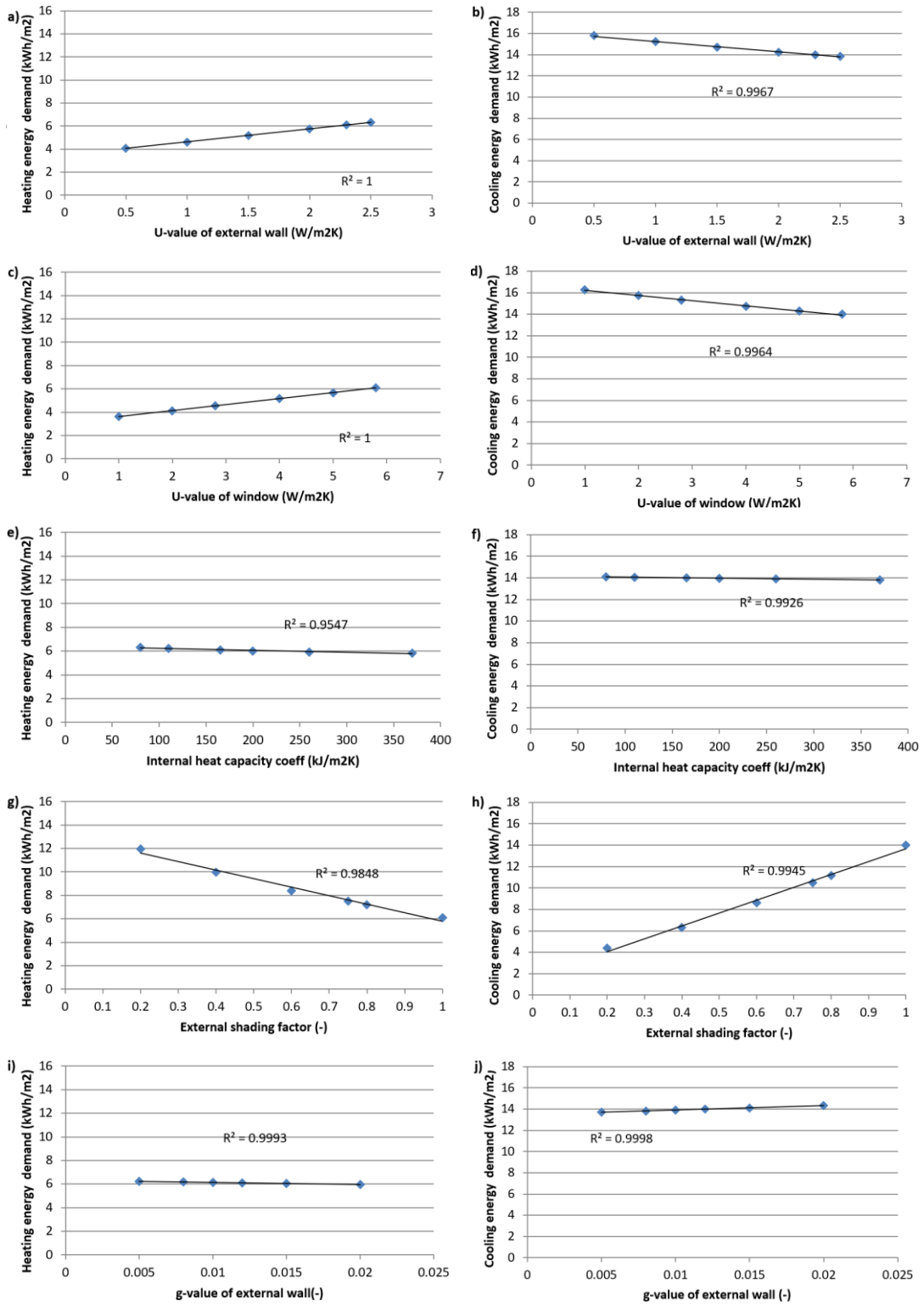


Figure 3-18: Correlation between heating and cooling energy consumption for a,b) U-value of external wall, c,d) U-value of window, e,f) internal heat capacity coefficient, g,h) external shading factor, i,j) g-value of external wall, k,l) air infiltration rate, m,n) g-value of glazing, o) heating COP, p) cooling COP and q,r) U-value of roof.

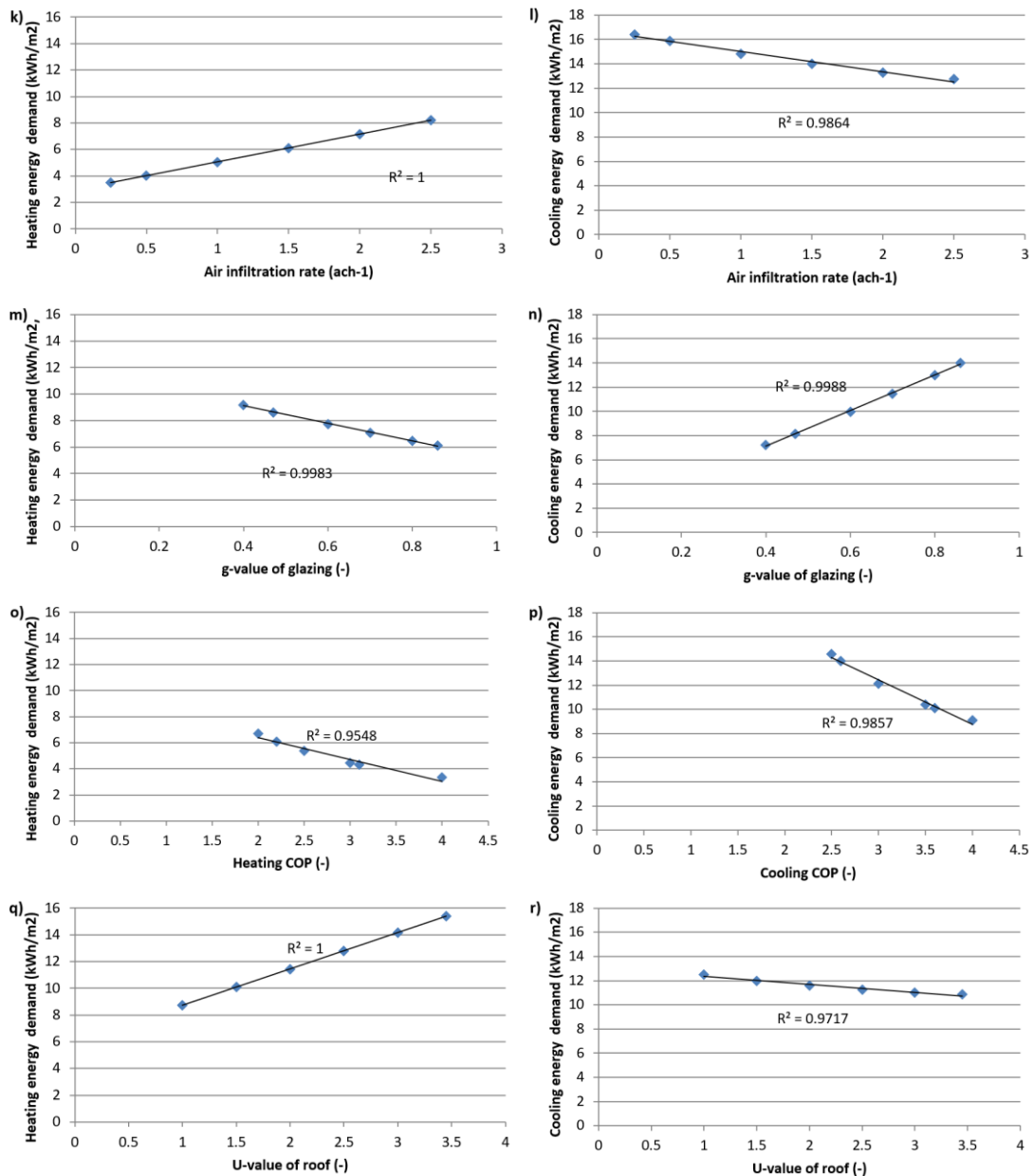


Figure 3-18, continued : Correlation between heating and cooling energy consumption for a,b) U-value of external wall, c,d) U-value of window, e,f) internal heat capacity coefficient, g,h) external shading factor, i,j) g-value of external wall, k,l) air infiltration rate, m,n) g-value of glazing, o) heating COP, p) cooling COP and q,r) U-value of roof.

3.6 Development of retrofit measures

Seven practical building retrofit measures were evaluated for the case study building: external wall insulation, roof insulation, change windows, air infiltration control, additional window overhang, enclosed communal staircase, and energy-efficient AC. A selection of retrofit options for each retrofit measure

is developed according to Section 2.7 reported in the literature review. The retrofit measures studied were summarised in Table 3-8.

Retrofit measure one: External wall insulation

The external wall is not insulated; it has a high U-value ($2.3 \text{ W/m}^2\text{K}$) which experiences heat loss in winter by transmission (Table 3-5). Section 2.7.2 reviewed that common insulation materials used in the HSCW zone are extruded polystyrene (XPS) and expanded polystyrene (EPS) insulation. EPS insulation was used in this study, as Liu et al. (2015) showed that EPS is the most economical external wall insulation material for residential buildings in the HSCW zone. The thermophysical parameters of EPS are referenced from Chinese design standard, with a conductivity of 0.03 W/mK , specific heat of 1380 J/kgK , and density of 30 kg/m^3 (MOUHRD, 2010a). Section 2.7.2 reported that popular insulation thicknesses employed for residential buildings in the HSCW zone are 10mm (Ouyang et al., 2009; Xiaotong Wang et al., 2015), 15mm (Ouyang et al., 2011), 20mm (Gao et al., 2014; Xi Wang et al., 2015; Yao and Xu, 2010; Zhao et al., 2015), 25mm (Yu et al., 2008), and 30mm (Ge et al., 2018; Pan et al., 2018). Accordingly, these five thicknesses of EPS insulation for external walls were tested.

Retrofit measure two: Roof insulation

The roof is not insulated; it has a high U-value ($3.45 \text{ W/m}^2\text{K}$) that experiences heat loss in winter by transmission, at the top flats specifically (Table 3-5). Similar to external wall insulation, EPS insulation was used in this study since Yu et al. (2011) revealed that EPS is the most economical roof insulation material for residential buildings in the HSCW zone. Section 2.7.3 reviewed that typical insulation thicknesses are 20mm (Xiaotong Wang et al., 2015), 30mm (Xi Wang et al., 2015), 40mm (Ouyang et al., 2011, 2009) and 50mm (Ge et al., 2018). As a result, these four types of EPS insulation for roofs were tested.

Retrofit measure three: Double-glazed windows

Single-glazed windows have a high U-value ($5.8 \text{ W/m}^2\text{K}$) and g-value (0.87), experiencing heat loss by transmission in winter which increases heating energy consumption, as well as solar heat gain in summer which increases

cooling energy consumption. Double-glazed windows reduce heat loss by transmission, whilst low emissivity (low-e) windows reduce solar heat gain. Section 2.7.5 reviewed types of double-glazed windows used for residential buildings in the HSCW zone, where the window construction reported has a considerable variation, with U-values ranging from 1.6 to 4.0 W/m²K and g-values of glazing ranging from 0.34 to 0.84. Interestingly, the selection of the combination of U-values and g-values of windows potentially does not exist. As an example, Gou et al. (2018) evaluated windows a combination of U-values and g-values as possible inputs to find the most efficient double-glazed windows, yet some of the input combinations potentially did not exist, which reduces the reliability of predictions. Hence, this study selected five types of double-glazed windows based on the Chinese design standard:

- 6mm outermost windowpane; a 12mm air gap; and 6mm innermost windowpane, aluminium window frames, with a U-value of 3.9 Wm²K and g-value 0.85, similar to the selection of Yao and Xu (2010; U-value of 3.6 Wm²K and g-value 0.84) or Fu et al. (2017; U-value of 4.0 Wm²K and g-value 0.75) ;
- 6mm outermost windowpane; a 12mm air gap; and 6mm innermost windowpane, uPVC window frames, with a U-value of 2.8 Wm²K and g-value 0.75, similar to the selection of Ouyang et al. (2009; U-value of 2.85 Wm²K and g-value 0.7)
- 6mm outermost windowpane with solar control; a 12mm air gap; and 6mm innermost windowpane, uPVC window frames, with a U-value of 2.8 Wm²K and g-value 0.54, similar to the selection of Zhao et al. (2015; U-value of 2.8 Wm²K and g-value 0.5);
- 6mm outermost low-e windowpane; a 12mm air gap; and 6mm innermost windowpane, uPVC window frames, with a U-value of 1.9 Wm²K and g-value 0.54, similar to the selection of Yang et al. (2015; U-value of 2.1 Wm²K and g-value 0.43) ;
- 6mm outermost low-e windowpane; a 12mm argon gap; and 6mm innermost windowpane, uPVC window frames, with a U-value of 1.5 Wm²K and g-value 0.54.

The material properties used for the windows tested above are discussed as follows: uPVC (polyvinyl chloride) window frames have conductivity of 0.17 W/mK, specific heat of 900 J/kgK, and density of 1390 kg/m³; Aluminium window frames have conductivity of 160 W/mK, specific heat of 880 J/kgK, and density of 2800 kg/m³; Low-e windowpanes have conductivity of 0.9 W/mK and solar transmittance of 0.6; and clear windowpanes have conductivity of 0.9 W/mK and solar transmittance of 0.775.

Retrofit measure four: Air infiltration control

Air infiltration rate is high (1.5 ach⁻¹); it increases heat loss by ventilation in winter (Table 3-5). There is no guidance on the required air infiltration rate in newly built Chinese dwellings. Nevertheless, Chinese ventilation standard defines a minimum ventilation rate of 0.5 ach⁻¹ base on the floor area of the case study flat. Furthermore, the literature review in Section 2.7.4 reported that an air infiltration rate of 0.44 to 1 ach⁻¹ is typical. Besides, Chinese design standard suggested an infiltration rate of 1.0 ach⁻¹ for new residential buildings (MOUHRD, 2010). Health problems occur when air infiltration rates are below 0.5 ach⁻¹, and mechanical ventilation would be required (Fu et al., 2017). Thus, three types of air infiltration rate were tested: 1.0 ach⁻¹, 0.7 ach⁻¹, and 0.5 ach⁻¹.

Retrofit measure five: Additional window overhang

There is no additional window overhang in the case study flat; installing window overhang can reduce solar gain of windows. Yao et al. (2018) tested window overhang length of 0.5m; Yu et al. (2008) tested overhang lengths from 0.3 to 1.5m, and found that the reduction diminished for overhang lengths of 1.0 to 1.5m. Thus, three types of horizontal overhang length were tested: 0.3m, 0.5m and 1.0m (Figure 3-19).

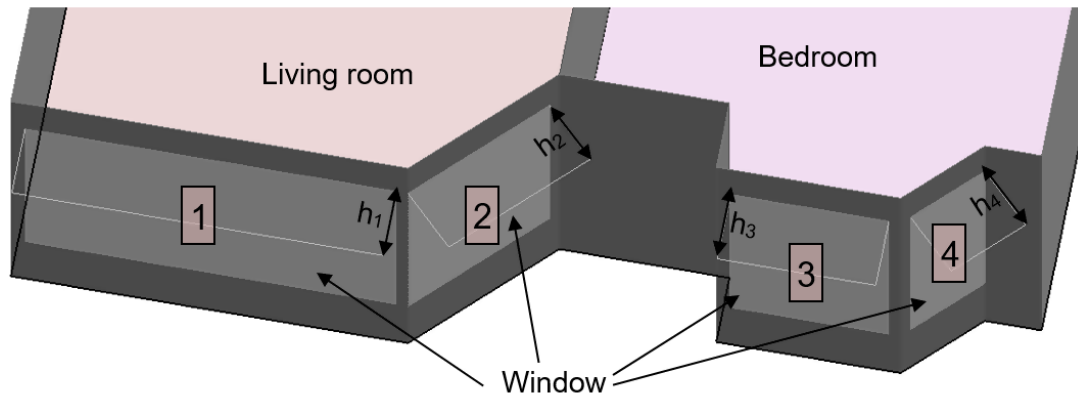


Figure 3-19: Location of proposed additional window overhang installed in the case study flat, where h refers to the overhang length.

Retrofit measure six: Enclosed communal staircase

The communal staircase of the case study flat is exposed to outdoor conditions; this is typical of multi-storey buildings in the representative area. Nevertheless, previous findings often did not consider enclosing communal staircases as a retrofit measure, since they develop simplified box models (Gong et al., 2012) or only study a middle floor flat in a building (Yao et al., 2018) to reduce simulation time. The effect of an enclosed communal staircase has been studied twice (Ouyang et al., 2011, 2009); however, they simply included the floor area of the communal corridor to the simulated floor area of the flat for the dynamic thermal model, which reduced the reliability of predicted energy savings. Therefore, in this study, the outdoor communal corridor in the case study building is converted from “with outdoor condition” (Figure 3-20a) to “fully indoor condition with external walls and window” (Figure 3-20b). In other words, the three communal staircases located inside the outdoor communal corridor are removed, and each floor has a communal corridor with fully indoor condition (Figure 3-20b). Additionally, an extension is proposed in the left where a new enclosed communal staircase is built and the entrance staircase from the ground floor to the second floor is removed. To simplify the modelling process, only the enclosed communal corridor was modelled (Figure 3-20b). Subsequently, three combinations of material to enclose the communal staircase were tested:

- Exclusion of windows and external walls without insulation
- Single-glazed windows and external walls without insulation
- Double-glazed windows and external walls with insulation

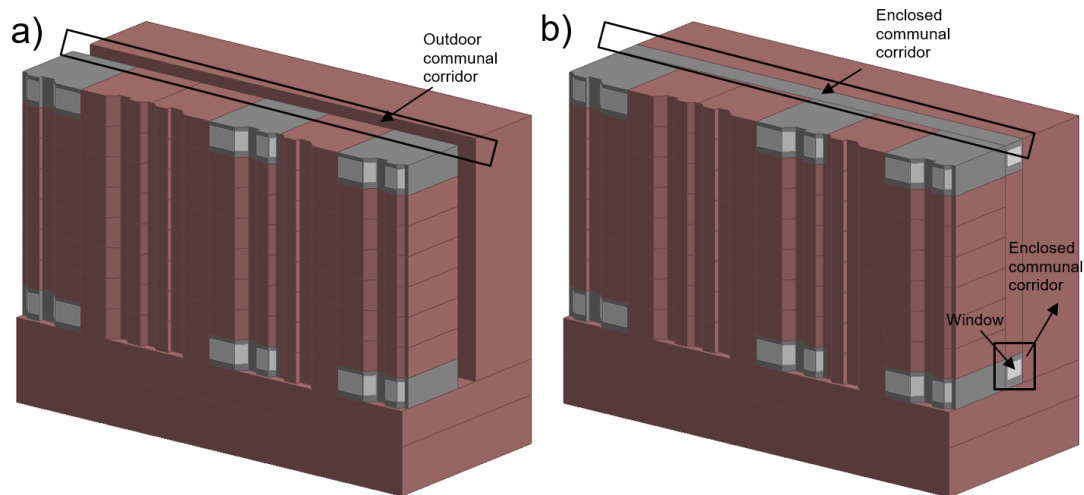


Figure 3-20: DTM of the case study building, a) before enclosed communal staircase, b) after enclosed communal staircase in axonometric view

As for the two cases with windows, the windows are assumed to be opened when the outdoor temperature is above 17°C, similar to the case study building defined in Section 3.4.4.

CIBSE guide A (CIBSE, 2015) suggested that the assumption that ventilation openings can be represented by orifice flow equations (equation 3-1), enables estimates to be made of ventilation rates using standard formulae for simple building layouts. For the enclosed communal corridor, two windows are installed in the two ends of the corridor (Figure 3-20b). Thus, standard formulae for estimating airflow rates for simple building layouts (openings on opposite sides) was used; also, this study assumes only airflow rate due to wind alone is accounted. Subsequently, equation 3-5 and 3-6 was used to calculate the ventilation rates, the wind speed (u) was determined by the average value of the hourly wind speed when windows are opened annually (Table 3-4). ΔC_p was 0.8, referenced from wind pressure coefficient data from CIBSE guide A (CIBSE, 2015), under the category of low-rise building, length to width ratio of 2:1 and surrounded by obstructions equivalent to half the height of the building. The area of the window in the two ends of the corridor are 1.5m² each, with maximum openable percentage of 70%. Thus, using equation 3-5 and 3-6, the calculated ventilation rate is 6.2 ach⁻¹.

$$Q = C_d A_w u (\Delta C_p)^{0.5} \quad (3-5)$$

$$\frac{1}{A_w^2} = \frac{1}{A_1^2} + \frac{1}{A_2^2} \quad (3-6)$$

Where Q is the volumetric flow rate through the opening (m³/s), C_d is the discharge coefficient assumed to be 0.61 (CIBSE, 2015), A₁ is the area of the opening on one side and A₂ is the area of the opening on the other side (m²), u is the wind velocity and ΔC_p is the pressure difference across the opening (Pa).

Retrofit measure seven: Energy-efficient AC

From Section 2.7.7, a few researchers evaluated energy-efficient AC together with other passive retrofit measures. As an example, Gong et al. (2012) tested AC with heating and cooling COP of 3.1; similarly Gao et al. (2014) tested AC with heating COP of 3.5 and cooling COP of 3.3; and Li et al. (2019) tested AC with heating and cooling COP of 3.5 and 4.0. However, split-type air conditioners often have a heating COP lower than cooling COP (Pulido-Arcas et al., 2016), where the ratio of heating COP to cooling COP is 83% from the Chinese design standard (MOHURD, 2010a). Therefore, the cooling COP of air conditioners was selected from the Chinese regulation governing the energy efficiency grades for room air conditioners issued in 2010 (MOHURD, 2010c). As the heating COP for the heat pump component is not defined in the regulation, heating COP was assumed to be 82.6% of cooling COP (section 3.3.3). Three variations of energy efficient AC according to energy efficiency grades (Grades 1, 2, and 3) of the Chinese standard (MOHURD, 2010c) were tested.

- Increase heating COP from 2.2 to 2.7, cooling COP from 2.6 to 3.2;
- Increase heating COP from 2.2 to 2.9, cooling COP from 2.6 to 3.4;
- Increase heating COP from 2.2 to 3.1, cooling COP from 2.6 to 3.6;

Table 3-8: Summary of selected seven practical retrofit measures.

Retrofit measure	Pre-retrofit	Retrofit measure	Post-retrofit
1.External wall insulation	U-value = 2.3 W/m ² K	10mm EPS insulation	U-value = 1.3 W/m ² K
		15mm EPS insulation	U-value = 1.07 W/m ² K
		20mm EPS insulation	U-value = 0.91 W/m ² K
		25mm EPS insulation	U-value = 0.79 W/m ² K
		30mm EPS insulation	U-value = 0.7 W/m ² K
2.Roof insulation	U-value = 3.45 W/m ² K	20mm EPS insulation	U-value = 1.31 W/m ² K
		30mm EPS insulation	U-value = 0.99 W/m ² K
		40mm EPS insulation	U-value = 0.79 W/m ² K
		50mm EPS insulation	U-value = 0.65 W/m ² K
3.Double-glazed windows	U-value = 5.88 W/m ² K, g-value = 0.87	Double glazed window without solar control, aluminium frame	U-value = 3.9 W/m ² K, g-value = 0.85
		Double glazed window without solar control, uPVC frame	U-value = 2.8 W/m ² K, g-value = 0.75
		Double glazed window with solar control, uPVC frame	U-value = 2.8 W/m ² K, g-value = 0.54
		Double glazed low-e window, uPVC frame	U-value = 1.9 W/m ² K, g-value = 0.54
		Double glazed argon filled low-e window, uPVC frame	U-value = 1.5 W/m ² K, g-value = 0.54
4.Air infiltration control	Air infiltration rate = 1.5 ach ⁻¹	Reduce air infiltration rate by 0.5 ach ⁻¹	Air infiltration rate = 1.0 ach ⁻¹
		Reduce air infiltration rate by 0.8 ach ⁻¹	Air infiltration rate = 0.7 ach ⁻¹
		Reduce air infiltration rate by 1.0 ach ⁻¹	Air infiltration rate = 0.5 ach ⁻¹
5.Additional window overhang	Overhang length = 0 m	Horizontal overhang with length of 0.3m	Overhang length = 0.3m
		Horizontal overhang with length of 0.5m	Overhang length = 0.5m
		Horizontal overhang with length of 1.0m	Overhang length = 1.0m
6.Enclosed communal staircase	Staircase outdoor conditions	Exclusion of windows and external walls without insulation	
		Single-glazed windows and external wall without insulation	
		Double-glazed windows and external wall with insulation	
7.Energy-efficient AC	Heating COP = 2.2, Cooling COP = 2.6	Energy efficiency Grade 3 air conditioner	Heating COP = 2.7, Cooling COP = 3.2
		Energy efficiency Grade 2 air conditioner	Heating COP = 2.9, Cooling COP = 3.4
		Energy efficiency Grade 1 air conditioner	Heating COP = 3.1, Cooling COP = 3.6

3.7 Metered annual electricity consumption: Secondary data

As reviewed in Section 2.5.3, it is critical to compare predicted energy consumption with measured data to increase the reliability of results. In the UK, annual electricity consumption collected from electricity meters is available from the government website down to post-code level (HM Government, 2019a). As an example, postcode AB10 1BB has six meters with an annual electricity consumption of 17000 kWh in 2017. The measured building energy consumption in the case of UK buildings can thus be easily deduced.

However, government statistics of this kind are vastly insufficient in China. The only data available for the public in Chongqing is from the Municipal Bureau of Statistics of Chongqing, (2019), which reported merely a single figure with a total annual household electricity consumption of 205.04 million MWh in 2018. This value applies to all households in Chongqing municipality, with a 34 million population and roughly 12.7 million households. Therefore, the estimated household electricity consumption per household is 1614 kWh. There is not any available data on the household electricity consumption by end-use, therefore the proportion of heating and cooling energy consumption is not available from the statistical data.

Due to the lack of data regarding household electricity consumption by end-use from government reports, many researchers collected monthly electricity bills from energy suppliers throughout a year for a number of residential flats in different cities in the HSCW zone (Chen et al., 2013, 2009, 2008; Gu et al., 2013; Hu et al., 2013; Ouyang et al., 2011, 2009). Subsequently, the space heating and cooling energy consumption can be predicted by subtracting the average monthly use in non-space heating and cooling period (autumn and spring) from the monthly total energy consumption in space heating and cooling period (summer and winter). This method was commonly used by researchers in China to estimate the space heating and cooling energy consumption from energy (electricity) meters and was reviewed in Section 2.6.4.2. Performing a secondary analysis using existing data can have the electricity meter readings collected throughout multiple cities in the HSCW zone, where households with different AC operating schedules were covered.

Twelve studies were reviewed in section 2.6.4.2; seven studies (Chen et al., 2013, 2009, 2008; Gu et al., 2013; Hu et al., 2013; Ouyang et al., 2011, 2009) are selected for the purpose of this research as they contain both heating and cooling energy consumption (Table 3-9). Note that these are average values because data from a number of households were collected. The annual space heating and cooling energy consumption ranged from 7.67 to 16.92 kWh/m². The percentage of electricity consumption attributed to heating and cooling ranged from 17 to 53%. Subsequently, information from Table 3-9 will be used in this thesis to compare the DTM predictions with measured data.

Table 3-9: Heating and cooling electricity (energy) consumption collected from electricity meters from various households in residential buildings.

Heating energy consumption (kWh/m ²)	Cooling energy consumption (kWh/m ²)	Total energy consumption (kWh/m ²)	% of heating and cooling to household energy consumption	Number of households	Reference
2.2	9.32	11.52	30%	204	(Chen et al., 2009)
3.65	10.32	13.97	53%	18	(Ouyang et al., 2011)
5.51	6.77	12.28	34%	22	(Ouyang et al., 2009)
7.42	9.5	16.92	17%	26	(Gu et al., 2013)
/	/	7.67	30%	241	(Chen et al., 2013)
4.30	8.27	12.57	26%	261	(Hu et al., 2013)
3.99	6.83	10.82	28%	60	(Chen et al., 2008)

It is worthwhile to note that the space heating and cooling energy consumption in the HSCW zone is much lower than other developed countries. For example, the annual household space heating energy consumption in the UK was 17449 kWh from the English housing survey (HM Government, 2017). In Osaka, Japan, the space cooling electricity consumption ranged from 1000 to 7000 kWh, in which the usage in the lower band exceeds the average usage in the HSCW zone. In Chongqing, China, the average household electricity consumption (including space heating, space cooling, lighting, and equipment) is 1614 kWh.

A national standard for energy consumption of buildings was issued in 2016 in China (MOUHRD, 2016). This includes a suggested threshold of annual electricity consumption of 3100 kWh per household in the HSCW zone, including lighting and equipment electricity consumption. As the mean percentage of heating and cooling to household electricity consumption is 30% from the seven studies in Table 3-6; hence, the threshold of space heating and

cooling energy consumption was 930 kWh per household, this data was used in the city scale study in Chapter 6.

The metered annual electricity consumption was published a decade previously (from 2008 to 2013). However, annual weather and climate is changing, and thus the measured annual heating and cooling electricity consumption can be higher or lower, depending on the outdoor air temperature. Subsequently, the monthly average outdoor air temperature of year 2000, 2005, 2010, 2015 and 2019 are compared (Table 3-10), collected from an online database (Karl, 2019) ; results showed that the average annual outdoor air temperature was the highest for year 2010 (19.3°C) and lowest for year 2000 and 2019 (18.7°C). Furthermore, winter was warmer in 2010 comparing to 2019, i.e., outdoor air temperature in January 2010 was 9.8°C, higher than January 2019 (8.1°C); summer was warmer in 2010 comparing to 2019, i.e., outdoor air temperature in July 2010 was 30.1°C, higher than July 2019 (27.4°C). Also, note that this thesis uses Typical Meteorological Year (TMY) for Chongqing via EnergyPlus website, the average annual outdoor temperature for year 2000, 2005, 2010, 2015 and 2019 are higher than the TMY weather data by 0.6°C. Thus, this thesis may over-predict heating energy consumption, and under-predict cooling energy consumption. Moreover, if the measurement is repeated in 2019, the metered annual electricity consumption can be lower in winter and higher in summer.

Table 3-10: Monthly and annual average outdoor air temperature for year 2000, 2005, 2010, 2015, 2019 and TMY weather data used in DesignBuilder

Year	2000	2005	2010	2015	2019	Average (2000, 2005, 2010, 2015, 2019)	TMY weather data
Jan	8.1	7.9	9.8	9.2	8.1	8.6	8.1
Feb	9.6	9.9	11.4	11.2	10.5	10.5	10.3
Mar	14.7	14.3	15.4	16.1	14.0	14.9	13.7
Apr	18.5	20.9	17.4	19.3	21.5	19.5	18.7
May	24.4	23.3	22.7	22.6	20.8	22.8	23.0
Jun	25.8	27.4	24.9	25.5	24.6	25.6	25.2
Jul	29.0	30.2	30.1	27.9	27.4	28.9	28.1
Aug	27.3	26.5	29.5	27.4	30.2	28.2	27.6
Sep	23.8	27.1	25.7	23.7	24.4	24.9	24.2
Oct	20.2	18.3	19.3	20.2	18.8	19.4	18.4
Nov	13.4	14.9	15.3	15.7	13.6	14.6	14.6
Dec	10.1	9.1	9.5	9.2	10.1	9.6	9.3
Average	18.7	19.2	19.3	19.0	18.7	19.0	18.4

3.8 Summary

This chapter provided an overview of the methods regarding calibrating a dynamic thermal model for a typical flat, evaluation of energy saving retrofits for a typical residential building, and large-scale residential energy saving retrofits. Moreover, it described the selection of the representative area in Chongqing, as well as the selection of a typical residential building as a case study in the representative area. Subsequently, the geometries and justification of building parameters (summarised in Table 3-5) of the case study building were discussed. After that, a selection of options for each retrofit measure were described (summarised in Table 3-8). Finally, measured data, i.e., metered annual electricity consumption gathered from previous researchers, was used to compare with the DTM predictions presented in this thesis.

Chapter 4 : Calibration of a dynamic thermal model for building fabric parameters in a case study flat

4.1 Introduction

In this Chapter, Objective 2 is addressed. The aim of this chapter is to create a calibrated dynamic thermal model of the case study flat (Section 3.4.2), using predicted sensitivity of energy demand of various building fabrics and measured data, in order to increase the reliability of model predictions when evaluating energy saving retrofits in Chapter 5.

Section 4.2 presents the development of a steady-state model (hereby steady-state model). A steady-state model prescribed by ISO 13790:2008 was developed initially by Taylor (2016), using excel spreadsheets, to predict energy demand for houses in the UK. The procedures to adjust input parameters in the steady-state model to fit the context of the HSCW zone is described.

Section 4.3 presents the comparison of the predicted monthly energy demand using the steady-state model and a dynamic thermal model.

Section 4.4 presents the predicted sensitivities of building fabric parameters, which include external wall construction, window construction and air infiltration rate; these parameters are altered within a range developed supported from Section 2.6.3. Subsequently, the sensitivity of annual energy demand of these building fabric parameters can be used to inform the model calibration process in Section 4.7.

Section 4.5 presents the procedure and analysis of the measured indoor air parameters in the case study flat. This included indoor air temperature, indoor relative humidity, indoor air velocity, and external wall temperature of the

outdoor communal corridor, which were all measured in five-minute intervals for a one-week period in April.

Section 4.6 presents the development of a customised weather file for the one-week measurement period. Parameters required in the weather files include dry bulb temperature, wet bulb temperature, atmospheric pressure, relative humidity, dew point temperature, global solar radiation, normal solar radiation, diffuse solar radiation, and wind speed. These were all measured in five-minute intervals for a one-week period in April on site.

Section 4.7 presents the model calibration process. To start with, a sensitivity analysis was conducted to evaluate the effects of three building fabric parameters selected in Section 4.4, where these parameters were altered using the same range developed in Section 4.4, to improve the model's predictions of indoor air temperatures. Subsequently, the parameters which had the potential to improve the predictions of indoor air temperature were adjusted in the base case model to generate a refined model. Finally, the sensitivity was compared with the annual sensitivity of energy demand in Section 4.4.

4.2 Development of a steady-state model

This section explores the procedures of developing a steady-state model for the context of the HSCW zone. Although dynamic thermal simulation is selected as the building energy modelling tool in this thesis, the development of steady-state models is a reliable way to collect valuable insights on building performance and energy demand through a preliminary study when input data are not sufficient for the development of DTM.

The main inputs required in the steady-state model are transmission and ventilation parameters, heat gains from internal heat sources, solar parameters, climate data, description of the building and building components; system and use, and comfort requirements (set-point temperature and ventilation rates). The main output of the model is annual and monthly energy demand for space heating and cooling. In order to calculate the heating energy

demand and cooling energy demand in the monthly steady-state model, the heat transfer and heat gain are calculated (Equations 4-1 and 4-2). The model was developed using excel spreadsheets (Figure 4-1) by using equations listed in Appendix A.

$$Q_{H,nd} = Q_{H,ht} - \eta_{H,gn} Q_{gn} \quad (4-1)$$

$$Q_{C,nd} = Q_{gn} - \eta_{C,ls} Q_{C,ht} \quad (4-2)$$

where $Q_{H,nd}$ is the heating energy demand, $Q_{H,ht}$ is the total heat transfer for heating, $\eta_{H,gn}$ is the dimensionless gain utilisation factor, Q_{gn} is the total heat gain, $Q_{C,nd}$ is the cooling energy demand, $\eta_{C,ls}$ is the dimensionless loss utilisation factor, $Q_{C,ht}$ is the total heat transfer for cooling.

Input & results		Area / m ²		U-value / Wm ⁻² K ⁻¹		Proportion of area facing...		Window		Wall		Heating & ventilation		Value		Units	
7	Dimensions & U-values	60	120	2	2.5	West	0.19	0.19	0.19	0.19	Air changes per hour	3.00	h ⁻¹				
8	Ground	25	25	4.8	4.8	South-west	0.31	0.31	0.31	0.31	Time fraction when ventilation present	0.417	-				
9	Wall	60	60	1.9	1.9	South	0.00	0.00	0.00	0.00	Fraction of hours in a week with normal heating set-point	0.298	-				
10	Window	120	120	2	2	South-east	0.19	0.19	0.19	0.19	Fraction of days in a week with normal cooling set-point	0.714	-				
11	Roof	25	25	4.8	4.8	East	0.31	0.31	0.31	0.31	Heating set-point temperature	21.0	°C				
12	Total floor area	60	60	1.9	1.9	North-east, North and North-west	0.31	0.31	0.31	0.31	Cooling set-point temperature	26.0	°C				
13	Ceiling height	2.5	2.5	m	m						Internal gains per unit floor area	20	Wm ⁻²				
14	Internal heat capacity coefficient	110	110	kJk ⁻¹ m ⁻²	kJk ⁻¹ m ⁻²												
15	Location	Midlands	Midlands														
16	Standard calculation or test	Std calc	Std calc														
17	Results: calculated energy demand																
23	Heating energy demand	kWh	4376	3557	2416	1616	1372	628	610	666	956	1531	2495	3872	24496		
24	Cooling energy demand	kWh	17	17	24	31	43	53	65	58	43	29	19	17	414		
25	Heating energy demand per unit floor area	kWh/m ²	36.5	29.6	20.1	15.1	11.4	6.9	5.1	5.5	8.0	12.8	20.8	32.3	204.1		
26	Cooling energy demand per unit floor area	kWh/m ²	0.1	0.1	0.2	0.3	0.4	0.4	0.5	0.5	0.4	0.2	0.2	0.1	3.5		

Figure 4-1: Monthly quasi-steady-state calculation spreadsheet (BSI, 2008).

The case study flat was used as an example in this thesis to develop a steady-state model. All the thermal zones modelled in the case study flat were assumed to have the same heating and cooling set-point temperature, as well as the same heating, cooling and internal heat gains schedules. Furthermore, the internal floor, internal ceiling, and also two internal walls connected to the nearby flats were considered to be adiabatic.

Note that the comparison was performed based on the condition of a single-thermal zone model, which is different from the multi-zone model as described in Section 3.4.2. This was to avoid increasing the complexity of the calculations with regard to the steady-state model (which is intended as a simplified model). Therefore, the case study flat modelled, described in Section 3.4.2, was assumed to have the same heating and cooling set-point temperature, as well

as the same heating, cooling, and internal heat gains schedules. Moreover, the ISO13790:2008 standard does not recommend the application of developing a multi-zone coupling steady-state model, since it ignores the dynamic interactions between the thermal zones, thereby making the direct comparison with dynamic thermal models not entirely realistic.

Seven input parameters need to be specified in the steady-state model which are different to the inputs for the representative dynamic thermal (see section 3.4): internal heat capacity coefficient, external shading factor, internal shading factor, reduction factor intermittent heating, reduction factor for intermittent cooling, fraction with ventilation, and window to wall ratio. Thermal mass of a building can be determined by the value of internal heat capacity coefficient (BSI, 2008); medium weight construction was assumed according to external wall construction (internal heat capacity coefficient is 165 kJ/m²K according to ISO 13790:2008). External shading factor represents a reduction of incident solar radiation due to permanent shading of the surface from other buildings, trees and overhangs; no external shading was assumed for the case study flat (section 3.4). Internal shading factor represents the reduction of incident solar radiation due to shading of the surface from blinds; no internal shading was assumed for the case study flat (section 3.4).

Considering medium energy users (see Section 3.3.5 and Figure 3-16), heating was operated for 5 hours and cooling was operated for 6 hours in the living room. In the bedroom, cooling was operated for 3 hours. To account for intermittent heating and cooling in the steady-state model, reduction factor for intermittent heating (equation 4-3) and reduction factor for intermittent cooling (equation 4-4) were calculated. Heating energy demand was calculated by multiplying the reduction factor for intermittent heating by energy required for continuous heating. Cooling energy demand was calculated by multiplying the reduction factor for intermittent cooling by energy required for continuous cooling.

$$a_{H,red} = 1 - 3(\tau_{H,0}/\tau)\gamma_H(1 - f_{H,hr}) \quad (4-3)$$

$$a_{C,red} = 1 - 3(\tau_{C,0}/\tau)\gamma_C(1 - f_{C,hr}) \quad (4-4)$$

Where $a_{H,red}$ is the dimensionless reduction factor for intermittent heating, $f_{H,hr}$ is the fraction of the number of hours in the week with a normal heating set-point (17.7°C for this study), $a_{C,red}$ is the dimensionless reduction factor for intermittent cooling, $f_{C,hr}$ is the fraction of the number of days in the week with a normal cooling set-point (27.9°C for this study).

Table 4-1 summarised the input parameters used to develop a base case model using the steady-state model of the case study flat with a floor area of 49.3m².

Table 4-1: Input parameters used for the steady-state model.

Parameter	Base case
Simulated floor area (m ²)	49.3
External wall area (m ²)	9.74 (Front), 16.59 (Rear)
External window area (m ²)	8.42 (Front), 1.49 (Rear)
U-value of external wall (W/m ² K)	2.3
U-value of window (W/m ² K)	5.8
g-value of window (-)	0.87
Air infiltration rate (ach ⁻¹)	1.5
Internal heat capacity coefficient (kJ/m ² K)	165
External shading factor (-)	1.0
Internal shading factor (-)	1.0
Frame area fraction (-)	0.1
Fraction of the number of hours in the week with a normal heating set-point (-)	0.21
Fraction of the number of days in the week with a normal cooling set-point (-)	1
Heating set-point temperature (°C)	17.7
Cooling set-point temperature (°C)	27.9
Internal heat gain (W/m ²)	4.9

In the steady-state model, vertical solar radiation data (beam plus diffuse solar irradiance) from eight building orientations (west, south-west, south, south-east, east, north-east, north and north-west) are required. In the UK, vertical solar radiation data for different orientations can be collected from CIBSE Guide J (CIBSE, 2002). However, this data does not exist in the context of China. A fully prescribed hourly horizontal-vertical translation method was provided by Duffie and Beckman in their book *Solar Engineering of Thermal Processes* (Duffie and Beckman, 2013). Subsequently, an excel spreadsheet based on the hourly horizontal-vertical translation method to predict vertical solar radiation data from different building orientations was developed (Jack,

2015). Equation 4-5 lists the correlation to calculate the total (beam plus diffuse) solar irradiance reaching vertical facade in eight orientations.

$$I_T = (I_b + I_d A_i) R_b + I_d (1 - A_i) \left(1 + \frac{\cos \beta}{2}\right) \left(1 + f \sin^3 \left(\frac{\beta}{2}\right)\right) + I \rho_g \left(1 - \frac{\cos \beta}{2}\right) \quad (4-5)$$

where I_T is the total solar irradiance, I_b is the beam irradiance, I_d is the diffuse irradiance, A_i is the anisotropy index, R_b is the geometric factor, β is the orientation of the surface (90° for vertical walls), f is the modulating factor, and ρ_g is the ground reflectance, and the value is assumed to be 0.2 (Jack 2015). All the preliminary calculations to derive total solar irradiance are further discussed in Appendix B.

An empirically defined correlation, which expressed 1st to 4th-degree polynomials by relating diffuse fraction k_d (the ratio of diffuse to global solar radiation) with the clearness index k_t (ratio of the global to extra-terrestrial solar radiation), was developed. There are many correlations to derive diffuse fraction k_d (the ratio of diffuse to global solar radiation) according to the literature, which affects the accuracy of predicted vertical solar radiation. Duffie and Beckman recommend using Erbs et al.'s (1983) correlation (Equation 4-6; Duffie and Beckman, 2013). However, these models need to account for local climatic differences (Jacovides et al., 2006). In China, an empirically defined correlation was derived to estimate the diffuse fraction k_d (Equation 4-7; Jin et al., 2004). The correlation was validated with actual measurements from two meteorological stations in Chongqing.

$$k_d = 1 - 0.09k_T \quad \text{for } k_T \leq 0.22$$

$$k_d = 0.9511 - 0.16049k_T + 4.388k_T^2 - 16.638k_T^3 + 12.336k_T^4 \quad \text{for } 0.22 < k_T \leq 0.8$$

$$k_d = 0.165 \quad \text{for } k_T > 0.8 \quad (4-6)$$

$$k_d = 0.987 \quad \text{for } k_T < 0.2$$

$$k_d = 1.292 - 1.447k_t \quad \text{for } 0.2 \leq k_T < 0.75$$

$$k_d = 0.209 \quad \text{for } k_t > 0.75 \quad (4-7)$$

Solar radiation data in London were collected from CIBSE guide J. The data showed that west and east orientations have similar solar radiation throughout the year. In winter, solar radiation in south orientation doubled that in west and east orientations. In summer, solar radiation in south, west, and east orientations are similar (Figure 4-2). When using the horizontal-vertical translation method to predict vertical solar radiation, solar radiation in west orientation was slightly lower (20 W/m²) than east orientation in summer; north orientation was also predicted in the model, and it showed lower (40 W/m²) solar radiation in summer when compared to east and south orientations. Similar to CIBSE guide J, solar radiation in south orientation doubled that in west, east, and north orientation in winter (Figure 4-3). Thus, the horizontal-vertical translation method showed good accuracy in predicting vertical solar radiation.

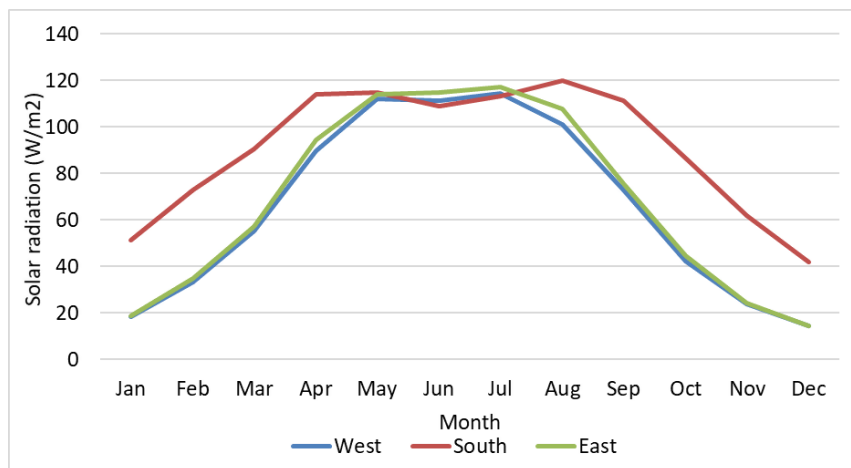


Figure 4-2: Vertical solar radiation in London collected from CIBSE guide J.

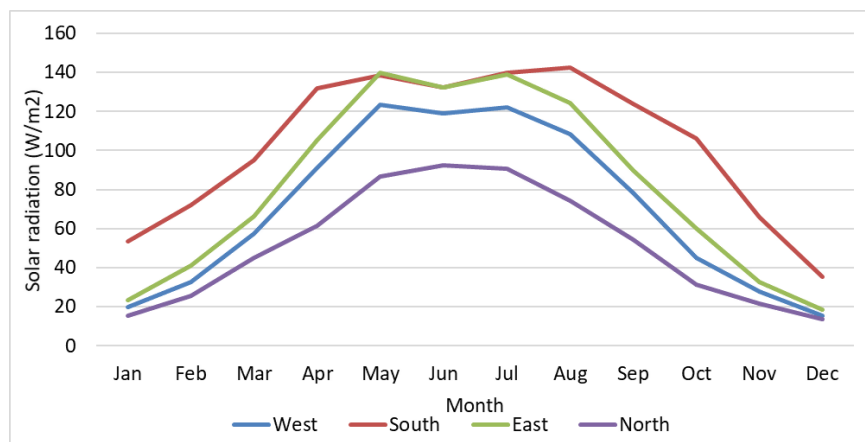


Figure 4-3: Vertical solar radiation in London predicted from horizontal-vertical translation method.

Subsequently, the model was used to predict vertical solar radiation in Chongqing. In London, latitude is 51.5°N and longitude is -0.13°E. In Chongqing, latitude is 29.4°N and longitude is 106.9°E. Monthly outdoor temperature in Chongqing is higher than in London throughout the year (Figure 4-4). Solar radiation in west, south, east and north orientations are similar (30 W/m²) in winter. Interestingly, the solar intensity is similar to London despite the low latitude in Chongqing. This is reflected from the average annual solar radiation is around 1000 kWh/m² in Chongqing with the intensity is similar to the UK (Muneer et al., 2012). In summer, the solar intensity increased by four times (90W/m²) compare to winter for west, south and north orientation. For east orientation, the solar intensity is the highest (120W/m²). Therefore, more solar heat gain can be obtained from the east-facing façade in summer in Chongqing (Figure 4-5).

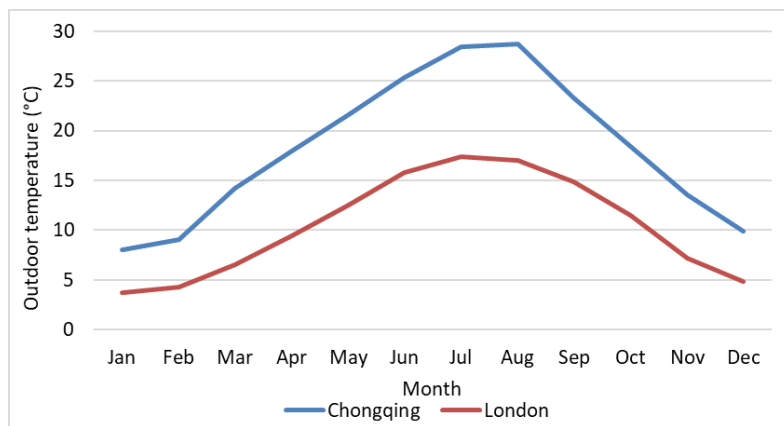


Figure 4-4: Monthly outdoor temperature in Chongqing and London.

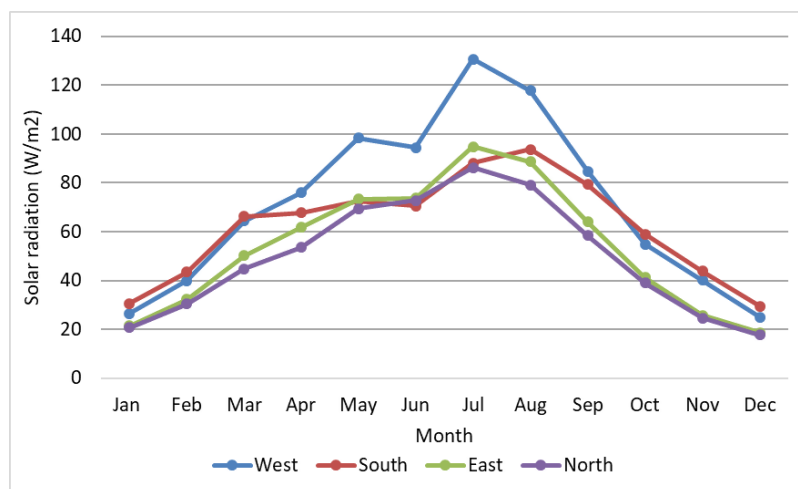


Figure 4-5: Vertical solar radiation in Chongqing predicted from horizontal-vertical translation method.

4.3 Comparison of predicted energy demand using single-zone steady-state and dynamic thermal models

The single-zone steady state model was used to perform preliminary calculations to inform decisions and select inputs for the DTM. The prediction from the steady-state model was compared with dynamic thermal simulation (which performs simulation in hourly interval), so as to predict the validity of the prediction from the steady-state model. Subsequently, a single-zone DTM (with the same building parameters as the steady-state model) was developed for the purpose of this research to compare the results with the steady-state model.

With respect to annual heating energy demand, the steady-state model predicted 660 kWh and the DTM predicted 672 kWh, with a 2% difference. For annual cooling energy demand, the steady-state model predicted 1793 kWh and the DTM predicted 1555 kWh, with a 16% difference. When considering annual total energy demand, the steady-state model predicted 2450 kWh and the DTM predicted 2220 kWh, with a 10% difference. Nonetheless, when looking at the difference regarding monthly energy demand, the difference was 18% for heating in February, while the difference was more considerable for cooling, with a 40% difference in May (Figure 4-6). Results seem to suggest that the prediction of the steady-state model is more reliable for heating than cooling. A possible reason is that the reduction factor for intermittent cooling is defined as a fraction of the number of days in the week with a normal cooling set-point. As for the case study flat, the reduction factor for intermittent cooling is one, since the same cooling set-point was used throughout a week. Using a similar method, the fraction of the number of days in a week is also one for low and high energy users defined in Section 3.4.4; this will lead to the same predicted cooling energy demand for the three energy users, which is, in fact, not the case.

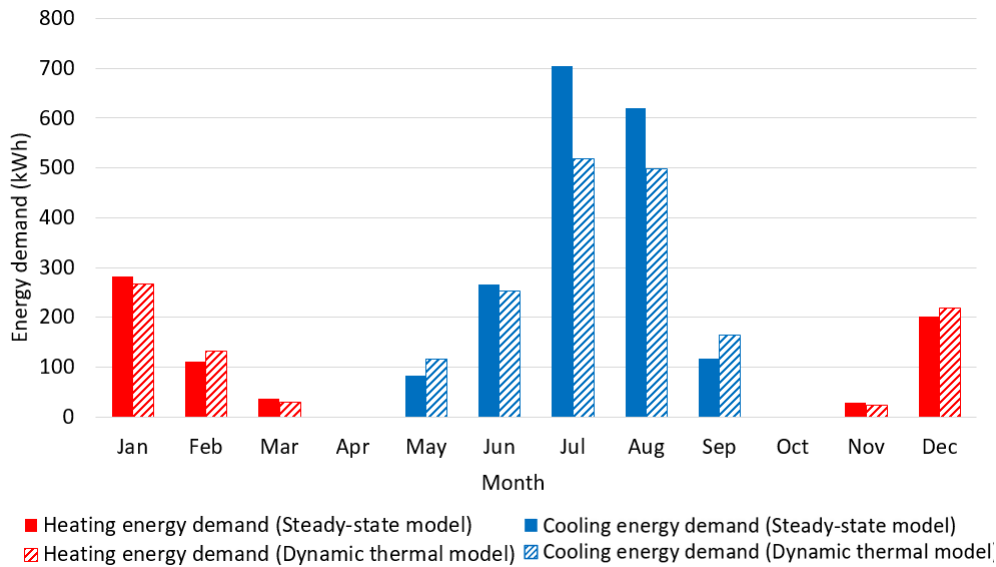


Figure 4-6: Comparison of predicted monthly heating and cooling energy demand with a single-zone steady-state model and dynamic thermal model for the case study flat.

4.4 Sensitivity analysis of building fabric parameters

4.4.1 Development of uncertainty bands for building fabric parameters

Building fabric parameters used in the development of a dynamic thermal model were justified in Section 3.4.4. Yet, identifying the influence of building fabric parameters on energy demand helps to pinpoint the sensitive parameters, where the sensitive parameters can be focused on when calibrating a dynamic thermal model in Section 4.7. The sensitivity of four building fabric parameters (U-value of external wall, U-value of window, g-value of window and air infiltration rate) are investigated in this thesis; as from literature review (Section 2.6.3), these parameters have a large variation, and thus may influence the predicted energy demand.

Differential sensitivity analysis was selected to evaluate the sensitivity of building fabric parameters, it involved varying one input for each simulation whilst the remaining inputs stay fixed at the base case (Lomas and Eppel, 1992). Sensitivity of three building fabric input parameters (external wall construction, window construction, and air infiltration rate) were evaluated. Low band (minimum value) was defined as the effect of a decrease in the input parameter value. High band (maximum value) was defined as the effect of an increase in the input parameter value. All input parameters were varied from

the base case values to the high band and to the low band (Table 4-2). Heating and cooling energy demand was predicted for each case, with a total of six simulations. The justification of the selected parameters from Table 4-2 are as follows:

- External walls construction: U-value of external wall varied from 1.97 to 3.67 W/m²K base on 15 studies (see Section 2.6.3.2). A U-value of 1.96 W/m²K represents solid clay brick construction (Yao et al., 2018), whilst a U-value of 3.67 W/m²K represents reinforced concrete construction (Yu et al., 2018).
- Windows construction: U-value of windows varied from 4.7 to 6.4 W/m²K and g-value of windows varied from 0.7 to 0.95 based on 15 studies (Table 2-19). A U-value of 4.7 W/m²K and g-value of 0.7 represents 5 mm single-glazed windows with plastic window frame (Ouyang et al., 2009); whereas a U-value of 6.4 W/m²K and g-value of 0.95 represents 3 mm single-glazed windows with steel frame (McNeil et al., 2016).
- Air infiltration rate: Air infiltration rate varied from 1 to 2 ach⁻¹ (see Section 2.6.3.6). An air infiltration rate of 1 ach⁻¹ represents residential buildings with poor air infiltration performance (Yu et al., 2013); where an infiltration rate of 2 ach⁻¹ represents residential buildings very poor air infiltration performance (McNeil et al., 2016).

Table 4-2: Uncertainty bands for building fabric parameters.

Building fabric parameter	Base case	Low band	High band
U-value of external wall (W/m ² K)	2.3	1.97	3.67
U-value of windows (W/m ² K)	5.8	4.7	6.4
g-value of windows (-)	0.87	0.7	0.95
Air infiltration rate (ach ⁻¹)	1.5	1	2

The percentage change of energy consumption due to uncertainty (P_l and P_h) respective to the base case was calculated by equation 4-8 for the low band and equation 4-9 for high band.

$$P_l = \frac{E_b - E_l}{E_b} \times 100\% \quad (4-8)$$

$$P_h = \frac{E_b - E_h}{E_b} \times 100\% \quad (4-9)$$

Where P_l and P_h are the percentage of energy reduction caused by uncertainty of low band and high band of building fabric parameters, defined in Table 4-2. E_l , E_b and E_h are the energy consumption for low band, base case and high band building fabric parameters respectively.

4.4.2 Predicted sensitivities of building fabric parameters using a steady-state model

In Figure 4-7, the blue bar represents the percentage change of energy demand due to a decrease in input parameter value (low band); whereas the red bar represents the percentage change of energy demand due to an increase in input parameter value (high band). As an example, reductions of the U-value of the external wall (from 2.3 to 1.97 W/m²K) led to a heating energy demand reduction of 6% (low band) but cooling energy demand increased by 2%. Meanwhile, the increase of the U-value of the external wall (from 2.3 to 3.67 W/m²K) caused a heating energy demand increase of 26% (high band), but a cooling energy demand reduction of 7%. As for other building fabric parameters, the uncertainty (blue and red bar) of air infiltration rate is the highest (35%) when considering heating energy demand, with external wall construction ranking second (32%). Considering cooling energy demand, uncertainty of window construction (25%) is the highest, with air infiltration rate ranking second (11%). However, when considering total energy demand, uncertainty of window construction (15%) is the highest, because the predicted cooling energy demand is more substantial than heating energy demand according to Section 4.3 (Figure 4-7).

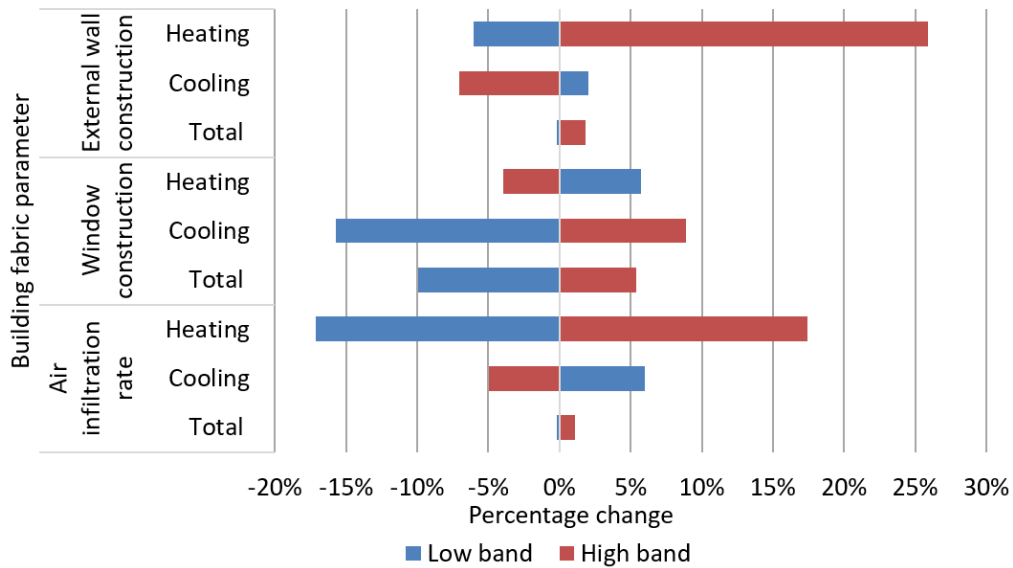


Figure 4-7: Bar chart representation of sensitivity of building fabric parameters using steady-state model. Blue bar represents the percentage change of energy demand due to a decrease in input parameter value (low band). Red bar represents the percentage change of energy demand due to an increase in input parameter value (high band).

4.4.3 Predicted sensitivities of building fabric parameters using a dynamic thermal model

This sub-section aims to compare the predicted sensitivities of the building fabric parameters using the steady-state model (Section 4.4.2) and using the multi-zone DTM developed in Section 3.4, the results were presented in Figure 4-8.

Concerning the comparison of steady-state model and DTM, results suggested that uncertainty of external wall construction for steady-state model (32%) is higher than DTM (17%) considering heating energy demand; whereas the uncertainty of cooling energy demand is higher for the steady-state model (9%) when compared with DTM (3%). As for uncertainty of window construction, both the uncertainty of heating and cooling energy demand for the steady-state model (10% and 25%) is higher than DTM (5% and 18%). Moreover, the uncertainty of air infiltration rate is similar for the steady-state model (35%) and DTM (33%) considering heating energy demand; whilst the uncertainty of cooling energy demand is higher for the steady-state model (11%) when compared with DTM (2%). When considering total energy demand, uncertainty of window construction is the highest (15%), with external wall construction and air infiltration rate having the smallest uncertainty (1%), since the increase

of heating and cooling cancel out. For the DTM, uncertainty of window construction and air infiltration rate are similar (11%), with external wall construction having the smallest uncertainty (3%).

For the DTM, variation of the three-building fabric parameters influences the predicted energy demand in the case study flat, with air infiltration rate having the highest influence (uncertainty of 11.1% for total energy demand), followed by window construction and external wall construction.

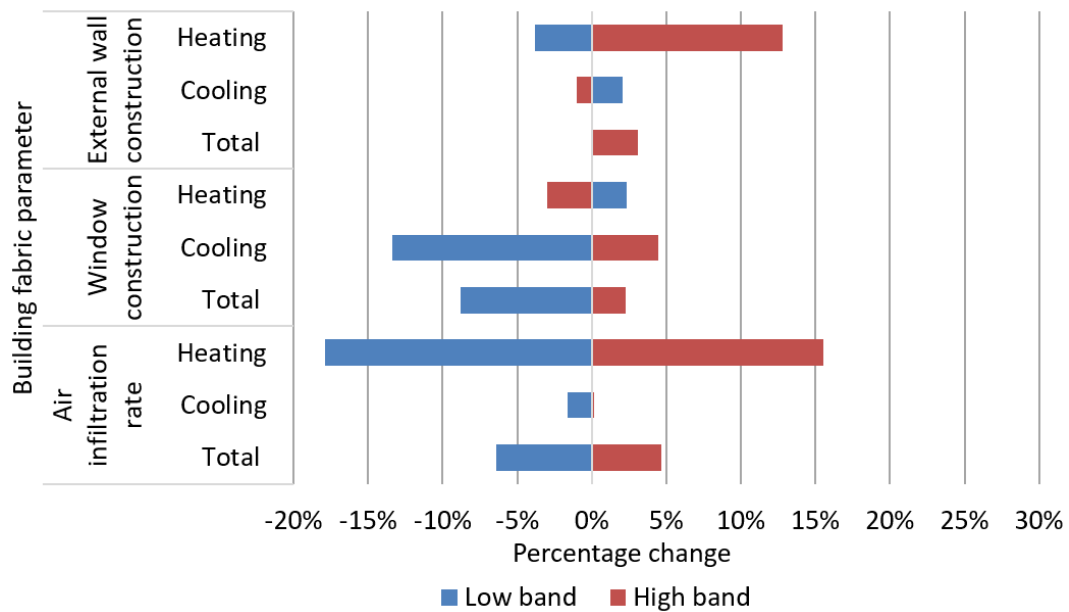


Figure 4-8: Bar chart representation of sensitivity of building fabric parameters using dynamic thermal model. Blue bar represents the percentage change of energy demand due to a decrease in input parameter value (low band). Red bar represents the percentage change of energy demand due to an increase in input parameter value (high band).

4.5 Indoor air measured conditions of the case study flat

4.5.1 Measurement set-up

To increase the reliability of the DTM predictions of energy saving retrofits in Chapter 5, measurements of indoor environmental parameters were undertaken between 7th April 2017 (15:00) and 13th April 2017 (16:00) in the living room when the flat was unoccupied, and the windows were closed. Seven indoor environmental parameters were measured with the specification of the measuring instrument illustrated in Table 4-3. These measurements were done by LoHCool on my behalf, i.e., LoHCool installed and collected these data specifically for this research.

Table 4-3: Technical specification of measuring instruments (source: Yao, 2017).

Parameter	Equipment	Test frequency	Precision
Indoor air temperature	HOBO UX100-003 Temp/RH recorder	5 minutes	$\pm 0.21^{\circ}\text{C}$
Indoor humidity	HOBO UX100-003 Temp/RH recorder	5 minutes	$\pm 3.5\%$
Indoor air velocity	HOBO T-DCI-F900-S-O	1 minute	$\pm 10\%$ or $\pm 0.05\text{m/s}$ (take the highest value)
External wall temperature	Type K thermocouple	5 minutes	$\pm (0.15\% + 1^{\circ}\text{C})$
AC electricity consumption	HOBO CTV-A	1 minute	$\pm 2.1\%$

Four sensors that measure indoor temperature (H1T, H2T, H3T, H4T), indoor relative humidity (H1RH, H2RH, H3RH, H4RH), and indoor air velocity (H1V, H2V, H3V, H4V) were clipped on the chairs, shown in Figure 4-9 with red boxes, with a height of 0.95m above the floor. One sensor which measures indoor temperature (HCT), indoor relative humidity (H1RH) and indoor carbon dioxide concentration (HCO_2) was placed on the table, shown on Figure 4-9 with a yellow box, with a height of 0.85m above the floor (Figure 4-10). The setting of the measurement was in accordance with the Chinese standard (Evaluation standard for indoor thermal environment in civil buildings; MOUHRD, 2012).

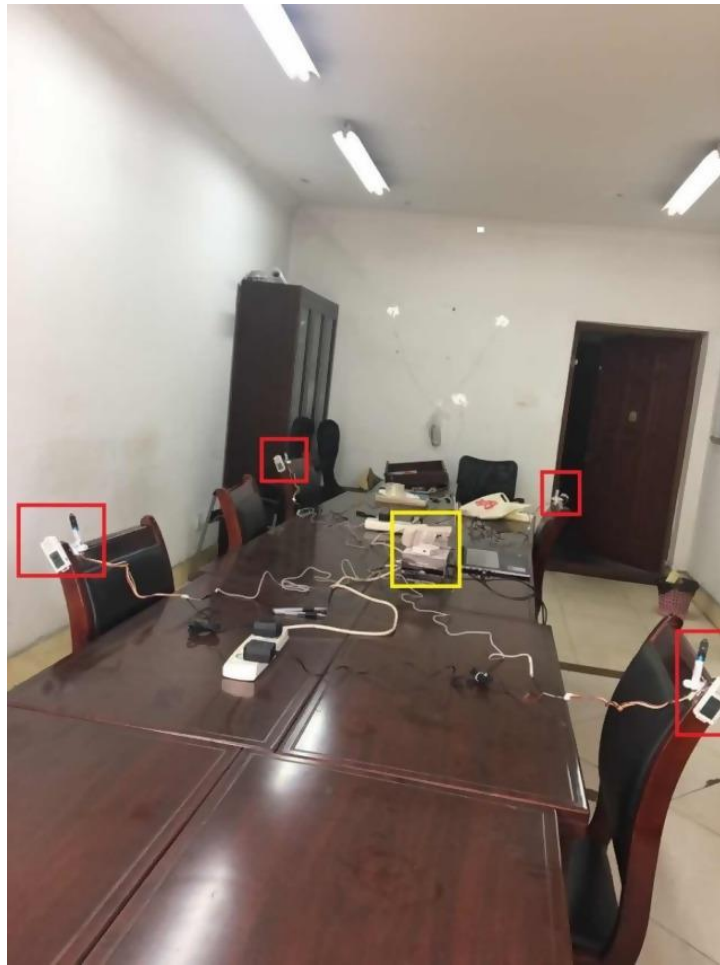


Figure 4-9: View of living room and location of sensors (source: Yao, 2017).

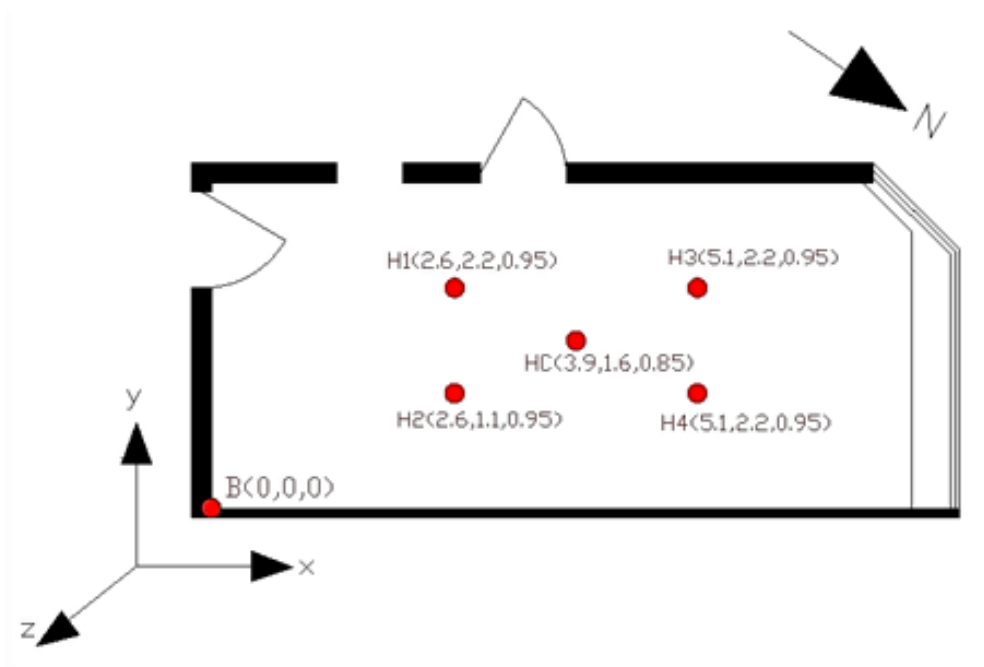


Figure 4-10: Plan view of the sensors' locations in the living room, in coordinates for x,y,z in meters from internal corner B (original source: Yao, 2017).

External wall temperatures against the outdoor communal corridor were measured with four thermocouples (Figure 4-11). The setting of the measurement was in accordance with the Chinese standard (Standard for energy efficiency test of residential buildings; MOUHRD, 2009), which suggests a minimum of four thermocouples should be used for measurement with one of them close to the centre. Thus, four thermocouples were placed on the inside and outside of the external wall (Figure 4-11). As there was a fire hydrant in the centre, two configurations of measurement were considered. The first configuration placed the sensors VI3 and VO3 close to the centre, near the fire hydrant, the measurement starts from 7th April 2017, 15:00 to 10th April 2017, 16:00 (Figure 4-12). The second configuration spread the sensors evenly. The sensors were placed close to each other so that they were closer to the centre, and no sensor was placed next to the fire hydrant; the measurement started from 10th April 2017, 16:00 to 13 April 2017, 16:00 (Figure 4-12).



Figure 4-11: Location of the thermocouples used to measure external wall temperature for two configurations, with red boxes showing thermocouples and blue boxes showing fire hydrant (source: Yao, 2017).

The AC electricity consumption was measured by a clamp meter, shown in Figure 3-24, highlighted red. It is a split type air conditioner, with an Energy

Efficiency Ratio (EER) and COP of 3.59 and 3.49 respectively. Heating and cooling capacity are 3950(+760) W and 3550W respectively (Figure 4-13). The AC load throughout the measurement period was zero.

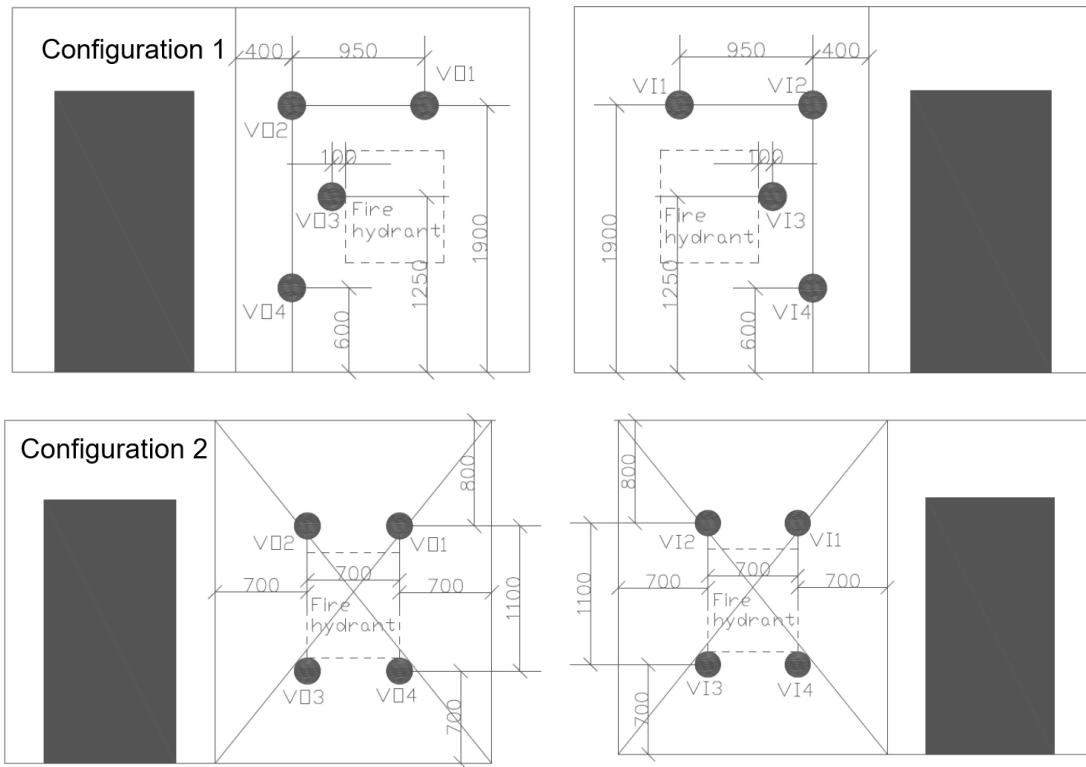


Figure 4-12: Naming of the thermocouples used to measure external wall temperature with dimensions for two configurations (original source: Yao, 2017).



Figure 4-13: Location of the clamp meter to measure AC electricity consumption (source: Yao, 2017).

4.5.2 Analysis of measured indoor air temperature

Indoor air temperature ranged from 19.5 to 23.5°C during the measurement period, from 7th April 2017 (15:00) to 13th April 2017 (16:00). The minimum indoor air temperature difference, as shown in Figure 4-14, was 0.014°C, and the maximum temperature difference was 1.18°C. Indoor air temperature recorded by sensor HCT was around 0.5°C higher than the other four sensors from 7/4 to 10/4, but the difference reduced in later days (11/4 to 13/4). Sensors H3T and H4T recorded the highest temperature (maximum 0.8°C difference) in the afternoon on the 7th, 8th, 12th, and 13th of April, because sensors H3T and H4T were closer to the façade (2.6 m away), with potentially higher exposure to solar radiation in the afternoon, resulting in a higher temperature recorded (Figure 4-14).

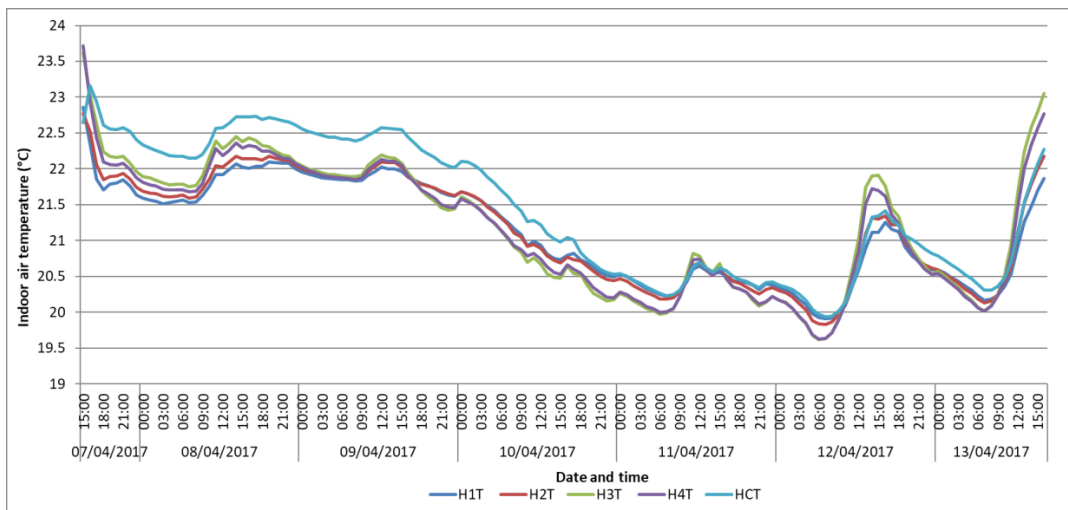


Figure 4-14: Measured indoor room temperature for different sensors.

From Section 4.4.1, two configurations of measurement were considered when measuring the external wall temperatures against the outdoor communal corridor. The results from the sensors were reviewed, and they both provided very similar readings; therefore, the measurement results from the two configurations were averaged. The outdoor wall temperature ranged between 18 to 22.5°C; the maximum outdoor temperature difference was 0.7°C and the minimum difference was 0.092°C, during the measurement period. Measured data between the four sensors had a small difference, with a maximum difference of 0.5°C (Figure 4-15).

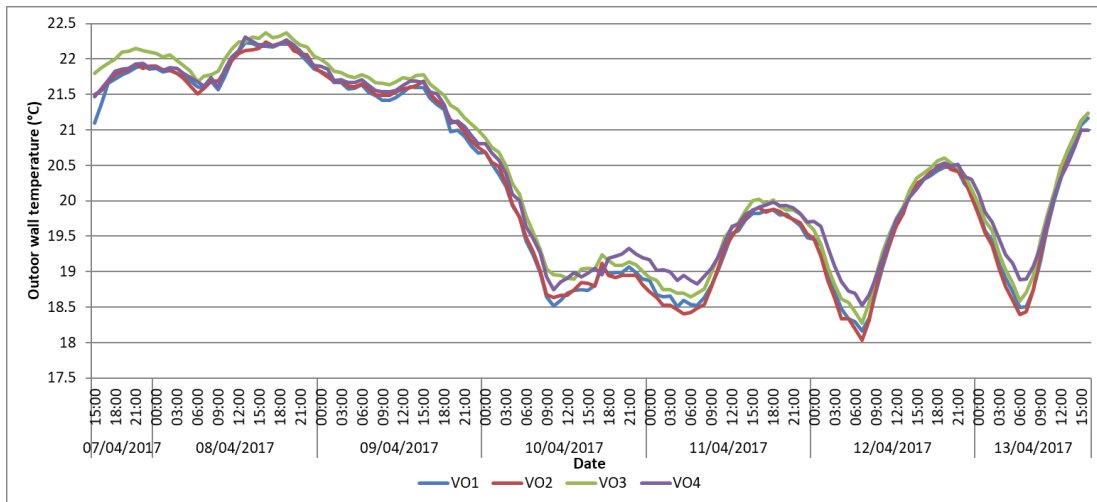


Figure 4-15: Measured outdoor wall temperature for different sensors.

Internal surface temperatures of the external wall towards the communal corridor varied between 20 to 23°C; the maximum indoor temperature difference was 1.67°C, and minimum indoor temperature difference was 0.4°C, during the measurement period. Sensors placed at the upper parts of the wall (VI1, VI2), and sensors placed at the lower parts (VI3, VI4) had similar variations, and the indoor surface temperature difference between the two groups of sensors (sensors placed at the upper and lower parts of the wall) was 0.5°C, due to buoyancy and warm air accumulating towards the ceiling. Although the temperature of sensor VI4 was 1°C lower than sensor VI3 at the beginning of the measuring period, the indoor surface temperature difference only stayed for several hours (Figure 4-16).

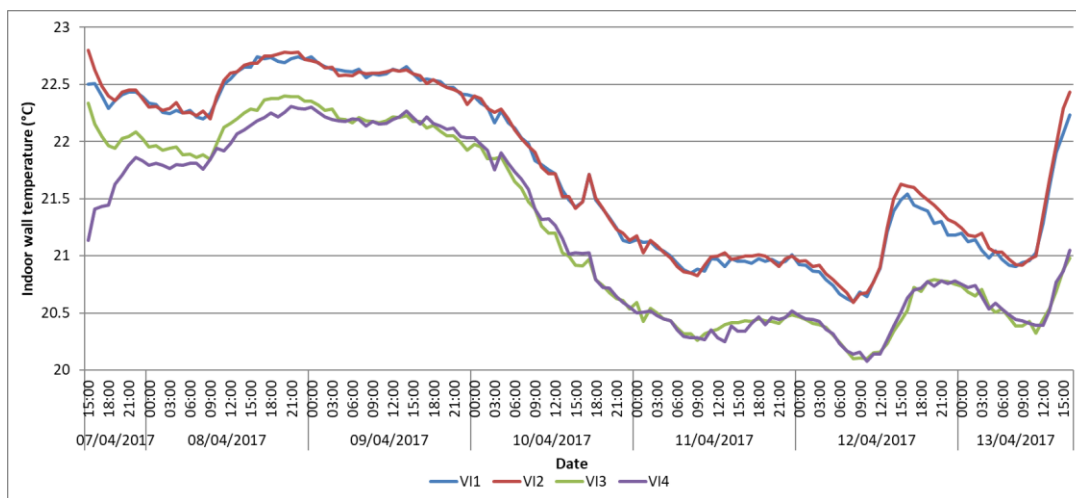


Figure 4-16: Measured indoor wall temperature for different sensors.

The temperature difference between outdoor air temperature and outdoor wall temperature was compared. Results showed that the maximum temperature difference was predicted in the morning (6:00) at 10/4, 12/4, and 13/4; outdoor wall temperature was 4°C higher than the outdoor air temperature. In the afternoon (15:00), outdoor wall temperature was 6°C lower than outdoor air temperature (Figure 4-17). This shows that the external wall facing internal street behaves as a semi-exposed wall, due to shading from a nearby apartment block (Figure 4-17).

Measured indoor air temperature was taken as the average of all five sensors shown in Figure 4-14. The indoor wall temperature was measured to be higher than the indoor air temperature throughout the measuring period, except on the afternoons of 7/4, 12/4, and 13/4, when outdoor air temperature increased rapidly. Possible reasons were because all windows were closed and had a small air change rate; thus, heat transfer by ventilation was low.

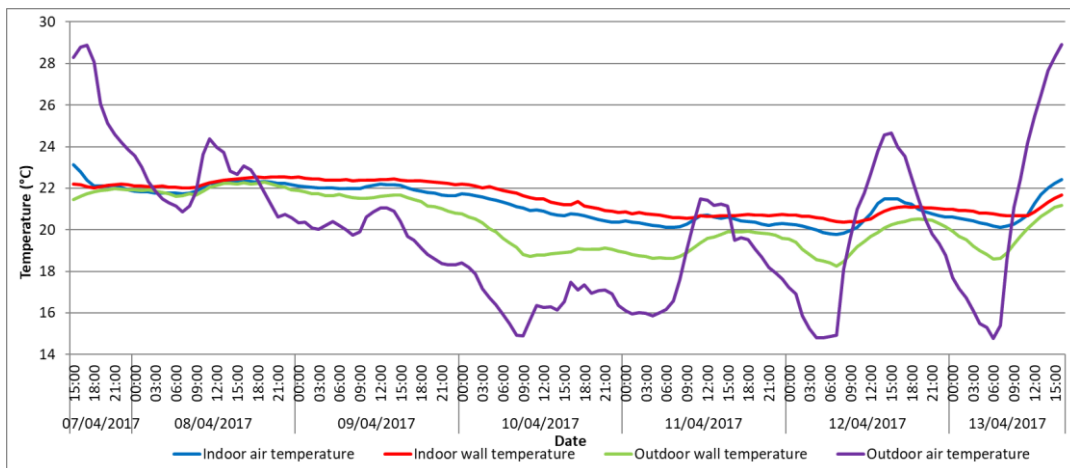


Figure 4-17: Comparison between measured indoor air temperature, indoor wall temperature, outdoor wall temperature, and outdoor air temperature.

4.5.3 Analysis of measured indoor relative humidity

The indoor relative humidity ranged between 45 to 80%, during the measurement period for the four sensors. The minimum relative humidity difference was 2.30%, and the maximum relative humidity difference was 7.37% for the four sensors. Relative humidity measured by sensor H4RH was constantly lower than other sensors by a difference of 5% during the whole

measurement period; also, measurement from sensor HCRH was constantly higher than other sensors by a difference of 5% from 10/4 to 13/4 (Figure 4-18).

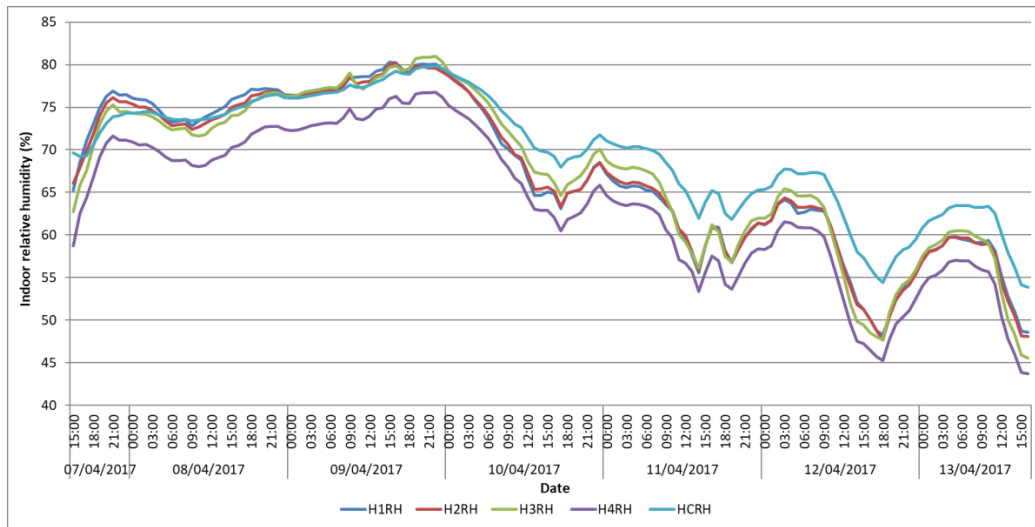


Figure 4-18: Measured indoor relative humidity for different sensors.

Indoor relative humidity was between 50 to 80%, and it was usually lower than outdoor relative humidity, which was between 30 to 100%. The indoor relative humidity remained 60 to 80% in the first four days (7/4 to 11/4), where the outdoor relative humidity was high (70 to 100%). The indoor relative humidity decreased in the last three days, as the weather was sunny and outdoor relative humidity decreased rapidly in the afternoon (Figure 4-19).

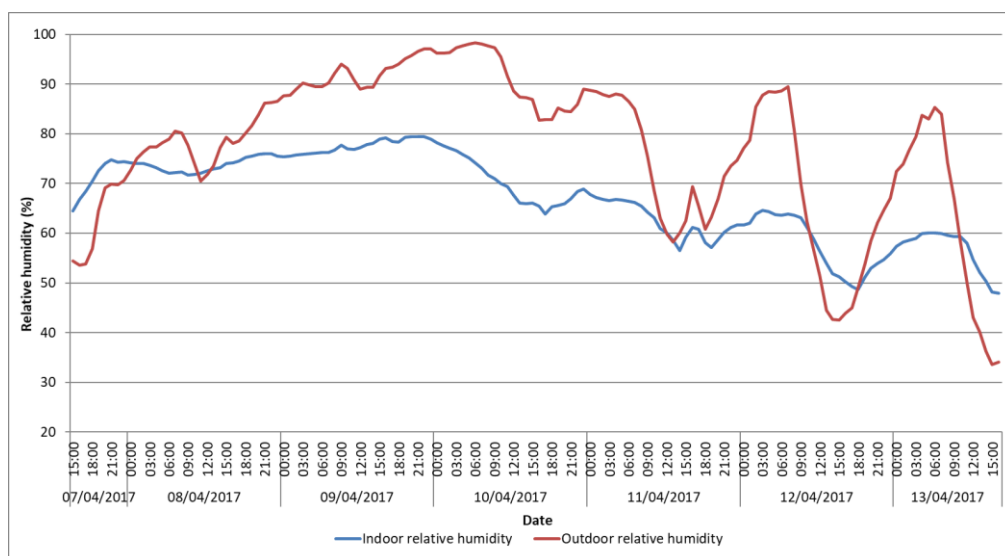


Figure 4-19: Comparison between measured indoor and outdoor relative humidity.

4.5.4 Analysis of measured indoor air velocity

The indoor air velocity ranged from 0.02 to 0.05 m/s during the measurement period for the four sensors (H1V, H2V, H3V and H4V). The maximum indoor air velocity difference between sensors was 0.02 m/s, and minimum indoor air velocity difference between sensors was 0 m/s. The indoor air velocity throughout the measurement period was less than 0.05 m/s, and the average value was 0.03 m/s (Figure 4-20).

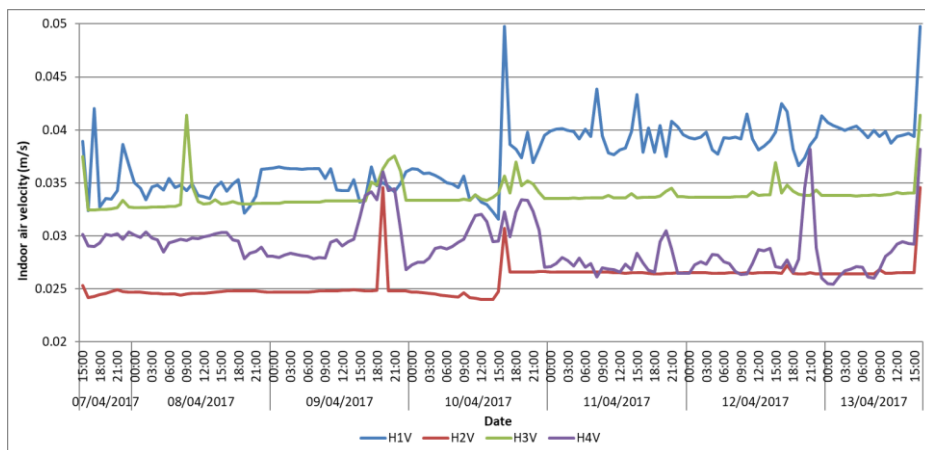


Figure 4-20: Measured indoor air velocity for different sensors.

The indoor air velocity of four sensors was averaged and compared with outdoor wind speed. The indoor air velocity was much lower than outdoor wind speed, and it was almost constant. This indicates that the flat had low air infiltration rate as the windows were closed; the indoor air velocity was not affected by outdoor wind speed (Figure 4-21).

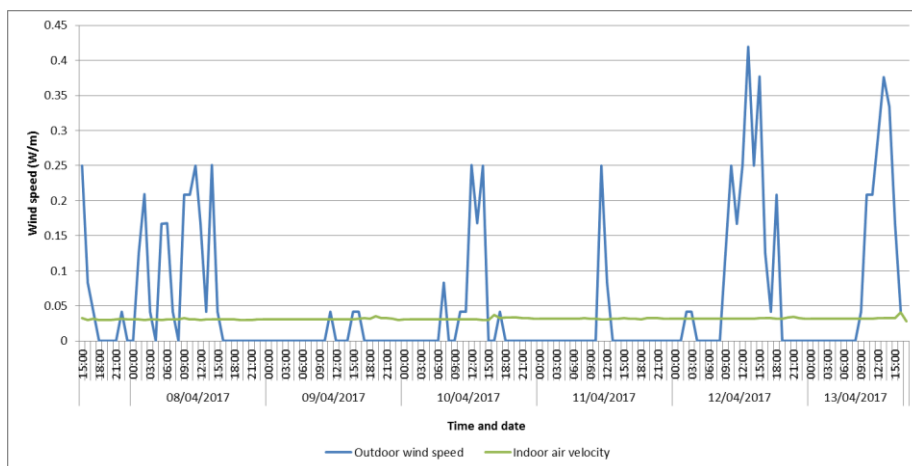


Figure 4-21: Comparison between indoor air velocity and outdoor wind speed.

4.6 Development of a customised weather file

4.6.1 Weather file construction

After analysing the measured indoor air temperature of the case study flat, the next step is to develop a customised weather file, so as to perform model calibration in Section 4.7.

Dry bulb temperature is the air temperature measured, freely exposed to air but shielded from radiation and moisture (ASHRAE, 2018). Relative humidity is the ratio of the partial pressure of water to the equilibrium vapour pressure of water (ASHRAE, 2018). Global solar radiation is the solar radiation measured on a horizontal surface (ASHRAE, 2018). Gust speed is defined as the maximum wind speed measured in each interval (5 minutes), and wind speed is defined as the average wind speed measured in each interval (5 minutes; Harper et al., 2008). Wet-bulb temperature is the adiabatic saturation temperature; dew-point temperature is the temperature of moist air saturated at a given pressure with the same humidity ratio as that of a given sample of moist air (ASHRAE, 2018).

Real-time weather data were collected from a weather station located in Chongqing University, which is close (~1 km distance) to the case study building. The period of measurement was from 7th April 2017, 00:00 to 14th April 2017, 00:00. The dry-bulb temperature, atmospheric pressure, relative humidity, global solar radiation, wind speed, gust speed, and wind direction were recorded in 5-minute intervals; the resolution of data was up to 3 decimal places. Hourly weather data were calculated by averaging measurements in 5 minutes intervals.

Elements (Big Ladder Software, 2019) was used, which is an open-source software tool to create and edit custom weather files for building energy modelling (Figure 4-22).

Date/Time	Dry Bulb Temperature [C]	Wet Bulb Temperature [C]	Atmospheric Pressure [kPa]	Relative Humidity %	Dew Point Temperature [C]	Global Solar [Wh/m2]	Normal Solar [Wh/m2]	Diffuse Solar [Wh/m2]	Wind Speed [m/s]
2005/01/01 @ 00:00:00	6.4	6.1	99.49	96	5.83	0	0	0	2.5
2005/01/01 @ 01:00:00	6.3	6.08	99.49	97	5.88	0	0	0	2.5
2005/01/01 @ 02:00:00	6.1	5.95	99.49	98	5.83	0	0	0	0
2005/01/01 @ 03:00:00	5.7	5.83	99.49	99	5.57	0	0	0	0
2005/01/01 @ 04:00:00	5.1	5.1	99.49	100	5.12	0	0	0	0
2005/01/01 @ 05:00:00	4.6	4.6	99.49	100	4.61	0	0	0	0
2005/01/01 @ 06:00:00	4.2	4.2	99.49	100	4.21	0	0	0	0
2005/01/01 @ 07:00:00	4	4	99.49	100	4.01	0	0	0	0
2005/01/01 @ 08:00:00	4.1	4.03	99.49	99	3.97	8	0	8	2
2005/01/01 @ 09:00:00	4.4	4.26	99.49	98	4.12	62	0	62	2
2005/01/01 @ 10:00:00	4.8	4.52	99.49	96	4.23	121	0	121	2
2005/01/01 @ 11:00:00	5.3	4.8	99.49	93	4.27	174	0	174	2
2005/01/01 @ 12:00:00	6.1	5.44	99.49	91	4.76	209	0	209	2
2005/01/01 @ 13:00:00	7	6.16	99.49	89	5.33	220	0	220	2
2005/01/01 @ 14:00:00	8.1	7.06	99.49	87	6.09	204	0	204	2

Figure 4-22: Interface of Elements (a customise weather editing tool).

4.6.2 Analysis of the weather data collected

Wet-bulb temperature, dew-point temperature, normal solar radiation, and diffuse solar radiation were not measured at the weather station. However, these values can be predicted by correlating other measured weather parameters. Wet-bulb and dew-point temperature can be predicted from the measured outdoor air temperature and relative humidity using the correlations in the psychrometric chart; these equations are listed in ASHRAE handbook fundamentals (ASHRAE, 2018).

The wind speed was higher than 0.25 m/s for less than 10% of the measurement period and 70% of the time the wind speed was 0 m/s (Figure 4-23a). The gust speed was lower than 3 m/s during the measurement period (Figure 4-23b). The wind direction was predominately west, with some of them facing north-west, south-west and north (Figure 4-23c). However, as the wind speed was low, the wind direction potentially did not have a considerable influence on the DTM in the measurement period.

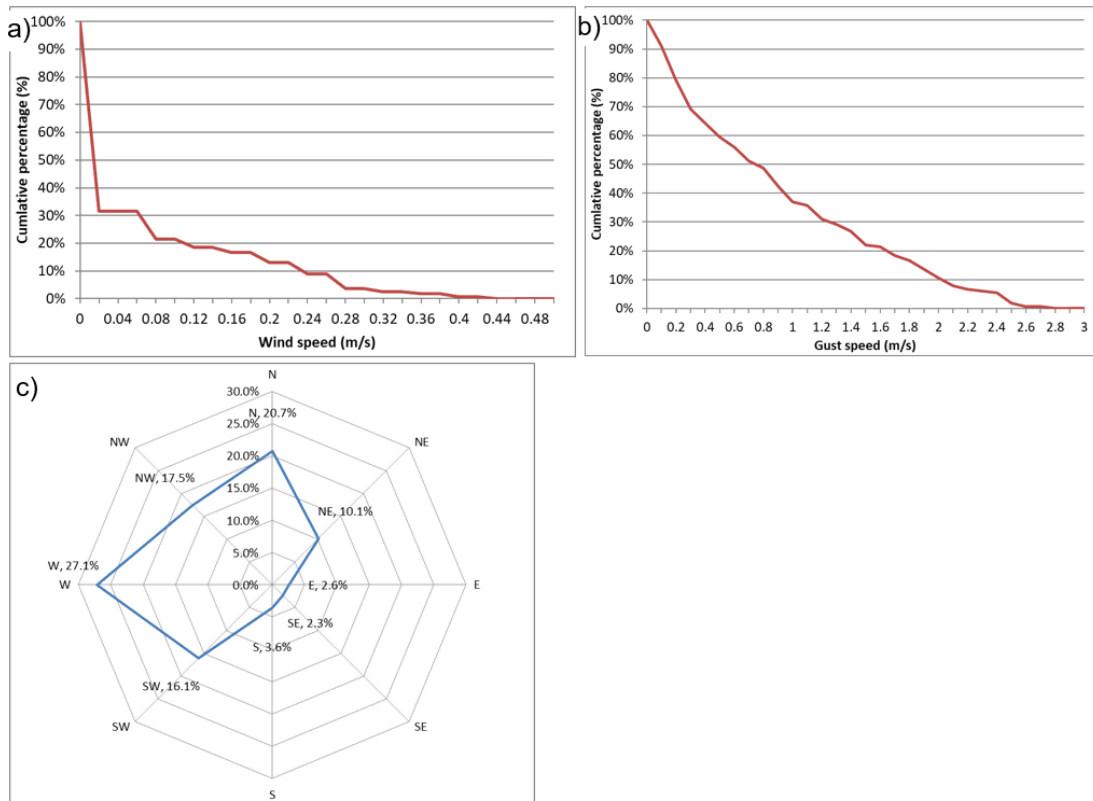


Figure 4-23: a) Cumulative percentage of wind speed, b) cumulative percentage of gust speed, c) wind direction for the measurement period.

The outdoor air temperature was between 14 to 30°C, and the relative humidity was between 30 to 100% during the measurement period (Figure 4-24). When outdoor air temperature increased, the relative humidity decreased because the water moisture content in the air stayed the same. Four days (7/4, 11/4-13/4) have larger temperature variation with higher temperatures in the afternoons, and the reason is these days were sunny (Figure 4-25). Three days (8/4-10/4) have smaller temperature variation with lower temperatures in the afternoons, and the reason is these days were rainy or cloudy (Figure 4-25). The moisture content of air lay between 0.008 to 0.015 kg/kg of dry air during the measurement period. In the first three days (7/4-9/4), the moisture content was high (0.0014 kg/kg dry air). During the morning of 10/4, the moisture content of air dropped from 0.0014 kg/kg dry air to 0.0010 kg/kg dry air, the moisture content of air then remained low (0.0010 kg/kg dry air) for the remaining days (Figure 4-26).

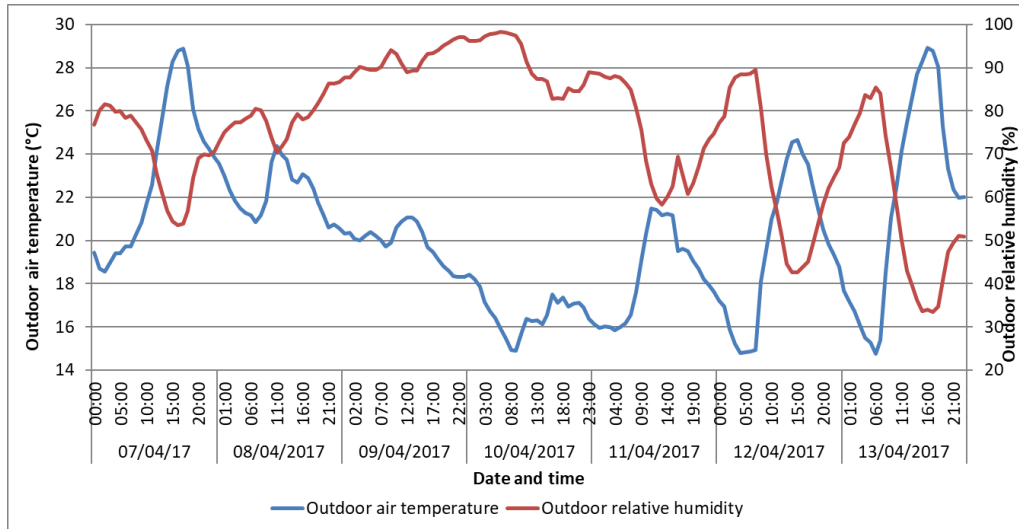


Figure 4-24: Outdoor air temperature and relative humidity for the measurement period.

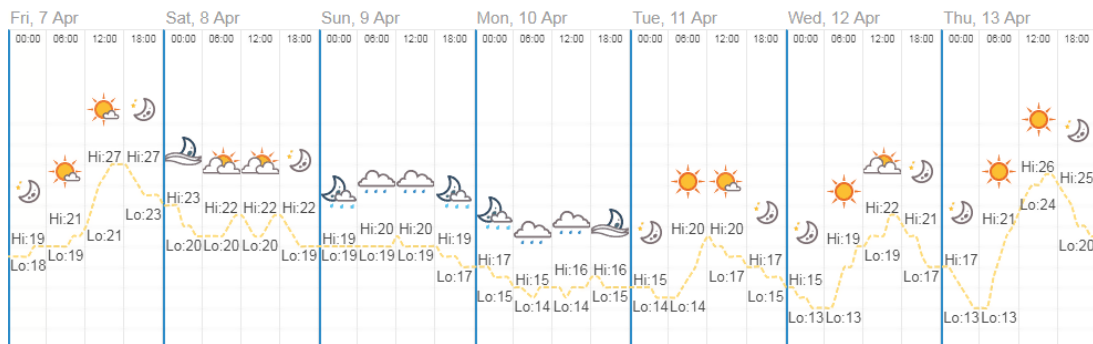


Figure 4-25: Weather conditions for the measurement period (Thorsen, 2019).

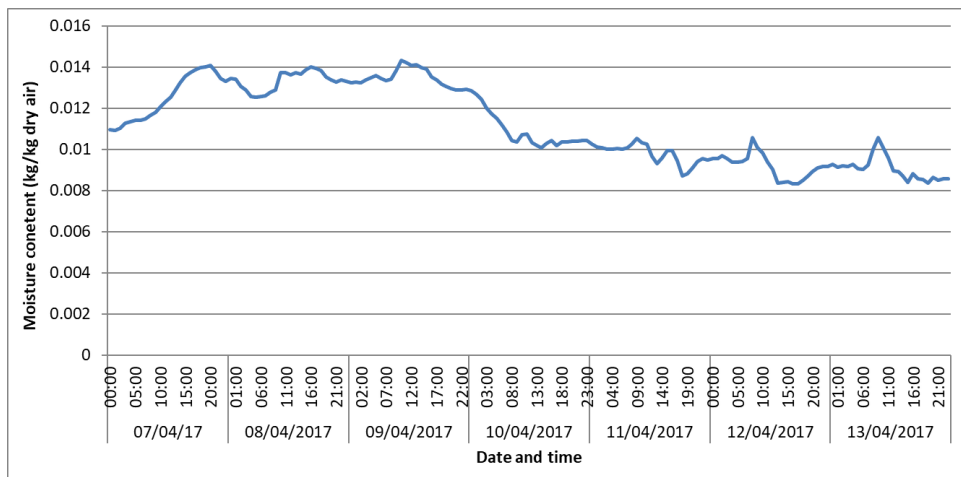


Figure 4-26: Moisture content of outdoor air for the measurement period.

Using equations from Appendix B, the diffuse and beam radiation can be predicted from measured global horizontal solar radiation (Figure 4-27). The process is similar to the hourly horizontal-vertical translation model developed in section 4.2.2 to predict vertical solar radiation. On sunny days (7/4, 11/4,

and 13/4), the beam radiation is higher than diffuse radiation, the global radiation peaks at 700 to 900 W/m². On cloudy or partly sunny days (8/4 and 11/4), the diffuse radiation is higher than beam radiation, the global radiation peaks at 400 to 500 W/m². In a rainy day (9/4 and 10/4), the beam radiation is zero, and the diffuse radiation is equal to global radiation, the global radiation peaks at 100 W/m².

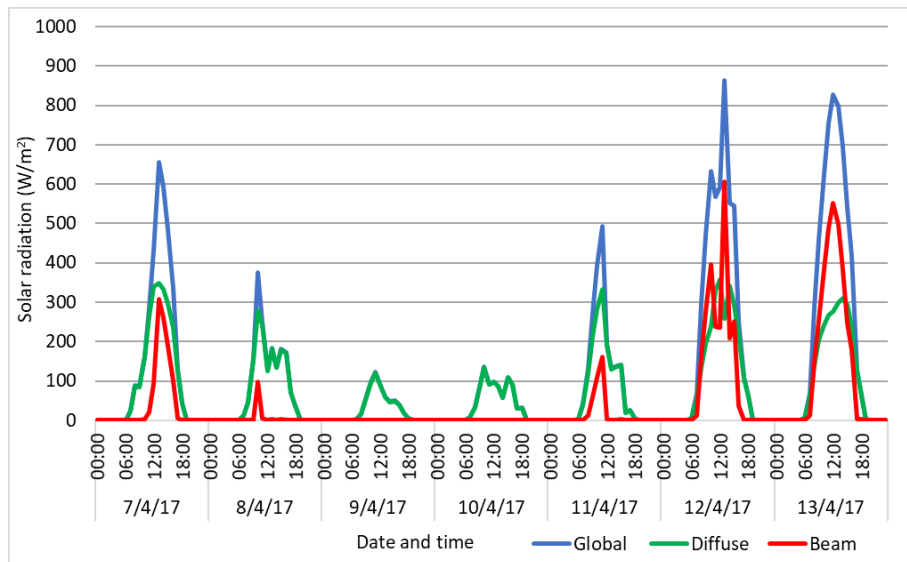


Figure 4-27: Prediction of diffuse and beam radiation from global horizontal solar radiation.

4.7 Calibration of a dynamic thermal model for a case study flat

To sum up this chapter, the measured indoor air temperature (Section 4.5) was compared with the predicted indoor air temperature by a DTM using customised weather data (Section 4.6). A sensitivity analysis using the same uncertainty band developed in Section 4.4 was then conducted to evaluate the effects of building fabric parameters on improving the DTM predictions of indoor air temperature. Subsequently, the building fabric parameters which had the potential to improve the predictions of indoor air temperature were adjusted in the DTM developed in Section 3.4 to generate a refined model.

Dynamic thermal simulation was performed from 7th April 2017 (00:00) to 14th April 2017, (00:00), since weather data were collected during this period, where the measurements were taken from 7th April 2017 (15:00) and 13th April

2017 (16:00). Results revealed that the DTM over-predicted the indoor temperatures significantly, with an average 2°C over-prediction during the measurement period (Figure 4-28). This is due to a vast difference between the thermal condition (wall, floor, ceiling, and indoor air temperature) of the case study apartment for the simulation and measurement at the start of the period.

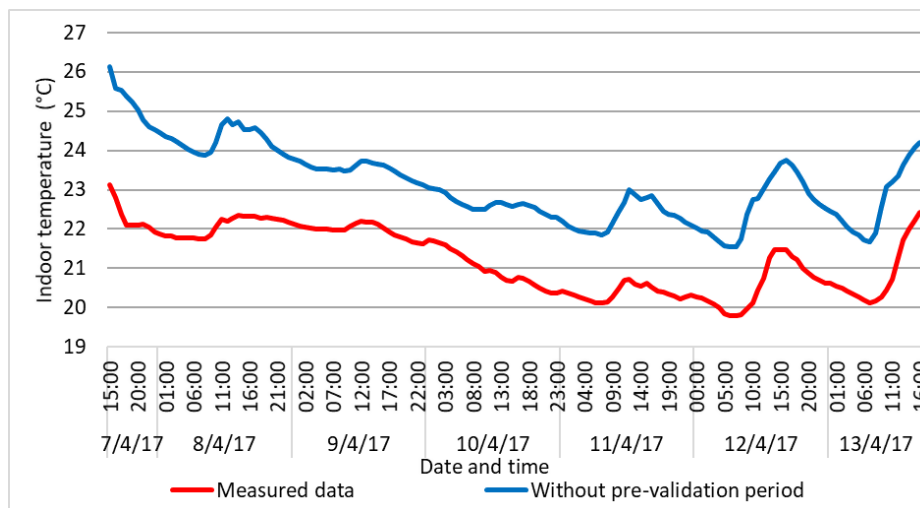


Figure 4-28: Comparison between measured and simulated temperature without pre-validation period.

To improve the accuracy of dynamic thermal simulation, a pre-validation period of two weeks (24/3/2017 to 6/4/2017) was introduced, in order to match the thermal condition of the apartment before 7/4/2017. Therefore, the whole simulation period was extended from one week (7/4/2017-13/4/2017) to three weeks (24/3/2017-13/4/2017). This is important as previous researchers have measured indoor air temperature to calibrate DTM in residential buildings in China (Fu et al., 2017; Li et al., 2019; Short et al., 2018), but a pre-validation period was not introduced, potentially leading to a massive difference between the thermal condition of the DTM and measurement at the start of the measurement period. Subsequently, weather data for the pre-validation period were collected from an online database (Karl, 2019), since measured weather data were not available for the additional two week period. Only outdoor air temperature and relative humidity were obtained from the online database, and the resolution of data was up to 0 decimal places. By introducing the pre-validation period, the simulated indoor air temperature becomes lower than the measured indoor air temperature (Figure 4-29).

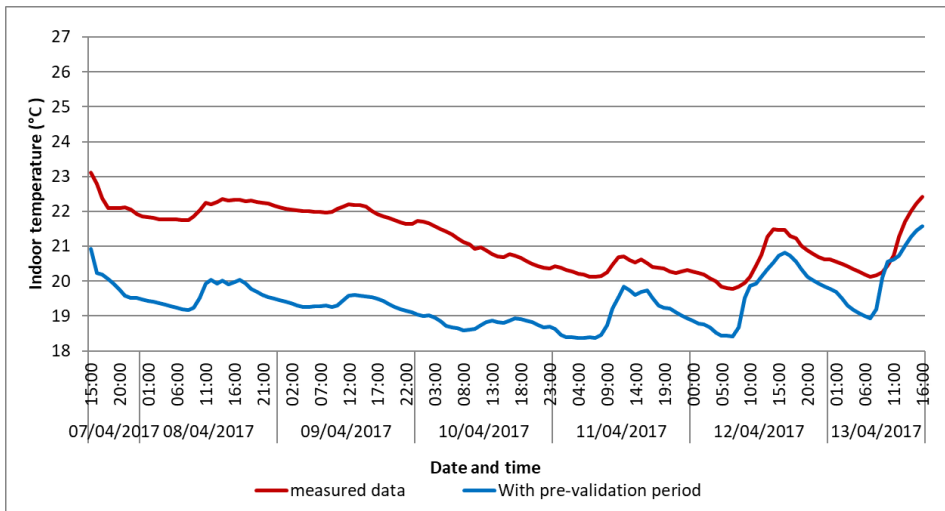


Figure 4-29: Comparison between measured and simulated temperature with pre-validation period.

The outdoor air temperatures from the weather data collected from an online database (Karl, 2019) were compared with the weather data collected in the measurement period, from 7th April 2017 (00:00) to 14th April 2017, (00:00), in order to examine the discrepancy between the two data sources. The outdoor air temperature from measured data was always higher (0 to 3°C) than the online source base (Figure 4-30). The reason is the weather station for the online data source is located at the airport in Chongqing, which is in the rural area, and the weather station for weather data collected from LoHCool is located at Chongqing University, which is in the city centre and affected by urban heat island effect.

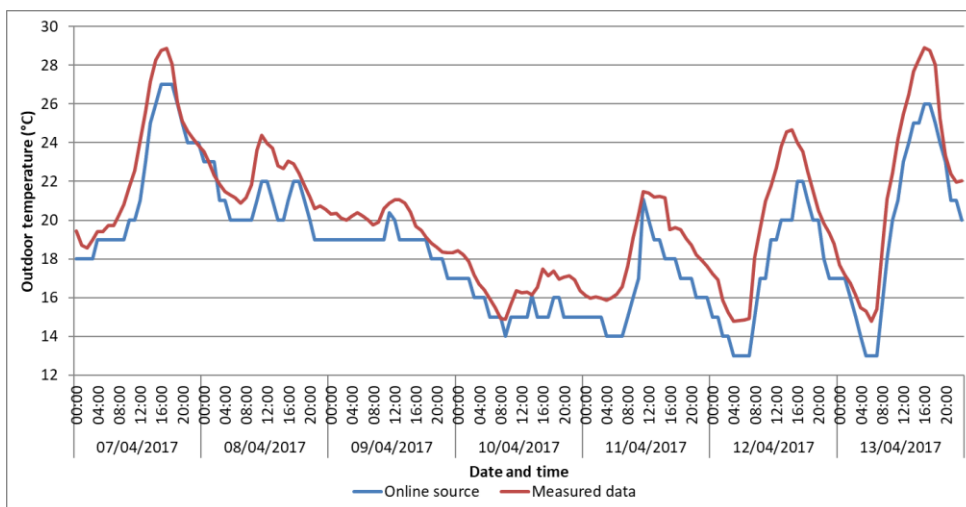


Figure 4-30: Comparison between online source and measured data during the measurement period.

The difference between outdoor air temperature for the last few days (4/4/2017 to 6/4/2017) in the pre-validation period (24/3/2017 to 6/4/2017) leads to the under-prediction of indoor air temperature. Thus, the outdoor air temperature collected from the online database was increased to reduce the error between simulated and measured temperature. Four new cases were tested by increasing outdoor air temperature of the pre-validation period (24/3/2017 to 6/4/2017) by 1°C, 1.5°C, 2°C, and 2.5°C.

Instead of collecting weather data for the pre-validation period from an online database, another solution is to repeat the weather data in the measurement period (7/4/2017 to 13/4/2017) for the pre-validation period (Figure 4-30). As the outdoor temperature for the last few days in the pre-validation period (4/4 to 6/4) was higher when repeating the weather data in the measurement period compared to the online database. Four new cases were tested by decreasing outdoor air temperature of the pre-validation period (24/3/2017 to 6/4/2017) by 0.5°C, 1°C, 1.5°C, and 2°C. Statistical metrics of Mean Bias Error (MBE) and Coefficient of Variation of Root Mean Square Error (CvRMSE) were used to compare the simulated and measured indoor air temperature during the measurement period. Another metric is the temperature difference between the starting hour (15:00 in 7/4/2017) of the measurement and the simulation. Results suggested that cases 4, 8, and 9 have the lowest MBE, CvRMSE, and starting temperature difference (Table 4-4).

Table 4-4: MBE and CvRMSE for different options of adjustment when compared to simulated temperature.

Case	Type of data for pre-validation period	Change to outdoor air temperature	MBE	CvRMSE	Starting temp. difference (°C)
1	Online source	No change	-8.50%	9.25%	-2.19
2		+1°C	-3.08%	4.76%	-2.54
3		+1.5°C	-2.08%	3.67%	-0.56
4		+2°C	-0.95%	3.02%	-0.22
5		+2.5°C	-2.57%	3.76%	-0.43
6	Repeat measured data	No change	2.53%	3.33%	1.05
7		-0.5°C	1.51%	2.72%	0.75
8		-1°C	-0.30%	2.49%	0.22
9		-1.5°C	-0.94%	2.72%	0.03
10		-2°C	0.42%	2.48%	0.26

Figure 4-31 shows a graphical plot of the selected cases 4, 8, and 9. The model underpredicts in the first few days and it overpredicts in the last few days, but the discrepancy between measured and simulated indoor air temperature has improved significantly before the pre-validation period is introduced. By observing Figure 4-31, case 8 has the closest match with measured data in the first few days, which is also reflected by the fact that MBE and CvRMSE are the lowest for case 8.

Therefore, by performing dynamic thermal simulation for three weeks (24/3/2017-13/4/2017), including the pre-validation period (24/3/2017 to 6/4/2017), the difference between the thermal condition (wall, floor, ceiling, and indoor air temperature) of the case study flat for the simulation and measurement at the start of the period was minimised, with an MBE of -0.3% and CvRMSE of 2.49%.

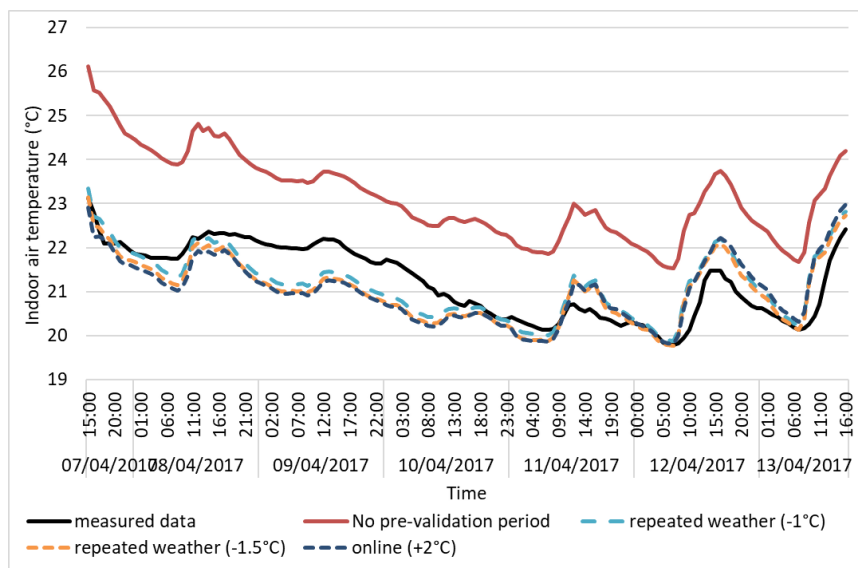


Figure 4-31: Comparison between measured and base case indoor air temperature for the selected pre-validation period.

A sensitivity analysis using the same uncertainty band developed in Section 4.4 was then conducted to evaluate the effects of building fabric parameters on improving the DTM predictions of indoor air temperature, summarised in Table 4-5.

Table 4-5: Building fabric parameters used in model calibration

Building fabric parameter	Base case	Low band	High band
U-value of external wall (W/m ² K)	2.3 (Table 3-5)	1.97 (Yao et al., 2018)	3.67 (Yu et al., 2008)
U-value of windows (W/m ² K)	5.8 (Table 3-5)	4.7 (Ouyang et al., 2009)	6.4 (McNeil et al., 2016)
g-value of windows (-)	0.87 (Table 3-5)	0.7 (Ouyang et al., 2009)	0.95 (McNeil et al., 2016)
Air infiltration rate (ach ⁻¹)	1.5 (Table 3-5)	1 (Yu et al., 2013)	2 (McNeil et al., 2016)

Results suggested that the variation of indoor temperature is insignificant for external wall construction (U-value of external wall; Figure 4-32), and window construction (U-value and g-value of windows; Figure 4-33). This indicates the variation of these parameters do not affect the model calibration process. Nevertheless, results from Section 4.4.3 suggested that the variation of total energy demand is significant for both external wall and window construction (Figure 4-32 and 4-33). Since the annual dynamic thermal simulation is carried out to evaluate the sensitivity of building fabric parameters, where the indoor and outdoor temperature difference can be massive (in winter). This led to substantial transmission heat loss of building fabric; thus, measures (e.g. reducing the U-value of the external wall) led to a considerable reduction in heating energy demand. As the measurements were performed for one-week mid-season, the indoor and outdoor temperature difference was small.

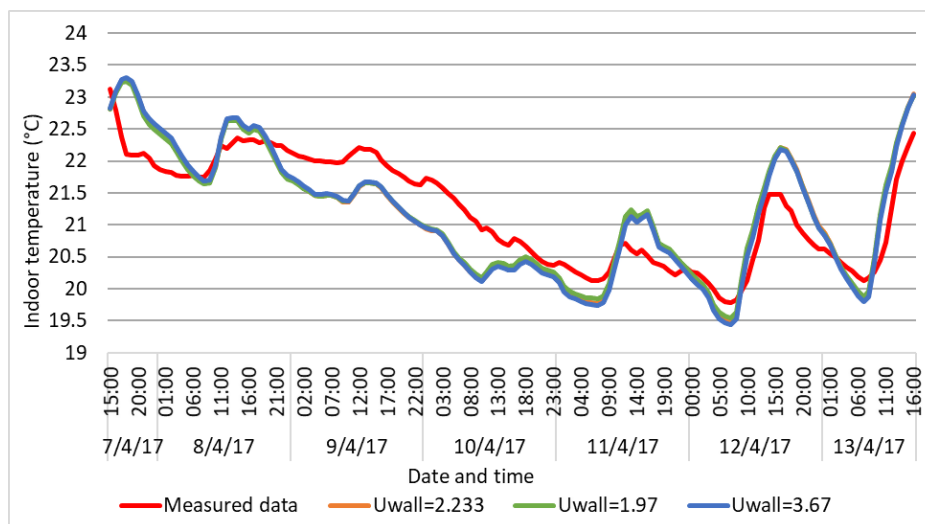


Figure 4-32: Variation of indoor temperature for three walls' U-values.

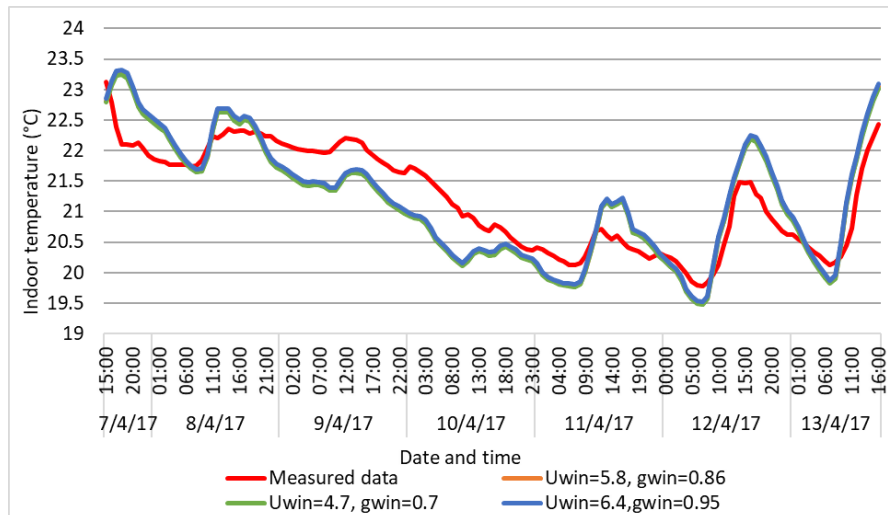


Figure 4-33: Variation of indoor temperature for three windows' U-value and g-value.

On the contrary, the variation of indoor temperature is significant for the air infiltration when compared to the other two building fabric parameters (Figure 4-34). In Section 4.4.3, air infiltration rate was presented as the most sensitive parameter when considering total energy demand. This is also reflected in the model calibration process, where the change of indoor temperature is significant when the air infiltration rate is varied. The indoor air temperature difference can be up to 1°C, where differences for other building fabric parameters are close to zero. Results suggested that an air infiltration rate of 1.0 ach⁻¹ gives MBE = 0.39%, CvRMSE = 2.1% and air infiltration rate of 2.0 ach⁻¹ gives MBE = -0.92%, CvRMSE = 3.0%. Yet, MBE did not improve when compare with base case with an air infiltration rate of 1.5 ach⁻¹ (-0.3%). Therefore, none of the three variants improved the prediction of indoor air temperature, and the final DTM used to evaluate energy saving retrofits in Chapter 5 is the same as the model start with in this Chapter.

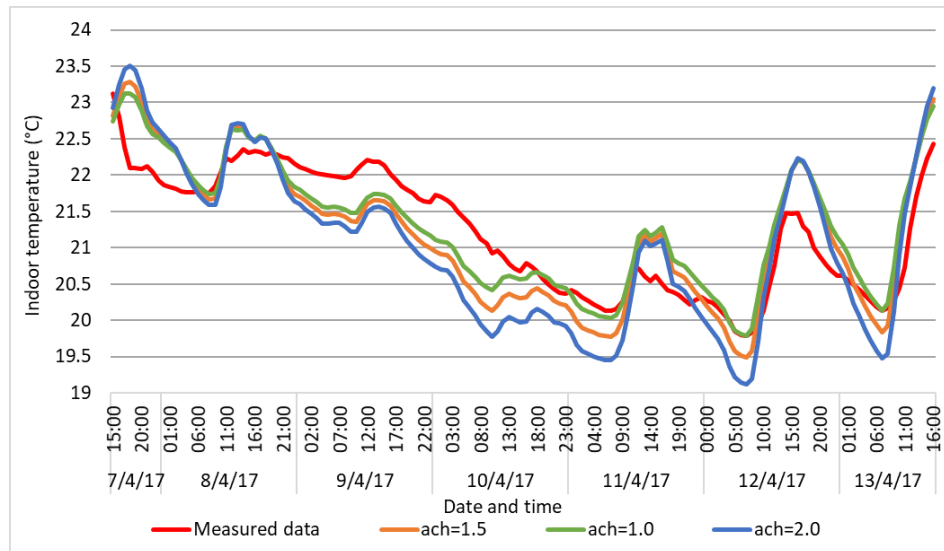


Figure 4-34: Variation of indoor temperature when air infiltration is changed.

4.8 Limitations of calibration performed

The monitoring for this research took place for a short, unoccupied period (1-week) in the case study flat. The measurements included hourly indoor air temperature, which was used to compare with the simulated indoor air temperature. As only indoor air temperature was measured, only three variants (U-value of external wall, U-value and g-value of window, and air infiltration rate) were altered within a reasonable range to test if it improved the accuracy of predicted indoor air temperature. Results showed that variation of indoor temperature is insignificant for three parameters (U-value of external wall, U-value of window and g-value of window); for air infiltration rate, MBE for 1 ach⁻¹ was 0.39% and 2 ach⁻¹ was -0.92%, where MBE did not improve when compare with base case with an air infiltration rate of 1.5 ach⁻¹ (-0.3%). Therefore, none of the three variants improved the prediction of indoor air temperature, and the final DTM used to evaluate energy saving retrofits in Chapter 5 is the same as the model start with in this Chapter.

This research attempted to calibrate the DTM, but data was not adequate; however, the simulated hourly indoor air temperatures matched the measured indoor air temperatures and thus the DTM of this study was verified.

Monitoring in future projects should measure hourly AC electricity consumption in the heating and cooling season, along with indoor air temperature, in all the thermal zones (In this case: living room, bedroom, kitchen and wetroom) in the flat. Moreover, perform surveys in the flat, to record AC operating schedule, window opening schedule, and heat gain due to lighting, occupant, and equipment for each thermal zone.

4.9 Discussion

This chapter presented the calibration of a DTM of the case study flat, using predicted sensitivity of energy demand of various building fabrics and measured indoor air temperature, in order to increase the reliability of model predictions.

The comparison of the steady-state model and dynamic thermal model revealed that the predicted cooling energy demand was the same for the three energy users. This is aligned to the findings by Kokogiannakis et al. (2008), which predicted the same results using steady-state model for the same two intermittent cooling settings (10 and 12 hours of cooling); however, the prediction from DTM varied by 20%. Since ISO13790:2008 standard suggested that “fraction of the number of hours in the week with a normal cooling set-point” was used, due to the diurnal pattern of the weather and the effect of the building thermal inertia. The standard suggested that a switch-off of air conditioner has a smaller effect on the energy needed for cooling than a switch-off of heating energy demand. This implies that a switch-off of air conditioners during evening/night will only slightly change the energy needed for cooling, except during very warm months or in the case of high internal heat gains. Therefore, the time fraction for intermittency in the cooling mode is based on the number of days per week with cooling instead of number of hours per week as for the heating mode. Nevertheless, the case study building may have different conditions as stated in the standard. To start with, summer temperature is high, and it may fall into the criteria of very warm months defined in the standard. Also, the air conditioner is primarily operated in evening/night (17:00-22:00), instead of a switch off as defined in the standard.

As for the sensitivity analysis of building fabric parameters, the uncertainty bands developed are supported and developed according to literature. For instance, the range of U-value of external wall was 1.97 to 3.67 W/m²K in this thesis. However, the findings are in contrast to L. Xu et al. (2013), which evaluated the range of U-value of external from 0.3 to 1.96 W/m²K, including newly built buildings. Since L. Xu et al. (2013) failed to develop the uncertainty bands with reference to literature. This led to the under-prediction of the sensitivity of the energy demand due to the uncertainty of external wall construction. Moreover, this thesis predicts the sensitivity of energy demand of window construction by varying both U-value of window and g-value of window. However, this is contrary to the findings from L. Xu et al. (2013), as L. Xu et al. (2013) investigated the sensitivity of U-value of window and g-value of window separately, where some of the combinations did not exist as a window construction.

With regards to the comparison of measured and simulated indoor air temperature, an average of 2°C over-prediction during the one-week measurement period in April 2017 was found. This is aligned to findings by Short et al. (2018), where the diurnal variation of measured and simulated indoor air temperature has a 2°C difference at the most extensive divergence. Furthermore, this thesis introduced a pre-validation period by extending the whole simulation period from one week to three weeks, and thus the prediction difference was reduced. However, no action was performed by Short et al. (2018) to improve the fit, even though Short et al. (2018) reported a 2°C difference in winter and 1°C difference in summer at the start of the simulation period. If Short et al. (2018) introduced a pre-validation period, the prediction difference could be further reduced.

Finally, the calibration of the DTM revealed that the external wall and window construction were not sensitive to indoor air temperature but were sensitive to the air infiltration rate. However, the results are not in line with the results as the predicted sensitivities of building fabrics, in which the external wall and window construction also varies according to energy demand for the sensitivity analysis. This may be because the measurement was performed in mid-season, where the temperature difference between indoors and outdoors is

small. Additionally, owing to the fact that MBE and CvRMSE were not improved when adjusting the air infiltration rate parameter, the model did not meet the calibration criteria. Nevertheless, this is the first study which attempted to calibrate a DTM for a residential building in the HSCW zone; it can provide useful insights for future studies which perform DTM calibration in a similar condition.

The next chapter aims to quantify the performance of energy saving retrofits of the case study building.

Chapter 5 : Energy saving retrofits for a case study building

5.1 Introduction

In this Chapter, Objective 3 is addressed. First, energy and thermal comfort performance of the case study flat was predicted, using the DTM developed in Section 3.4. After that, the investigation is expanded to other flat locations and the whole case study building. Finally, an optimum combination of retrofit measures (developed in Section 3.5) for reducing energy consumption and thermal discomfort is evaluated in the case study building.

Section 5.2 presents the energy and thermal comfort performance of a case study flat before retrofit. This includes a comparison of measured monthly energy consumption (selected from Section 3.6) with the predicted monthly energy consumption (using the DTM developed in Section 3.4) for the three energy users. Moreover, the thermal comfort conditions are evaluated using the thermal comfort evaluation metrics developed in Section 3.6.2.

Section 5.3 presents the energy and thermal comfort performance for different flat locations before retrofit. Section 2.5.4 showed the importance of evaluating the location of the flat within an apartment building, and thus Section 3.4.3 selected twelve types of flats to be modelled out of 96 flats in the case study building. This section compares the prediction difference of energy and thermal comfort performance considering the categories of flats modelled and the case study flat.

Section 5.4 presents the energy and thermal comfort performance for the whole case study building before retrofit, i.e., all the 96 flats in the case study building are considered. The results are then compared with the case study flat.

Section 5.5 presents the selection of an optimum combination of retrofit measures from the list of retrofit options. Heating and cooling energy consumption reduction, combined with the summer and winter thermal discomfort hours reduction, were predicted for the selected options for each retrofit measure developed in Section 3.5. An optimum option for each retrofit measure was selected based on the ability to reduce energy consumption and thermal discomfort hours.

Section 5.6 presents the performance of the selected retrofit measures in other flat locations in the case study building to compare the effectiveness of the selected retrofit measures in each flat.

Section 5.7 presents the cost of retrofitting the case study building, and a cost-benefit analysis of the proposed energy saving retrofit measures.

5.2 Energy and thermal comfort performance of a case study flat: Pre-retrofit conditions

5.2.1 Predicted energy performance

For the case study flat, the energy consumption for different types of energy users varies significantly. In this chapter, energy consumption is referred to as space-conditioning electricity consumption. The predicted annual energy consumption for the three energy users were presented in Table 5-1. The low energy user consumes half of the total energy consumption used by the high energy user. The proportion of energy consumption for heating and for cooling is about 40/60 for all three types of energy users (Table 5-1).

In Section 3.6 seven studies which collected electricity consumption from energy meters in different households were presented, however only two studies by Ouyang et al. (2011, 2009) reported the monthly electricity consumption for the households measured; hence, these were used to evaluate the predictions of annual and monthly energy consumption of the case study flat using DTM. Heating energy consumption measured by Ouyang et al. (2011, 2009) was found to be 3.65 and 5.51 kWh/m², with a mean value of 4.58 kWh/m². Cooling energy consumption was found to be 6.77 and 10.32

kWh/m², with a mean value of 8.55 kWh/m². Therefore, the total (heating and cooling) measured energy consumption from Ouyang et al. (2011, 2009) was 13.1 kWh/m², which is in line with the results of the research reported in Table 5-1.

Table 5-1: Annual energy consumption for three energy users and monitoring studies.

	Heating energy consumption (kWh/m ²)	Cooling energy consumption (kWh/m ²)	Total energy consumption (kWh/m ²)	Heating and cooling ratio
Low energy users	3.38	5.85	9.24	40/60
Medium energy users	4.92	7.22	12.14	40/60
High energy users	6.84	9.52	16.35	40/60
Measurements by Ouyang et al. (2011, 2009)	4.58	8.55	13.1	40/60

Considering the predicted monthly energy consumption, November to March is the heating season with zero cooling energy consumption; April and October are the transition seasons (heating and cooling energy consumption are less than 0.1 kWh/m²), and May to September is the cooling season with zero heating energy consumption. Comparing with the measured energy consumption by Ouyang et al. (2011, 2009), the measured heating energy consumption lies between the prediction from medium and high energy users in January, February, and March. In December, the measured heating energy consumption was lower than the prediction from low energy users (Figure 5-1). The measured cooling energy consumption by Ouyang et al. (2011, 2009) was higher than the prediction from high energy users in July and August. In June and September, the measured cooling energy consumption was lower than the prediction from low energy users, and in May, the measurement lay between the prediction from medium and high energy users (Figure 5-1).

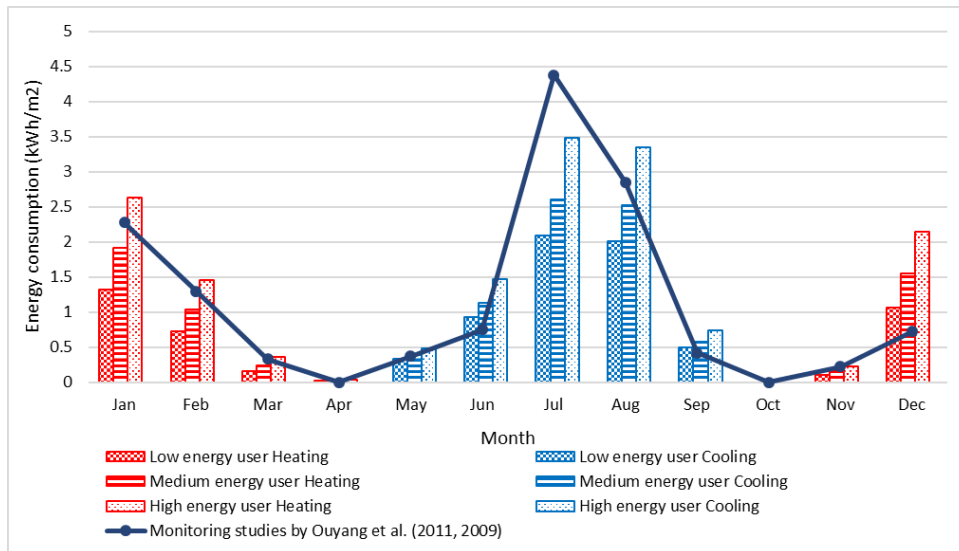


Figure 5-1: Predicted monthly energy consumption for different energy users in case study flat.

5.2.2 Predicted thermal comfort performance

The mean monthly indoor air temperature in winter (December, January, and February) and summer (June, July, and August) during occupied hours was predicted for living room and bedroom. Figure 5-2 showed the monthly average indoor air temperature without AC for the case study flat. The lower boundary of comfort range was the heating set-point (17.7°C), and the higher boundary of comfort range was the cooling set-point (27.9°C). In winter, the average indoor air temperature was below the comfort range from December to February, with January being the coldest month. During January the average indoor air temperature was 9.81°C in the bedroom and 10.04°C in the living room, with an average indoor air temperature of 11.05°C for the two rooms during occupied hours. A survey study by Guo et al. (2015) of measured indoor air temperature in various households for residential buildings in the HSCW zone reported a median indoor temperature of unheated rooms of 12.1°C with a range of $10\text{-}14^{\circ}\text{C}$, which is in line with the results of the research reported here.

In summer, the average indoor air temperature above the comfort range was from June to August. August was the hottest month with an average indoor air temperature of 30.7°C in the bedroom and 30.9°C in the living room, with an average indoor air temperature of 30.7°C across the two zones. Indoor air temperature predicted in the bedroom and living room was similar (less than

0.1°C) (Figure 5-2). Zhang et al. (2013) measured indoor air temperature in various households (without AC) within residential buildings in the Hot Summer and Warm Winter (HSWW) zone in summer. The HSWW zone (25-30°C) has average outdoor temperature similar to the HSCW zone (25-29°C) in summer. Results from Zhang et al. (2013) found that the average surveyed indoor air temperature was 30.1°C, which is in line with the results of the research reported here.

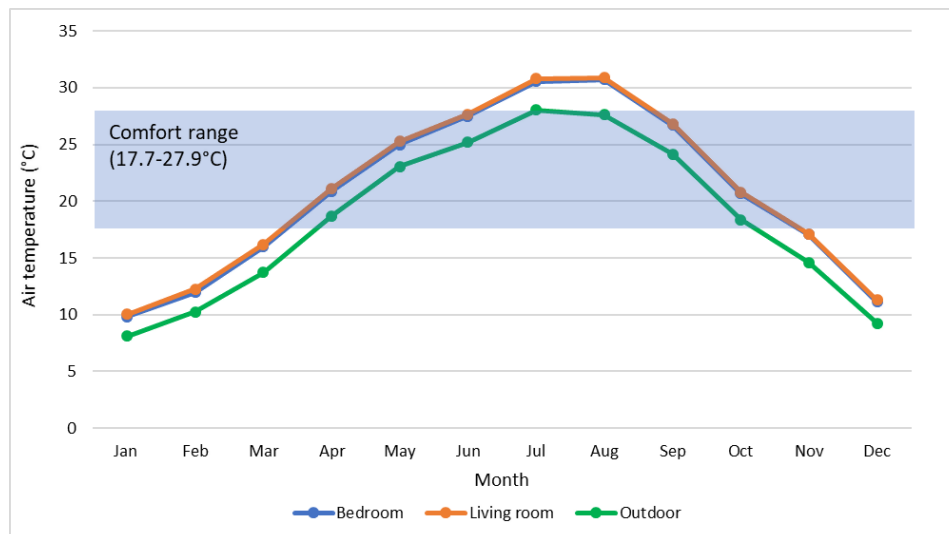


Figure 5-2: Predicted monthly indoor air temperature without AC.

When AC operation with medium energy users was considered, the average indoor air temperature in winter increased significantly to 16.1°C in the living room and increased to 12.6°C in the bedroom during occupied hours (Figure 5-3). Although no heating was operated in the bedroom, the indoor air temperature was higher than the case without AC. This may be due to the heat transfer between the internal wall separating the living room and bedroom, as heating was operated in the living room in the evening. The mean indoor air temperature for the living room and bedroom was 14.4°C, which is in line with the results reported in Gou et al. (2014), with a median measured indoor air temperature of heated rooms of 15.3°C.

In the summer with AC operation with medium energy users, the average indoor air temperature above the comfort range is from June to August, with August being the hottest month. In August there is an average indoor air temperature of 28°C in the bedroom and 29.2°C in the living room, with an

average indoor air temperature of 28.6°C across the two zones (Figure 5-3). B. Li et al. (2018) measured indoor air temperature in various households for residential buildings in the HSCW zone and reported an average indoor air temperature of 28.2°C in July and August, which is in line with the results of the research reported here.

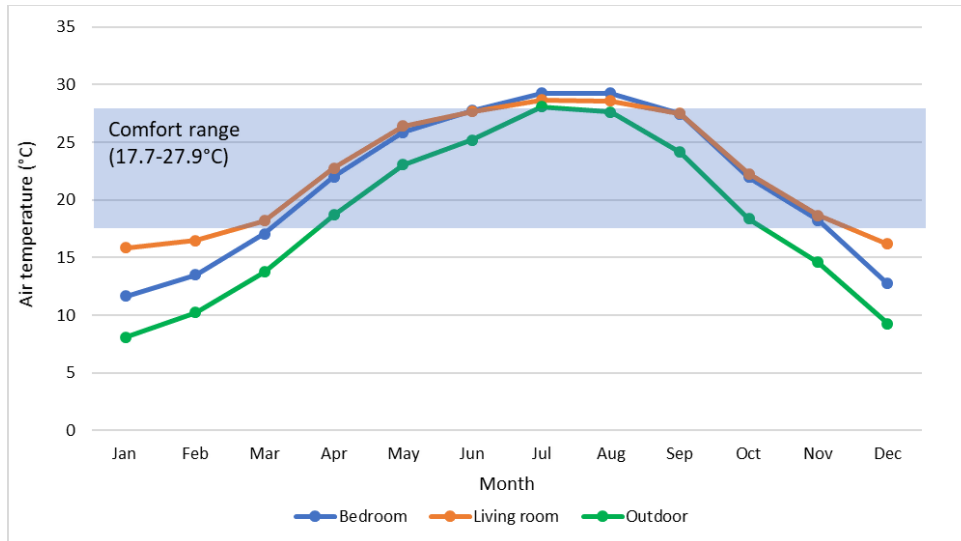


Figure 5-3: Predicted monthly indoor air temperature with medium energy users.

Winter discomfort hours is defined as the number of hours annually with an indoor air temperature lower than 17.7°C (selected based on the heating set-point) in the living room and bedroom. Summer discomfort hours is defined as the number of hours annually with an indoor air temperature higher than 27.9°C (selected based on the cooling set-point) in the living room and bedroom. Note that the annual occupied hour was 2920 hours in the living room and 2555 hours in the bedroom, with a total occupied hour of 5475 hours.

Results from the DTM suggested that as the living room occupied 2920 hours annually, there were 941 discomfort hours in winter and 736 discomfort hours in summer. The percentage of discomfort hours annually is 57.4% in occupied hours. The bedroom is occupied for 2555 hours annually, with 869 discomfort hours in winter and 570 discomfort hours in summer. The percentage of discomfort hours annually is 56.3% during occupied hours. In all spaces combined, they are occupied for 5475 hours annually, with 1810 discomfort hours in winter and 1306 discomfort hours in summer. The percentage of discomfort hours annually is 56.9% discomfort during occupied hours.

5.3 Energy and thermal comfort performance of different flat locations: Pre-retrofit conditions

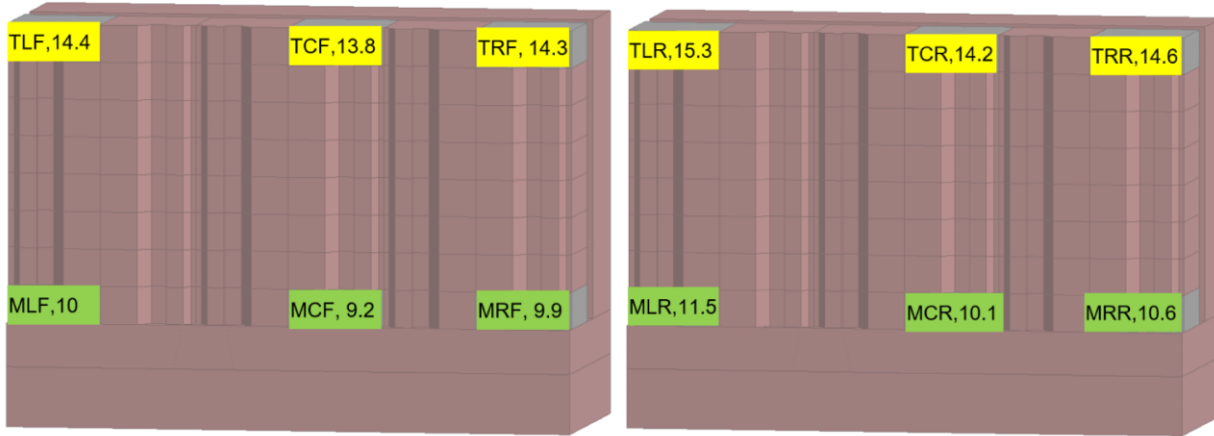
5.3.1 Predicted energy consumption

Methods to evaluate different flats in the case study building were developed in Section 3.3.3, in which twelve types of flats were selected to be modelled out of 96 flats in the building (see Figure 5-4). The twelve types of flats can be further divided into four groups of flats in response to different exposed roof/wall to floor area ratios (Table 5-2). The exposed wall/roof to floor area ratio was calculated by the sum of roof and wall area exposed to outdoor conditions divided by floor area. The twelve types of flats have different energy performance because the exposed roof/wall to floor area ratio and building orientation varied. The base case total energy consumption for the twelve types of flats for the three energy users was predicted (Figure 5-4).

Table 5-2: Exposed roof/wall to floor area ratio for twelve types of flats in the case study building.

Flat	Exposed roof area (m ²)		Exposed external wall area (m ²)		Exposed roof/wall to floor area ratio		
	Living room	Bedroom	Living room	Bedroom	Living room	Bedroom	Whole flat
MCF, MCR	0	0	12.9	11.5	0.26	0.23	0.49
MLF, MRF, MLR, MRR	0	0	12.9	23.6	0.26	0.48	0.74
TCF, TCB	29.2	15.4	12.9	11.5	0.85	0.55	1.4
TRF, TLF, TRR, TLR	29.2	15.4	12.9	23.6	0.85	0.79	1.64

a) Low energy users



b) Medium energy users



c) High energy users



Key		Code
MLF: Middle Left Front	MLR: Middle Left Rear	MCF, 12.1
MCF: Middle Centre Front	MCR: Middle Centre Rear	Flat position
MRF: Middle Right Front	MRR: Middle Right Rear	Total energy consumption in kWh/m ²
TLF: Top Left Front	TLR: Top Left Rear	Colour: Green (<12 kWh/m ²)
TCF: Top Centre Front	TCR: Top Centre Rear	Yellow (12-16 kWh/m ²)
TRF: Top Right Front	TRR: Top Right Rear	Orange (16-20 kWh/m ²)
		Red (>20 kWh/m ²)

Figure 5-4: Energy consumption for different flat locations for three energy users.

For front flats, the percentage changed compared to case study flats in annual energy consumption for middle corner flats increased from low energy users (8% to 9%) to high energy users (12% to 13%). The difference between top flats is similar, with an increase in energy consumption with low (50% to 56%), medium (57% to 63%) and high (60% to 67%) energy users. For middle rear facing flats, the percentage change is more substantial (12%) for low energy users and smaller (10%) for high energy users, with an average of 11% increase in energy consumption. For corner flats facing the rear, the order of percentage change increased from low to high energy users. For top flats facing the rear, the energy consumption increase was similar to top flats facing front with 42% to 55% increase, with a difference of 5% when compared to top flats facing front (Figure 5-5).

The annual energy reduction shows large variation when different energy users are considered (Figure 5-4); the difference between a low and high energy user is doubled. Also, energy consumption for low energy users in top flats (16 kWh/m²) can be higher than medium energy users in medium flats (15 kWh/m²), which reflects the importance of identifying the energy consumption in top flats (Figure 5-4).

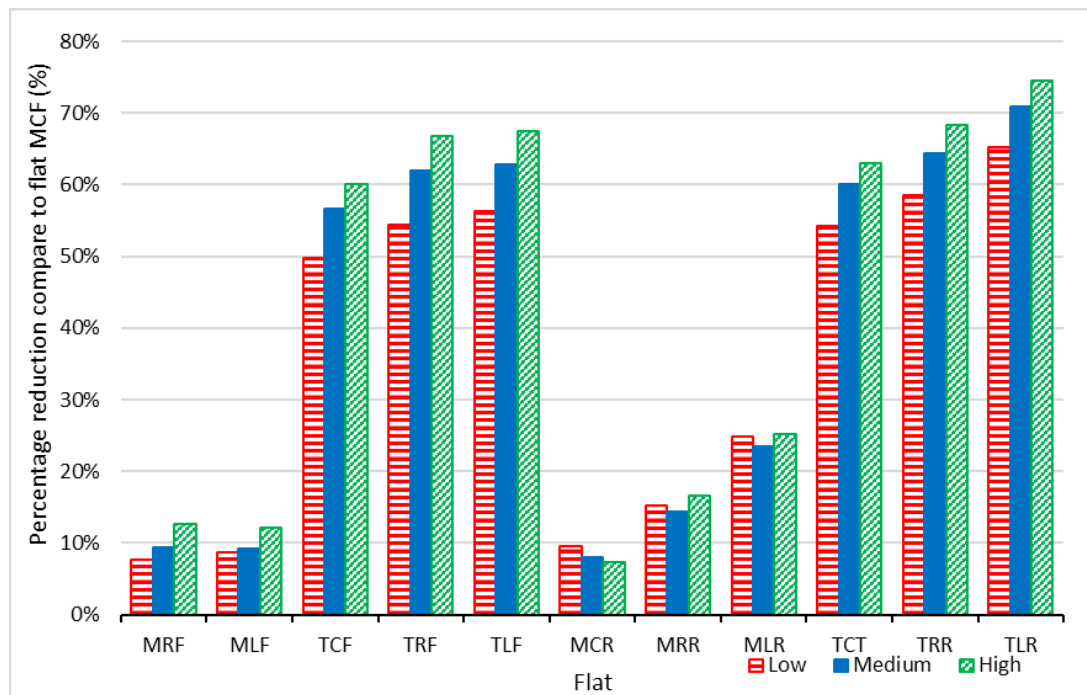


Figure 5-5: Percentage change in energy consumption for different energy users when compare to flat MCF

The energy consumption performance for six types of flats located at the front was quantified by calculating the percentage change of energy consumption when compared to flat MCF (case study flat). Results showed that flat TCF consumed 57% more energy annually, but middle corner flats (flats MLF and MRF) consumed 9% more energy annually. This was due to the larger exposed roof/wall to floor area ratio for flat TCF compared to the middle corner flats (flats MLF and MRF; Table 5-2). In the middle corner flats, change of heating energy consumption (9%) was similar to cooling energy consumption (10%), whereas in flat TCF, the change of heating energy consumption (89%) was much bigger than cooling energy consumption (35%). Additionally, variation between flats MLF and MRF was minimal, also between flats TLF and TRF. Thus, the evidence suggested that solar heat gain from external walls in left and right flats was similar (Figure 5-6).

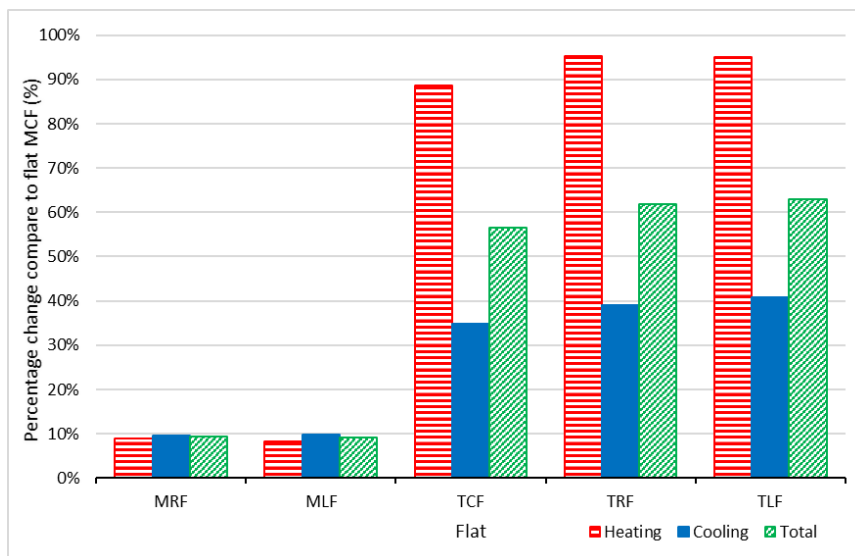


Figure 5-6: Percentage change in energy consumption when compared to flat MCF.

For the middle centre flat facing rear (flat MCR), annual heating energy consumption was 12.3% lower than flat MCF, and the annual cooling energy consumption was 21.8% higher than flat MCF. Because the flat facing front was oriented 30° to the north and the flat facing rear was oriented 30° to the south, flat MCR experienced more solar heat gain which increased cooling energy consumption but decreased heating energy consumption.

The energy consumption performance for six types of flats located at the rear is quantified by calculating the percentage change of energy consumption

when compared to flat MCR. Results showed that both flat MLR and flat MRR consumed more energy annually than flat MCR, with flat MLR consumed the highest energy among three flats. In particular, the difference was more substantial for cooling energy (16% increase for flat MLR compared to a 4% increase for flat MRR) compared with heating energy (11% increase for both flats). The reason may be due to the orientation of the exposed external wall of flat MLR. Top flats consumed double the heating energy when compared to flat MLR, but cooling energy only increased by 20%. Heating energy consumption was 4% lower and cooling energy consumption was 8% higher for flat TCR compared with flat TCF; thus the change due to orientation (front and rear flats) was smaller for top centre flats compared to middle centre flats. Interestingly, the cooling energy consumption difference when compared with flat MCR was similar for flats MLR (15.9%) and TCR (19.6%), whereas for front flats the difference was large (10% and 35% for MLF and TCF respectively) (Figure 5-7).

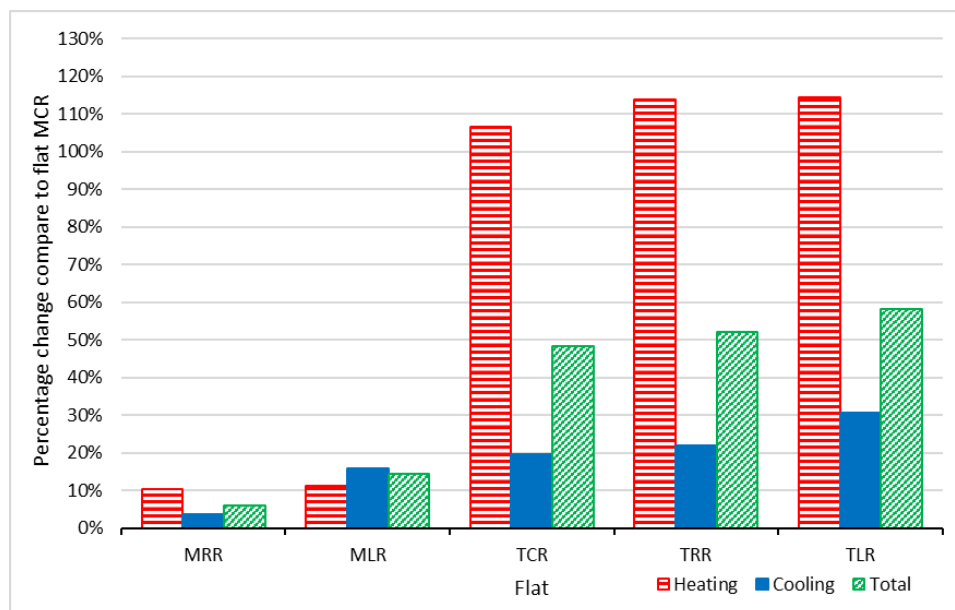


Figure 5-7: Percentage change in energy consumption when compared to flat MCR.

5.3.2 Predicted thermal comfort performance

The thermal comfort performance for the six types of flats located at the front is quantified by calculating the absolute change in thermal discomfort hours when compared to flat MCF; note that total discomfort hours is the sum of winter and summer discomfort hours. Similar to energy consumption, the result

showed that the top flats had poor thermal comfort performance, experiencing an increase of 400 hours annually compared to flat MCF, but the middle corner flat experienced an increase of 75 hours. The difference in thermal discomfort hours for flats TCF, TRF, and TLF was the same (400 more discomfort hours), but the energy consumption of these three flats was different. Winter discomfort hours in the top flats (2160 hours) were higher than the middle flats (1810 hours) by 350 hours. The increase in summer discomfort hours was not as large (50 hours increase; Figure 5-8).

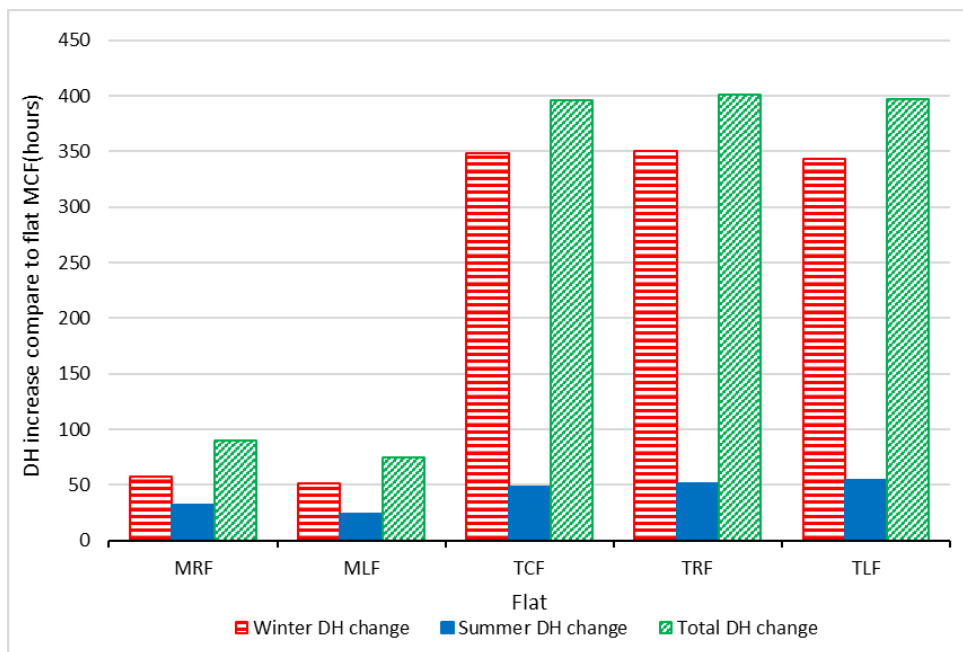


Figure 5-8: Discomfort hours (DH) increase for different flat locations when compared to flat MCF.

For the block of flats facing the rear, top floor flats had an increase in winter discomfort hours (400 hours) but a decrease in summer discomfort hours (50 hours). The total discomfort hours increase was slightly larger for flat TLR (50 hours). Similarly, flat MRR had an increase in winter discomfort hours but a decrease in summer discomfort hours, leading to a small increase in total discomfort hours (20 hours). However, for the case of flat MLR, both heating and cooling discomfort hours increased, with total discomfort hours increase of 100 hours when compared to flat MCR (Figure 5-9).

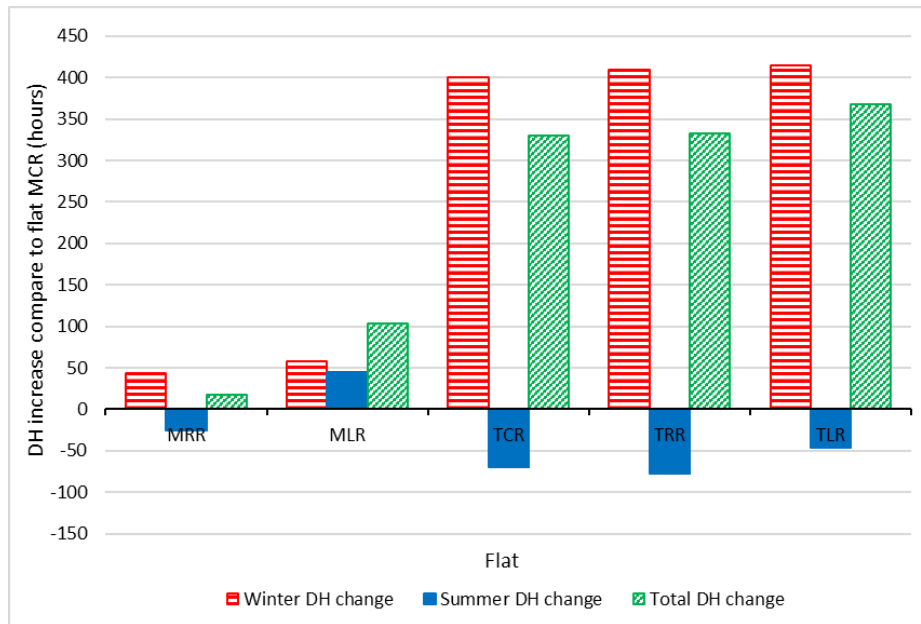


Figure 5-9: Discomfort hours (DH) increase for different flat locations when compared to flat MCR.

5.4 Energy and thermal comfort performance of the whole case study building: Pre-retrofit conditions

5.4.1 Predicted energy consumption

Section 5.3 predicted the energy consumption for the twelve types of flats in the case study building. Subsequently, the whole building's energy consumption was calculated by adding energy consumption of all the flats (96 flats) in the building. Flats MCF and MCR represented 28 flats in the building; flats MRF, MLF, MRR, and MLR represented seven flats in the building; flats TCF and TCR represented four flats in the building; and flats TRF, TLF, TRR, and TLR represented one flat in the building. The average energy consumption per floor area of the building was calculated by dividing the built area (4732.8 m²) by total energy consumption for 96 flats (equation 5-1).

$$E = (28 \times E_{MCF} + 7 \times E_{MRF} + 7 \times E_{MLF} + 4 \times E_{TCF} + E_{TLF} + E_{TRF} + 28 \times E_{MCR} + 7 \times E_{MRR} + 7 \times E_{MLR} + 4 \times E_{TCR} + E_{TLR} + E_{TRR})/96 \quad (5-1)$$

Where E is the predicted energy consumption for the whole case study building, E_{MCF} , E_{MRF} , E_{MLF} , E_{TCF} , E_{TLF} , E_{TRF} , E_{MCR} , E_{MRR} , E_{MLR} , E_{TCR} , E_{TLR} and E_{TRR} are

the predicted energy consumption for flats MCF, MRF, MLF, TCF, TLF, TRF, MCR, MRR, MLR, TCR, TLR, and TRR respectively.

The prediction from dynamic thermal simulation revealed that both heating and cooling energy consumption are under-predicted when the case study flat is considered instead of the whole case study building for all three energy users. As Section 5.3.1 showed that case study flat (flat MCF) had the lowest energy consumption among all the flats investigated; furthermore, top flats consumed 60% more energy than the case study flat. Therefore, when modelling only the case study flat, it experienced an under-prediction of 8% for heating, 18% for cooling, and 14% for total energy consumption compared to modelling the whole case study building. Moreover, the percentage of under-predictions for low (14%) and high (15%) energy users were similar for total energy consumption. When compared to measurements by Ouyang et al. (2011, 2009), discussed in Section 5.2.1, medium energy users predicted 16% more heating energy, with a total of 5% over-prediction for energy consumption (Table 5-3).

Table 5-3: Annual energy consumption for three energy users of the case study flat and building.

	Heating energy (kWh/m ²)	Cooling energy (kWh/m ²)	Total energy (kWh/m ²)
Low energy users (flat)	3.38	5.85	9.23
Low energy users (building)	3.62	6.88	10.50
Medium energy users (flat)	4.92	7.22	12.15
Medium energy users (building)	5.33	8.52	13.85
High energy users (flat)	6.84	9.51	16.35
High energy users (building)	7.55	11.25	18.80
Measurements from Ouyang et al., (2011, 2009)	4.58	8.55	13.13

5.4.2 Predicted thermal comfort

When considering the whole case study building, the calculation of discomfort hours utilises the same method as energy consumption (equation 5-1).

Results suggested that the winter discomfort hours was 1812 hours (2 hours higher than the case study flat) and summer discomfort hours was 1390 hours (82 hours higher than case study flat), with a total discomfort hour of 58.5%,

which is 1.6% higher than case study flat. Therefore, it is vital to consider the case study building as a whole when evaluating retrofit performance.

5.5 Selection of an optimum combination of retrofit measures in reducing energy and thermal discomfort for a case study building

Section 3.5 developed a list of options for each of the retrofit measures, and this section aims to predict energy consumption and thermal discomfort hours by applying the retrofit options for each retrofit measure. Subsequently, the optimum retrofit option which achieves the highest energy and thermal discomfort hour reduction was selected for each retrofit measure. The evaluations for external wall insulation, double-glazed windows, improved air tightness, added window overhang, enclosed communal staircase, and energy efficient ACs were performed in the case study flat; whereas evaluation for roof insulation was performed in the top floor flat on the centre facing front.

Retrofit measure one: External wall insulation

For external wall insulation, the predicted heating energy consumption reduction was 9.2% if 30 mm EPS insulation was employed; however, the predicted cooling energy increased by 1.5%. The total energy consumption reduction was 2.9% because the base case cooling energy consumption was higher than heating energy consumption.

When considering thermal comfort, predicted winter discomfort hours reduced by 70 hours for 30 mm EPS insulation, and summer discomfort hours increased by 35 hours. However, the total discomfort hour reduction was the highest (37 hours reduction) for 25 mm EPS insulation, with a U-value for the external wall of 0.79 W/m²K. Moreover, Figure 5-10 showed that energy consumption and thermal discomfort reduction were less effective when the thickness of EPS insulation increased. In fact, the largest reduction occurred for 10 mm EPS insulation (2% reduction for energy consumption) when compared to no EPS insulation. Therefore, 25 mm was selected as the optimum EPS insulation thickness, with a U-value of 0.79 W/m²K (Figure 5-10).

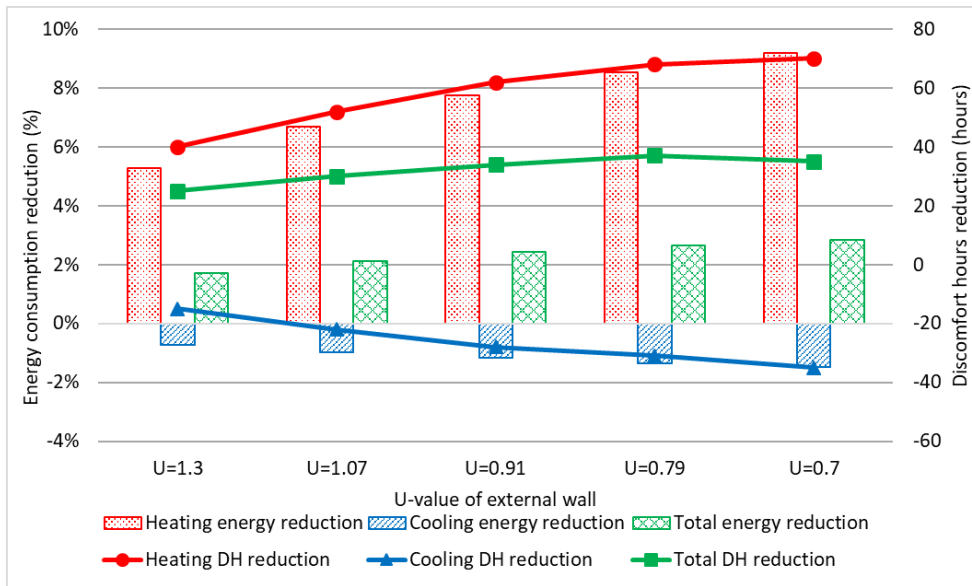


Figure 5-10: Energy consumption and discomfort hours reduction for external wall insulation (flat MCF).

Retrofit measure two: Roof insulation

Flat TCF was used as a base case to analyse the optimum retrofit measure for roof insulation, as the ceiling for the case study flat is adiabatic. Note that the base case energy consumption for flat TCF was 57% higher than flat MCF, as discussed in Section 5.2.

Considering energy consumption reduction, the worst-performing retrofit option was 20 mm EPS insulation (U-value of roof = 1.31 W/m²K), where the total energy reduction was 22%. The best performing retrofit option was 50 mm EPS insulation, which reduced total energy consumption by 27%. Interestingly, the total energy consumption with 50 mm EPS insulation was 13.7 kWh/m², which was higher than the total energy consumption for flat MCF pre-retrofit (12.15 kWh/m²). Considering thermal discomfort hours reduction, winter discomfort hours reduced by 260 hours for 50 mm EPS insulation, but summer discomfort hours remained the same (49 hours) for all the four insulation thicknesses investigated. This lead to a total thermal discomfort reduction of 320 hours with 50 mm EPS insulation. Similar to energy consumption, the thermal discomfort hours after 50 mm EPS insulation was 58.2% for flat TCF, higher than flat MCF pre-retrofit (56.9%). Therefore, 50 mm roof insulation was selected as the optimum retrofit measure for roof (Figure 5-11).

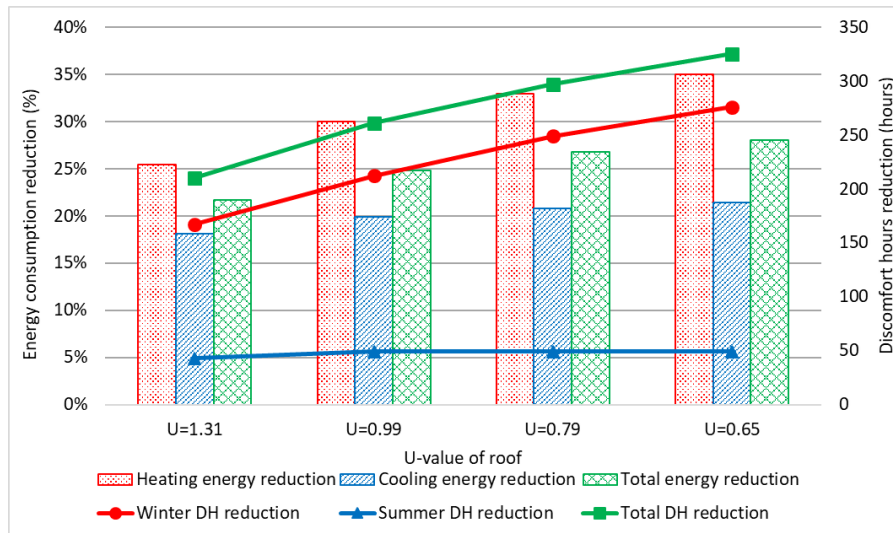


Figure 5-11: Energy consumption and discomfort hours reduction for roof insulation (flat TCF).

Retrofit measure three: Double-glazed windows

When replacing single-glazed windows with double-glazed, all options in Figure 5-12 showed a reduction in total energy consumption, with low-e argon double-glazing (U-value of 1.5 W/m²K and g-value of 0.54) having the highest total energy reduction of 15.7%. It is interesting that the reductions of U-value of window and g-value of window counteract each other, i.e., heating energy reduced when U-value of window decreased, and heating energy increased when g-value of window decreased. On the other hand, cooling energy reduced when g-value of window decreased, and cooling energy increased when U-value of window increased.

When considering thermal comfort, winter thermal discomfort hours increased for all five options of double-glazed windows, with the highest 49 hours increase for double-glazed windows with solar control (U-value of 2.8 W/m²K and g-value of 0.54). In summer, thermal discomfort hours decreased for all five options of double-glazed windows, with the highest reduction of 131 hours for double-glazed windows with solar control (U-value of 2.8 W/m²K and g-value of 0.54). Percentage point of reduction of total energy consumption and thermal discomfort hours is large when g-value reduced from 0.75 to 0.54. When the U-value of window reduced from 2.8 to 1.9 W/m²K, the percentage point of reduction of total energy consumption increased slightly by 1%, because heating energy increased by 5% but cooling energy decreased by 2%. For thermal discomfort hours, the trend was similar to energy consumption,

with a reduction of total thermal discomfort hours by 17 hours. When the U-value of window further reduced from 1.9 to 1.5 W/m²K, the total energy consumption remained the same and total discomfort hours further reduced by 10 hours. Thus, the window with a U-value of 1.9 W/m²K and g-value of 0.54 was selected (Figure 5-12).

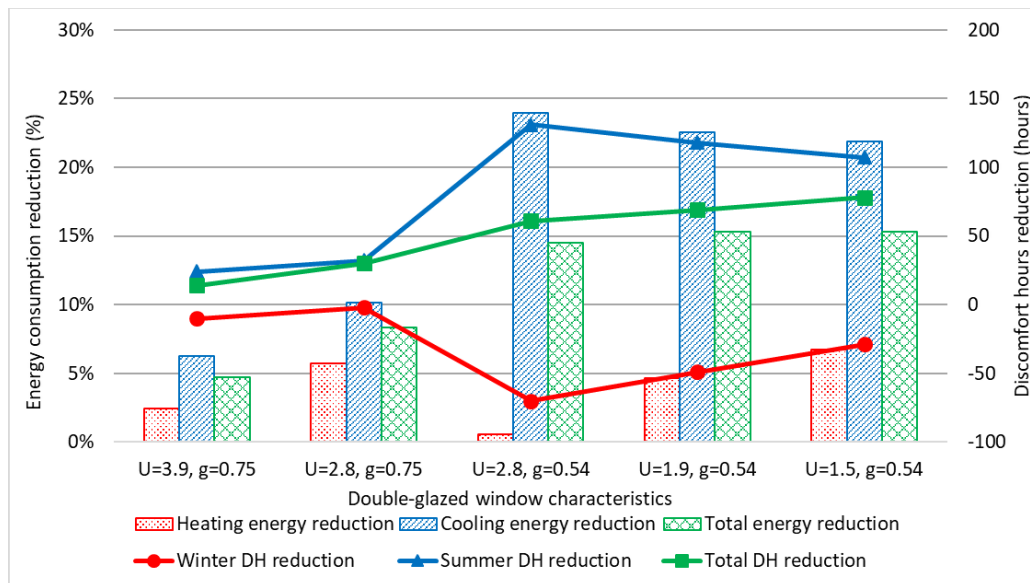


Figure 5-12: Energy consumption and discomfort hours reduction for double-glazed windows (flat MCF).

Retrofit measure four: Reduced air leakage

For reducing air infiltration rate, heating energy consumption had the largest reduction with 31% when air infiltration rate was 0.5 ach⁻¹, where total energy reduction was 14.3%. For thermal comfort, winter thermal discomfort hours reduced by 155 hours when air infiltration rate was 0.5 ach⁻¹. However, summer thermal discomfort hours increased by 178 hours, leading to a net 23 hours increase in total thermal discomfort hours. Considering total discomfort hours reduction, an air infiltration rate of 1 ach⁻¹ performs the best with a 20 hours reduction; however, the total energy reduction is the lowest (7%) in this case among the three options of air infiltration rate. Therefore, considering both energy consumption and thermal discomfort reduction, an air infiltration rate of 0.7 ach⁻¹ was selected (Figure 5-13).

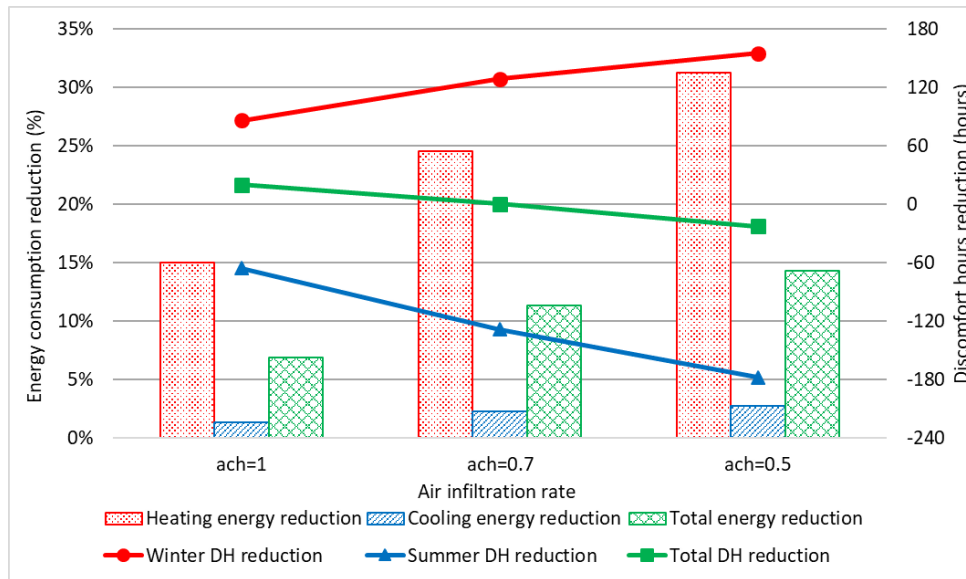


Figure 5-13: Energy consumption and discomfort hours reduction for reducing air infiltration rate (flat MCF).

Retrofit measure five: Add window overhang

For additional window overhang, heating energy consumption increased by 2% for overhang length of 1 m and cooling energy decreased by 11.5%, leading to a total energy reduction of 6%. For thermal comfort, winter thermal discomfort hours increased by 37 hours for overhang length of 1 m, however, summer discomfort hours decreased by 54 hours, with a net 17 hours reduction in total thermal discomfort hours. When overhang length increased from 0.3 m to 1 m, the total thermal discomfort hours reduction was similar (16 hours), and total energy reduction increased slightly (2 to 6%). Interestingly, the total thermal discomfort hours reduction was 17 hours for an overhang length of 0.5 m. Because an overhang length of 1 m led to a massive increase (37 hours) of winter thermal discomfort hours, which reduce total discomfort hours by 1 hour when compare to an overhang length of 0.5 m, despite a 52 hours reduction of summer discomfort hours. Therefore, considering both energy consumption and thermal discomfort reduction, overhang length of 0.5 m was selected in this study (Figure 5-14)

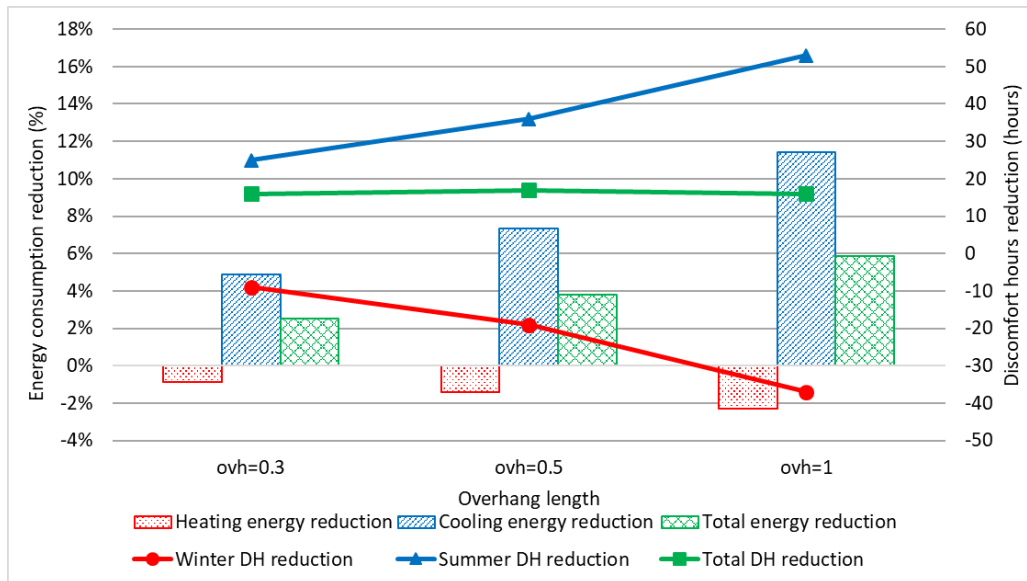


Figure 5-14: Energy consumption and discomfort hours reduction for additional overhang (flat MCF).

Retrofit measure six: Enclosed communal staircase

Total energy consumption and thermal discomfort hours reduced when the staircase was enclosed for all three options (exclusion of windows and external walls without insulation; single-glazed windows and external walls without insulation; double-glazed windows and external walls with insulation). For the case of double-glazed windows and external walls with insulation, it was assumed the parameters of the selected retrofit measures (25 mm EPS external wall insulation, double-glazed windows with low-e coating, air infiltration rate of 0.7 ach^{-1} and overhang length of 0.5 m) were used. Results showed that an enclosed communal staircase with option double-glazed windows and external walls with insulation performed the best among the three options, achieving a 10% reduction of total energy consumption and 68 hours reduction of total thermal discomfort hours. Therefore, the option with double-glazed windows and external walls with insulation was selected for an enclosed communal staircase (Figure 5-15).

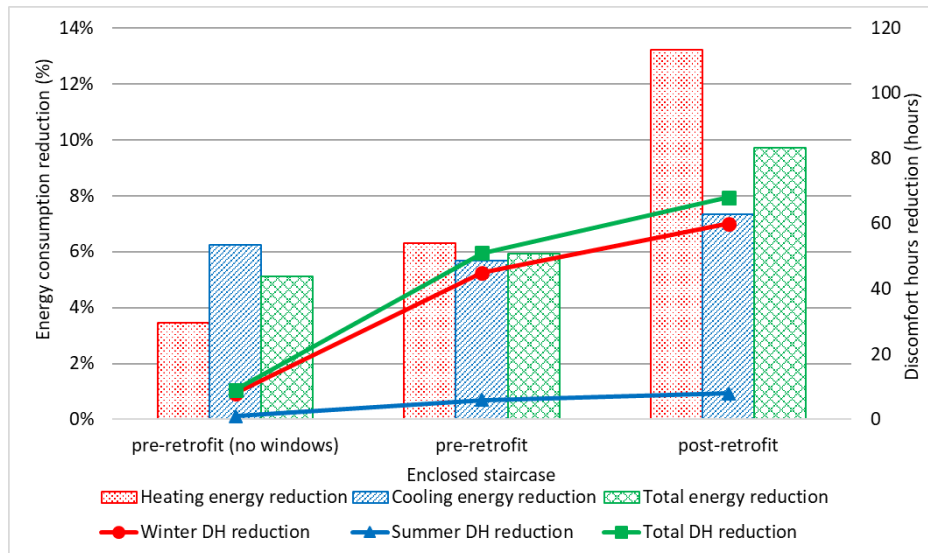


Figure 5-15: Energy consumption and discomfort hours reduction for enclosed communal staircase (flat MCF).

Retrofit measure seven: Energy-efficient AC

Energy-efficient AC provide similar heating, cooling, and total energy reduction, with Grade 1 AC achieving the highest total energy reduction of 28%. Thermal discomfort hours are unchanged for energy-efficient AC because the operating hours of AC do not change after the retrofit. Therefore, Grade 1 air conditioner was selected considering energy reduction (Figure 5-16).

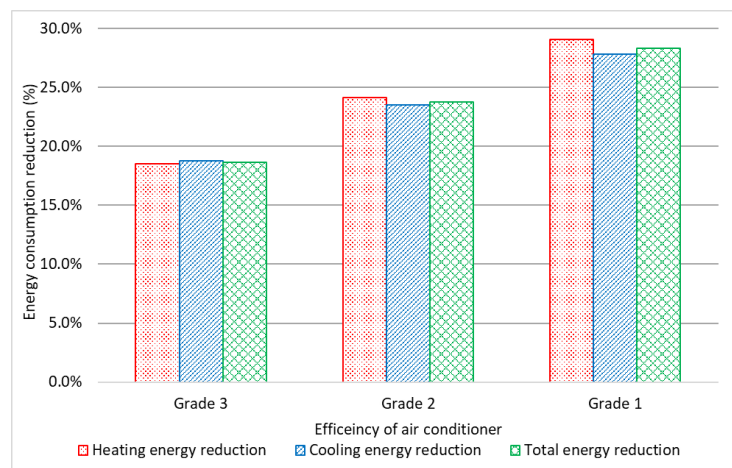


Figure 5-16: Energy consumption and discomfort hours reduction for energy-efficient AC (flat MCF).

Table 5-4 summarised the selected seven optimum combinations of retrofit measures in reducing energy consumption and thermal discomfort hours

Table 5-4: Selection of optimum combination of retrofit measures.

Retrofit measure	Details	Changes in the dynamic thermal model
1	External wall insulation with 25mm EPS insulation	U-value of external wall reduces from 2.3 to 0.79 W/m ² K
2	Roof insulation with 50mm EPS insulation	U-value of roof reduced from 3.45 to 0.65 W/m ² K
3	New double-glazed low-e window with solar control	U-value of window reduces from 5.9 to 1.9 W/m ² K, g-value of window reduces from 0.87 to 0.47
4	Reduce air infiltration rate	Air infiltration rate reduces from 1.5 to 0.7 ach ⁻¹
5	Additional overhang	Overhang length of 0.5m is installed
6	Enclosed communal staircase with single-glazed windows in internal corridor	Staircase from semi-indoor condition to fully indoor condition
7	Energy-efficient AC with Grade 1	Heating COP increases from 2.2 to 3.1, cooling COP increases from 2.6 to 3.6

5.6 Predicted energy and thermal discomfort reduction for the selected retrofit measures for the case study building

5.6.1 Predicted retrofit performance in the case study flat

The selected optimum combination of retrofit measures from Section 5.5 (Table 5-4) was evaluated in the case study flat (flat MCF). Results revealed that the energy saving retrofits performed differently when considering heating, cooling, and total energy consumption. Considering building fabric retrofit measures, reduced air infiltration (25%) and enclosed communal staircase (13%) resulted in the two highest heating energy reductions, while double-glazed windows (23%) and additional overhang (7%) resulted in the two highest cooling energy reductions. But when combining heating and cooling, double-glazed windows (15%) and reduced air infiltration (11%) ranked the first and second. When combining all the building fabric retrofit measures, the total energy reduction was 45%, where heating energy reduction (62%) was more substantial than cooling energy reduction (33%). The heating and cooling energy reduction for energy-efficient AC was the highest among all retrofit measures, but the energy reduction (28%) of energy-efficient AC was lower than the case of combining all building fabric retrofit measures (Figure 5-17).

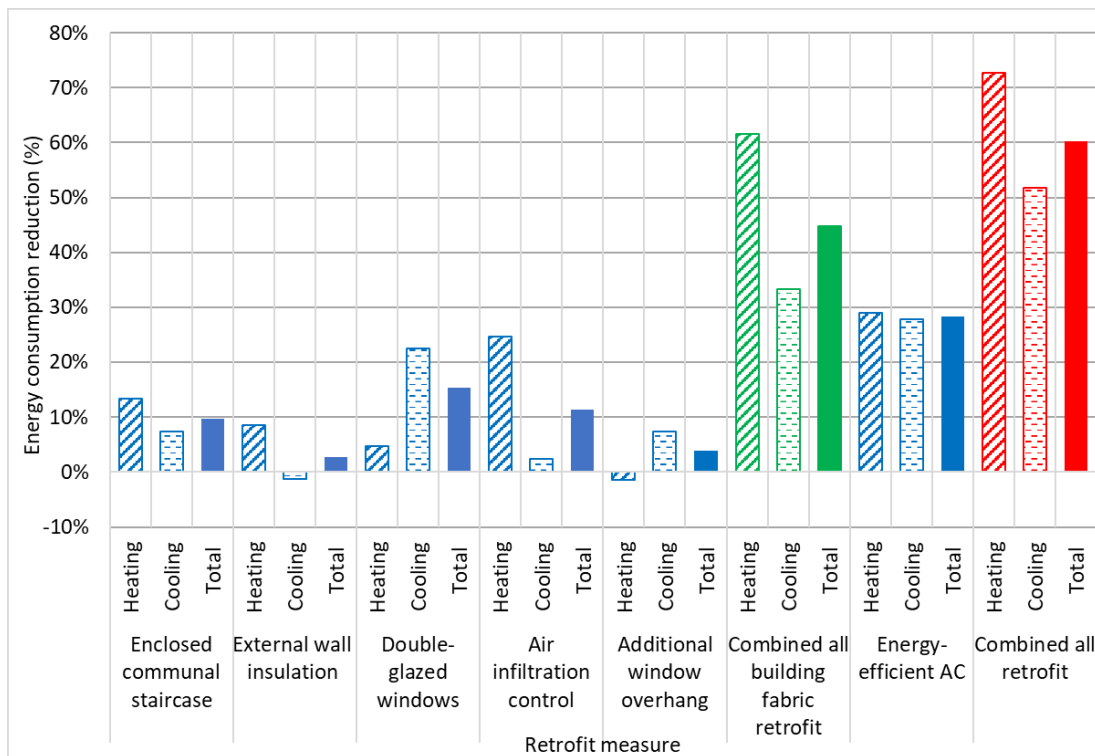


Figure 5-17: Percentage of heating, cooling and total energy reduction after retrofit with medium energy users.

Considering different (low, medium, and high) energy users, the percentage of energy reduction when combining all retrofit measures was similar for the three energy users (60% to 62%). It is interesting to note that the percentage of energy reduction for enclosed communal staircase, double-glazed windows, reduced air infiltration rate and additional overhang were similar (1% difference) for different energy users; whereas the energy reduction for external wall insulation was smaller (1.8%) for low energy users and larger (4.2%) for high energy users when compared to medium energy users (2.7%). Therefore, medium energy users can be used to predict the percentage of energy reduction of retrofit measures with reasonable accuracy (Figure 5-18).

With respect to different energy users for absolute value (in kWh/m²) reduction, results suggested that the absolute values of energy reduction show a considerable variation when compared with the case of percentage of energy reduction (Figure 5-18). As an example, for the case of combining all retrofit measures, the energy reduction was 5.55 kWh/m², 7.33 kWh/m² and 10.16 kWh/m² for low, medium, and high energy users respectively, where the difference between a low and high energy user is two folded (Figure 5-19).

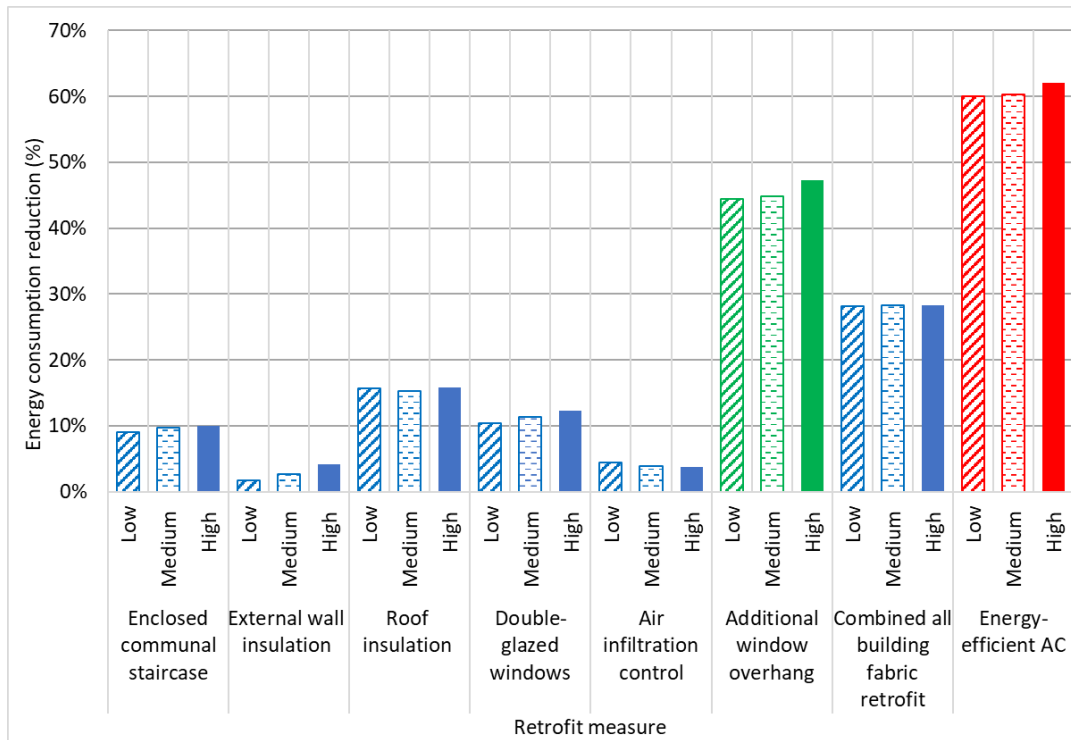


Figure 5-18: Percentage of energy reduction after retrofit with low, medium, and high energy users.

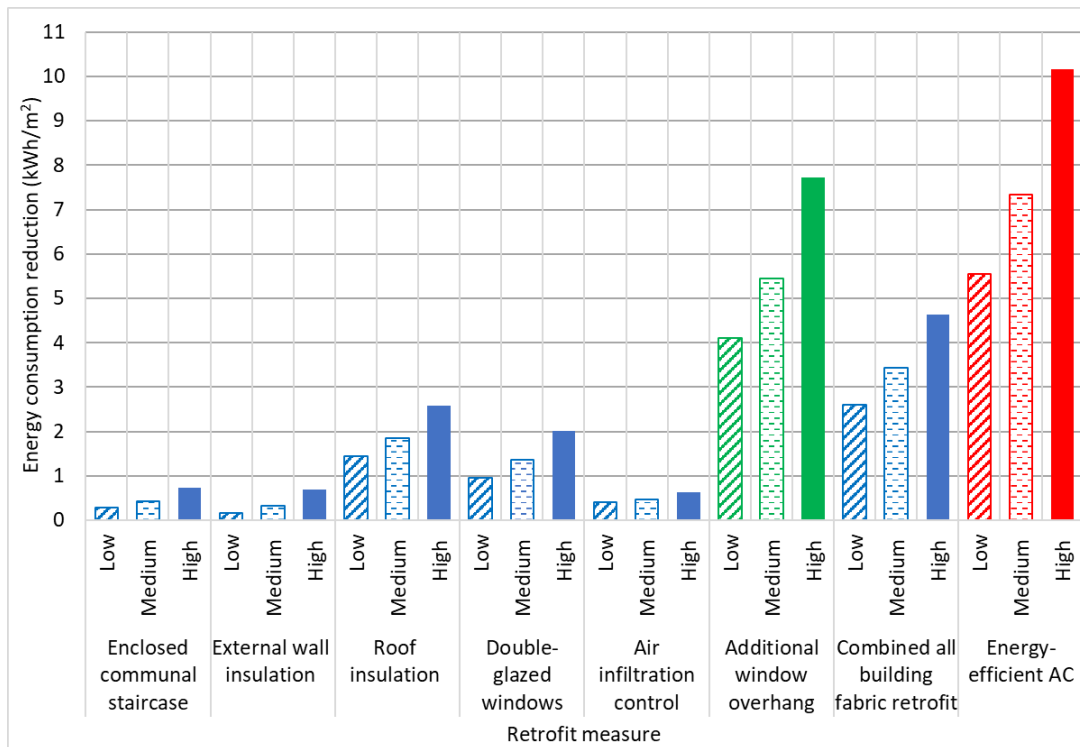


Figure 5-19: Absolute value of energy reduction after retrofit for case study flat with low, medium, and high energy users.

Considering thermal comfort improvements after retrofitting in terms of indoor air temperature increase, results suggested that the monthly average indoor

air temperature increased from 11.05°C to 14.7°C in winter seasons (December to February). It is worth noting that before retrofit, average indoor air temperature in March (16.1°C) and November (17.1°C) lay outside the comfort range; whilst when all retrofit measures were employed, the average indoor air temperature in March (18.8°C) and November (21.0°C) increases, and they lies inside the comfort range. As a result, winter thermal comfort conditions improved after retrofit measures are introduced. In summer seasons (July to August), the average indoor air temperature remained the same (30.7°C) after retrofit (Figure 5-20).

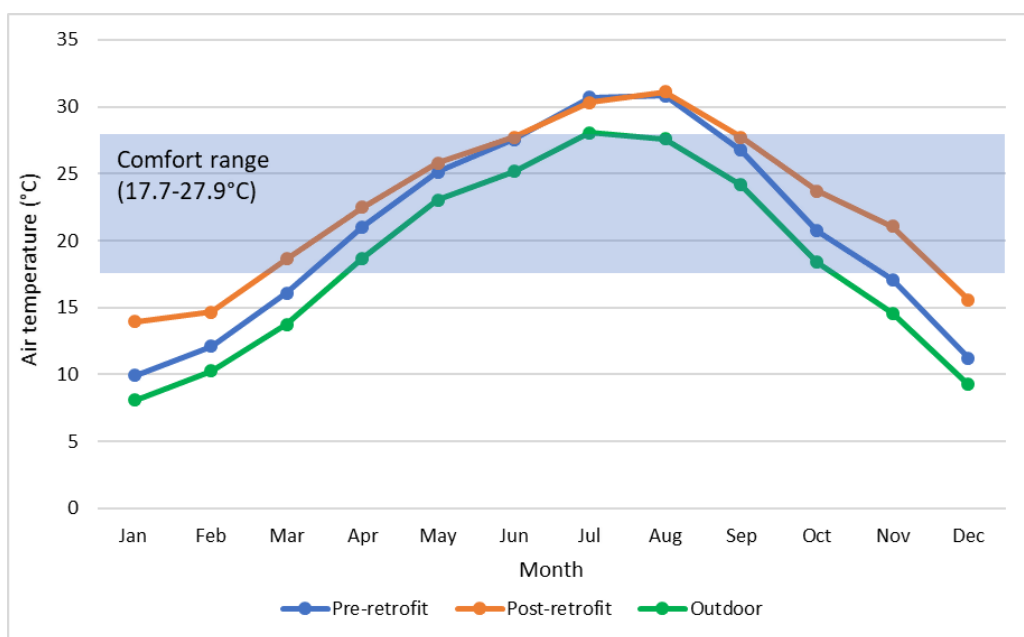


Figure 5-20: Comparison between indoor air temperature before and after retrofit and outdoor air temperature.

When looking at thermal discomfort hours reduction, reduced air infiltration rate (129 hours) and external wall insulation (68 hours) resulted in the highest and second-highest winter thermal discomfort hours reduction, while double-glazed windows (118 hours) and additional overhang (34 hours) resulted in the highest and second-highest cooling energy reduction. However, when assessing annual discomfort hours, double-glazed windows and enclosed communal staircase have the best performance because a reduced air infiltration rate dramatically increases thermal discomfort hours (129 hours). The negative effect of retrofits is more prevalent when evaluating thermal comfort, with double-glazed windows increasing winter discomfort hours by 49

hours, and external wall insulation increasing summer discomfort hours by 31 hours (Figure 5-21).

Therefore, results indicated that the optimum combination of retrofit measures is more effective at reducing heat loss in winter (343 hours decrease), but less effective at reducing heat gain in summer (10 hours increase). Nevertheless, summer overheating is prevented when the proposed combination is selected.

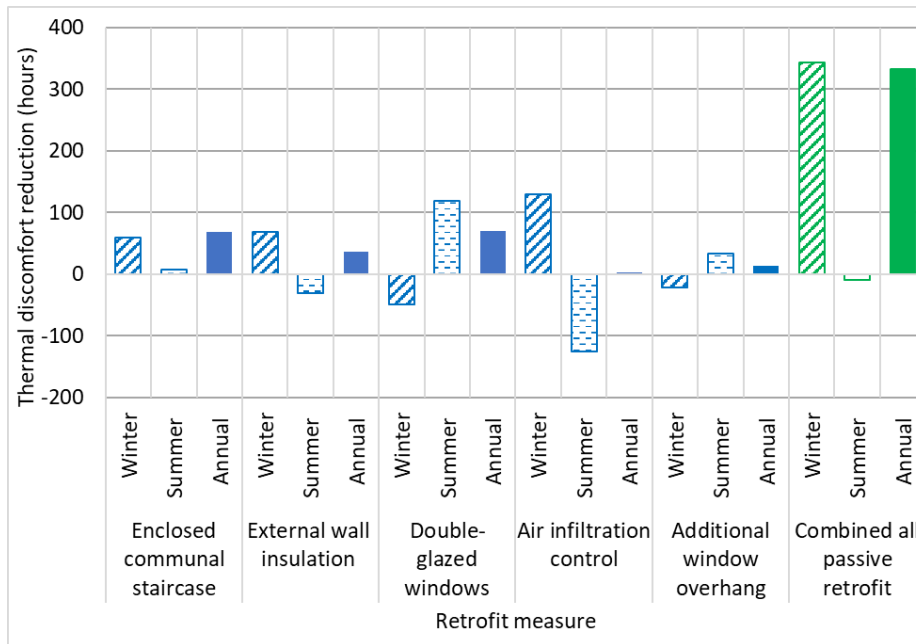
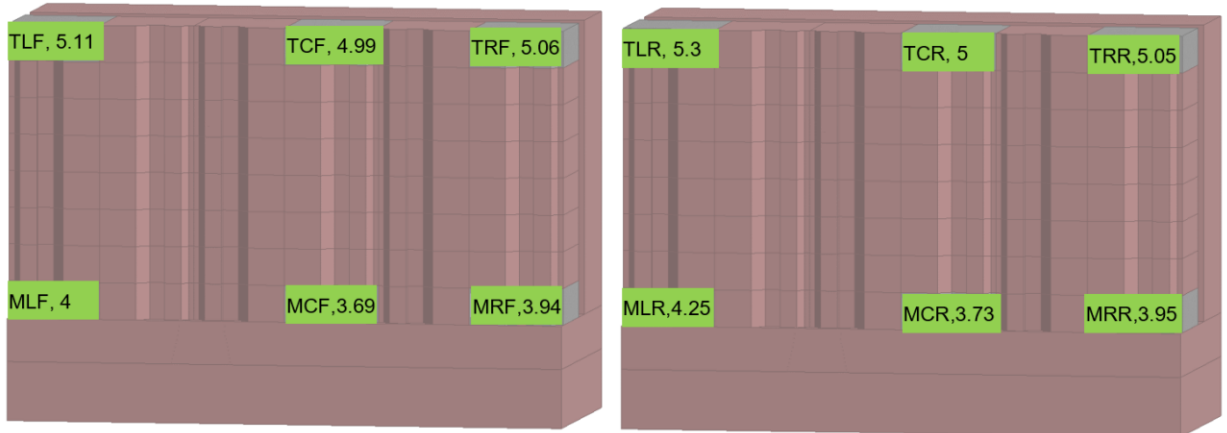


Figure 5-21: Thermal discomfort hours for winter, summer and annual reduction after retrofit.

5.6.2 Predicted retrofit performance for different flat positions in the building

When the optimum combination of all retrofit measures was employed for different flat positions in the case study building, the percentage point of total energy reductions for low (59% to 65%), medium (60% to 66%), and high (62% to 68%) energy users were similar (Figure 5-22). Furthermore, the difference in energy consumption between middle flats and top flats was reduced. However, Figure 5-22 only presented the case of combined retrofit measures; the heating and cooling energy reduction of individual retrofit measures may vary when considering different flat positions compared to the case study flat. Subsequently, the performance of individual retrofit measures is further investigated for different flat positions and compared with the results of flat MCF presented in Section 5.6.1.

a) Low energy users



b) Medium energy users



c) High energy users



Key		Code
MLF: Middle Left Front	MLR: Middle Left Rear	MCF, 3.69
MCF: Middle Centre Front	MCR: Middle Centre Rear	Total energy consumption in kWh/m ²
MRF: Middle Right Front	MRR: Middle Right Rear	Flat position
TLF: Top Left Front	TLR: Top Left Rear	Colour: Green (<12 kWh/m ²)
TCF: Top Centre Front	TCR: Top Centre Rear	Yellow (12-16 kWh/m ²)
TRF: Top Right Front	TRR: Top Right Rear	Orange (16-20 kWh/m ²)
		Red (>20 kWh/m ²)

Figure 5-22: Total energy consumption when seven retrofit measures were employed for different flat locations for three energy users.

With regards to the energy saving retrofits in the middle floor flat on the centre facing rear (building orientation of main facade faces S30°W), the performance of energy saving retrofits was different when compared to the case study flat. The best performing two retrofit measures for heating were reduced air infiltration rate and enclosed communal staircase; for cooling the best two performing were double-glazed windows and additional overhang. Cooling energy reduction was higher for flat MCR as the main facade faced 30° south, with higher solar radiation in summer. When combining heating and cooling, double-glazed windows (20%) and reduced air infiltration rate (10%) ranked the first and second. Combining all the passive retrofit measure, the total energy reduction can be up to 46%, which is larger than flat MCF (42%; Figure 5-23).

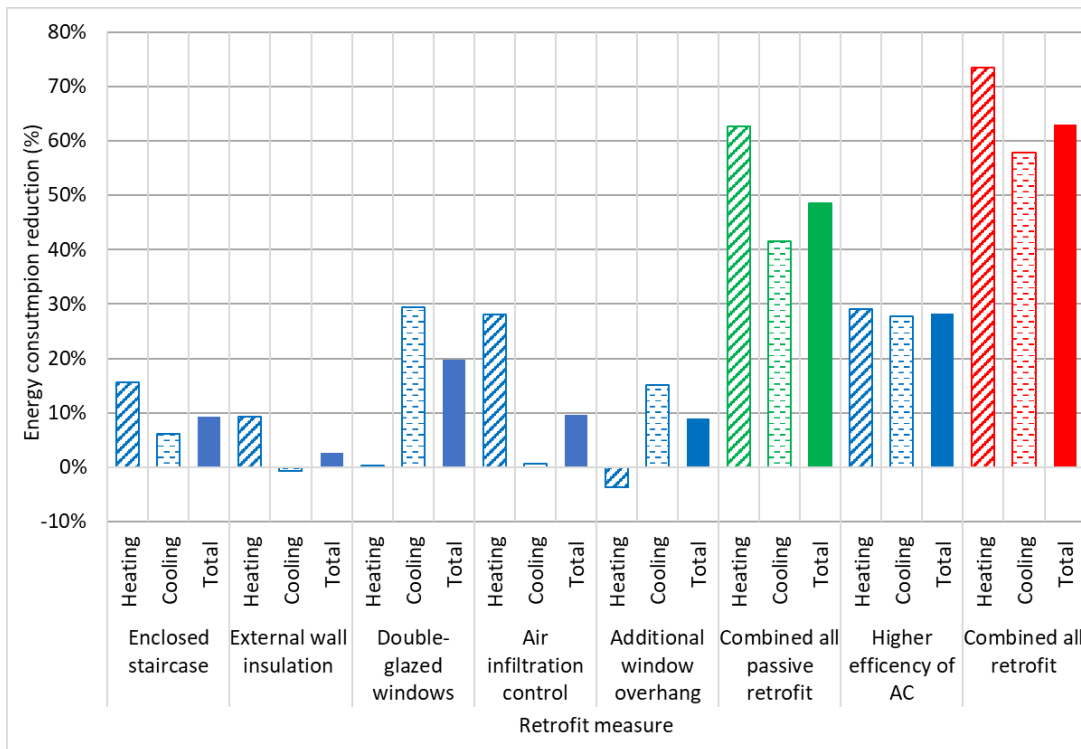


Figure 5-23: Percentage of heating, cooling and total energy consumption after retrofit with medium energy users for flat MCR.

Considering energy saving retrofits in the top floor flat on the centre facing front (flat TCF), roof insulation resulted in the largest heating (35%) and cooling (21%) energy reduction. Moreover, the second-best performing measure was reduced air infiltration rate with 8% total energy reduction. Enclosed communal staircase achieved a higher cooling energy reduction (8%) than heating energy

reduction (3%) with a total energy reduction of 6%. Interestingly, other building fabric retrofit measures were less effective at reducing energy consumption when compared to the case study flat, with total energy reduction of less than 10% (Figure 5-24).

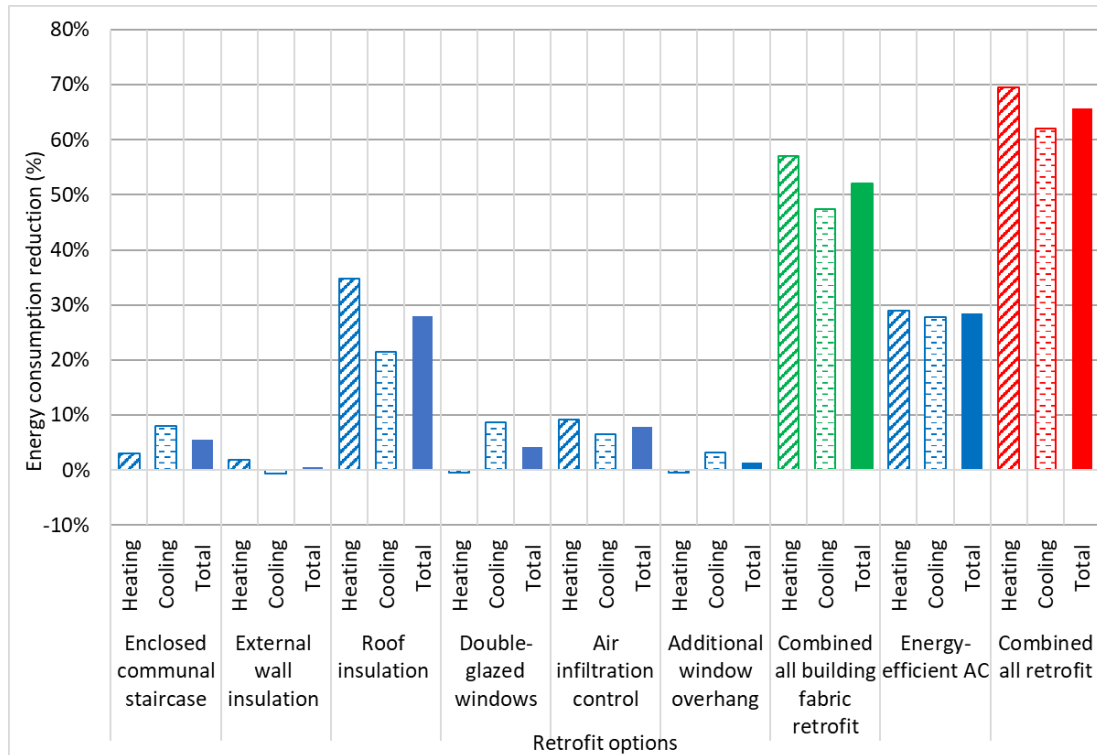


Figure 5-24: Percentage of heating, cooling and total energy consumption after retrofit with medium energy users for flat TCF.

Considering thermal comfort conditions, in flat MCR, where the main facade faces 30° to the south, reduced air infiltration rate (114 hours) was the most effective at improving winter discomfort, while double-glazed windows (196 hours) and additional overhang (108 hours) were effective at improving summer discomfort. When compared to the case study flat, enclosed communal staircase and external wall insulation were less effective in improving winter thermal discomfort, leading to winter discomfort hours for combined retrofit increasing by 10 hours. However, double-glazed windows were more effective in improving summer thermal discomfort, with summer discomfort hours for combined retrofit decreasing by 80 hours (Figure 5-25).

Regarding the thermal comfort conditions in flat TCF, the trend was similar to energy consumption, where roof insulation was the most effective retrofit measure, reducing winter discomfort hours by 300 hours. Yet, the reduction of

total thermal discomfort hours of other retrofit measures was less than 20 hours (Figure 5-26).

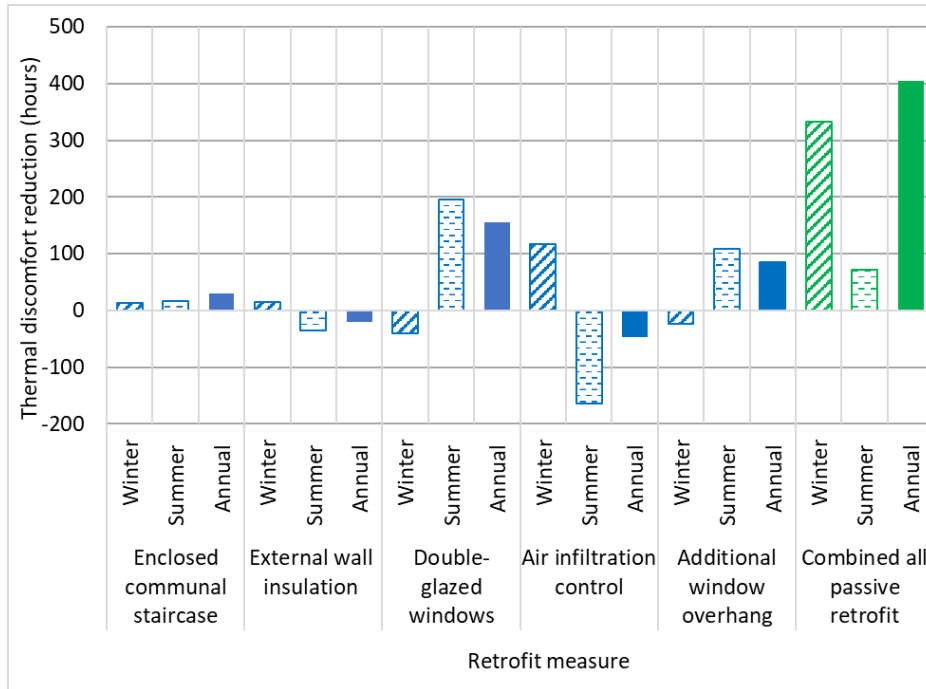


Figure 5-25: Thermal discomfort hours reduction for winter, summer, and annual reduction after retrofit for flat MCR.

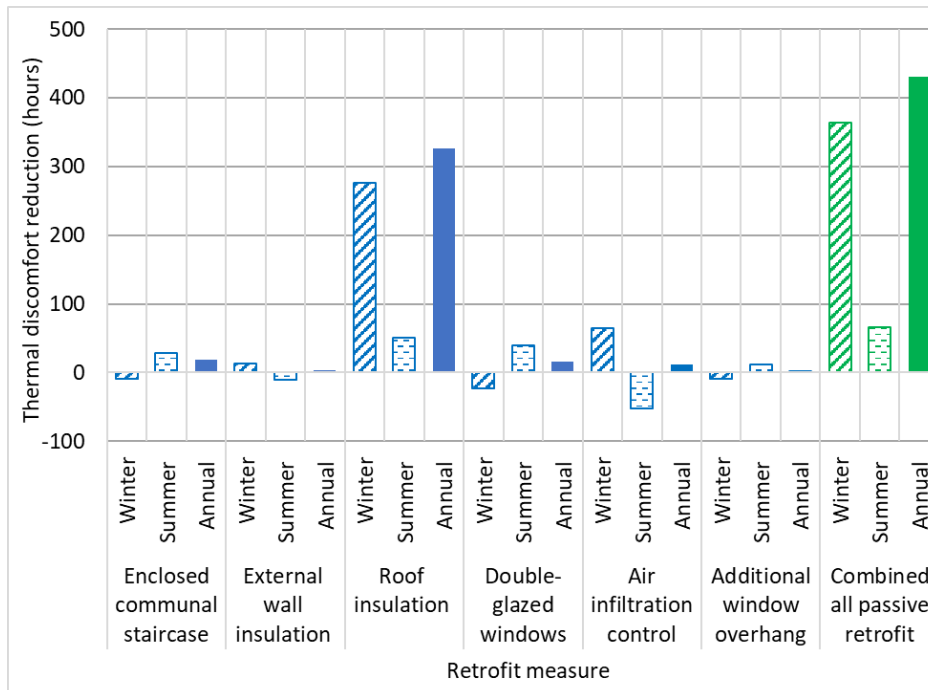


Figure 5-26: Thermal discomfort hours reduction for winter, summer, and annual reduction after retrofit for flat TCF.

5.6.3 Predicted retrofit measures for the whole case study building

Using the same method developed in Section 5.5, the energy consumption for the whole case study building with 96 flats can be predicted. Accordingly, the effect of individual retrofit measures on total energy reduction in building scale for the three energy users are evaluated. Results showed that the percentage of energy reduction for low (61.8%), medium (62.4%), and high energy users (63.9%) were similar for combined retrofit (Figure 5-27); all of the retrofit measures have a percentage variation of less than 2% for different energy users, but the absolute value varies significantly (6.41 to 11.91 kWh/m²) (Figure 5-28), the results showed a similar trend when compared to flat MCF (Figure 5-28).

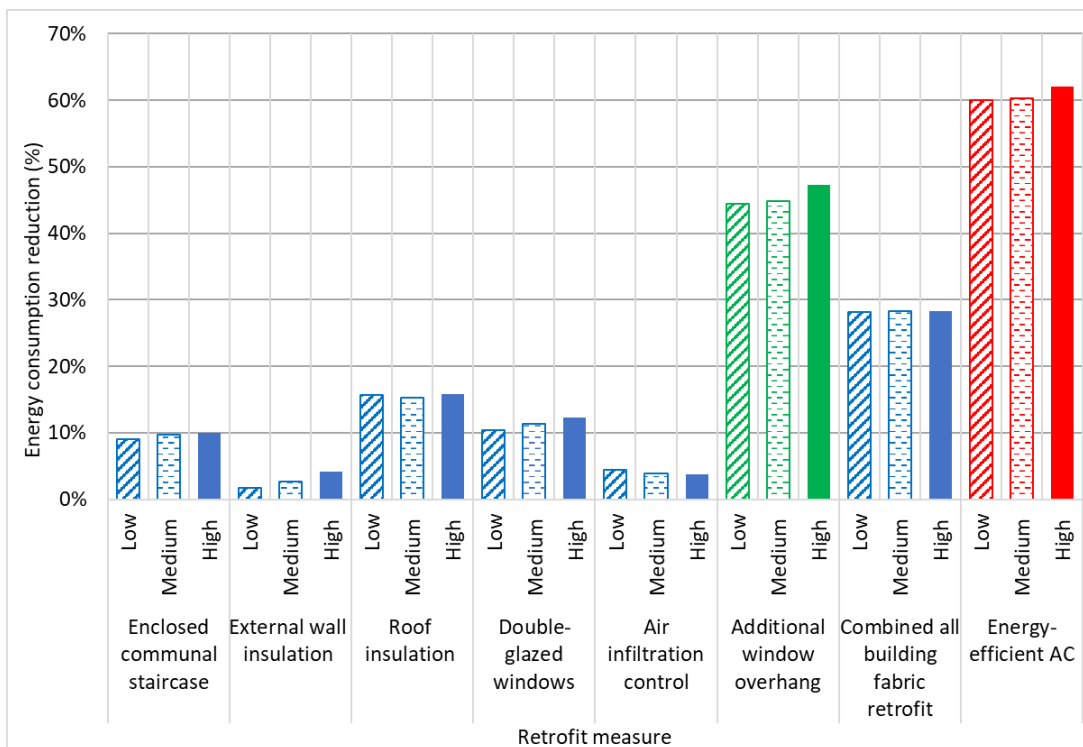


Figure 5-27: Percentage of energy reduction after retrofit for the whole case study building with low, medium and high energy users.

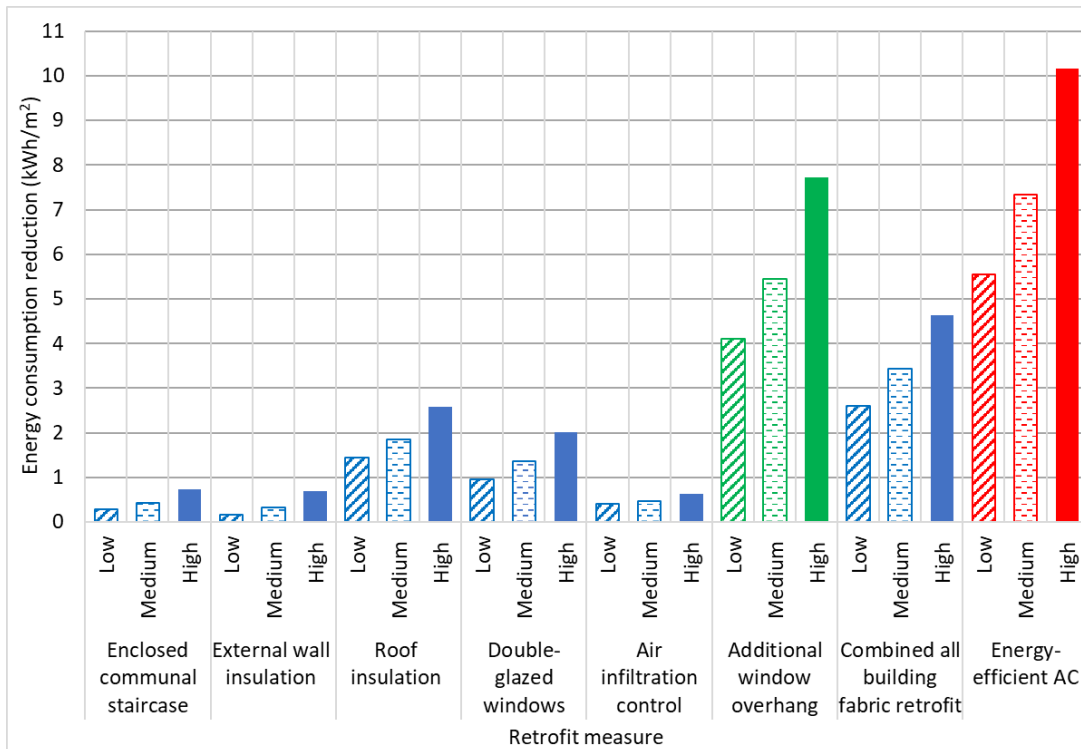


Figure 5-28: Absolute value of energy reduction after retrofit for the whole case study building with low, medium and high energy users.

To sum up the analysis, all the outputs (heating, cooling, and total energy reduction) of twelve types of flats (see Figure 5-22) and the whole case study building (Figure 5-27) for medium energy users were compared (Figure 5-29). Results indicated that double-glazed windows (15%) and reduced air infiltration rate (10%) rank the first and second considering all the twelve types of flats modelled. Furthermore, the total energy reduction was 48% when all passive retrofit measures were combined, which is larger than flat MCF (42%). Of all the retrofit measures, the most substantial variation was roof insulation, since middle floor flats do not benefit from EPS roof insulation, as the ceiling is assumed to be adiabatic for the DTM developed in this study. This led to the energy reduction of the whole case study building (4%) which is much lower than the energy reduction for top flats (30%). Another point which is worth noting is that enclosed communal staircase (3% to 16%) and reduced air infiltration rate (9% to 28.1%) had a considerable variation for heating energy reduction, whereas double-glazed windows (8% to 29%) had a considerable variation for cooling energy reduction. When combining all passive retrofit measures, the variation for heating (56 to 63%) was lower than cooling energy reduction (33% to 49%) for different flat locations. Additionally, the energy

reduction for energy-efficient AC was the same for different flat locations and whole case study building (Figure 5-29).

The graphs showing all the outputs for low and high energy users are not presented, because results showed that the percentage point change of the three energy users were similar for the whole case study building (Figure 5-27). Regarding different flat locations, when combining all retrofit measures, the range of total energy reduction for low energy users was 58.9% to 64.9% and high energy users was 62% to 67.9%, where medium energy users achieved a 60.3% to 66.5% reduction. Similar to the whole case study building (Figure 5-28), the range of absolute total energy reduction for low (3.7 to 5.3 kWh/m²), medium (4.8 to 6.9 kWh/m²), and high (6.2 to 9.3 kWh/m²) energy users varied significantly by flat location. For example, the reduction in the top corner flat facing south (flat TLR) for medium energy users (6.9 kWh/m²) was higher than the reduction of middle centre flat facing north (flat MCF) for high energy users (6.2 kWh/m²).

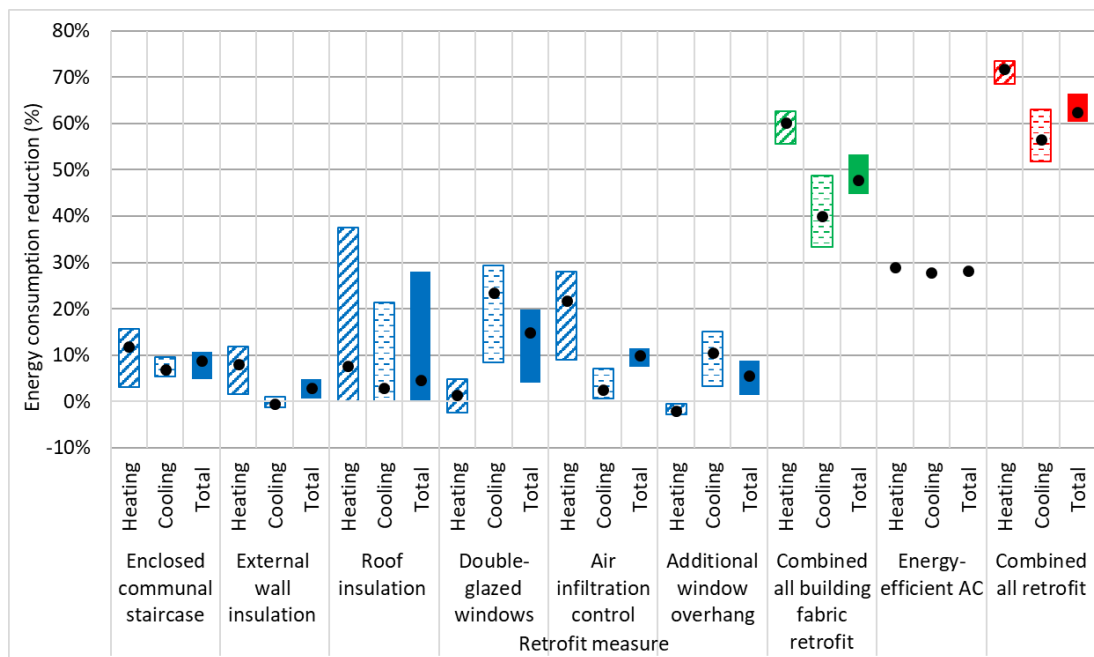


Figure 5-29: Variation of heating, cooling, and total energy consumption after retrofit with medium energy users for different housing units, with black dots representing the entire case study building.

When the whole building is considered, the performance of retrofit measures was similar to the case study flat. The performance of roof insulation was similar to external EPS insulation, with 35 hours reduction of thermal

discomfort hours in winter (Figure 5-30). For combined retrofit, winter thermal discomfort hours reduced by 10 hours, but summer thermal discomfort hours increased by 50 hours. Results from Figure 5-28 show that most of the flats have thermal discomfort hours in summer reduced by up to 117 hours. Winter thermal discomfort hours were more effectively reduced when all the retrofit measures were employed, with a range of 283 to 394 hours (Figure 5-30).

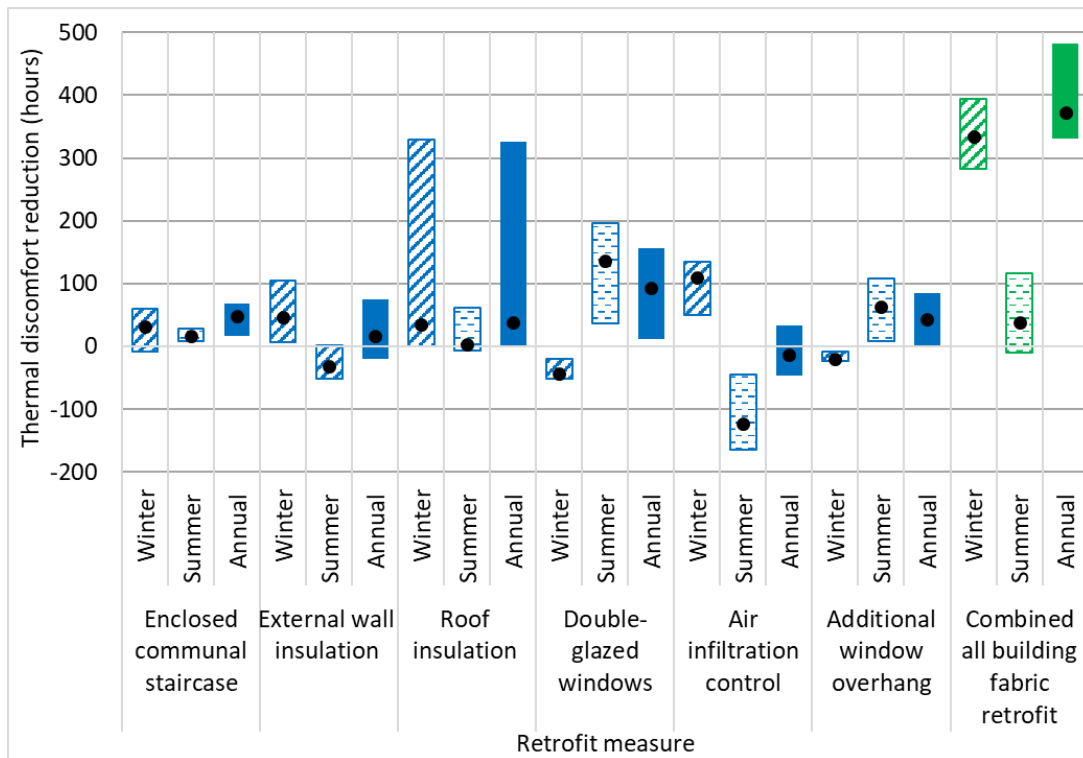


Figure 5-30: Variation of thermal discomfort hours reduction for winter, summer, and annual reduction after retrofit for different housing units, with black dots representing the entire case study building.

5.7 Retrofit cost

The approximate cost of the proposed combination of seven practical retrofit measures was calculated using locally established construction cost estimates, the Chongqing engineering cost information, dated in December 2018 (Chongqing Cost, 2018). The payback period of the combined retrofit measures was predicted, in order to evaluate the feasibility of the implementation of the selected retrofit measures in the case study building. Payback period is determined by equating the net present value of savings to the net present value of the costs associated with a retrofit measure (Chidiac

et al., 2011). Net present value (NPV) is calculated by applying an investment rate to the value in the present, in contrast to some future value it will have when it has been invested at compound interest. However, Y. Liu et al. (2018) stated that the use of NPV requires an informed selection of an appropriate discount rate, where information of this kind, such as the cost of finance to retrofit the case study building, is not available to determine the discount rate. Therefore, a static investment payback period (in number of years), calculated by the material cost divided by the electricity saved in a year for the retrofit measure(s) investigated, was used for the purpose of this study; since this metric neglects the discount rate and inflation rate, as opposed to NPV.

Product life (life span) of passive retrofit measures varies, for example Short et al. (2018) assumed a product life of 30 years, whereas Ouyang et al. (2009) assumed 40 years, and Li et al. (2019) performed a parametric study by assuming 15, 25, and 35 years of product life. For the purpose of this study, the product life of the passive retrofit measures is assumed to be 30 years, based on the mean value of the above three studies listed. On the other hand, the product life of split-type air conditioners is 12 years (H. Yu et al., 2015), almost one third the length of passive retrofit measures. However, a previous study (Li et al., 2019) assumed the same product life for passive retrofit measures and air conditioners. Subsequently, this study assumes 30 years of product life for the selected six passive retrofit measures and 12 years of product life for air conditioners. Thus, if the calculated payback period is shorter than the calculated product life, the retrofit measure is cost-efficient.

The electricity price in Chongqing is 0.57 RMB/kWh (0.0644 GBP/kWh) (The exchange rate for RMB¥ to GBP£ is taken as 0.113 – the yearly average rate between May 2018 and Apr 2019; oanda.com). To put the price into context, the electricity price in the UK was 0.125 GBP/kWh in 2018 (HM Government, 2019b).

The cost of retrofit is predicted for medium energy users (Table 5-5). Results from Table 5-5 represent the calculated net present value of retrofit, in which the initial retrofit cost for improving building fabric or AC efficiency should be lower than the calculated value so that the retrofit is economically feasible.

The material cost of external wall insulation, roof insulation, and double-glazed windows can be estimated from Chongqing engineering cost information. To start with, the price of external wall EPS insulation is RMB¥110 (GBP£12.4) per m² (Chongqing Cost, 2018). Area required for 25 mm external wall EPS insulation was 12.9 m² for the external wall of each flat, and an extra 12 m² for each corner flat. The total EPS insulation required for the building is 1622 m², thus, the material cost is predicted to be RMB¥178,420. As for the material cost of double-glazed windows, the price of a low-e double-glazed window is RMB¥150/m² for the windowpane plus RMB¥220/m² for the uPVC window frame, with combined a cost of RMB¥370/m² after-tax (Chongqing cost, 2018). The total window area replacement required is 10 m², and thus the material cost was roughly RMB¥3700 per flat and RMB¥355,200 for the whole building. Considering the material cost of roof insulation, the price of 50 mm EPS roof insulation is RMB¥220 (GBP£24.8) per m² (Chongqing Cost, 2018). The area required for 50 mm EPS roof insulation was 54.1 m², with 324.6 m² for all roof units in the case study building, and thus the total material cost is roughly RMB¥17,560 for the whole building.

The information on the cost of overhangs, enclosed communal staircase, and air infiltration rate cannot be estimated based on Chongqing engineering cost information. These associated costs are estimated according to Y. Liu et al. (2018), who performed a cost-benefit analysis for a residential building in China with a built area of 10180 m². The construction cost was calculated to be RMB¥601,578, which excluded external wall insulation, roof insulation, and double-glazed windows. Therefore, by extrapolating the construction cost to the case study building with a built area of 4730 m², the construction cost is estimated to be RMB¥280,000. Subsequently, the total estimated cost of all building fabric retrofit for the case study building is estimated to be RMB¥831,180.

According to the manufacturer's catalogue for air conditioners in China, the price of Grade 1 air conditioner in China is roughly RMB¥2400 (Midea air conditioner, 2500W; midea.com). As the living room and bedroom are assumed to have an air conditioner, replacing the cost of two air conditioners

is RMB¥4800. Thus, material cost for the whole case study building is RMB¥460,800 for replacing air conditioners.

Although results from Table 5-5 revealed that all the retrofit measures, except roof EPS insulation, are cost-inefficient for all the three energy users. The proposed combination of retrofit measures can improve thermal comfort conditions significantly in the case study building (Section 5.4.2), and thus its application is vital to future proofing of buildings. Additionally, the implementation of all the retrofit measures is critical as some retrofit measures (e.g. external wall insulation) aim to reduce heating energy consumption, whilst some measures (e.g. additional overhang) aim to reduce cooling energy consumption even for high energy users.

Table 5-5: Payback period for low, medium, and high energy users, with a product life of 30 years for building fabric retrofit and 12 years for energy-efficient AC.

Retrofit measure	Material cost (RMB¥)	Payback period for low energy users (years)	Payback period for medium energy users (years)	Payback period for high energy users (years)
External wall EPS insulation	178420	356	170	78
Roof EPS insulation	17560	15	10	7
Double-glazed windows	355200	79	64	47
Combined all building fabric retrofit	831180	63	47	33
Energy efficient AC	460800	58	44	32
Combined all retrofit	1291980	75	56	40

5.8 Discussion

An AC operating schedule was developed according to the quantified hourly percentage of AC operation for a typical day based on survey studies (Chen et al., 2011, 2010; Hu et al., 2013; Yoshino et al., 2006). Results showed that the predicted heating and cooling energy consumption are in line with the metered electricity consumption collected from Ouyang et al. (2011, 2009). However, the findings are in contrast to the predicted heating and cooling energy consumption in existing modelling studies (Li et al., 2019; X. Li et al., 2018; Short et al., 2018; L. Xu et al., 2013; Yao et al., 2018) reviewed in Section 2.6.4.1, which was approximately doubled than the prediction here; since all

these existing studies missed to quantify hourly percentage of AC operation for a typical day based on survey studies. This led to the over-prediction of energy reduction of retrofit measures evaluated in these studies, and hence an uninformed selection of the optimum combination of retrofit measures. This thesis is believed to be the first study in which the predicted energy consumption in DTM is in line with the measured energy consumption. By doing so, an informed quantification of the retrofit measures was performed.

When assessing thermal comfort performance, the evaluation criteria in this thesis was based on a comprehensive survey performed by B. Li et al. (2018) in the HSCW zone. As the results suggested (Section 5.2.2), only 43.1% of occupied hours lie in the comfort zone (17.7-27.9°C) for the case study flat. This is in line with the survey results from B. Li et al. (2018), which suggested that 44.7% of occupied hours lie in the comfort zone. Yet, the findings are contrary to Yao et al. (2018), which predicted that 22% of occupied hours (halved the occupied hours when compare to the prediction here) lie in the comfort zone for residential buildings in the HSCW zone built before building regulations. As Yao et al. (2018) failed to consider the acceptable temperature range of occupants, and assumed a comfort range of 18-26°C according to Chinese design standard. Thus, this shows the importance of using HSCW zone thermal comfort criteria to predict the thermal comfort performance in flats in the HSCW zones, so that the actual performance can be predicted in building energy models.

Regarding the effect of flat location in a residential building, a 10% increase was predicted for both heating and cooling energy consumption for middle left (flat MLF) and middle right (flat MRF) flats compared to the case study flat (oriented N30°E). The findings are in opposition to Yao (2012), which predicted middle right flats consumed 18% more heating and cooling energy, whereas middle left flats consumed 7% more cooling energy and 34% more heating energy, when compared to middle centre flats. Nevertheless, Yao (2012) missed to consider the intermittent heating and cooling AC operating schedule (where heating is not operated in the bedroom for medium energy users); and assumed a 24-hour continuous heating and cooling AC operating schedule to simplify the DTM. Therefore, a higher heating energy difference due to the

effect of flat location was predicted by Yao (2012); as the middle left and right flats have one extra external wall with free access to the external environment when compare to the middle centre flat, where the heat loss due to transmission in the flat increases.

Considering the effect of external wall insulation, this thesis predicted that 2% energy reduction can be achieved for an optimum insulation thickness of 25 mm. This findings are in contrast to Ouyang et al. (2009), which predicted a larger (6%) percentage of energy reduction when external wall insulation was employed (with 10 mm insulation thickness). As this thesis assumed an intermittent AC operating schedule based on the fact that occupants use more cooling than heating. Therefore, despite a heating energy reduction of 8%, cooling energy increased by 1%, leading to a net reduction of 2% reduction in this study. Nonetheless, Ouyang et al. (2009) assumed 24-hours continuous operation of air conditioners, and the predicted heating energy consumption doubled that of cooling energy consumption pre-retrofit, causing an over-prediction of percentage decrease when external wall insulation was employed.

Concerning the effect of roof insulation, this thesis predicted a significant energy reduction (27%) when the optimum insulation thickness of 50 mm is employed. The findings are opposed to Ouyang et al. (2009), which predicted a smaller (7%) percentage of energy reduction when roof insulation was employed (with 40 mm insulation thickness). This is because the DTM developed in this thesis modelled different flat locations individually (i.e., middle flat and top flat), where Ouyang et al. (2009) modelled the building as a whole. This thesis suggests that when the whole building is considered, adding 40 mm roof insulation predicted a 5% energy reduction, which is according to the findings by Ouyang et al. (2009). Therefore, this study shows that although roof insulation achieves a small percentage of energy reduction in building level, it is a critical retrofit measure for the flats located on the top floor.

This thesis predicted an air infiltration rate of 0.7 ach^{-1} is the optimum, and can achieve a 12% energy reduction. The maximum potential energy reduction was 15% (in which a 30% heating and 2% cooling energy reduction was

achieved) for an air infiltration rate of 0.5 ach^{-1} . Nonetheless, the findings are contrary to Zhao et al. (2015), which predicted a 30% energy reduction when air infiltration rate was reduced from 1.5 to 0.44 ach^{-1} , where the predicted heating energy is halved and there was a 5% reduction for cooling. It may be due to the fact that Zhao et al. (2015) failed to develop a highly detailed DTM for the case study building; instead, Zhao et al. (2015) used a simplified box model ($10 \times 10 \times 3 \text{ m}$) for dynamic thermal simulation, where the volume specified in the model (300 m^3) was larger than the living room and bedroom in this study. This caused the increased prediction in heating energy due to the higher ventilation heat loss for a larger volume.

This thesis predicted that an optimum overhang with a length of 0.5 m can achieve a 4% total energy reduction, with a 7% reduction in cooling energy consumption but a 2% increase heating energy consumption. As additional window overhang decreased solar heat gain to the windows, which reduced cooling energy in summer but increased heating energy in winter. The findings are contrary to Yu et al. (2008), which suggested that a 1.5m horizontal overhang only provided a 4% cooling energy reduction and increased 1.9% of heating energy, leading to a 2% total energy reduction (halved the reduction predicted when compare with this thesis). The difference is due to Yu et al. (2008) predicted the heating energy doubled cooling energy pre-retrofit, in which the effect of cooling energy reduction due to additional window overhang reduced .

Regarding enclosing communal staircase, DTM predicted a 10% reduction for total energy, with a 12% heating reduction and 8% cooling reduction. The predictions are contrary to Ouyang et al. (2009), which predicted a 4% energy reduction (halved the energy reduction predicted in this thesis) after the communal staircase was enclosed. As Ouyang et al. (2009) simply extended the building energy model to include the staircase (i.e., reduce shape coefficient from 0.38 to 0.32), and failed to model the communal staircase in detail, i.e., the heat exchange between the external wall connecting the communal staircase and case study flat was not considered. Therefore, this study shows that enclosing the communal staircase is a beneficial retrofit measure to reduce energy consumption.

This chapter selected an optimum combination of retrofit measures which improved winter discomfort but did not cause overheating in summer. However, the evaluation was performed in the case study building, which is an eight-storey residential complex with one-bedroom flats. The next chapter will investigate the possibility of simplifying the DTM and evaluate the retrofit performance of the selected combination of retrofit measures on a city scale.

Chapter 6 : Large scale residential energy saving retrofits

6.1 Introduction

In this Chapter, Objective 4 and 5 are addressed. Sections 6.2 to 6.4 presents the development and selection of the most computationally efficient model for the city-scale study. When evaluating energy savings, building performance and occupants' comfort for retrofits on a single flat, a highly complex and computationally detailed DTM can be used; however, such evaluations at a city-scale require less input complexity. Throughout a city, there are residential buildings with a different number of storeys and bedrooms when compared to the case study building. Hence, archetypal buildings, which are statistical composites of the features found within a category of buildings in a city, can be used to model large-scale energy saving retrofits in the HSCW zone (An et al., 2017; Hu et al., 2016; Li et al., 2019; Zhe Wang et al., 2015b). In order to generate building archetypes, different building designs in the city were identified (Reinhart and Cerezo Davila, 2016). In the HSCW zone, 83% of households live in apartment buildings in urban areas (THUBERC, 2017) and thus the case study building represents 83% of building stock, which indicates significant energy savings if retrofit measures are employed.

Section 6.5 presents the development of residential building archetypes in the HSCW zone. Three segmentation parameters (number of bedrooms, number of storeys, and energy users) are defined to design a city-scale model. The case study building consists of one-bedroom flats. However, two-bedroom flats and three-bedroom flats are also typical in the HSCW zone. The number of bedrooms causes variation of predicted building energy consumption per square meter for residential buildings in the HSCW zone (Li et al., 2019; Zhe Wang et al., 2015b). Moreover, the case study building is an eight-storey

residential building; however, there are residential buildings of different heights in the HSCW zone (X. Li et al., 2018), which causes variation of predicted building energy consumption per square meter. Note that 90% of households in the HSCW zone use split-type AC, and the control of these systems is performed manually (THUBERC, 2017). Thus, three energy users are developed to represent the vast differences between energy usage by different types of occupants. Subsequently, these three parameters, i.e., number of bedrooms, number of storeys and energy users, are defined to design a city-scale model.

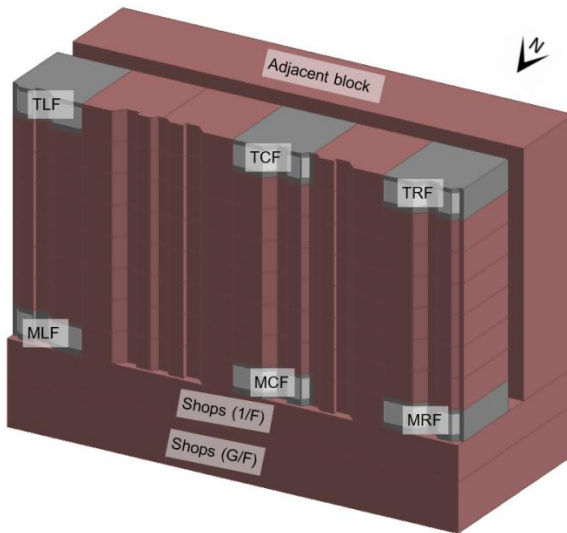
Section 6.6 presents the predicted energy consumption for the twelve building archetypes developed in Section 6.5, and the energy saved when the proposed retrofit measures, developed in Chapter 5, is employed.

Section 6.7 presents the city-scale energy saving retrofit contribution for the representative area in Chongqing, with 321 residential buildings and a built area of 4.07 million m².

6.2 Calculating building level energy consumption

When evaluating energy saving retrofits in a flat scale for the case study building in Chapter 5, twelve types of flats were developed. However, the number of categories of flats can be reduced when evaluating energy saving retrofits in a building scale; in order to decrease simulation time, but in the same time provide good accuracy of the predicted energy consumption.

The case study building has six types of flats facing front and six types of flat facing rear. When calculating building level energy consumption, only the flats facing front were considered, and the building orientation was changed from N30°E to north when evaluating large-scale residential energy saving retrofits in this section (Figure 6-1).



Key
 MLF: Middle Left Front
 MCF: Middle Centre Front
 MRF: Middle Right Front
 TLF: Top Left Front
 TCF: Top Centre Front
 TRF: Top Right Front

Figure 6-1: 3D representation of the studied building in the DTM software showing the location of selected flats for building scale simulation.

Four options by reducing number of categories of flats to calculate building level energy consumption were listed as follows:

- Option one modelled six types of flats, the building level energy consumption was calculated by equation 6-1;
- Option two modelled four categories of flats (as of option one, but flat MLF and flat TLF were replaced by adiabatic blocks), building level energy consumption was calculated by equation 6-2;
- Option three modelled two categories of flat (as of option two, but flat MRF and TRF were replaced by adiabatic blocks), building level energy consumption was calculated by equation 6-3;
- Option four only modelled the middle centre flat (as of option three, but flat TCF was replaced by adiabatic block), building level energy consumption was calculated by equation 6-4.

$$E_1 = (28 \times E_{MCF} + 7 \times E_{MRF} + 7 \times E_{MLF} + 4 \times E_{TCF} + E_{TLF} + E_{TRF})/48 \quad (6-1)$$

$$E_2 = (28 \times E_{MCF} + 14 \times E_{MRF} + 4 \times E_{TCF} + 2 \times E_{TRF})/48 \quad (6-2)$$

$$E_3 = (42 \times E_{MCF} + 6 \times E_{TCF} + E_{TRF})/48 \quad (6-3)$$

$$E_4 = E_{MCF} \quad (6-4)$$

Where E_1 , E_2 , E_3 , and E_4 represent options 1, 2, 3, and 4 for calculating building energy consumption. E_{MCF} , E_{MRF} , E_{MLF} , E_{TCF} , E_{TRF} , E_{TLF} represent the energy

consumption for the middle centre, middle right, middle left, top centre, top right, and top left flats (Figure 6-1).

The predicted building level energy consumption in kWh/m² of the four options are presented in Table 6-1. Results suggest that when six types of flats were considered (option one), the predicted heating energy consumption was 5.54 kWh/m² and cooling energy consumption is 7.94 kWh/m². When the four categories of flats were considered (option two), the total energy consumption increased by 1%. As Section 5.2 showed that predicted energy consumption for corner left (MLF, TLF) and corner right flats (MRF, TRF) was similar, with less than 1% difference. Interestingly, when two categories of flat (middle centre and top centre flats) were considered (option three), the total energy consumption only decreased by 1% when compared to option one. As Section 5.2 showed that top flats consumed 60% more energy than middle flats, the difference between middle corner flats is smaller (10% increase compared to middle centre flat). Therefore, it was possible to omit corner flats and still achieve building level energy consumption within 1% when compared to option one. Furthermore, the simulation time was halved when compare to option one. Nevertheless, when only one category of flat was modelled (option four), the total energy consumption decreased by 10% compared to option one; thus it is essential to include top flats when calculating building level energy consumption. As a result, option 3 (with flat MCF and TCF modelled) was selected to calculate building energy consumption.

Table 6-1: Predicted building level energy consumption in kWh/m² for the four options.

Option	Flats modelled	Heating (kWh/m ²)	Cooling (kWh/m ²)	Total (kWh/m ²)
1	MLF, MCF, MRF, TLF, TCF, TRF	5.54	7.94	13.49
2	MCF, MRF, TCF, TRF	5.54	8.05	13.59
3	MCF, TCF	5.47	7.93	13.4
4	MCF	4.92	7.65	12.57

6.3 Development of the LoD required for energy modelling of the case study building

Nine LoD were developed using the DTM representative of the residential building stock in the HSCW zone (case study building), to study the impacts on the computed building level energy consumption and identify the most computationally efficient model. LoD1 has the highest level of detail and LoD9 has the lowest level of detail. The LoD reflects the shortage of suitable data at one end of the scale (LoD9), and the effort involved implementing a detailed model at the other (LoD1). The details of the nine variants are as follows:

LoD1: Highest level of detail

LoD1 has the highest level of detail, which is used to evaluate energy saving retrofit in flat scale in Chapter 5, it has a simulated floor area of 49.3 m², with the following details modelled in each flat:

- Simulated area includes lettable space,
- Exact window location and size of the bay windows,
- All the five thermal zones (living room, bedroom, wetroom, kitchen and corridor) are modelled,
- Window frame and dividers,
- Effect of shading from the adjacent block of flats,
- Floor to ceiling height consider ceiling void and floor height,
- Thermal zones are separated by internal walls,
- Flats on one floor are separated by internal walls.

LoD2: Wall thickness

As of LoD1 but include internal and external wall thickness (4.8m²), and the floor area was increased to 54.1 m² (Figure 6-2). By doing so, the floor area increment of the living room was 2 m², bedroom was 0.8 m², and kitchen was 1.1 m²; the floor area of the corridor and wetroom remained the same. Note that all the thermal parameters of the walls remained the same compare to LoD1.

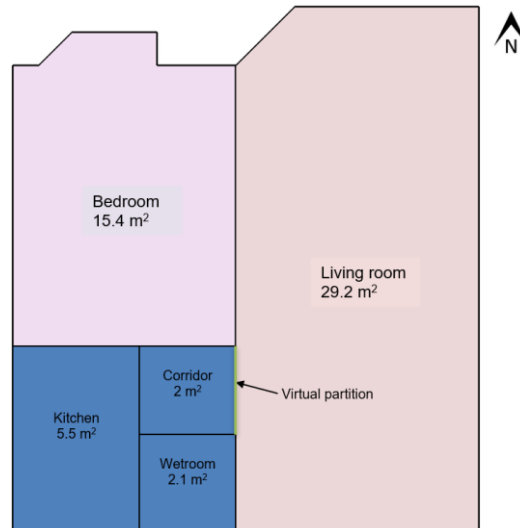


Figure 6-2: DTM of the case study flat with a plan view, including wall thickness.

LoD3: Bay windows

As of LoD2 but the bay windows was replaced with a less detailed single windowpane (hereby “new windows”) for the living room and bedroom (Figure 6-3). The area of the new windows (10 m²) was the same as bay windows (10 m²) to ensure a valid comparison. Subsequently, the window to wall ratio increased from 44% to 50% due to the decrease of the external wall area, with a reduction of 20% for living room and bedroom. When bay windows were replaced, the orientation of the new windows face north. The area of the window frame and dividers were the same for LoD3 when compare to LoD2 (Figure 6-4). Moreover, the floor area of the flat for LoD3 (54.1 m²) remained the same as LoD2 (54.1m²), with the floor area of living room reduced by 1 m² and floor area of bedroom increased by 1 m² compared to LoD2 (Table 6-2).

Table 6-2: Window to wall ratio of the main facade for the case study flat.

	Zone	Total area of external wall (m ²)	Total area of window (m ²)	Total area (m ²)	Window to wall ratio
LoD2	Living room	4.52	6.85	11.4	60.34%
	Bedroom	8.36	3.14	11.5	27.34%
	Main facade	12.88	9.99	22.9	43.8%
LoD3	Living room	3.51	6.85	10.36	66.2%
	Bedroom	6.38	3.14	9.52	33.0%
	Main facade	9.89	9.99	19.88	50.3%

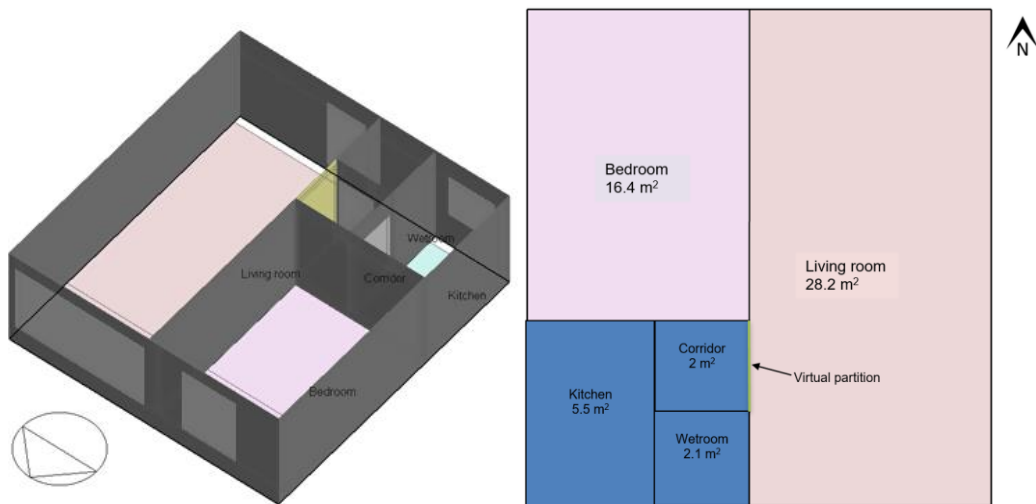


Figure 6-3: DTM of the case study building for LoD3, showing an axonometric view of the building (left) and plan view of a flat (right).

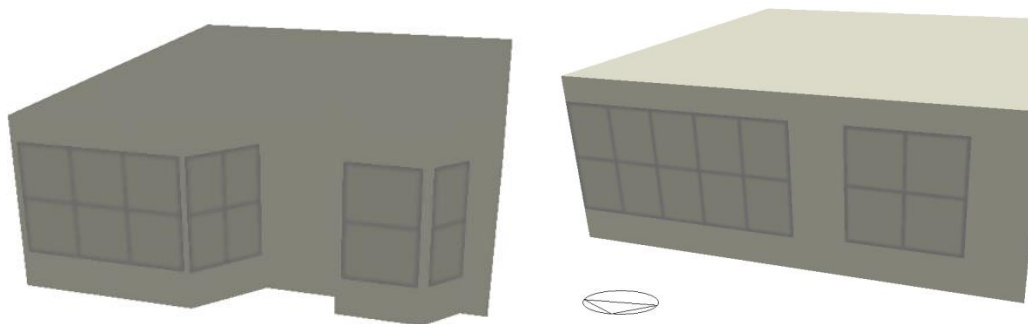


Figure 6-4: DTM of the case study flat showing window frames for LoD2 (left) and LoD3 (right).

LoD4: External door and thermal zones

As of LoD3 but the three unoccupied thermal zones (kitchen, corridor and wetroom) were combined into one unoccupied thermal zone, by removing internal partitions connecting the auxiliary area (Figure 6-5). Since the kitchen (occupied between 18:00-19:00 for cooking with a heat gain of 10.8 W/m^2) was combined with corridor and wetroom (without heat gains) to one thermal zone. Therefore, the heat gain from the kitchen was scaled based on the floor area to the auxiliary area, with a heat gain of 6.3 W/m^2 (Figure 6-5).

Furthermore, LoD4 excluded external doors connecting the living room and outdoor communal corridor, and the external door area was replaced by the external wall. As the U-value of the external wall ($2.3 \text{ W/m}^2\text{K}$) and U-value of the external door ($2.75 \text{ W/m}^2\text{K}$) are similar, this change will only have a small impact on the computed energy consumption.

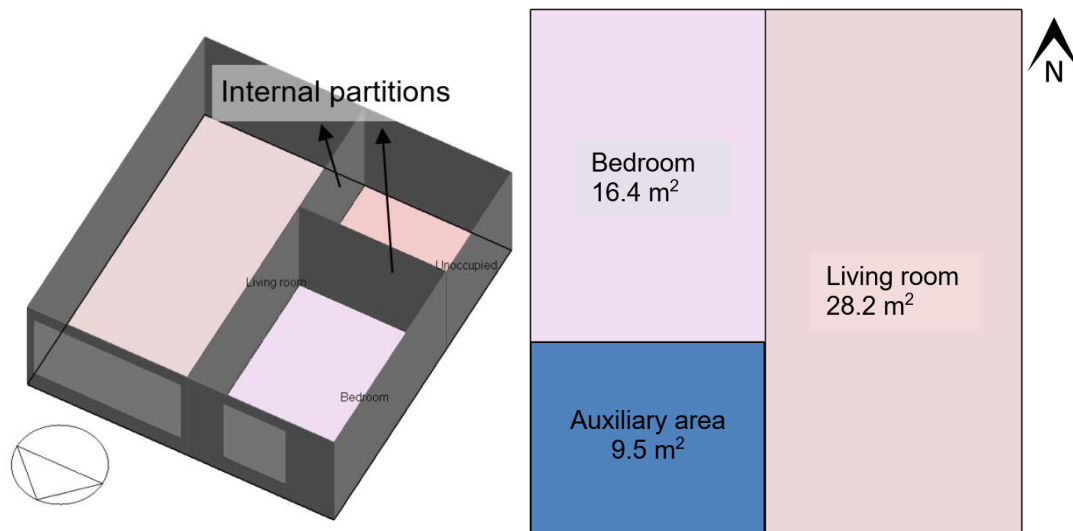


Figure 6-5: DTM of the case study building combining unoccupied thermal zones (LoD5), showing an axonometric view of the flat (left) and plan view of the flat (right).

LoD5: Window frames and dividers

As of LoD4 but window frames and dividers were excluded; instead, the window frame and dividers area were replaced by the external wall to keep the window area the same as LoD4 for a valid comparison. In the living room, the window area was 5.8 m^2 , with a frame area of 0.55 m^2 , and divider area of 0.52 m^2 . In the bedroom, the window area was 2.6 m^2 , with a frame area of 0.34 m^2 , and divider area of 0.16 m^2 . Subsequently, the external wall area of the living room increased by 1.1 m^2 , and for the bedroom a 0.5 m^2 increment.

LoD6: Adjacent block

As of LoD5 but the effect of shading from the adjacent block of flats was not modelled (Figure 6-6)

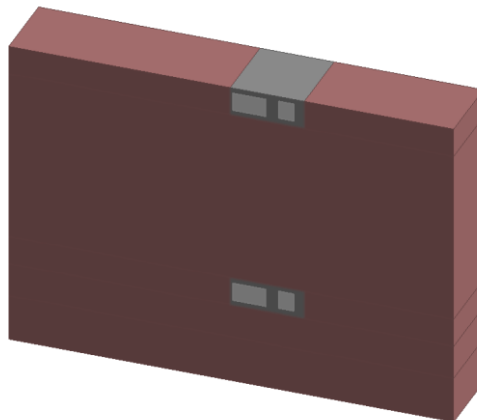


Figure 6-6: 3D representation of the studied building in the DTM software showing the excluded adjacent block.

LoD7: Floor to ceiling height

As of LoD6 but the ceiling (0.26 m) and floor height (0.14 m) were excluded for the calculation of the floor to ceiling height. Therefore, the floor to ceiling height increased from 2.4 m to 2.8 m, and the volume of the flat increased from 130 m³ to 151 m³.

LoD8: Single-thermal zone model

As of LoD7 but the internal walls connecting the thermal zones (living room, bedroom and auxiliary area) were replaced by virtual partitions, so that the flat was modelled as a single-thermal zone. The virtual partition acts as a partition between two zones which exists purely to sub-divide the space and has no corresponding wall in the actual building (DesignBuilder, 2019).

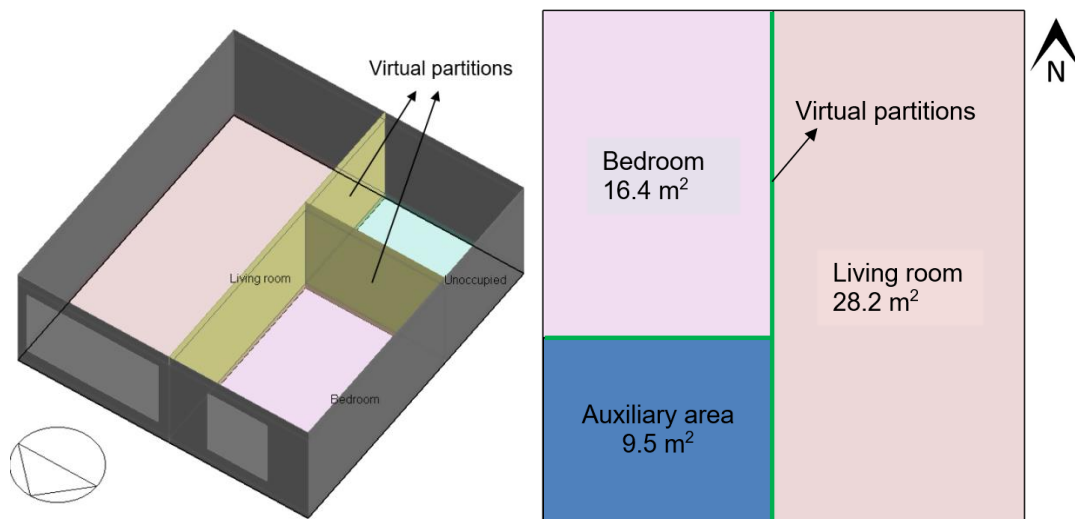


Figure 6-7: DTM of the case study building combining unoccupied thermal zones (LoD5), showing an axonometric view of the flat (left) and plan view of the flat (right).

LoD9: Whole floor model

As of LoD8 but the internal walls connecting the flats in the same floor were removed, in which the whole floor was modelled (Figure 6-8a). Since the ratio of the living room was 50%, the bedroom was 30%, and the auxiliary area was 20% of the flat area (Figure 6-7); thus, the floor area of the whole floor model was a multiple of six of the case study flat (Figure 6-8b). Also, windows in the living room (34.8 m²) and bedroom (15.8 m²) of LoD9 were a multiple of six when compared to LoD8 (Figure 6-8).

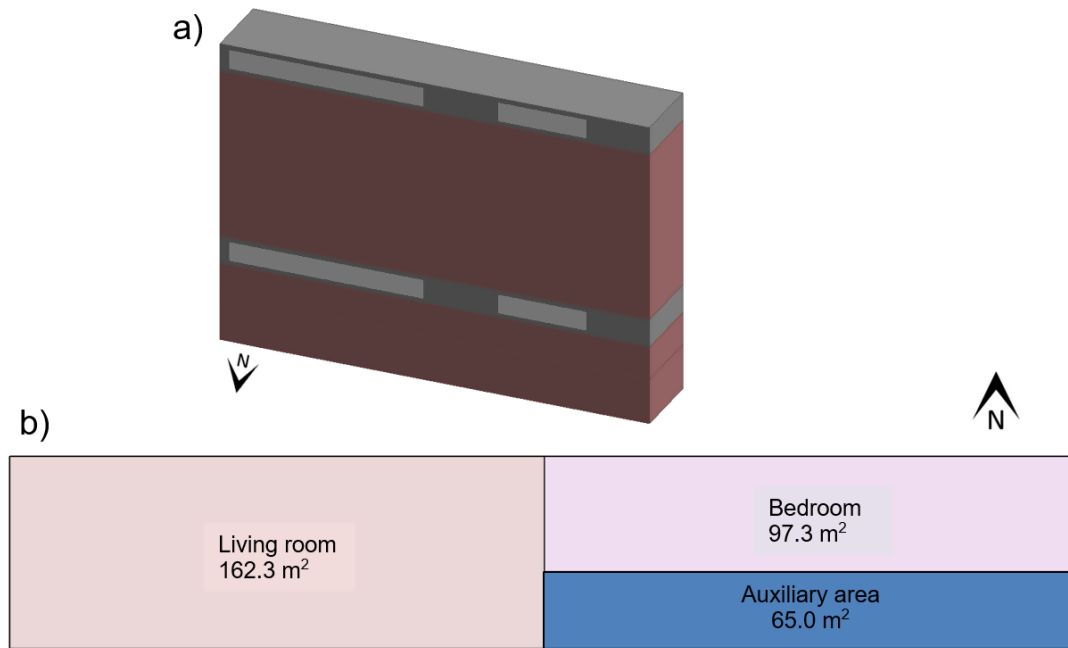


Figure 6-8: DTM of the case study building with whole floor model, showing a) axonometric view of the building and b) plan view of the flat .

6.4 LoD selection for a city-scale study

The percentage difference of building level energy consumption for LoD2 to LoD9 was compared with LoD1 using equation 6-5. The percentage difference of building level energy consumption for LoD2 to LoD9 was also compared respective with the previous LoD using equation 6-6.

$$P_{LoDi} = \frac{E_{LoDi} - E_{LoD1}}{E_{LoD1}} \times 100\% \quad (6-5)$$

$$S_{LoDi} = \frac{E_{LoDi} - E_{LoDi-1}}{E_{LoDi-1}} \times 100\% \quad (6-6)$$

Where P_{LoDi} is the percentage of building level energy consumption reduction for $LoDi$, $i = 2$ to 9 when compared to LoD1, S_{LoDi} is the percentage of building level energy consumption reduction for $LoDi$, $i = 2$ to 9 when compared to the previous LoD

Predicted annual building level (in MWh for all the 48 flats facing front) heating energy demand for LoD1 to LoD9 were presented in Figure 6-9 in red bar. Results revealed that the percentage differences for LoD1-6 are within the -5% to 5% range for P_{LoDi} and S_{LoDi} , which showed that the level of detail does not cause a considerable variation of the total building heating energy demand.

Using LoD2 predicted heating energy demand is less by 1.7% when compared to LoD1, in response to the floor area increase by 4.8 m² for the case study flat. Using LoD3 predicted heating energy demand is less by 0.4% when compared to LoD2; since the floor area of the living room decreased and bedroom increased when bay windows were excluded. For medium energy users, AC operated five hours daily in the living room but zero hours in the bedroom for heating, thus leading to a decrease in heating energy demand. Using LoD4 predicted heating energy demand is more by 3.5% when compared to LoD3; owing to the fact that heat loss due to building fabric increased in the auxiliary area when kitchen, corridor, and wetroom were combined to form one thermal zone. Subsequently, the building fabric heat loss between the two internal walls from auxiliary area connecting the bedroom and living room increased and lead to increased heating energy demand. Using LoD5 predicted heating energy demand is more by 0.2% when compare to LoD4; as LoD5 has external wall construction (U-value of 2.3 W/m²K) instead of aluminium window frames and windows (U-value of 5.88 W/m²K), which decrease heat loss due to building fabric. Using LoD6 predicted heating energy demand is less by 0.2% when compared to LoD5; in view of the fact that removal of the adjacent block increased solar heat gain to the facade facing the rear.

Changes throughout LoD7 to LoD9 caused a considerable variation (over 5% increase or decrease for P_{LoDi} and S_{LoDi}) on building level heating energy demand. Using LoD7 predicted heating energy demand is more by 7% when compared to LoD6; since LoD7 excluded the ceiling and floor height, which increased volume of the flat from 130 to 151 m³ and thus heating energy demand increased. Using LoD8 predicted heating energy demand is significantly more by 22% when compared to LoD7; due to the heating being operated from 17:00-23:00 in the living room, where during this operation period, heating did not operate in the bedroom and auxiliary area. Therefore, the indoor air temperature of the bedroom and the auxiliary area was lower than the living room. Subsequently, there was heat loss by transmission through the internal wall connecting the auxiliary area and living room, and the internal wall connecting the bedroom to the living room. When replaced by

virtual partitions, heat loss by transmission through the internal walls was not modelled, thus leading to the reduction of heating energy demand. Using LoD9 predicted heating energy demand is less by 7% when compared to LoD8; for the reason that the heat gain increased from solar and internal heat gain was larger than the heat loss increased from transmission and ventilation when the DTM was scaled up from one flat to the entire floor by six times.

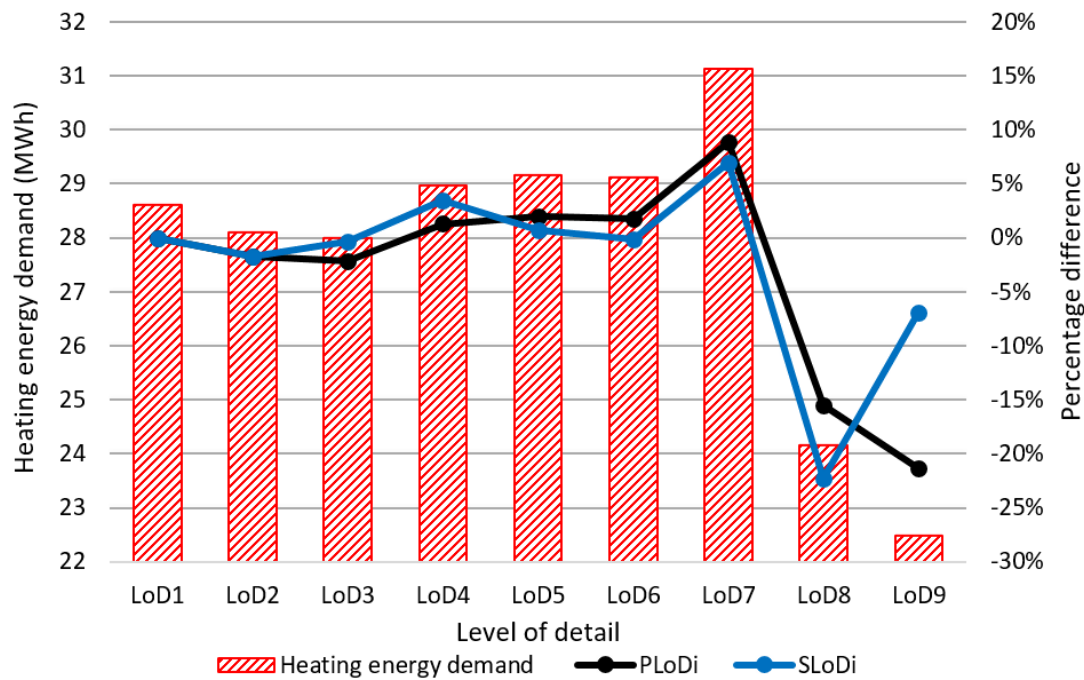


Figure 6-9: Annual building level heating energy demand, the percentage difference of building level energy consumption for LoD2 to LoD9 compared with LoD1 (P_{LoDi}), and the percentage difference of building level energy consumption for LoD2 to LoD9 compared respective with the previous LoD (S_{LoDi}).

Predicted annual building level (in MWh for all the 48 flats facing front) cooling energy demand for LoD1 to LoD9 were presented in Figure 6-10 in blue bar. The predicted cooling energy demand using the nine LoDs showed a different trend when compared to the predicted heating energy demand in Section 6.4.2. Results indicate that using LoD2 predicted cooling energy demand is more by 2% when compare to LoD1; as the increased floor area led to increased internal heat gain. Using LoD4 predicted cooling energy demand is less by 1% when compare to LoD3; since ventilation heat loss increased when three thermal zones were reduced to one thermal zone (decreasing the average temperature in unoccupied zones). LoD5 increased cooling energy demand because the U-value of wall increased.

Changes in LoD3 and LoD6 caused a considerable variation (over 5% increase or decrease for P_{LoDi} and S_{LoDi}) on building level cooling energy demand, but not for heating energy demand. Using LoD3 predicted cooling energy demand is significantly less by 12% when compared to LoD2, but heating energy demand only decreased by 0.4%. This is due to the solar heat gain from the window in summer decreasing by 20% for LoD3 when compare to LoD2, where internal heat gain remained unchanged, leading to a reduction in cooling energy demand. When comparing LoD2 with LoD3, the reduction in heating energy demand due to the reduction of transmission heat loss outweighs the increase in heating energy demand due to the reduction of solar heat gain, which leads to a net reduction of heating energy demand (Table 6-2). These two effects led to a net small reduction (0.4%) of heating energy demand when bay windows were excluded. Using LoD6 predicted cooling energy demand is more by 9% when compared to LoD5, but heating energy demand only decreased by 0.2%. Since the global horizontal solar radiation in Chongqing was low ($70 \text{ Wh/m}^2/\text{day}$) in winter, leading to the small decrease in heating energy demand when shading from the adjacent block was excluded.

Changes in LoD7 to LoD9 does not cause a considerable variation of the total building cooling energy demand, but not for heating energy demand. Using LoD7 predicted cooling energy demand is more by 1% when compared to LoD6, but heating energy demand increased by 7%. This showed that the volume increase has less of an impact on cooling energy demand than heating energy demand. Using LoD8 predicted cooling energy demand is less by 4% when compared to LoD7, but heating energy demand decreased by 22%. This indicates that the exclusion of zoning has less of an impact on cooling energy demand than heating energy demand. Possible reasons are the temperature difference between the bedroom and the living room is smaller in summer than winter. Using LoD9 predicted cooling energy demand is less by 3% when compared to LoD8, but heating energy demand decreased by 7%.

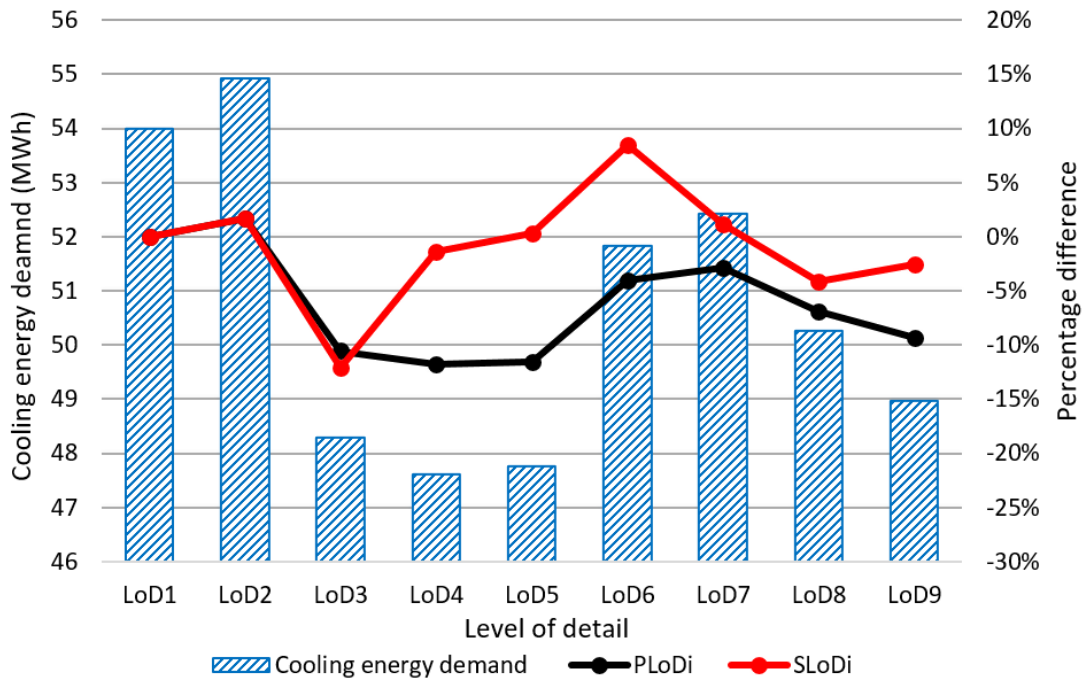


Figure 6-10: Annual building level cooling energy demand, the percentage difference of building level energy consumption for LoD2 to LoD9 compared with LoD1 (P_{LoDi}), and the percentage difference of building level energy consumption for LoD2 to LoD9 compared respective with the previous LoD (S_{LoDi}).

Predicted annual building level (in MWh for all the 48 flats facing front) total energy demand for LoD1 to LoD9 were presented in Figure 6-11 in green bar. With regards to the total energy demand in the case study building, LoD3, LoD6, and LoD8 led to more substantial changes, with S_{LoDi} greater than -5% or +5%. Furthermore, LoD3 and LoD6 are insensitive to heating but sensitive to cooling and LoD8 is sensitive to both heating and cooling.

Impact of the model complexity on computer run time was presented in Figure 6-12. All simulations were performed on the same machine (an HP ProBook 6470b running an Intel Core i5-3320M CPU at 2.6GHz with 8GB RAM). The execution time is shown for each LoD of the case study building in black bar in Figure 6-12. Note that the value returned by DesignBuilder is an elapsed time and so depends on other processes being carried out by the computer; the data presented should, therefore, be seen as indicative rather than precise. Note that in Figure 6-12, P_{LoDi} was calculated as the summation of the absolute value of P_{LoDi} for heating and cooling; and S_{LoDi} was calculated as the summation of the absolute value of S_{LoDi} for heating and cooling.

Results suggested that the main decreases in execution time occurred with LoD3 (50% decrease), LoD4, LoD6, and LoD8. Further, LoD2, LoD5, LoD7, and LoD9 did not change the simulation time because the geometry did not change but excluded information in DesignBuilder. Using the calculated percentage difference, an LoD will be selected with a selection criterion of maximum 10% difference of the above metrics. Subsequently, LoD6 was selected to develop an archetype for the city-scale model. As the absolute heating and cooling energy demand difference was the smallest (5%) from LoD3-9. LoD7 was not selected because the combined cooling and heating percentage difference for LoD7 (12%) was larger than LoD6 (5%). LoD5 was not selected, seeing as the difference between LoD5 and LoD1 was large (-6%); also the simulation time was 20% higher than LoD6.

As a result, LoD6 is selected for the city-scale study. This also showed that it is possible to omit information of wall thickness, bay windows, internal and external doors, detailed information about unheated and cooled thermal zones, and window frames. With heating energy demand, the correct ceiling height (volume of the flat) and internal zoning need to be specified for the flat.

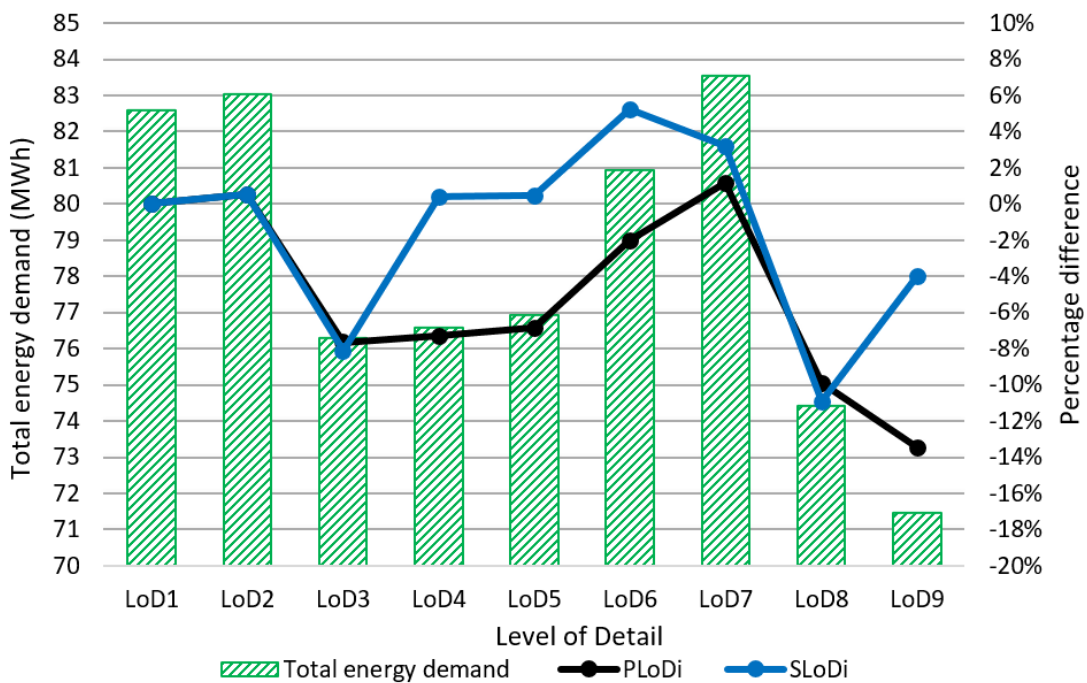


Figure 6-11: Annual building level total energy demand, the percentage difference of building level energy consumption for LoD2 to LoD9 compared with LoD1 (P_{LoDi}), and the percentage difference of building level energy consumption for LoD2 to LoD9 compared respective with the previous LoD (S_{LoDi}).

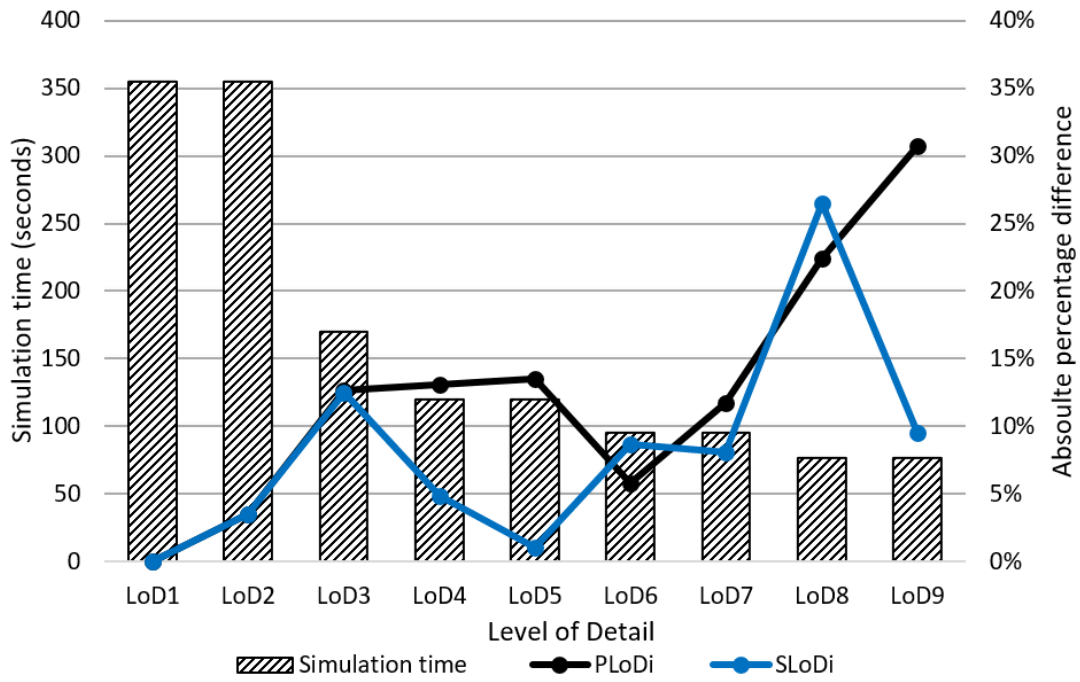


Figure 6-12: Absolute percentage difference and simulation time for various LoDs, the percentage difference of building level energy consumption for LoD2 to LoD9 compared with LoD1 (P_{LoDi}), and the percentage difference of building level energy consumption for LoD2 to LoD9 compared respective with the previous LoD (S_{LoDi}).

6.5 Development of building archetypes for city-scale study

6.5.1 Parameter 1: Number of bedrooms

In the UK, the English housing survey provided average floor areas for different types of dwellings (HM Government, 2017); however, such a report is not available in China. The national statistics of China suggested average living area per person of 29.3 m² in Chongqing (NBS, 2017). Accordingly, the ratio of living rooms, bedrooms, kitchens, and toilets needs to be determined. A new methodology was developed by collecting floor plans of residential buildings with dimensions from existing studies. Subsequently, ten floor plans of residential buildings were collected from eight studies (Ichinose et al., 2017; Meng et al., 2019; Short et al., 2019, 2018; Yao, 2012; Yu et al., 2009a, 2008; W. Yu et al., 2015), summarised in Figure 6-13. Each layout consisted of different arrangement of zones (living room, bedroom, kitchen, and toilet) derived from the floor plans, summarised in Table 6-3. Note that throughout the ten case study buildings, it is typical to have a mix of floor area uses in each building. For example, one out of four are one-bedroom flats, and three out of four are two-bedroom flats in a building (Figure 6-13a), whereas in another building, two out of four are two-bedroom flats and two out of four are three-bedroom flats (Figure 6-13h).

The mean floor area of different zones of flats is summarised in Table 6-4 from Table 6-3. Table 6-4 shows that the living room area was about half (47%) of the flat for one-bedroom flats but that percentage decreased for two-bedroom flats (42%), and three-bedroom flats (36%). The combined area of bedrooms increased, with the area of the bedroom about one-third (33%) of the total flat for one-bedroom flats, 42% for two-bedroom flats, and just under half for three-bedroom flats (45%). The reason for the smaller increase from two- to three-bedroom flats is because the floor area of bedroom three is smaller. An interesting thing to note is the combined area of kitchen and toilet decreased from one-bedroom (20%) to two-bedroom flats (16%) but increased again for three-bedroom flats (18%). This is because some of the three-bedroom flats had two toilets, which increased the combined floor area.

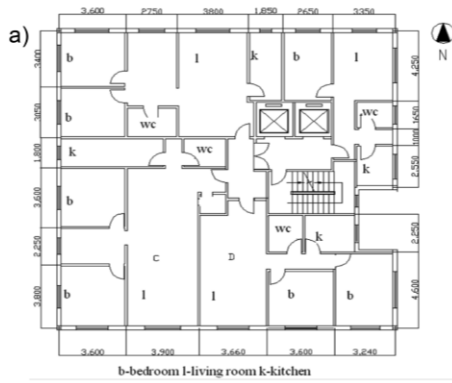
The mean floor area of one-bedroom flats was 36 m², for two-bedroom flats it was 66 m², an increase of 30m² (70% when compared to one-bedroom flats). Mean floor area of three-bedroom flats was also 27 m² larger than two-bedroom flats. Li et al. (2019) assumed the floor area of one-bedroom flats was 35 m², two-bedroom flats was 70 m² and three-bedroom flats was 105 m². Further, assuming there are two occupants in one-bedroom flats, three occupants in two-bedroom flats, and four occupants in three-bedroom flats.

Table 6-3: Floor area of different zones for typical residential buildings as found previous studies.

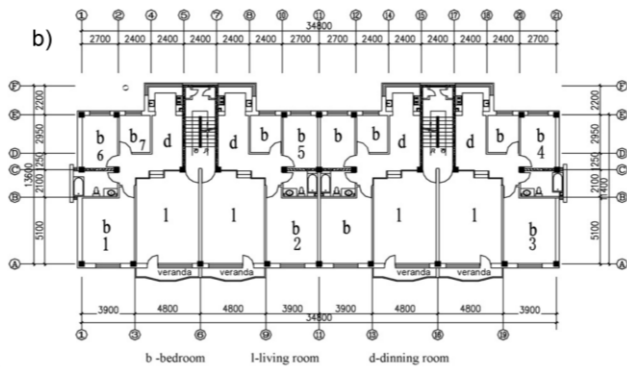
	Bedroom 1	Bedroom 2	Bedroom 3	Living room	Toilet	Kitchen	Reference
One-bedroom flat	12.1	/	/	16.9	3.0	4.4	Case study building
	11.3	/	/	14.2	3.5	4.7	(Yu et al., 2009a)
	14	/	/	16.2	3.6	3.6	(Short et al., 2018)
	10.9	/	/	20.3	1.8	4.8	(Short, 2019)
Two-bedroom flat	13.7	14.9	/	25	5	6.3	(Yu et al., 2009a)
	9.4	12.9	/	16	3.8	3.8	(Short et al., 2018)
	10.9	10.9	/	20.3	1.8	4.8	(Short, 2019)
	13.3	14.3	/	25	6.25	5.9	(Meng et al., 2019)
	12.9	25.7	/	41	4.4	8.1	(Yao, 2012)
Three-bedroom flat	12.5	16.8	/	39	3.6	10.5	(W. Yu et al., 2015)
	7.1	11.3	19.9	34.6	5.6	12.4	(Yu et al., 2008)
	17.2	17.2	17.2	46.6	7.7	16.5	(Ichinose et al., 2017)
	7.6	12.2	14.4	8.9	3.5	3.9	(Short, 2019)
	13.3	15	15.5	38	13.1	5.9	(Meng et al., 2019)
	9.9	13.9	16	32.8	4.4	7.2	(Yao, 2012)
	12.5	16.2	16.8	42	10.8	10.5	(W. Yu et al., 2015)

Table 6-4: Mean value of floor area for different zones according to Table 6-3 for typical residential buildings.

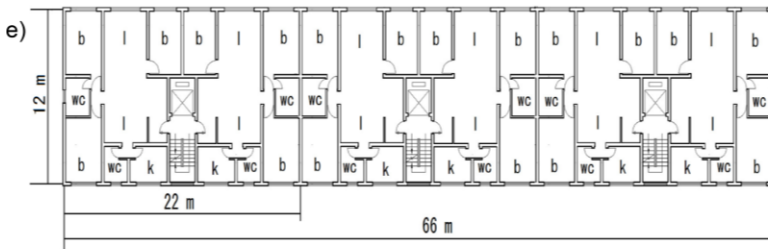
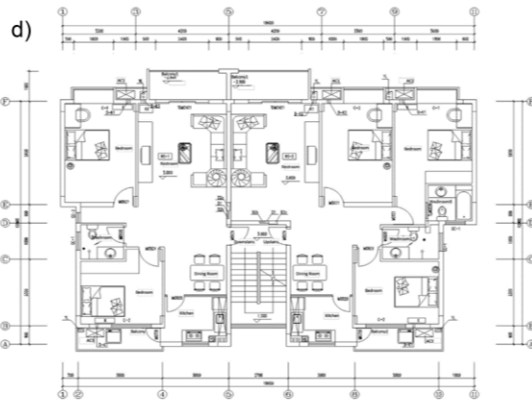
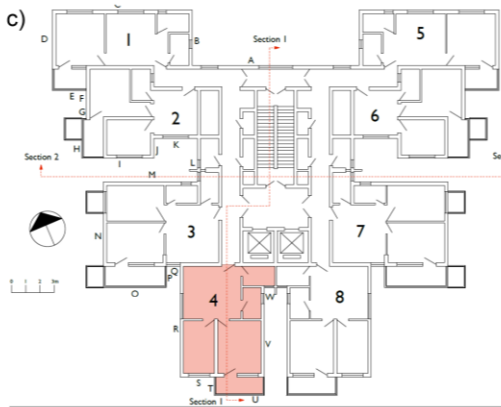
No. of bedroom		Bedroom 1	Bedroom 2	Bedroom 3	Living room	Toilet	Kitchen	Total
One	Area (m ²)	12.1	/	/	16.9	3.0	4.4	36.3
	Percentage	33%	/	/	47%	8%	12%	100%
Two	Area (m ²)	12.1	15.9	/	27.7	4.1	6.5	66.4
	Percentage	18%	24%	/	42%	6%	10%	100%
Three	Area (m ²)	11.3	14.3	16.6	33.8	7.5	9.4	92.9
	Percentage	12%	15%	18%	36%	8%	10%	100%



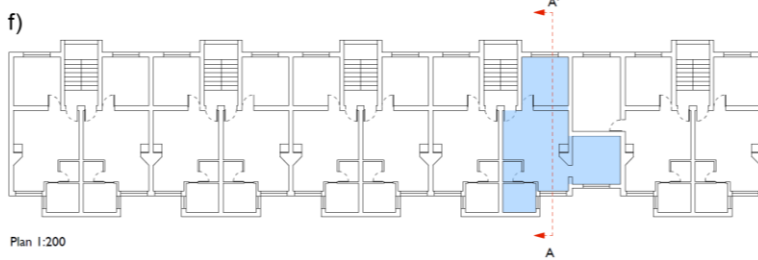
b-bedroom l-living room k-kitchen



b -bedroom l-living room d-dinning room



l: Living room, b: Bedroom, k: Kitchen, wc: Water closet.



Plan 1:200

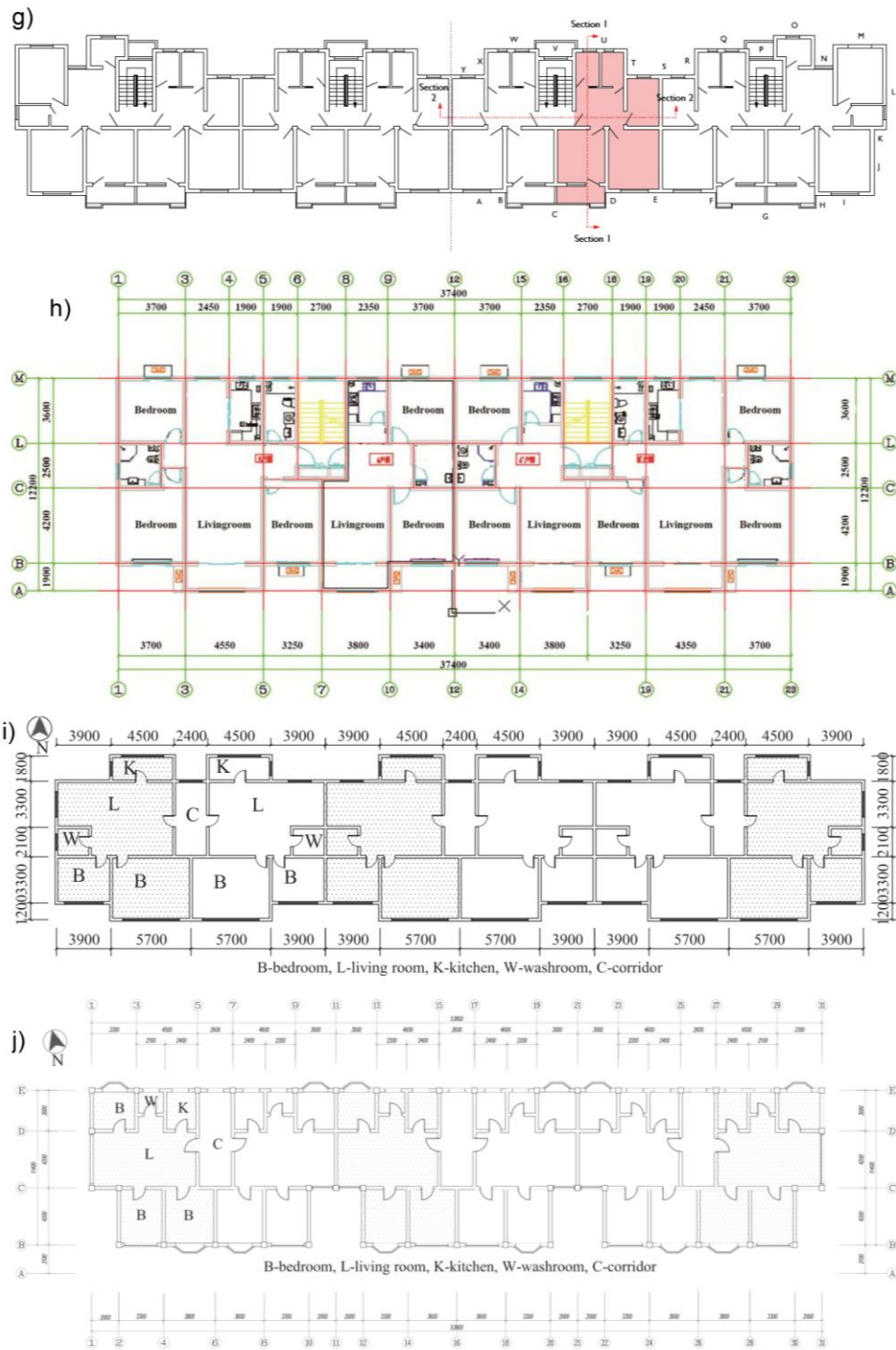


Figure 6-13: Typical floor plans for residential buildings in the HSCW zone as found in study a) Yu et al. (2009b), b) Yu et al. (2008), c) Short et al. (2018), d) W. Yu et al. (2015), e) Ichinose et al. (2017), f) Short et al. (2019), g) Short et al. (2019), h) Meng et al. (2019), i) Yao (2012) and j) Yao (2012).

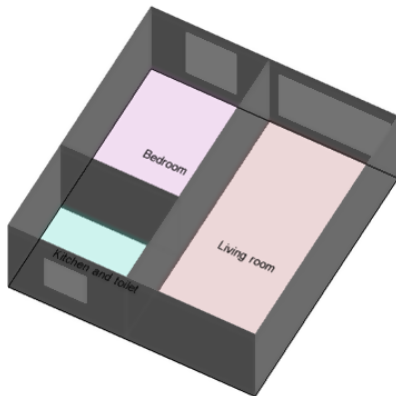
For the purpose of this study, the building archetype with one-bedroom was assumed to have the same area as the case study flat, with the level of detail reduced from LoD1 to LoD6 (Section 6.2). The total floor area of two-bedroom flats increased by 8 m² compared to the case study flat. Interestingly, the floor area of the living room, kitchen, and toilet remained unchanged, with a floor area of bedroom increase of 50%. Therefore, the floor area of the bedroom increased in the DTM (Figure 6-14b), with the window to wall ratio remaining unchanged (Table 6-6). Two bedrooms were modelled in one-single zone, assuming three occupants with the same AC operating schedule in the bedrooms, defined in Section 3.5.3. The floor layout of the two-bedroom flat was the same as the case study flat, i.e., the living room had a window facing front, bedroom had a window facing front, and the auxiliary area had a window facing the rear. Also, the shorter side width of the flat remained unchanged. For the three-bedroom flat, the floor area of bedroom increased by 26 m² (2.5 folded) compared to case study flat, living room increased by 6 m² (20%), and kitchen and toilet increased by 7 m² (70%). The development of the building archetype with three-bedrooms was the same as two-bedrooms (Figure 6-14c), with the window to wall ratio and floor layout unchanged (Table 6-6).

Table 6-5: Floor area of thermal zones assumed in flats with different bedrooms.

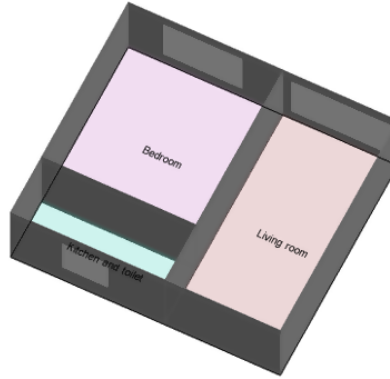
	Bedroom (m ²)	Living room(m ²)	Kitchen and toilet (m ²)	Total (m ²)
Case study flat	16	28	10	54
Two-bedroom flat	28	28	10	66
Three-bedroom flat	42	34	17	93

The most up-to-date 2010 census data provided information regarding number of bedrooms for each household in urban areas in Chongqing municipality (NBS, 2010). Because less than 9% of households have four or more bedrooms, these minor household categories are not considered in this study. From the census data, the percentage of households with one bedroom was 24%, with two bedrooms was 42%, and with three bedrooms was 34%.

a) one-bedroom flat



b) two-bedroom flat



c) three-bedroom flat

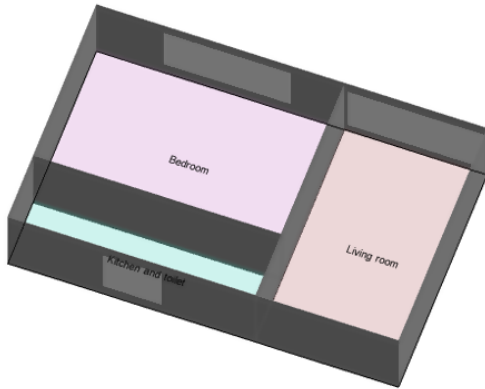


Figure 6-14: Axonometric view of flats with different number of bedrooms.

Table 6-6: Window to wall ratio of flats with different number of bedrooms.

	Zone	Total area of external wall (m ²)	Total area of window (m ²)	Total area (m ²)	Window to wall ratio
Case study flat	Living room	3.51	6.85	10.36	66%
	Bedroom	6.38	3.14	9.52	33%
	Kitchen & toilet	8.08	1.44	9.52	15%
Two-bedroom flat	Living room	3.51	6.85	10.36	66%
	Bedroom	9.3	4.58	13.88	33%
	Kitchen & toilet	11.77	2.11	13.88	15%
Three-bedroom flat	Living room	4.25	8.24	12.49	66%
	Bedroom	14.52	7.15	21.67	33%
	Kitchen & toilet	18.42	3.25	21.67	15%

6.5.2 Parameter 2: Building height

According to the Code for Design of Civil Building in China (MOHURD, 2005), the urban residential building stock in the HSCW zone can be classified into four types with regards to the number of storeys: low-rise (from one to three floors); multi-storey (from four to six floors); middle high-rise (from seven to

nine floors); and high rise (ten or more floors). However, a range of the number of storeys was specified for each type, i.e., a low-rise building can be a one, two, or three-storey building, which has different building energy consumption. In the representative area with 321 residential buildings, number of storeys of each residential building was collected and categorised as follows:

- 10% are low-rise buildings (31 buildings), the average number of storeys is 2.5; thus a three-storey building was modelled (Figure 6-15a);
- 16% are multi-storey buildings (51 buildings), the average number of storeys is 5.2; thus a five-storey building was modelled (Figure 6-15b);
- 38% are middle high-rise buildings (122 buildings), the average number of storeys is 8.1; thus an eight-storey building was modelled (Figure 6-15c);
- 36% are high-rise buildings (117 buildings), the average number of storeys is 16.2; thus a 16-storey building was modelled (Figure 6-15d).

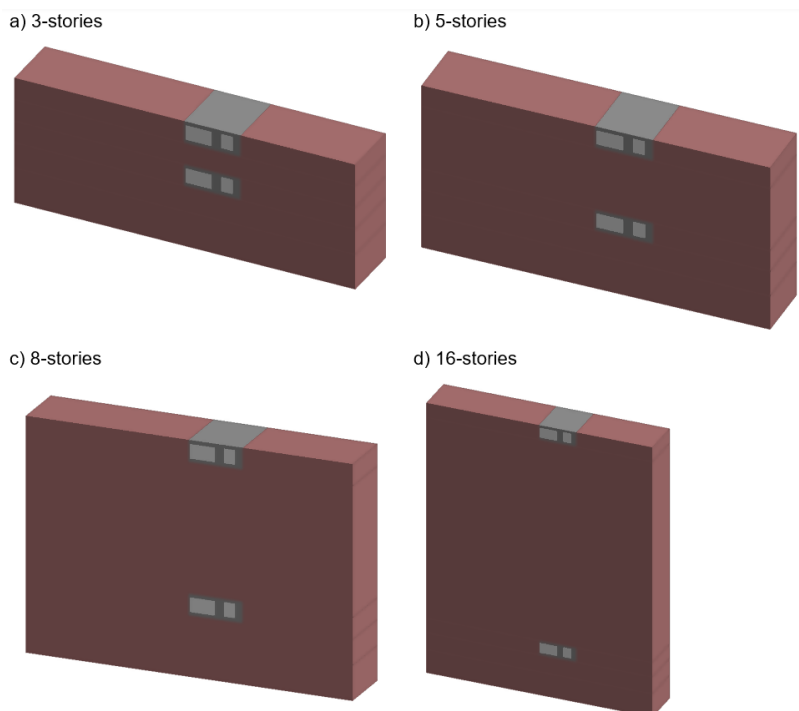


Figure 6-15: Dynamic thermal models with different number of stories (one-bedroom flat).

6.5.3 Parameter 3: Energy users

90% of households in the HSCW zone use a split-type air conditioner, which operates manually (THUBERC, 2017). Thus, only this type of energy usage pattern was considered in the city-scale model. Three scenarios which

correspond to the three energy users developed from Section 3.5 are used to represent the vast differences between energy use by different types of occupants. The energy users are assumed to be equally probable because no information about the percentage of households for each energy user exists.

6.5.4 Summary of building archetypes selected

Section 6.5.1, 6.5.2, and 6.5.3 justified the three parameters selected when developing building archetype for the city-scale study, summarised in Figure 6-16.

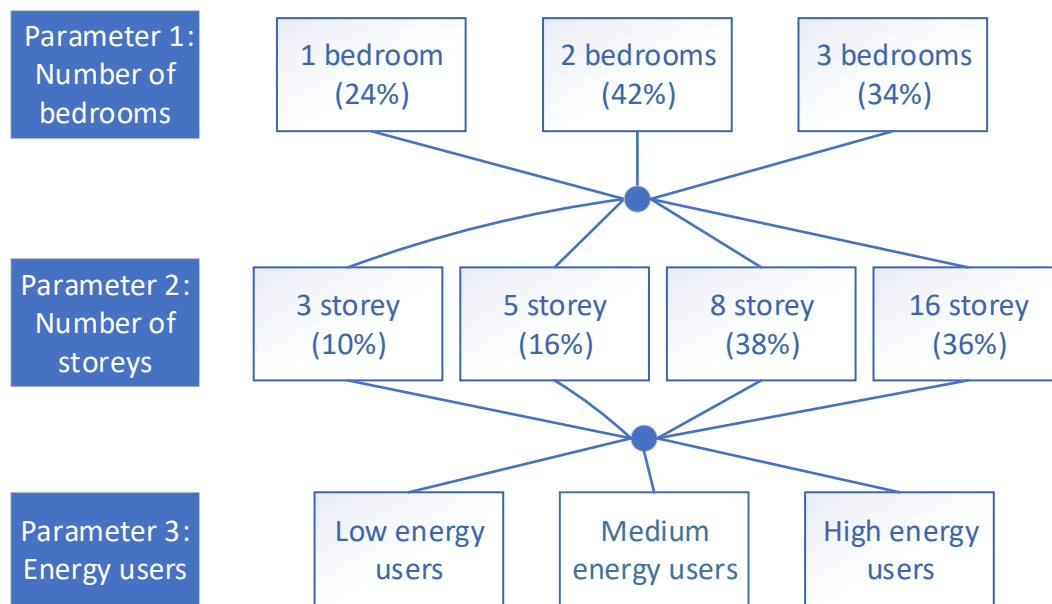
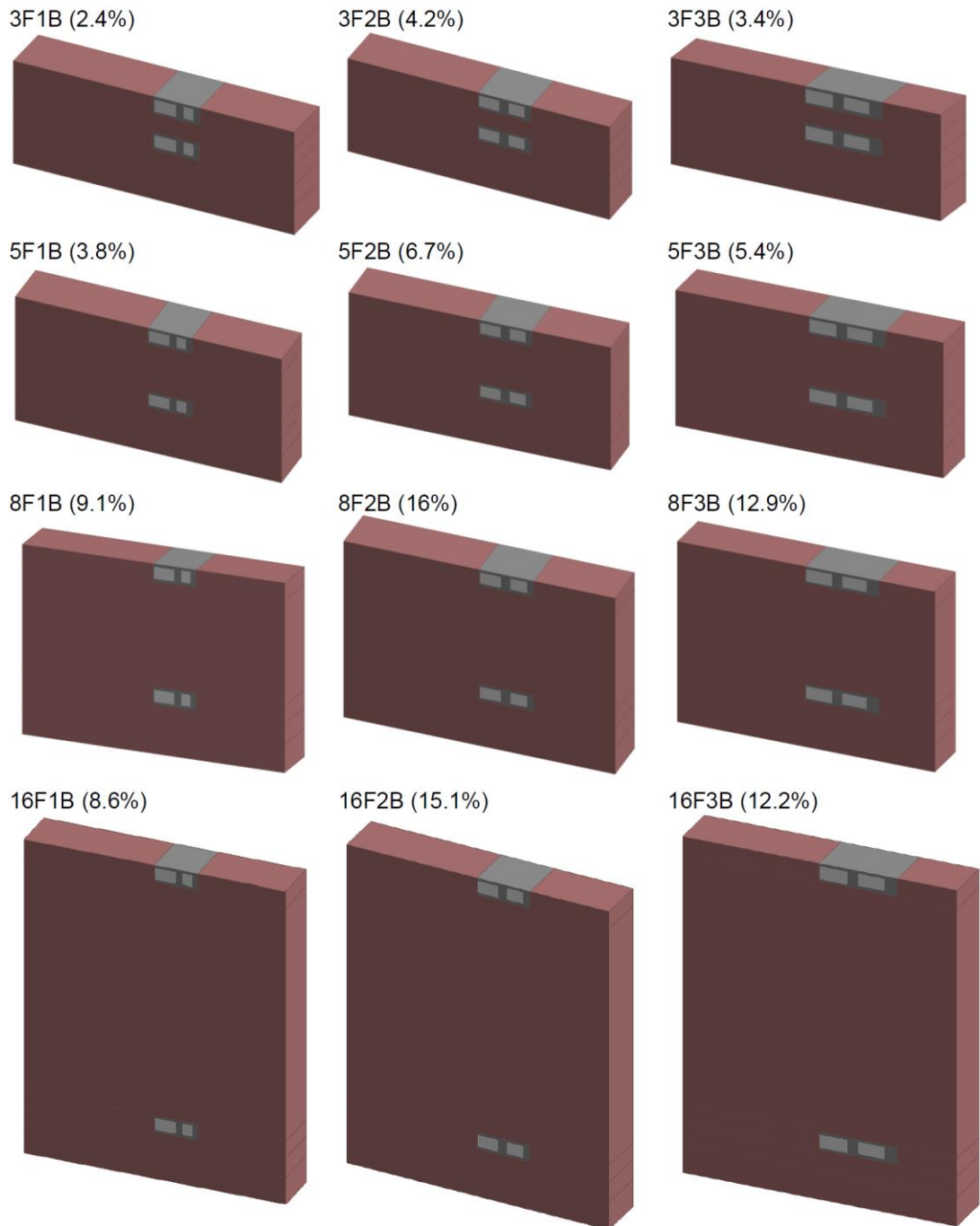


Figure 6-16: Parametric tree of the selected building archetypes.

Subsequently, twelve archetypes are developed accounting for number of bedrooms and building height (Figure 6-17).



Key

3F1B: Three storeys building with one-bedroom flats	8F1B: Eight storeys building with one-bedroom flats
3F2B: Three storeys building with two-bedroom flats	8F2B: Eight storeys building with two-bedroom flats
3F3B: Three storeys building with three-bedroom flats	8F3B: Eight storeys building with three-bedroom flats
5F1B: Five storeys building with one-bedroom flats	16F1B: 16 storeys building with one-bedroom flats
5F2B: Five storeys building with two-bedroom flats	16F2B: 16 storeys building with two-bedroom flats
5F3B: Five storeys building with three-bedroom flats	16F3B: 16 storeys building with three-bedroom flats

Figure 6-17: Dynamic thermal model for the selected twelve building archetypes in city-scale study.

6.6 Residential building archetypes energy saving retrofits

Predicted energy consumptions (in kWh/m²) of the twelve residential building archetypes are presented in Figure 6-18. The blue box refer to the range of metered energy consumption according to Section 3.6. Archetype 8F1B represents the case study building, which accounts for 7.9% of buildings in the representative area. For medium energy users, the predicted heating, cooling, and total energy consumption was 5.09 kWh/m², 7.68 kWh/m², and 12.77 kWh/m² respectively. The heating to cooling ratio was 40/60.

Heating energy consumption was the highest per square metre (5.93 kWh/m²) for a three-storey building and the lowest (4.84 kWh/m²) for a 16-storey building, with a 20% difference. The reason is that top flats consume twice as much heating energy as middle flats (Section 5.2), and the percentage of top flats in a three-storey building (33%) is larger than a 16-storey building (6%). The trend of cooling energy consumption is similar to that of heating energy consumption, where cooling energy consumption is the highest (8.01 kWh/m²) for a three-storey building and the lowest (7.58 kWh/m²) for a 16-storey building, with a 7% difference. Top flats consume 30% more cooling energy as middle flats (Section 5.2; Figure 6-18).

Heating energy consumption was 24% less for two-bedroom flats, and 40% less for three-bedroom flats than for one-bedroom flats. The reason is that for medium energy users, it is assumed that occupants do not use heating in the bedroom. Floor area of bedroom doubled for two-bedroom flats and tripled for three-bedroom flats, but the floor area of the living room did not increase for two-bedroom flats and increased by 20% for three-bedroom flats compared to one-bedroom flats. This caused the reduction of heating energy consumption per floor area. The reduction for cooling energy consumption was smaller because occupants operate AC for cooling for 3 hours in the bedroom, therefore increased floor area of bedroom led to increased cooling energy consumption. The cooling energy consumption per floor area reduced by 4% for two-bedroom flats and 7% for three-bedroom flats (Figure 6-18).

The range of total energy consumption for low (6.91 to 10.39 kWh/m²), medium (9.98 to 13.95 kWh/m²), and high (14.84 to 18.89 kWh/m²) energy users was extensive. The total energy consumption for low energy users with archetype 3F1B (10.39 kWh/m²) was 5% more than medium energy users with archetype 16F3B (9.98 kWh/m²). The variation due to the number of bedrooms and building height is the largest for low energy users, where energy consumption for archetype 3F1B was 34% more than archetype 16F3B; the increment was smaller for medium energy users (28%) and high energy users (21%; Figure 6-18).

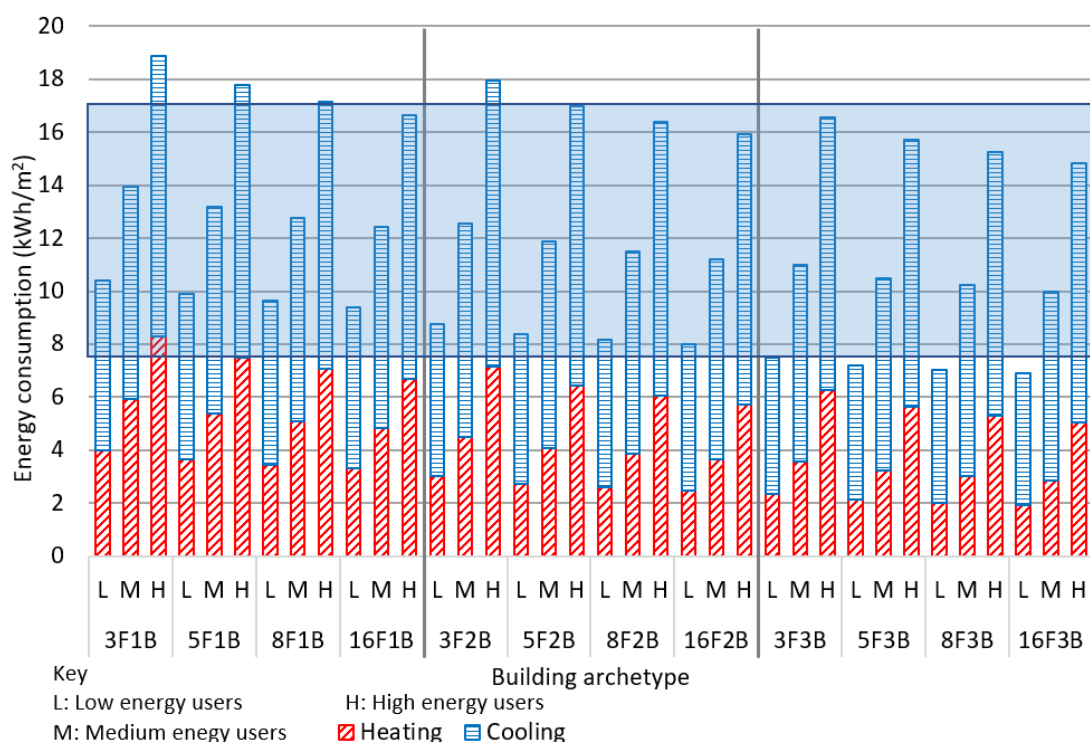


Figure 6-18: Predicted energy consumption for twelve residential archetypes with three energy users, with the blue box refer to the range of metered energy consumption from literature (7.7 to 17 kWh/m²).

In Figure 6-19, predicted energy consumptions (in kWh for each household) of the twelve residential building archetypes are presented. Results showed that the twelve residential archetypes were within the threshold (508 to 696 kWh) for low energy users. One archetype (5F3B) with an energy consumption of 976 kWh exceeded the threshold for medium energy users. However, ten archetypes (83% out of total) exceeded the threshold for high energy users. The highest energy consumption was archetype 3F3B, with an energy consumption of 1539 kWh, 65% higher than the threshold.

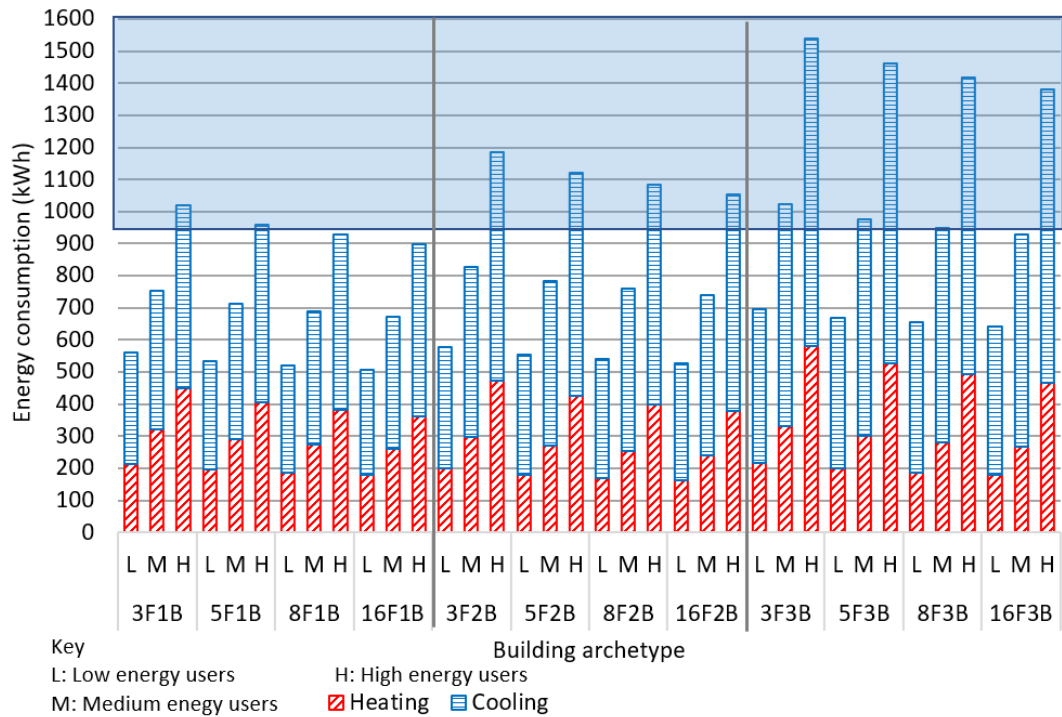


Figure 6-19: Predicted energy consumption in kWh per flat for twelve residential archetypes with three energy users, with the blue box refer to the range which exceed threshold suggested by Chinese regulation (>930 kWh/household).

When energy saving retrofit measures were employed, significant energy savings were predicted (Chapter 5). These retrofit measures were: 25 mm external wall insulation, 50 mm roof insulation, double-glazed low-e windows, air infiltration rate of 0.7 ach^{-1} , horizontal overhang of 0.5 m, and AC heating COP of 3.1 and cooling COP of 3.6.

The predicted energy consumptions (in kWh for each household) of the twelve residential building archetypes, along with the total percentage reduction (green line) after retrofit, were presented in Figure 6-20. Results showed that after the retrofit, space heating and cooling energy consumption were less than the threshold (930 kWh) for the twelve archetypes and three energy users. Note that when number of storeys varied, heating energy reduction remained unchanged but cooling energy reduction decreased when number of storeys increased; as the percentage of cooling energy reduction for top flats (60%) was larger than middle flats (50%). When number of bedrooms varied, the heating energy reduction increased slightly (from 73% to 75%) and cooling energy reduction decreased slightly (from 43% to 45%).

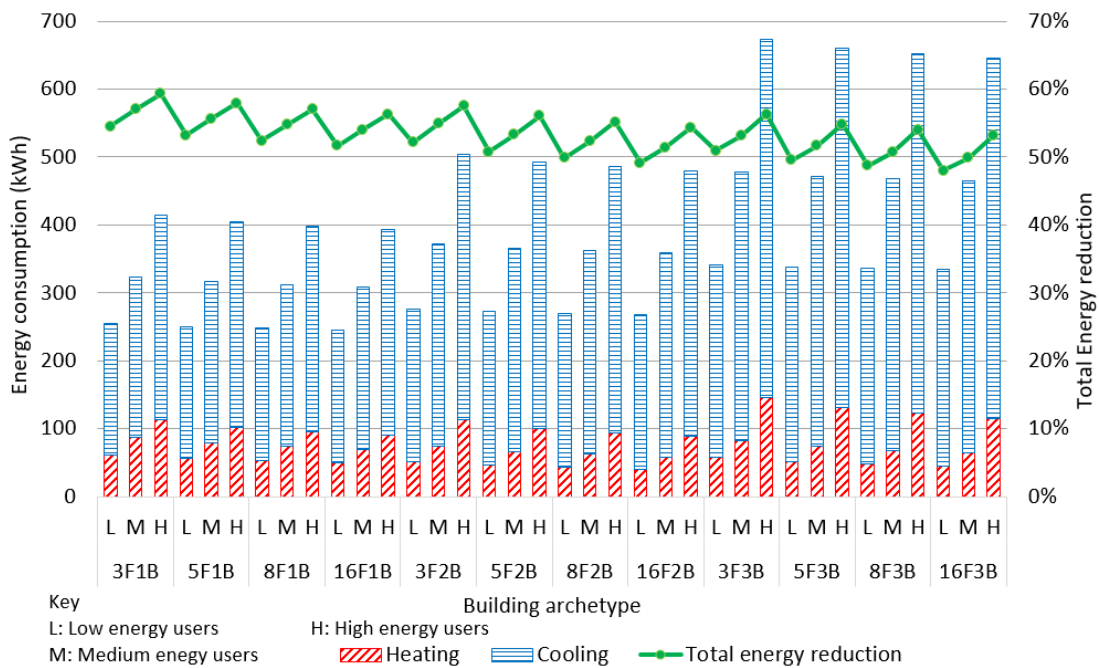


Figure 6-20: Predicted energy consumption in kWh per flat and total energy reduction post-retrofit for twelve residential archetypes with three energy users.

In Figure 6-21 and Figure 6-22, the correlation between number of storeys, number of bedrooms and energy users were presented. Number of bedrooms were quantified by floor area of flats. Energy users were quantified by the averaged heating and cooling AC operating hours, in living room and bedroom combined. Subsequently, the coefficient of determination (R^2) was calculated, to predict the correlation between total energy consumption with the number of storeys, number of bedrooms and energy users.

Results revealed that the energy users showed a strong correlation ($R^2 = 0.89$) to total energy consumption; thus, increasing AC operating hours led to the increase in energy consumption. However, number of storeys and number of bedrooms showed a weak correlation to energy consumption, although they showed a decreasing trend of energy consumption (Figure 6-21). In Figure 6-22, all the three parameters showed a weak correlation to energy consumption.

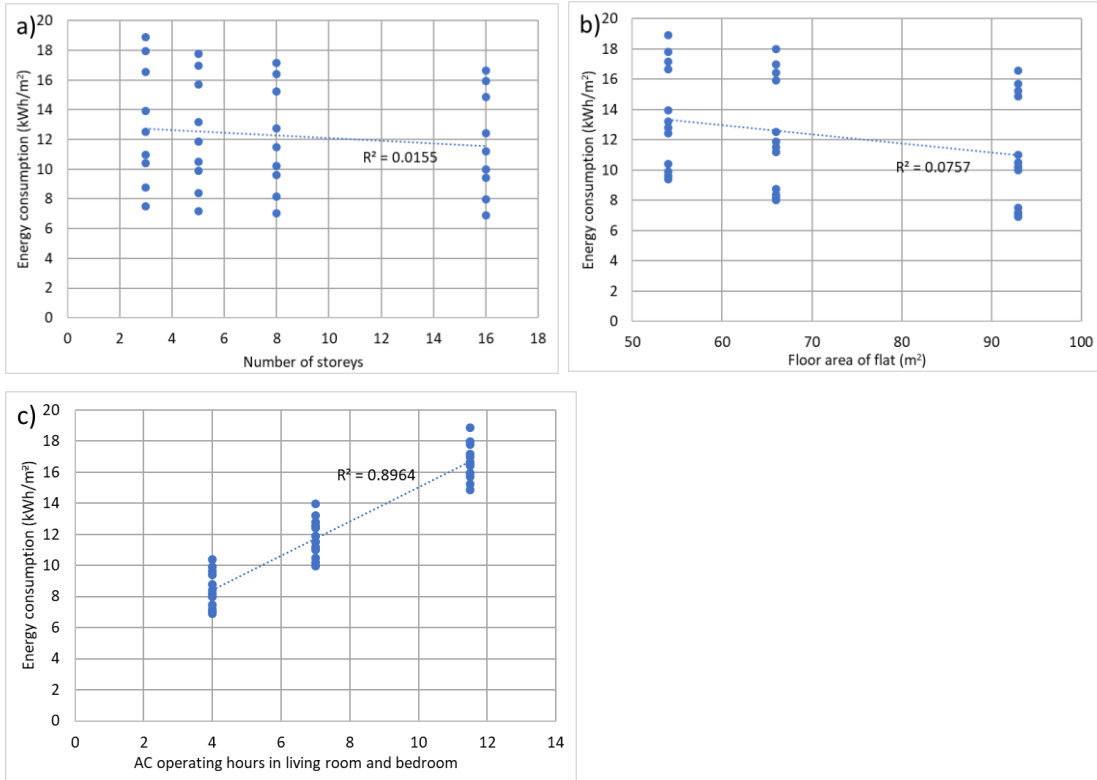


Figure 6-21: Correlation of a) number of storeys, b) number of bedrooms (quantified by floor area of flat) and c) energy users (quantified by averaged heating and cooling AC operating hours, in living room and bedroom combined), versus total energy consumption pre-retrofit in kWh/m².

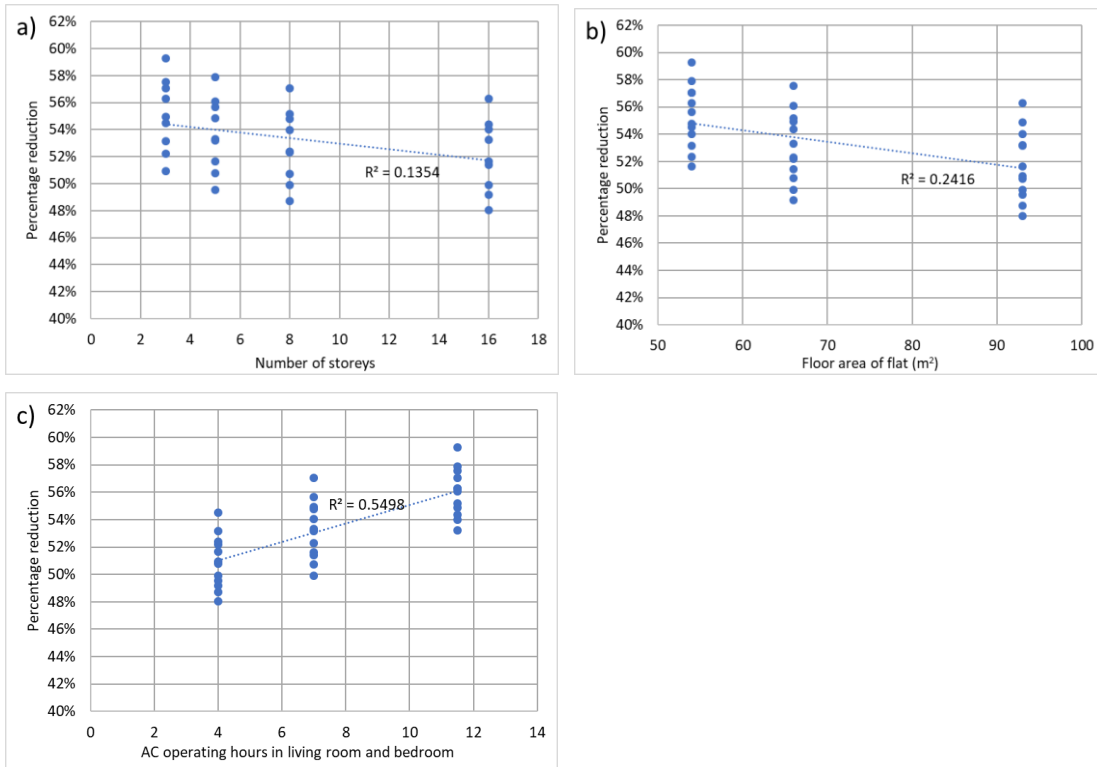


Figure 6-22: Correlation of a) number of storeys, b) number of bedrooms (quantified by floor area of flat) and c) energy users (quantified by averaged heating and cooling AC operating hours, in living room and bedroom combined) versus percentage of energy reduction after retrofit.

6.7 City-scale energy saving retrofits contribution

A representative area in Chongqing was selected with a population of 649,500, there were 321 residential apartment buildings built before building regulations, with a built area of 4.07 million m² (Section 3.3.1). Information including floor area, height, and built area of each building in the representative area were collected from LoHCool, based on field surveys and satellite images (details in Appendix C). Energy consumption (in kWh/m²) of the twelve residential building archetypes was predicted in Section 6.6; thus, the total built area for each archetype in the representative area was deduced, in order to evaluate energy saving retrofits at a city scale.

Built area per floor was collected for the 321 residential buildings (Appendix C). Note that the built area included communal area; whereas the predicted energy consumption of the twelve archetypes did not include communal area. Therefore, the communal area was excluded, and the percentage of communal area to the built area per floor was assumed to be 14%; based on the mean value according to five studies (Meng et al., 2019; Short et al., 2018; Yao et al., 2018; Yu et al., 2009a, 2008) and the case study building (Section 2.5.7).

Built area per floor was predicted for the four types of residential building with regards to the number of storeys, by calculating the mean built area per floor for the respective buildings (Table 6-7). Then, built area of the twelve archetypes was calculated by multiplying the built area per floor by the number of storeys and the number of buildings for each archetype according to Figure 6-17 (Table 6-8). Thus, the energy consumption in the representative area was predicted by summing the energy consumption for each archetype (calculated by multiplying the predicted energy consumption in kWh/m² by the built area).

Table 6-7: Mean built area per floor for four types of residential buildings in the representative area.

Type of residential building	Number of buildings	Mean built area per floor (m ²)	Mean built area per floor, excluding communal area (m ²)
Low-rise (1-3 storey)	31	590	510
Multi-storey (4-6 storey)	51	710	610
Middle high-rise (7-9 storey)	122	1030	890
High rise (≥10 storey)	117	1400	1200

Table 6-8: Total built area for twelve archetypes in the representative area.

Archetype	Built area per floor (m ²)	Number of storeys	Built area per building (m ²)	Number of buildings	Built area for each archetype (m ²)
3F1B	510	3	1530	17	26010
5F1B	610	5	3050	12	36600
8F1B	890	8	7120	26	185120
16F1B	1200	16	19200	23	441600
3F2B	510	3	1530	30	45900
5F2B	610	5	3050	20	61000
8F2B	890	8	7120	44	313280
16F2B	1200	16	19200	40	768000
3F3B	510	3	1530	24	36720
5F3B	610	5	3050	16	48800
8F3B	890	8	7120	36	256320
16F3B	1200	16	19200	33	633600

The predicted aggregated energy consumption in the representative area was presented in Figure 6-23. The heating and cooling energy consumption for all the residential buildings requiring retrofit was 32.9 TWh for medium energy users, 28% lower for low energy users and 43% higher for high energy users. 11.7 TWh (50%) of energy was reduced for low energy users reduced, 17.1 TWh (53%) of energy was reduced for medium energy users, and 25.7 TWh (55%) of energy was reduced for high energy users, if the proposed retrofit measures were employed.

In the future, as living standard increases, the AC operating hours will increase. Three scenarios are developed to analyse the effect of increased AC operating hours after retrofit:

- Scenario 1: The representative area consists mostly of low energy users with an energy consumption of 23.3 TWh. **After the retrofit, assume**

occupants switch to medium energy users, with an energy consumption of 15.4 TWh which will achieve a 30% reduction.

- Scenario 2: The representative area consists mostly of low energy users with an energy consumption of 23.3 TWh. After the retrofit, assume occupants switch to high energy users, with an energy consumption of 20.7 TWh which will achieve a 10% reduction.
- Scenario 3: The representative area consists mostly of medium energy users with an energy consumption of 32.5 TWh. After the retrofit, assume occupants switch to high energy users, with an energy consumption of 20.7 TWh which will achieve a 35% reduction.

Therefore, even in the worst-case scenario (scenario 2), the proposed retrofit measures can achieve a 10% energy reduction.

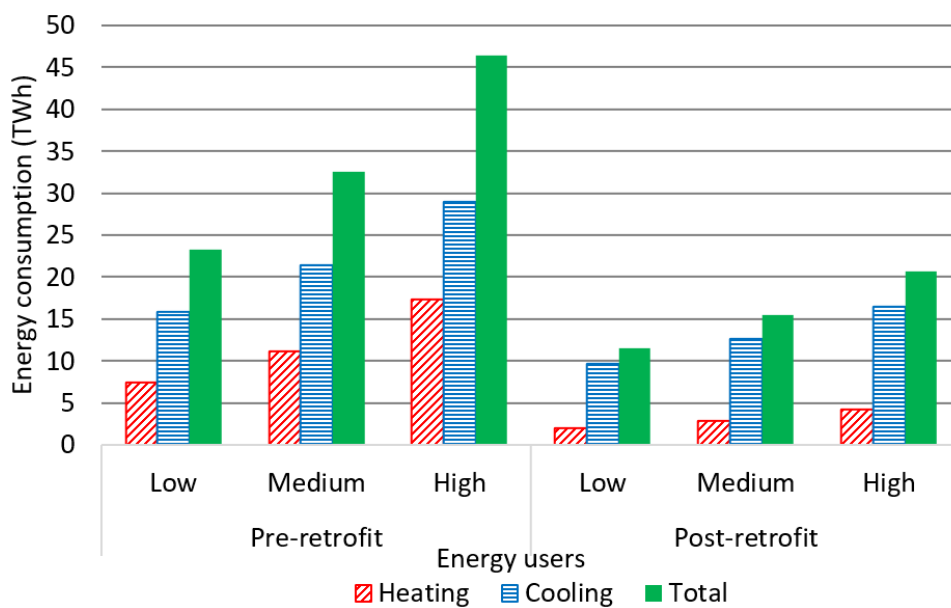


Figure 6-23: Space heating and cooling energy consumption pre-retrofit and post-retrofit in the representative area for three energy users.

Carbon dioxide (CO₂) emissions was predicted by multiplying annual energy consumption by CO₂ conversion factor. A direct emission conversion factor from tons of CO₂ per MWh (tCO₂/MWh), coal was selected for this study as it is the primary fuel used in China, with a conversion factor of 0.961 tCO₂/MWh (Krey et al., 2014).

The predicted CO₂ emission in tCO₂ was presented in Figure 6-24. The carbon dioxide emission reduction due to retrofits showed a similar trend with energy

reduction due to retrofits in Figure 6-23. A significant reduction of carbon dioxide emission was predicted, with 11,030 tCO₂ for low energy users, 16,500 tCO₂ for medium energy users, and 24,700 tCO₂ for high energy users, if the proposed retrofit measures were employed.

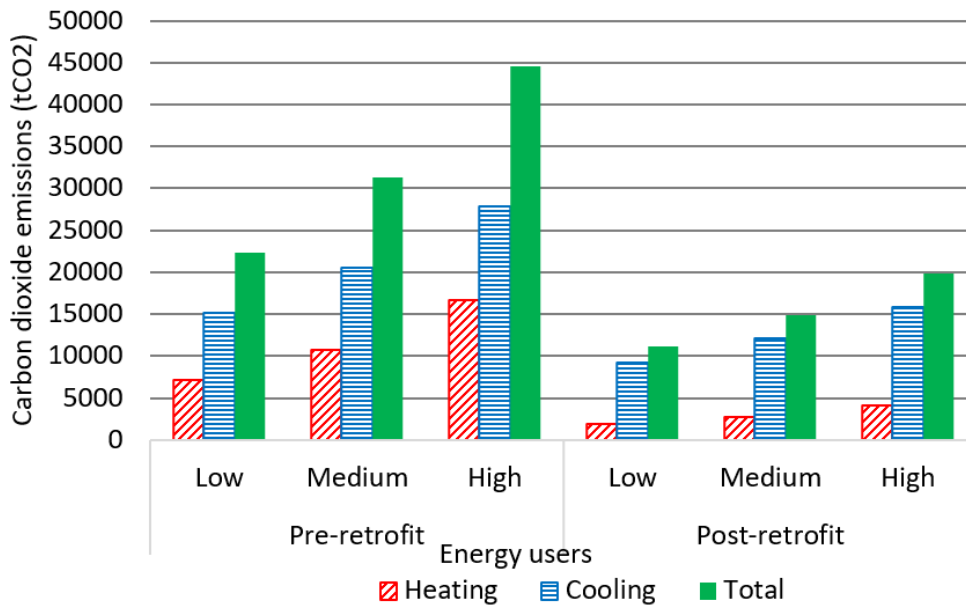


Figure 6-24: Carbon dioxide emissions pre-retrofit and post-retrofit in the representative area for three energy users.

6.8 Discussion

This chapter presents the identification of the most computationally efficient DTM, and evaluates the feasibility of the selected combination of retrofit measures at a city-scale.

A 0.4% heating energy reduction was predicted after removal of bay windows. This is aligned with Taylor et al. (2013), which predicted a heating energy reduction of 2.6% after removal of bay windows. Yet, Taylor et al. (2013) missed to consider the effect on cooling energy demand after removal of bay windows, where this thesis showed that a significant (12%) cooling energy reduction was resulted after removal of bay windows. Since solar heat gain from windows is reduced after removal of bay windows, and also the fabric transmission heat loss decreased in winter but not in summer. Therefore, in winter, the fabric transmission heat loss led to a reduction of heating energy demand, where the reduction of solar heat gain contributed to an increase of

heating energy demand, which balanced out and led to a net heating energy reduction of 0.4% in this thesis. In summer, the reduction of solar heat gain comprises the reduction in cooling energy demand, hence the 12% reduction after removal of bay windows.

Window frames and dividers had a small contribution in the heating load and equal to 1%. This was in line to results predicted by others, e.g. 3.5% reduction by Taylor et al. (2013). Yet, Taylor et al. (2013) missed to consider the effect on cooling energy demand, where this thesis showed that window frames and dividers had also a small contribution (1% reduction).

Single-thermal zone model (LoD8) had a significant contribution in the heating load, with a 25% reduction; but it had a small contribution in the cooling load, with a 5% reduction. The findings are opposed to Taylor et al. (2013), in which a 4% heating energy reduction was predicted. Since Taylor et al. (2013) assumed a different heating set-point for the living room (21°C) and all other areas in the house (18°C), where they have the same heating schedule; when the internal zoning was removed, the heating set-point of the whole flat was adjusted to 18.5°C. However, living room and bedroom had a different heating schedule, and this thesis showed that the internal wall separating bedroom and living room plays an essential role in increasing heat loss in the living room, as the living room is the only space with heating for medium energy users. Therefore, removal of the internal wall led to a massive difference in the predicted energy demand.

Energy consumption increased when number of bedrooms (floor area of a flat) decreased, since the ratio of bedroom area to flat area increased when number of bedrooms increase, and occupants' use AC more frequently in living room than bedroom. For instance, a 25% increase was predicted for energy consumption for one-bedroom flats (12.8 kWh/m²) compared with three-bedroom flats (10.2 kWh/m²), for an eight-storey building. However, the findings are in contrast to Li et al. (2019), in which energy consumption only increased by 3% when floor area of a flat increased (from 35 to 170 m²). As Li et al. (2019) failed to consider the ratio of bedroom area to flat area changes for flats with different number of bedrooms, i.e., Li et al. (2019) assumed the

bedroom area accounts for 50% of the flat area, for one-bedroom, two-bedroom, and three-bedroom flats; leading to a similar predicted energy consumption across the flats with different floor area.

Energy consumption increased when number of storeys decreased, as the ratio of top flats (which consume 60% more energy than middle flats) in buildings with larger number of storeys is smaller. For instance, a 13% increase was predicted for energy consumption for a three-storey building (12.4 kWh/m²) compared with a 16-storey building (14 kWh/m²), for one-bedroom flats. The findings are aligned to X. Li et al. (2018), which predicted a 5% increase in energy consumption for an eight-storey building compared to a 26-storey building.

The aggregated energy consumption in the representative area was predicted to be 32.9 TWh (medium energy users) before retrofit. The findings are in contrast to X. Li et al. (2018), where the predicted energy consumption was 153 TWh in the same representative area. Since X. Li et al. (2018) failed to create an occupancy profile that represented a large number of households, when using building energy model to predict the energy consumption in the representative area.

Chapter 7 : Conclusions

7.1 Introduction

This thesis set out to develop seven energy-saving retrofit measures for urban residential buildings in China's HSCW zone, aiming to reduce carbon emissions and prevent summertime overheating. Dynamic thermal simulation was used to predict the energy reduction at a city-scale. The development of a representative Dynamic Thermal Model (DTM) for the case study building was achieved by characterising building parameters of the urban residential building stock. Following this, the sensitivity of energy demand of various building fabrics was predicted, so as to calibrate the DTM in a case study flat for one week using measured indoor air temperatures. The energy and thermal comfort performance of the developed retrofit measures was quantified, along with the selection of an optimum combination of retrofit measures, for the case study flat and different flat locations in the case study building. DTMs with nine computational Level of Detail (LoD) were developed, and the most computationally efficient model was identified, which was used to devise twelve residential building archetypes, which would enable energy reduction predictions for 321 residential buildings with a built area of 4.07 million m² in Chongqing, China.

7.2 Key findings

Retrofitting domestic building stock in China concluded the following findings:

- External wall insulation does not contribute to energy reduction, with only 2% of (annual space-conditioning) energy reduction;
- Double-glazed window is the best retrofit measure, with a 15% energy reduction. Note that outermost windowpane should be low-emissivity (low-e), since the cooling energy reduction in summer due to decrease of solar heat gain to the windows outweighs the heating energy increase in winter;

- Air infiltration control is the second-best retrofit measure, with a 10% energy reduction;
- Double-glazed window and air infiltration control are more suitable for wide implementation, since 30% energy can be reduced;
- Additional window overhang provides 8% reduction for south facing flats, but only 4% reduction for north facing flats;
- Enclosing previously external communal staircases is not commonly investigated; however, it is an effective retrofit measure, with a 10% reduction;
- Roof insulation is the key retrofit measure for top floor flats, with a 28% reduction, but it is less effective with middle floor flats;
- Energy-efficient AC can achieve 28% energy reduction; however, it does not improve occupants' thermal comfort.

The comparison between city, building and flat scale evaluation concluded the following findings:

- Before retrofit, a selected part of the city in Chongqing (321 apartment buildings) with built area of 4.07 million m² was predicted to consume 32.9 TWh of annual space-conditioning energy, a building (eight-storeys, one-bedroom apartments) with built area of 4730 m² consumes 82.5 MWh of energy, and a middle floor flat on the centre facing north with area of 49.3 m² consumes 600 kWh of energy;
- In a building scale, a high-rise (16 storey) building consumes 13% more energy than a low-rise (3-storey) building, and a one-bedroom flat building consumes 25% more energy than a three-bedroom flat in terms of kWh/m². Combined energy-saving retrofits varied from 48 to 59% in these buildings;
- Evaluation of twelve flat locations in a single building in the selected area revealed that top floor flats consume 60% more energy than middle floor flats, and south facing flats consume 8% more energy than north facing flats. Combined energy-saving retrofits varied from 60.3% to 66.5% in these twelve flats.

The building performance modelling approaches employed in this research allowed for the following findings:

- Simulation time of LoD1 (highest detail) is four times longer than LoD9 (lowest detail); however, the total energy demand for LoD9 is 13.5% less than LoD1. LoD6 was selected to develop city-scale model, which take 20% longer to simulate than LoD9, but the energy demand is 2% less than LoD1;
- When calibrating a DTM using measured indoor air temperatures in a flat, adding a pre-validation period by extending the simulation period can match the thermal condition of the flat before the measurement starts; thus, improve the reliability of calibration process;
- Monthly quasi-steady-state model overpredicts energy demand by 10% compare to DTM; thus, it can be used to collect valuable insights on energy demand when input data are not sufficient for the development of DTM. However, such steady-state model fails to predict hourly energy demand and indoor air temperature;
- Uncertainty band should be supported and developed according to evidence as it directly affects the ranking of the input parameter; window construction is the most sensitive parameter (11%), follow by air infiltration rate (10%) and external wall construction (3%).

7.3 Impact of work

7.3.1 Academia

A systematic review is performed to characterise building parameters to develop a representative DTM. The outputs can be useful to model building stock in developing countries, where government reports or data are not available.

Considering different levels of computational details at building scale before the development of city scale models can reduce simulation time and increase representativeness of the devised building archetypes in a city; thus, the reliability of predictions at a city scale can be improved.

The predicted annual space-conditioning energy from the three energy users (9.2 to 16.4 kWh/m²) developed matches with annual metered space-conditioning energy (7.7 to 17 kWh/m²) collected from secondary data; thus, the energy users developed represented a large number of households, where an informed quantification of the retrofit measures can be performed;

The acceptable temperature range of occupants in the HSCW zone was between 17.7 to 27.9°C, but the Chinese design standard of energy efficiency in residential buildings suggest a comfort range of 18 to 26°C; thus, using HSCW zone thermal comfort criteria to predict occupants' thermal comfort can represent a large number of households.

7.3.2 Government

The Chinese design standard for energy efficiency of residential buildings in the HSCW zone (MOHURD 2010a) has not been updated in a decade. The proposed retrofit measures from this thesis can offer insights to revise the design standard, e.g. air infiltration control, additional overhang, and energy-efficient AC are not discussed in the standard, yet they are effective retrofit measures for reducing energy consumption and improving thermal comfort according to this thesis.

Only 2% of the urban residential building stock was retrofitted between 2016-2020 as a government policy; however, 50 to 55% of the annual space-conditioning energy could be saved, if the proposed retrofit measures are implemented, which offer insights to increase the retrofit rate in the future policy.

In December 2016, the Energy Supply and Consumption Revolution Strategy (2016-2030) was announced as part of a national policy in China. The policy aims to reduce carbon dioxide emission by 60 to 65% relative to 2005 levels in 2030. Thus, retrofitting the domestic building stock in China can assist the government to reach the carbon dioxide emission goals.

7.3.3 Industry

The percentage of energy savings presented in the key findings from retrofitting domestic building stock in China, can provide advice to industry to employ suitable retrofit measures.

Retrofit projects are generally more complex and require more expertise than the process of demolition and rebuild. Thus, increasing the number of retrofit projects can potentially raise the market value of the building industry.

7.3.4 Society

Occupants can benefit directly from retrofit with a more energy-efficient and thermally acceptable living environment; thus, improve resident's living standard.

Retrofitting domestic building stock in China help occupants to reduce cost of electricity require to heat and cool flats to a thermally acceptable temperature.

Less carbon dioxide emission is resulted from energy-saving retrofits; hence, reduce air pollution in cities, along with fresher air, which promote a healthier environment.

Besides the aspect of energy saving, retrofit can overcome poor ventilation and damp problems, as well as the installation of modern facilities, which can enhance resident's health and wellbeing, especially with the elderly population.

7.4 Limitations and recommendations for future work

Indoor air measurements from a single building were collected in this study, which made possible to calibrate the DTM of this building. However, future work could focus on measurements at a larger scale that would allow for a larger study to be conducted.

The key findings from retrofitting domestic stock in China were predicted based on a typical residential building. Yet, future work could include more building designs in the HSCW zone, that would allow a larger study to be conducted.

The city of Chongqing was focused in this study, which is a major city in the HSCW zone with 33 million residents. Nevertheless, future work could contain more cities in the HSCW zone with different climatic conditions, that would allow for further energy savings to be achieved.

The Level of Detail (LoD) selection was based on the data collected in this study, which made possible to create a highly complex and computationally detail DTM. However, future work could test the LoD selection with different climatic conditions, that would make the case study more generalisable.

Twelve residential building archetypes were devised from the selected LoD in this study, which represented a large number of buildings in the HSCW zone. Nonetheless, future work could introduce additional parameters, such as shading from surrounding buildings, which was out of the scope of this research.

The built area of residential buildings in the representative area was based on the data collected in this study, which made possible to predict the aggregated annual space-conditioning energy in the city using DTM. Yet, future work could focus on other areas in the city, which would allow the investigation of different composition of building types.

References

- Abualdenien, J., Borrmann, A., 2019. A meta-model approach for formal specification and consistent management of multi-LOD building models. *Advanced Engineering Informatics*, 40, 135–153.
- ACH foam technologies, 2013. EPS vs XPS applies to applies comparison of rigid foam insulation.
- American Institute of Architects (AIA), Associated General Contractors (AGC) of America, 2019. Level of Development (LOD) Specification Part 1 & Commentary For Buidling Information Models and Data.
- An, J., Yan, D., Hong, T., Sun, K., 2017. A novel stochastic modeling method to simulate cooling loads in residential districts. *Applied Energy*, 206, 134–149.
- ASHRAE, 2018. ASHRAE handbook fundamentals. ASHRAE standard. American Society of Heating Refrigerating and Air-Conditioning Engineers, Atlanta, Georgia.
- ASHRAE, 2010. Thermal Environmental Conditions for Human Occupancy, ASHRAE Standard 55-2010. Atlanta, Georgia.
- Ballarini, I., Corgnati, S.P., Corrado, V., 2014. Use of reference buildings to assess the energy saving potentials of the residential building stock: The experience of TABULA project. *Energy Policy*, 68, 273–284.
- Ballarini, I., Corrado, V., Madonna, F., Paduos, S., Ravasio, F., 2017. Energy refurbishment of the Italian residential building stock: energy and cost analysis through the application of the building typology. *Energy Policy*, 105, 148–160.
- Barlow, S., Fiala, D., 2007. Occupant comfort in UK offices-How adaptive comfort theories might influence future low energy office refurbishment strategies. *Energy and Buildings*, 39, 837–846.
- Beizaee, A., 2016. Measuring and modelling the energy demand reduction potential of using zonal space heating control in a UK home.
- Berkelmans, L., Wang, H., 2012. Chinese Urban Residential Construction to 2040.
- Big Ladder Software, 2019. Elements User Guide [WWW Document]. URL <https://bigladdersoftware.com/projects/elements/docs/user-guide/>
- Biljecki, F., Ledoux, H., Stoter, J., 2016. An improved LOD specification for 3D building models. *Computers, Environment and Urban Systems*, 59, 25–37.

- Bou-saada, T.E., Haberl, J.S., 1995. An improved procedure for developing calibrated hourly simulation models. *5th International IBPSA Conference*, 475–484.
- Bruno, R., Pizzuti, G., Arcuri, N., 2016. The Prediction of Thermal Loads in Building by Means of the en ISO 13790 Dynamic Model: A Comparison with TRNSYS. *Energy Procedia*, 101, 192–199.
- BSI, 2008. BS EN ISO 13790:2008 Energy performance of buildings - Calculation of energy use for space heating and cooling.
- Cai, Z., Yin, Y., Wennerstern, R., 2013. From energy efficiency to integrated sustainability in housing development in China: A case study in a hot-summer/cold-winter zone in China. *Journal of Housing and the Built Environment*, 28, 329–344.
- CEN, 2007. EN 15251:2006 Indoor environmental input parameters for design and indoor air quality , thermal environment , lighting and acoustics. Brussels, Belgium.
- Central Compilation & Translation Press, 2016. The 13th Five-Year Plan for Economic and Social Development. Beijing, China.
- Central Compilation & Translation Press, 2011. The 12th Five-Year Plan for Economic and Social Development. Beijing, China.
- Chen, A., Chang, V.W.-C., 2012. Human health and thermal comfort of office workers in Singapore. *Building and Environment*, 58, 172–178.
- Chen, J., Wang, X., Steemers, K., 2013. A statistical analysis of a residential energy consumption survey study in Hangzhou, China. *Energy and Buildings*, 66, 193–202.
- Chen, S., Levine, M.D., Li, H., Yowargana, P., Xie, L., 2012. Measured air tightness performance of residential buildings in North China and its influence on district space heating energy use. *Energy and Buildings*, 51, 157–164.
- Chen, S., Li, N., Guan, J., Xie, Y., Sun, F., Ni, J., 2008. A statistical method to investigate national energy consumption in the residential building sector of China. *Energy and Buildings*, 40, 654–665.
- Chen, S., Li, N., Yoshino, H., Guan, J., Levine, M.D., 2011. Statistical analyses on winter energy consumption characteristics of residential buildings in some cities of China. *Energy and Buildings*, 43, 1063–1070.
- Chen, S., Yang, W., Yoshino, H., Levine, M.D., Newhouse, K., Hinge, A., 2015. Definition of Occupant Behavior in Residential Buildings and Its Application to Behavior Analysis in Case Studies. *Energy and Buildings*, 104, 1–13.
- Chen, S., Yoshino, H., Levine, M.D., Li, Z., 2009. Contrastive analyses on annual energy consumption characteristics and the influence mechanism between new and old residential buildings in Shanghai, China, by the

- statistical methods. *Energy and Buildings*, 41, 1347–1359.
- Chen, S., Yoshino, H., Li, N., 2010. Statistical analyses on summer energy consumption characteristics of residential buildings in some cities of China. *Energy and Buildings*, 42, 136–146.
- Chen, X., Yang, H., 2018. Integrated energy performance optimization of a passively designed high-rise residential building in different climatic zones of China. *Applied Energy*, 215, 145–158.
- Chidiac, S.E., Catania, E.J.C., Morofsky, E., Foo, S., 2011. A screening methodology for implementing cost effective energy retrofit measures in Canadian office buildings. *Energy and Buildings*, 43, 614–620.
- Chongqing Cost, 2018. Chongqing engineering cost information (in Chinese). Chongqing, China.
- Chongqing Minicipal Bureau of Statistics, 2017. Chongqing Minicipal Bureau of Statistics & NBS Survey Office in Chongqing, Chongqing Statistical Yearbook (in Chinese).
- CIBSE, 2015. CIBSE Guide A: Environmental design. The Chartered Institution of Building Services Engineers, London, UK.
- CIBSE, 2002. CIBSE Guide J.
- Coakley, D., 2014. Calibration of Detailed Building Energy Simulation Models to Measured Data using Uncertainty Analysis.
- Coakley, D., Raftery, P., Keane, M., 2014. A review of methods to match building energy simulation models to measured data. *Renewable and Sustainable Energy Reviews*, 37, 123–141.
- Cook, M., Short, A., 2009. A Handbook of Sustainable Building Design and Engineering: An Integrated Approach to Energy, Health and Operational Performance. Earthscan, UK.
- Corrado, V., Mechri, H.E., 2009. Uncertainty and Sensitivity Analysis for Building Energy Rating. *Journal of Building Physics*, 33, 125–156.
- Crawley, D.B., Hand, J.W., Kummert, M., Griffith, B.T., 2006. Contrasting the capabilities of building energy performance simulation programs. *Building and Environment*, 43, 661–673.
- Crawley, D.B., Hand, J.W., Kummert, M., Griffith, B.T., 2005. Contrasting the Capabilities of Building Energy Performance Simulation Programs. *Ninth International IBPSA Conference*, 43, 231–238.
- Crawley, D.B., Lawrie, L.K., Winkelmann, F.C., Buhl, W.F., Huang, Y.J., Pedersen, C.O., Strand, R.K., Liesen, R.J., Fisher, D.E., Witte, M.J., Glazer, J., 2001. EnergyPlus: Creating a new-generation building energy simulation program. *Energy and Buildings*, 33, 319–331.
- Creswell, J.W., 2009. Research Design: Qualitative, Quantitative and Mixed

Approaches (3rd Edition), Research Design: Qualitative, Quantitative, and Mixed Methods Approaches.

- Curtis, R.B., Birdsall, B., Buhl, W.F., Erdem, E., Eto, J., Hirsch, J.J., Olson, K.H., Winkelmann, F.C., 1984. The DOE-2 Building Energy Analysis Program. *ASEAN Conference on Energy Conservation in Buildings*,
- Dall'o', G., Galante, A., Torri, M., 2012. A methodology for the energy performance classification of residential building stock on an urban scale. *Energy and Buildings*, 48, 211–219.
- Dascalaki, E.G., Droutsa, K.G., Balaras, C.A., Kontoyiannidis, S., 2011. Building typologies as a tool for assessing the energy performance of residential buildings - A case study for the Hellenic building stock. *Energy and Buildings*, 43, 3400–3409.
- DesignBuilder, 2019. DesignBuilder manual v6.1.2.009. Stroud, UK.
- Du, C., Liu, H., Yu, W., Jin, Z., 2015. Field study of thermal environments and comfort to residential buildings in the five climate zones of China, in: The 7th International Conference of SuDBE2015. SuDBE, Reading, UK.
- Dudley, B., 2018. BP Statistical Review of World Energy.
- Duffie, J.A., Beckman, W.A., 2013. Solar Engineering of Thermal Processes, John Wiley & Sons, Inc., Hoboken, New Jersey. Solar Energy Laboratory, University of Wisconsin-Madison.
- Duran, O., 2018. Evaluation of retrofitting strategies for post-war office buildings.
- Erbs, D.G., Klein, S.A., Beckman, W.A., 1983. Estimation of Degree-Days and Ambient Temperature Bin Data from Monthly Average Temperatures. *ASHRAE Journal*, 60.
- EU commission, 2019. Energy labelling of air conditioners.
- Everett, B., 2007. Saving energy—how to cut energy wastage. Sustainable Energy, Opportunities and Limitations. Palgrave Macmillan.
- Fellows, R., Liu, A., 2008. Research Methods for Construction, Third. ed. West Sussex, UK, Blackwell Publishing Ltd.
- Feng, X., Yan, D., Wang, C., Sun, H., 2016. A preliminary research on the derivation of typical occupant behavior based on large-scale questionnaire surveys. *Energy and Buildings*, 117, 332–340.
- Firth, S.K., Lomas, K.J., Wright, A.J., 2010. Targeting household energy-efficiency measures using sensitivity analysis. *Building Research and Information*, 38, 24–41.
- Fu, X., Qian, X., Wang, L., 2017. Energy efficiency for airtightness and exteriorwall insulation of passive houses in hot summer and cold winter zone of China. *Sustainability (Switzerland)*, 9.

- Gao, Y., Xu, J., Yang, S., Tang, X., Zhou, Q., Ge, J., Xu, T., Levinson, R., 2014. Cool roofs in China: Policy review, building simulations, and proof-of-concept experiments. *Energy Policy*, 74, 190–214.
- Ge, J., Wu, Jiajing, Chen, S., Wu, Jindong, 2018. Energy efficiency optimization strategies for university research buildings with hot summer and cold winter climate of China based on the adaptive thermal comfort. *Journal of Building Engineering*, 18, 321–330.
- Georgiou, G., Eftekhari, M., Eames, P., 2013. Calibration and validation of residential buildings: 8 case studies of detached houses. *IBPSA*,.
- Gerrish, T., Ruikar, K., Cook, M., Johnson, M., Phillip, M., 2017. Using BIM capabilities to improve existing building energy modelling practices. *Engineering, Construction and Architectural Management*, 24, 190–208.
- Gong, X., Akashi, Y., Sumiyoshi, D., 2012. Optimization of passive design measures for residential buildings in different Chinese areas. *Building and Environment*, 58, 46–57.
- Gou, S., Li, Z., Zhao, Q., Nik, V.M., Scartezzini, J.L., 2015. Climate responsive strategies of traditional dwellings located in an ancient village in hot summer and cold winter region of China. *Building and Environment*, 86, 151–165.
- Gou, S., Nik, V.M., Scartezzini, J.L., Zhao, Q., Li, Z., 2018. Passive design optimization of newly-built residential buildings in Shanghai for improving indoor thermal comfort while reducing building energy demand. *Energy and Buildings*, 169, 484–506.
- Gu, Z.H., Sun, Q., Wennersten, R., 2013. Impact of urban residences on energy consumption and carbon emissions: An investigation in Nanjing, China. *Sustainable Cities and Society*, 7, 52–61.
- Gui, X., Ma, Y., Chen, S., Ge, J., 2018. The methodology of standard building selection for residential buildings in hot summer and cold winter zone of China based on architectural typology. *Journal of Building Engineering*, 18, 352–359.
- Guo, S., Yan, D., Cui, Y., Zhou, X., Peng, C., Zhu, A., 2014. Case studies and key questions of space heating in residential buildings in Yangtze River Basin.
- Guo, S., Yan, D., Peng, C., Cui, Y., Zhou, X., Hu, S., 2015. Investigation and analyses of residential heating in the HSCW climate zone of China: Status quo and key features. *Building and Environment*, 94, 532–542.
- Harper, B.A., Kepert, J.D., Ginger, J.D., 2008. Guidelines for converting between various wind averaging periods in tropical cyclone conditions, World Meteorological Organisation.
- Heiple, S., Sailor, D.J., 2008. Using building energy simulation and geospatial modeling techniques to determine high resolution building sector energy consumption profiles. *Energy and Buildings*, 40, 1426–1436.

- Hestnes, A.G., Kofoed, N.U., 2002. Effective retrofitting scenarios for energy efficiency and comfort: results of the design and evaluation activities within the OFFICE project. *Building and Environment*, 37, 569–574.
- HM Government, 2019a. Postcode level electricity statistics: 2017. UK.
- HM Government, 2019b. Updated energy and emissions projections 2018. UK.
- HM Government, 2017. English housing survey. UK.
- HM Government, 1965. Building and Buildings: The Building Regulations 1965, Building Regulations 1965. Her Majesty's Stationery Office, London, UK.
- Hogan, J., Watson, R., Huang, J., Siwei, L., Xiangzhao, F., Haiyin, L., 2001. China's energy efficiency design Standard for residential buildings in the "Hot-Summer/Cold-Winter" zone, in: Proc. 4th International Conference on Indoor Air Quality, Ventilation and Energy Conservation in Buildings. Changsha, Hunan, China, pp. 573–577.
- Hu, S., Yan, D., Cui, Y., Guo, S., 2016. Urban residential heating in hot summer and cold winter zones of China-Status, modeling, and scenarios to 2030. *Energy Policy*, 92, 158–170.
- Hu, S., Yan, D., Guo, S., Cui, Y., Dong, B., 2017. A survey on energy consumption and energy usage behavior of households and residential building in urban China. *Energy and Buildings*, 148, 366–378.
- Hu, T., Yoshino, H., Jiang, Z., 2013. Analysis on urban residential energy consumption of Hot Summer & Cold Winter Zone in China, *Sustainable Cities and Society*.
- Ichinose, T., Lei, L., Lin, Y., 2017. Impacts of shading effect from nearby buildings on heating and cooling energy consumption in hot summer and cold winter zone of China. *Energy and Buildings*, 136, 199–210.
- IEA, 2015a. Building Energy Use in China. Transforming Construction and Influencing Consumption to 2050. France.
- IEA, 2015b. Energy Technology Perspectives 2015: Mobilising Innovation to Accelerate Climate Action.
- International Energy Agency, 2015. CO2 emissions from fuel combustion, IEA Statistics.
- Jack, R., 2015. Building diagnostics : Practical Measurement of the Fabric Thermal Performance of Houses.
- Jacovides, C.P., Tymvios, F.S., Assimakopoulos, V.D., Kaltsounides, N.A., 2006. Comparative study of various correlations in estimating hourly diffuse fraction of global solar radiation. *Renewable Energy*, 31, 2492–2504.
- Jeong, B., Jeong, J.W., Park, J.S., 2016. Occupant behavior regarding the manual control of windows in residential buildings. *Energy and Buildings*,

127, 206–216.

- Ji, Y., Duanmu, L., 2017. Airtightness field tests of residential buildings in Dalian, China. *Building and Environment*, 119, 20–30.
- Jin, Z., Yezheng, W., Gang, Y., 2004. Estimation of daily diffuse solar radiation in China. *Renewable Energy*, 29, 1537–1548.
- Jing, S., Li, B., Tan, M., Liu, H., 2012. Impact of Relative Humidity on Thermal Comfort in Warm Environment. *Indoor and Built Environment*, 1–10.
- Jokisalo, J., Kurnitski, J., 2007. Performance of EN ISO 13790 utilisation factor heat demand calculation method in a cold climate. *Energy and Buildings*, 39, 236–247.
- Kang, K.-N., Song, D., Schiavon, S., 2013. Correlations in thermal comfort and natural wind. *Journal of Thermal Biology*, 38, 419–426.
- Karl, T.R., 2019. United States National Climatic Data Center [WWW Document]. URL <https://www.ncdc.noaa.gov/cdo-web/>
- Kim, G., Lim, H.S., Lim, T.S., Schaefer, L., Kim, J.T., 2012. Comparative advantage of an exterior shading device in thermal performance for residential buildings. *Energy and Buildings*, 46, 105–111.
- Kirimtat, A., Koyunbaba, B.K., Chatzikonstantinou, I., Sariyildiz, S., 2016. Review of simulation modeling for shading devices in buildings. *Renewable and Sustainable Energy Reviews*, 53, 23–49.
- Kokogiannakis, G., Strachan, P., Clarke, J., 2008. Comparison of the simplified methods of the ISO 13790 standard and detailed modelling programs in a regulatory context. *Journal of Building Performance Simulation*, 1, 209–219.
- Kolbe, T.H., 2009. Representing and Exchanging 3D City Models with CityGML 15–31.
- Kolokotsa, D., Diakaki, C., Grigoroudis, E., Stavrakakis, G., Kalaitzakis, K., 2009. Decision support methodologies on the energy efficiency and energy management in buildings. *Advances in Building Energy Research*, 3, 121–146.
- Köppen climate classification, 2016. China map of Köppen climate classification [WWW Document]. https://en.wikipedia.org/wiki/Geography_of_China#/media/File:China_map_of_K%C3%B6ppen_climate_classification.svg.
- Krey, V., Masera, O., Blanford, G., Bruckner, T., Cooke, R., Fisher-Vanden, K., Haberl, H., Hertwich, E., Kriegler, E., Mueller, D., Paltsev, S., Price, L., Schlömer, S., Ürge-Vorsatz, D., Vuuren, D. van, Zwicke, T., 2014. Annex II: Metrics & Methodology. In: *Climate Change 2014: Mitigation of Climate Change. Contribution of Working Group III to the Fifth Assessment Report of the Intergovernmental Panel on Climate Change*, 1281–1328.

- Lam, J.C., Hui, S.C.M., 1996. Sensitivity analysis of energy performance of office buildings. *Building and Environment*, 31, 27–39.
- Lang, S., 2004. Progress in energy-efficiency standards for residential buildings in China. *Energy and Buildings*, 36, 1191–1196.
- Lawrence Berkeley National Laboratory, 2016. Key China Energy Statistics 2016.
- Lee, W.L., Chen, H., 2008. Benchmarking Hong Kong and China energy codes for residential buildings. *Energy and Buildings*, 40, 1628–1636.
- Lengsfeld, K., Holm, A., 2007. Entwicklung und Validierung einer hygrothermischen Raumklima-Simulationssoftware WUFI®-Plus. *Bauphysik*, 29, 178–186.
- Li, B., Du, C., Yao, R., Yu, W., Costanzo, V., 2018. Indoor thermal environments in Chinese residential buildings responding to the diversity of climates. *Applied Thermal Engineering*, 129, 693–708.
- Li, B., Yao, R., Wang, Q., Pan, Y., 2014. An introduction to the Chinese Evaluation Standard for the indoor thermal environment. *Energy and Buildings*, 82, 27–36.
- Li, B., Yu, W., Meng, L., Nan, L., 2011. Climatic Strategies of Indoor Thermal Environment for Residential Buildings in Yangtze River Region, China. *Indoor and Built Environment*, 20, 101–111.
- Li, X., Yao, R., Liu, M., Costanzo, V., Yu, W., Wang, W., Short, A., Li, B., 2018. Developing urban residential reference buildings using clustering analysis of satellite images. *Energy and Buildings*, 169, 417–429.
- Li, X., Yao, R., Yu, W., Meng, X., Liu, M., Short, A., Li, B., 2019. Low carbon heating and cooling of residential buildings in cities in the hot summer and cold winter zone - A bottom-up engineering stock modeling approach. *Journal of Cleaner Production*, 220, 271–288.
- Li, Z., 2007. Study on the life cycle consumption of energy and resource of air conditioning in urban residential buildings in China. Beijing: Tsinghua University.
- Lin, B., Wang, Z., Liu, Y., Zhu, Y., Ouyang, Q., 2016. Investigation of winter indoor thermal environment and heating demand of urban residential buildings in China's hot summer - Cold winter climate region. *Building and Environment*, 101, 9–18.
- Ling, J., Li, Q., Xing, J., 2015. The influence of apartment location on household space heating consumption in multi-apartment buildings. *Energy and Buildings*, 103, 185–197.
- Liu, H., Wu, Y., Li, B., Cheng, Y., Yao, R., 2017. Seasonal variation of thermal sensations in residential buildings in the Hot Summer and Cold Winter zone of China. *Energy and Buildings*, 140, 9–18.

- Liu, J., Dai, X., Li, X., Jia, S., Pei, J., Sun, Y., Lai, D., Shen, X., Sun, H., Yin, H., Huang, K., Tan, H., Gao, Y., Jian, Y., 2018. Indoor air quality and occupants' ventilation habits in China: Seasonal measurement and long-term monitoring. *Building and Environment*, 142, 119–129.
- Liu, X., Chen, Y., Ge, H., Fazio, P., Chen, G., Guo, X., 2015. Determination of optimum insulation thickness for building walls with moisture transfer in hot summer and cold winter zone of China. *Energy and Buildings*, 109, 361–368.
- Liu, Y., Liu, T., Ye, S., Liu, Yisheng, 2018. Cost-benefit analysis for Energy Efficiency Retrofit of existing buildings: A case study in China. *Journal of Cleaner Production*, 177, 493–506.
- Lomas, K.J., Eppel, H., 1992. Sensitivity analysis techniques for building thermal simulation programs. *Energy and Buildings*, 19, 21–44.
- Ma, N., Li, Q., Meng, Q., Cao, A., Wang, J., 2015. Discussion of the Adaption of between Blinds Glass for Residential Buildings in Different Climate Regions of China Based on Energy Consumption Analysis. *Procedia Engineering*, 121, 1150–1157.
- Marini, D., Webb, L.H., Diamantis, G., Buswell, R. a, 2014. Exploring the Impact of Model Calibration on Estimating Energy Savings Through Better Space Heating Control.
- McNeil, M.A., Feng, W., de la Rue du Can, S., Khanna, N.Z., Ke, J., Zhou, N., 2016. Energy efficiency outlook in China's urban buildings sector through 2030. *Energy Policy*, 97, 532–539.
- Meng, X., YU, W., Zheng, C., Wang, D., Cao, X., 2019. Path Analysis of Energy-Saving Technology in Yangtze River Basin Based on Multi-Objective and Multi-Parameter Optimisation 28.
- MOHURD, 2017. Building Energy Conservation and Green Building Development “the 13th Five-Year Plan.”
- MOHURD, 2013a. Green Building Action Plan.
- MOHURD, 2013b. GB 50034-2013: Standard for lighting design of buildings (in Chinese). Beijing, China.
- MOHURD, 2013c. The minimum allowable values of the energy efficiency and energy efficiency grades for heat pump water heaters. Beijing, China.
- MOHURD, 2012a. Retrofit guidelines for existing residential buildings in Hot Summer and Cold Winter (HSCW) zone (in Chinese). Beijing, China.
- MOHURD, 2012b. GB 50736-2012: Design Code for Heating, Ventilation and Air Conditioning of Civil Buildings (in Chinese). Beijing, China.
- MOHURD, 2010a. JGJ 134-2010: Design standard for energy efficiency of residential buildings in Hot Summer and Cold Winter zone (in Chinese). Beijing, China.

- MOHURD, 2010b. Design standard for energy efficiency 65% of residential building (in Chinese), DBJ 50-071-2010 (in Chinese).
- MOHURD, 2010c. GB 12021.2-2010 :The minimum allowable values of the energy efficiency and energy efficiency grades for room air conditioners (in Chinese). Beijing, China.
- MOHURD, 2005. GB 50352-2005: Code for Design of Civil Buildings (in Chinese). Beijing, China.
- MOHURD, 2001. Design standard for energy efficiency of residential buildings in Hot Summer and Cold Winter zone (in Chinese), JGJ 134-2001 (in Chinese).
- MOHURD, 1995. JGJ 26-1995: Design standard for energy efficiency of residential buildings (in Chinese). Beijing, China.
- MOHURD, 1993. Thermal Design Code for Civil Building (in Chinese), GB 50176-93 (in Chinese).
- Monien, D., Strzalka, A., Koukofikis, A., Coors, V., Eicker, U., 2017. Comparison of building modelling assumptions and methods for urban scale heat demand forecasting. *Future Cities and Environment*, 3, 2.
- MOUHRD, 2016. National standard for Energy Consumption of Buildings. Beijing, China.
- MOUHRD, 2012. Evaluation standard for indoor thermal environment in civil buildings. Beijing, China.
- MOUHRD, 2009. Standard for energy efficiency test of residential buildings. Beijing, China.
- Muneer, T., Gueymard, C., Kambezidis, H., 2012. Solar radiation and daylight models. Taylor & Francis.
- Municipal Bureau of Statistics of Chongqing, 2019. Chongqing Statistical Yearbook 2019. China Statistics Press.
- Mustafaraj, G., Marini, D., Costa, A., Keane, M., 2014. Model calibration for building energy efficiency simulation. *Applied Energy*, 130, 72–85.
- Nageler, P., Zahrer, G., Heimrath, R., Mach, T., Mauthner, F., Leusbrock, I., Schranzhofer, H., Hoehenauer, C., 2017. Novel validated method for GIS based automated dynamic urban building energy simulations. *Energy*, 139, 142–154.
- NBS, 2018. China Statistical Yearbook 2018. Beijing, China.
- NBS, 2017. China Statistical Yearbook 2017 (in Chinese). Beijing, China.
- NBS, 2010. National Bureau of Statistics of People's Republic of China on Major Figures of the 2010 Population Census (in Chinese). Beijing, China.
- NDRC, 2016. Energy Supply and Consumption Revolution Strategy (2016-

- 2030). Beijing, China.
- Nguyen, A.T., Reiter, S., 2012. An investigation on thermal performance of a low cost apartment in hot humid climate of Danang. *Energy and Buildings*, 47, 237–246.
- Nicol, J.F., Humphreys, M.A., 2002. Adaptive thermal comfort and sustainable thermal standards for buildings. *Energy and Buildings*, 34, 563–572.
- Ormandy, D., Ezratty, V., 2012. Health and thermal comfort: From WHO guidance to housing strategies. *Energy Policy*, 49, 116–121.
- Ouyang, J., Ge, J., Hokao, K., 2009. Economic analysis of energy-saving renovation measures for urban existing residential buildings in China based on thermal simulation and site investigation. *Energy Policy*, 37, 140–149.
- Ouyang, J., Wang, C., Li, H., Hokao, K., 2011. A methodology for energy-efficient renovation of existing residential buildings in China and case study. *Energy and Buildings*, 43, 2203–2210.
- Ozaki, A., Tsujimaru, T., 2005. Prediction of Hygrothermal Environment of Buildings Based Upon Combined Simulation of Heat and Moisture Transfer and Airflow. *9th International IBPSA Conference*, 899–906.
- Pan, L., Xu, Q., Nie, Y., Qiu, T., 2018. Analysis of climate adaptive energy-saving technology approaches to residential building envelope in Shanghai. *Journal of Building Engineering*, 19, 266–272.
- Peng, C., Yan, D., Wu, R., Wang, C., Zhou, X., Jiang, Y., 2012. Quantitative description and simulation of human behavior in residential buildings. *Building Simulation*, 5, 85–94.
- Porritt, S.M., Cropper, P.C., Shao, L., Goodier, C.I., 2012. Ranking of interventions to reduce dwelling overheating during heat waves. *Energy and Buildings*, 55, 16–27.
- Pulido-Arcas, J.A., Perez-Fargallo, A., Rubio-Bellido, C., 2016. Multivariable regression analysis to assess energy consumption and CO2 emissions in the early stages of offices design in Chile. *Energy and Buildings*, 133, 738–753.
- Purdy, J., Beausoleil-Morrison, I., 2001. The significant factors in modelling residential buildings. *Proceedings of the 7th International Conference of the International Building Performance Simulation Association*, 207–214.
- Reinhart, C.F., Cerezo Davila, C., 2016. Urban building energy modeling - A review of a nascent field. *Building and Environment*, 97, 196–202.
- Sarafis, P., Sotiriadou, K., Dallas, D., Stavrakakis, P., Chalaris, M., 2010. Sick-building syndrome. *Journal of Environmental Protection and Ecology*, 11, 515–522.
- Sherman, M.H., Grimsrud, D.T., 1980. The Measurement of Infiltration using

- Fan Pressurization and Weather Data. *Proceedings, First Air Infiltration Centre Conference, Windsor, England, October 6-8, 1980*.
- Shimoda, Y., Fujii, T., Morikawa, T., Mizuno, M., 2004. Residential end-use energy simulation at city scale. *Building and Environment*, 39, 959–967.
- Short, C.A., Song, J., Mottet, L., Chen, S., Wu, J., Ge, J., 2018. Challenges in the low-carbon adaptation of China's apartment towers. *Building Research & Information*, 46, 1–32.
- Short, C.A., Song, J., Mottet, L., Chen, S., Wu, J., Yu, W., Xiong, J., Zhang, Q., Ge, J., Yao, R., Li, B., 2019. The Hot Summer-Cold Winter region in China: challenges in the low carbon adaptation of residential slab buildings to enhance comfort (unpublished).
- Silva, A.S., Almeida, L.S.S., Ghisi, E., 2016. Decision-making process for improving thermal and energy performance of residential buildings: A case study of constructive systems in Brazil. *Energy and Buildings*, 128, 270–286.
- Sokol, J., Cerezo Davila, C., Reinhart, C.F., 2017. Validation of a Bayesian-based method for defining residential archetypes in urban building energy models. *Energy and Buildings*, 134, 11–24.
- SolarGIS, 2015. Global Solar Radiation in China [WWW Document]. <http://solargis.com/assets/graphic/free-map/GHI/Solargis-China-GHI-solar-resource-map-en.png>.
- State Council, 2012. 12th Five-Year Plan for Energy Saving and Emission Reduction in China (in Chinese). Beijing, China.
- Su, X., Zhang, X., 2010. Environmental performance optimization of window-wall ratio for different window type in hot summer and cold winter zone in China based on life cycle assessment. *Energy and Buildings*, 42, 198–202.
- Swan, L.G., Ugursal, V.I., 2009. Modeling of end-use energy consumption in the residential sector: A review of modeling techniques. *Renewable and Sustainable Energy Reviews*, 13, 1819–1835.
- Tardioli, G., Kerrigan, R., Oates, M., O'Donnell, J., Finn, D., 2015. Data driven approaches for prediction of building energy consumption at urban level. *Energy Procedia*, 78, 3378–3383.
- Taylor, S., 2016. Monthly quasi-steady-state excel spreadsheet model.
- Taylor, S., Allinson, D., Firth, S., Lomas, K., 2013. Dynamic Energy Modelling of UK Housing: Evaluation of Alternative Approaches. *13th Conference of International Building Performance Simulation Association*, 745–752.
- Thorsen, S., 2019. Time and Date [WWW Document]. URL <https://www.timeanddate.com/>
- THUBERC, 2018. 2018 Annual Report on China Building Energy Efficiency (in

- Chinese).
- THUBERC, 2017. 2017 Annual Report on China Building Energy Efficiency (in Chinese).
- THUBERC, 2013. 2013 Annual Report on China Building Energy Efficiency (in Chinese).
- Turner, C., Frankel, M., 2008. Energy Performance of LEED ® for New Construction Buildings. *New Buildings Institute*, 1–46.
- Wang, B.-L., Takigawa, T., Yamasaki, Y., Sakano, N., Wang, D.-H., Ogino, K., 2008. Symptom definitions for SBS (sick building syndrome) in residential dwellings. *International Journal of Hygiene and Environmental Health*, 211, 114–120.
- Wang, Xi, Altan, H., Kang, J., 2015. Parametric study on the performance of green residential buildings in China. *Frontiers of Architectural Research*, 4, 56–67.
- Wang, Xiaotong, Lu, M., Mao, W., Ouyang, J., Zhou, B., Yang, Y., 2015. Improving benefit-cost analysis to overcome financing difficulties in promoting energy-efficient renovation of existing residential buildings in China. *Applied Energy*, 141, 119–130.
- Wang, Zhe, de Dear, R., Lin, B., Zhu, Y., Ouyang, Q., 2015a. Rational selection of heating temperature set points for China's hotsummer - Cold winter climatic region. *Building and Environment*, 93, 63–70.
- Wang, Zhe, Zhao, Z., Lin, B., Zhu, Y., Ouyang, Q., 2015b. Residential heating energy consumption modeling through a bottom-up approach for China's Hot Summer-Cold Winter climatic region. *Energy and Buildings*, 109, 65–74.
- Wu, J., Liu, C., Li, H., Ouyang, D., Cheng, J., Wang, Y., You, S., 2017. Residential air-conditioner usage in China and efficiency standardization. *Energy*, 119, 1036–1046.
- Xiong, J., Costanzo, V., Yao, R., Li, B., 2018. Assessing the natural ventilation cooling potential of residential buildings in the hot summer and cold winter zone of China.
- Xiong, J., Yao, R., Grimmond, S., Zhang, Q., Li, B., 2019. A hierarchical climatic zoning method for energy efficient building design applied in the region with diverse climate characteristics. *Energy and Buildings*, 186, 355–367.
- Xu, L., Liu, J., Pei, J., Han, X., 2013. Building energy saving potential in Hot Summer and Cold Winter (HSCW) Zone , China — Influence of building energy efficiency standards and implications. *Energy Policy*, 57, 253–262.
- Xu, P., Xu, T., Shen, P., 2013. Energy and behavioral impacts of integrative retrofits for residential buildings: What is at stake for building energy policy reforms in northern China? *Energy Policy*, 52, 667–676.

- Yan, D., Xia, J., Tang, W., Song, F., Zhang, X., Jiang, Y., 2008. DeST — An integrated building simulation toolkit Part I: Fundamentals. *Building Simulation*, 1, 95–110.
- Yang, Q., Liu, M., Shu, C., Mmereki, D., Hossain, U., Zhan, X., 2015. Impact Analysis of Window-Wall Ratio on Heating and Cooling Energy Consumption of Residential Buildings in Hot Summer and Cold Winter Zone in China 2015.
- Yao, J., 2014. An investigation into the impact of movable solar shades on energy, indoor thermal and visual comfort improvements. *Building and Environment*, 71, 24–32.
- Yao, J., 2012. Energy optimization of building design for different housing units in apartment buildings. *Applied Energy*, 94, 330–337.
- Yao, J., Xu, J., 2010. Effects of Different Shading Devices on Building Energy Saving in Hot Summer and Cold Winter Zone 5–8.
- Yao, R., 2017. Private communication, r.yao@reading.ac.uk, 29th May 2017.
- Yao, R., Costanzo, V., Li, X., Zhang, Q., Li, B., 2018. The effect of passive measures on thermal comfort and energy conservation. A case study of the hot summer and cold winter climate in the Yangtze River region. *Journal of Building Engineering*, 15, 298–310.
- Yao, R., Li, B., Liu, J., 2009. A theoretical adaptive model of thermal comfort – Adaptive Predicted Mean Vote (aPMV). *Building and Environment*, 44, 2089–2096.
- Ye, X.J., Zhou, Z.P., Lian, Z.W., Liu, H.M., Li, C.Z., Liu, Y.M., 2006. Field study of a thermal environment and adaptive model in Shanghai. *Indoor Air*, 16, 320–326.
- Yoon, J., Lee, E.J., Claridge, D.E., 2003. Calibration Procedure for Energy Performance Simulation of a Commercial Building. *Journal of Solar Energy Engineering*, 125, 251.
- Yoshino, H., Guan, S., Lun, Y.F., Mochida, A., Shigeno, T., Yoshino, Y., Zhang, Q.Y., 2004. Indoor thermal environment of urban residential buildings in China: Winter investigation in five major cities. *Energy and Buildings*, 36, 1227–1233.
- Yoshino, H., Yoshino, Y., Zhang, Q., Mochida, A., Li, N., Li, Z., Miyasaka, H., 2006. Indoor thermal environment and energy saving for urban residential buildings in China. *Energy and Buildings*, 38, 1308–1319.
- Yu, H., Tang, B.J., Yuan, X.C., Wang, S., Wei, Y.M., 2015. How do the appliance energy standards work in China? Evidence from room air conditioners. *Energy and Buildings*, 86, 833–840.
- Yu, J., Tian, L., Yang, C., Xu, X., Wang, J., 2013. Sensitivity analysis of energy performance for high-rise residential envelope in hot summer and cold winter zone of China. *Energy and Buildings*, 64, 264–274.

- Yu, J., Tian, L., Yang, C., Xu, X., Wang, J., 2011. Optimum insulation thickness of residential roof with respect to solar-air degree-hours in hot summer and cold winter zone of china. *Energy and Buildings*, 43, 2304–2313.
- Yu, J., Yang, C., Tian, L., 2008. Low-energy envelope design of residential building in hot summer and cold winter zone in China. *Energy and Buildings*, 40, 1536–1546.
- Yu, J., Yang, C., Tian, L., Liao, D., 2009a. Evaluation on energy and thermal performance for residential envelopes in hot summer and cold winter zone of China. *Applied Energy*, 86, 1970–1985.
- Yu, J., Yang, C., Tian, L., Liao, D., 2009b. A study on optimum insulation thicknesses of external walls in hot summer and cold winter zone of China. *Applied Energy*, 86, 2520–2529.
- Yu, W., Li, B., Jia, H., Zhang, M., Wang, D., 2015. Application of multi-objective genetic algorithm to optimize energy efficiency and thermal comfort in building design. *Energy and Buildings*, 88, 135–143.
- Zhang, S., Yang, X., Jiang, Y., Wei, Q., 2010. Comparative analysis of energy use in China building sector: Current status, existing problems and solutions. *Frontiers of Energy and Power Engineering in China*, 4, 2–21.
- Zhang, Y., 2015. Design criteria of built thermal environment for Hot Summer & Warm Winter zone of China. *Building and Environment*, 88, 97–105.
- Zhang, Y., Chen, H., Meng, Q., 2013. Thermal comfort in buildings with split air-conditioners in hot-humid area of China. *Building and Environment*, 64, 213–224.
- Zhang, Y., Chen, H., Wang, J., Meng, Q., 2015. Thermal comfort of people in the hot and humid area of China-impacts of season, climate, and thermal history. *Indoor Air*, 820–830.
- Zhao, M., Kunzel, H.M., Antretter, F., 2015. Parameters influencing the energy performance of residential buildings in different Chinese climate zones. *Energy and Buildings*, 96, 64–75.

APPENDICES

Appendix A: Steady-state model

The following equations discuss the parameters required to calculate the heating and cooling energy demand. In order to calculate the heating energy demand and cooling energy demand in the steady-state model (Equation A-1, A-2), the heat transfer and heat gain are calculated (Equation A-3 to A-5)

$$Q_{H,nd} = Q_{H,ht} - \eta_{H,gn} Q_{gn} \quad (A-1)$$

$$Q_{C,nd} = Q_{gn} - \eta_{C,ls} Q_{C,ht} \quad (A-2)$$

$$Q_{H,ht} = Q_{H,tr} + Q_{H,ve} \quad (A-3)$$

$$Q_{C,ht} = Q_{C,tr} + Q_{C,ve} \quad (A-4)$$

$$Q_{gn} = Q_{int} + Q_{sol} \quad (A-5)$$

where $Q_{H,nd}$ is the energy need for space heating, $Q_{H,ht}$ is the total heat transfer for heating mode, $\eta_{H,gn}$ is the dimensionless gain utilisation factor, Q_{gn} is the total heat gain, $Q_{C,nd}$ is the energy need for space cooling, $\eta_{C,ls}$ is the dimensionless loss utilisation factor, $Q_{C,ht}$ is the total heat transfer for the cooling mode, $Q_{H,tr}$ is the total heat transfer by transmission for heating mode, $Q_{H,ve}$ is the total heat transfer by ventilation in heating mode, $Q_{C,tr}$ is the total heat transfer by transmission for cooling mode, $Q_{C,ve}$ is the total heat transfer by ventilation in cooling mode, Q_{int} is the sum of internal heat gains over the given period, Q_{sol} is the sum of solar heat gains over the given period.

The following equations discuss the parameters required to calculate the heat transfer by transmission and ventilation for heating and cooling mode (Equation A-6 to A-11).

$$Q_{H,tr} = H_{tr,adj} (\theta_{int,set,H} - \theta_e) t \quad (A-6)$$

$$Q_{C,tr} = H_{tr,adj} (\theta_{int,set,C} - \theta_e) t \quad (A-7)$$

$$Q_{H,ve} = H_{ve,adj} (\theta_{int,set,H} - \theta_e) t \quad (A-8)$$

$$Q_{C,ve} = H_{ve,adj} (\theta_{int,set,C} - \theta_e) t \quad (A-9)$$

$$H_{tr,adj} = \sum_i A_i U_i \quad (A-10)$$

$$H_{ve,adj} = \rho_a c_a (q_{ve} f_{ve,t}) \quad (A-11)$$

where $H_{tr,adj}$ is the overall heat transfer coefficient by transmission (W/K), $\theta_{int,set,H}$ is the set-point temperature for heating (°C), θ_e is the temperature of

the external environment ($^{\circ}\text{C}$), t is the duration of the calculation step (ms), $H_{ve,adj}$ is the overall heat transfer coefficient by ventilation (W/K), $\theta_{int,set,C}$ is the set-point temperature for cooling ($^{\circ}\text{C}$), A_i is the area of element i of the building envelope (m^2), U_i is the thermal transmittance of element i of the building envelope ($\text{W}/\text{m}^2\text{K}$), $\rho_a c_a$ is the heat capacity of air per volume ($\text{J}/\text{m}^3\text{K}$), q_{ve} is the airflow rate of the building (m^3/s), $f_{ve,t}$ is the time fraction of operation of the building, calculated as the fraction of the number of hours per day (-).

The following equations discuss the parameters required to calculate heat gain. For internal heat gain, the heat gain from occupants, appliances and lighting are calculated (Equation A-12). For solar heat gain, the heat gain through window and opaque element are calculated (Equation A-13), detailed equations are included to calculate heat gain through window and opaque, the effective collecting area is calculated to account for solar shading by external or internal obstacles (Equation A-14, A-15).

$$Q_{int} = \Phi_{int,oc} + \Phi_{int,A} + \Phi_{int,L} \quad (\text{A-12})$$

$$Q_{sol} = \sum A_{sol,k} I_{sol,k} \quad (\text{A-13})$$

$$A_{sol,gl} = F_{sh,ob} F_{sh,gl} g_{gl} (1 - F_F) A_{w,p} \quad (\text{A-14})$$

$$A_{sol,op} = F_{sh,gl} g_{op} A_c \quad (\text{A-15})$$

where $\Phi_{int,oc}$ is the internal heat flow rate from occupants, $\Phi_{int,A}$ is the internal heat flow rate from appliances, $\Phi_{int,L}$ is the internal heat flow rate from lighting, $A_{sol,k}$ is the effective collecting area of surface k with a given orientation and tilt angle for window and opaque building elements, $I_{sol,k}$ is the solar irradiance per square meter of collecting area of surface k , with a given orientation and tilt angle, $F_{sh,ob}$ is the internal shading reduction factor, $F_{sh,gl}$ is the external shading reduction factor, g_{gl} is the g-value for window, F_F is the frame area fraction, $A_{w,p}$ is the overall projected area of the window element, A_c is the projected area of the opaque part, g_{op} is the g-value for opaque building elements.

Dynamic effects are taken into account by calculating the gain utilisation factor (equation A-16) and loss utilisation factor (equation A-17). In order to calculate the gain and loss utilisation factors, heat-balance ratio for the heating (equation

A-18) and cooling (equation A-19) were calculated. Also, numerical parameter depending on time constant for heating (equation A-20) and cooling (equation A-21) were calculated. In order to calculate the numerical parameter, time constant (equation A-22) was calculated, and also the reference numerical parameters for heating ($\alpha_{H,0}$) and cooling ($\alpha_{C,0}$) and reference time constant for heating ($\tau_{H,0}$) and cooling ($\tau_{C,0}$). ISO 13790 proposed a default value with $\alpha_{H,0} = \alpha_{C,0} = 1$ and $\tau_{H,0} = \tau_{C,0} = 15$.

$$\eta_{H,gn} = \begin{cases} \frac{1 - \gamma_H^{a_H}}{1 - \gamma_H^{a_H+1}} & \text{if } \gamma_H > 0 \text{ and } \gamma_H \neq 1 \\ \frac{a_H}{a_H + 1} & \text{if } \gamma_H = 1 \\ 1/\gamma_H & \text{if } \gamma_H < 0 \end{cases} \quad (\text{A-16})$$

$$\eta_{C,ls} = \begin{cases} \frac{1 - \gamma_C^{-a_C}}{1 - \gamma_C^{-(a_C+1)}} & \text{if } \gamma_C > 0 \text{ and } \gamma_C \neq 1 \\ \frac{a_C}{a_C + 1} & \text{if } \gamma_C = 1 \\ 1 & \text{if } \gamma_C < 0 \end{cases} \quad (\text{A-17})$$

$$\gamma_H = \frac{Q_{gn}}{Q_{H,ht}} \quad (\text{A-18})$$

$$\gamma_C = \frac{Q_{gn}}{Q_{C,ht}} \quad (\text{A-19})$$

$$a_H = a_{H,0} + \frac{\tau}{\tau_{H,0}} \quad (\text{A-20})$$

$$a_C = a_{C,0} + \frac{\tau}{\tau_{C,0}} \quad (\text{A-21})$$

$$\tau = \frac{C_m/3600}{H_{tr,adj} + H_{ve,adj}} \quad (\text{A-22})$$

where γ_H is the dimensionless heat-balance ratio for heating mode, a_H is the dimensionless numerical parameter depending on time constant for heating, $a_{H,0}$ is the dimensionless reference numerical parameter for heating, $\tau_{H,0}$ is the reference time constant for heating, γ_C is the dimensionless heat-balance ratio for cooling, a_C is the dimensionless numerical parameter depending on time constant for cooling, $a_{C,0}$ is the dimensionless reference numerical parameter for cooling, $\tau_{C,0}$ is the reference time constant for cooling, τ is the time constant, C_m is the internal heat capacity.

Appendix B: Calculation of vertical solar radiation

The solar time which account how the sun moves across the sky in different location in different time of the year was calculated by equation B-1 to B-3 (Duffie and Beckman, 2013; Jack, 2015).

$$\text{Solar time} = 4(L_{st} + L_{loc}) + E + ST \quad (B-1)$$

$$E = 229.2(0.000075 + 0.001868 \cos B - 0.032077 \sin B - 0.014615 \cos 2B - 0.04089 \sin 2B) \quad (B-2)$$

$$B = (n - 1) 360/365 \quad (B-3)$$

where L_{st} is the standard meridian of the local time zone (time zone in Chongqing is GMT +8:00, $L_{st}=15 \times 9=90^\circ$), L_{loc} is the longitude of the location, E is the equation of time in minutes, ST is the standard time in hours, n is the n^{th} day of the year and B is a constant

The cosine of the zenith angle which is the angle between the vertical and the line of the sun was calculated by the equation B-4 to B-7 (Duffie and Beckman, 2013; Jack, 2015).

$$\cos \theta_z = \cos \phi \cos \delta \cos \omega + \sin \phi \sin \delta \quad (B-4)$$

$$\delta = 23.45 \sin \left(360 \times \frac{284 + n}{365} \right) \quad (B-5)$$

$$\cos \theta = -\sin \delta \cos \phi \cos \gamma + \cos \delta \sin \phi \cos \gamma \cos \omega + \cos \delta \sin \gamma \sin \omega \quad (B-6)$$

$$\omega = 15 \times (\text{Local solar time} - 12) \quad (B-7)$$

where δ is the declination angle, n is the n^{th} day of the year, γ is the surface azimuth angle, ω is the hour angle, θ is the angle of incidence, ϕ is the latitude of the building, θ_z is the zenith angle.

The diffuse fraction k_d and the clearness index k_t was calculated by equation B-8 to B-10 (Duffie and Beckman, 2013; Jack, 2015).

$$I_{o,h} = \left(12 \times \frac{3600}{\pi}\right) G_{sc} \left(1 + 0.033 \cos \frac{360n}{365}\right) \quad (B-8)$$

$$\times \left(\cos \phi \cos \delta (\sin \omega_2 - \sin \omega_1)\right)$$

$$+ \pi \left(\frac{(\omega_2 - \omega_1)}{180}\right) \sin \phi \sin \delta$$

$$k_t = I_h / I_{o,h} \quad (B-9)$$

$$k_d = 0.987 \text{ for } k_T < 0.2 \quad (B-10)$$

$$k_d = 1.292 - 1.447k_t \text{ for } 0.2 \leq k_T < 0.75$$

$$k_d = 0.209 \text{ for } k_t > 0.75$$

where G_{sc} is the global solar constant, ω_1 and ω_2 are the hour angles at the start and end of the hour, I is the measured global solar radiation, $I_{o,h}$ is the extra-terrestrial radiation falling on a horizontal surface, k_t is the clearness index and k_d is the diffuse fraction

The hourly direct solar radiation (I_b) and diffuse solar radiation (I_d) was calculated by equation B-11 to B-13 (Duffie and Beckman, 2013; Jack, 2015)

$$I_{d,h} = k_d \times I_h \quad (B-11)$$

$$I_{b,h} = I_b \times \cos \theta \quad (B-12)$$

$$I_h = I_{b,h} + I_{d,h} \quad (B-13)$$

where $I_{d,h}$ is the diffuse solar radiation on a horizontal surface, $I_{b,h}$ is the direct solar radiation on a horizontal surface, I_b is the direct solar radiation, I_h is the measured global solar radiation on a horizontal surface, θ_z is the zenith angle, k_t is the clearness index and k_d is the diffuse fraction.

Appendix C: City scale geometrical parameters

Appendix C presents the geometrical parameters collected for the 321 residential buildings in the representative area.

Building number	Number of storeys	Aspect ratio	Building surface area to volume ratio	Built area	Built area per floor
B16	13	1.18	0.16	12138.01	933.6931
B18	7	1.27	0.26	3320.66	474.38
B19	7	1.71	0.27	2934.57	419.2243
B20	6	3.54	0.26	3138.21	523.035
B21	14	2.32	0.3	3562.25	254.4464
B26	6	2.06	0.23	3613.44	602.24
B27	6	1.53	0.19	6340.6	1056.767
B28	8	1.94	0.21	5180.27	647.5338
B29	6	1.84	0.18	7583.66	1263.943
B32	12	3.63	0.19	13514.48	1126.207
B34	11	3.14	0.18	22894.04	2081.276
B36	9	2.21	0.24	3619.09	402.1211
B38	8	1.77	0.14	24942.62	3117.828
B39	8	2.11	0.21	14356.61	1794.576
B40	18	1.81	0.12	56287.84	3127.102
B43	10	1.73	0.12	23018.88	2301.888
B44	8	2.48	0.2	9493.03	1186.629
B45	6	1.22	0.23	9249.78	1541.63
B46	9	3.21	0.21	14735.93	1637.326
B47	9	1.21	0.21	10048.41	1116.49
B48	6	1.58	0.25	4731.87	788.645
B49	2	1.29	0.34	1098.06	549.03
B56	27	1.05	0.1	61743.55	2286.798
B60	3	1.59	0.2	8162.36	2720.787
B68	8	2.66	0.19	7539.11	942.3888
B69	8	1.82	0.3	2068.82	258.6025
B70	15	2.53	0.13	31064.26	2070.951
B74	15	1.16	0.13	19021.74	1268.116
B75	13	1.19	0.15	13433.01	1033.308
B76	13	2.3	0.14	31833.42	2448.725
B77	24	1.18	0.14	39875.95	1661.498
B78	24	1.37	0.12	41284.32	1720.18
B79	10	3.57	0.19	17499.29	1749.929
B80	28	1	0.1	51761.88	1848.639
B82	32	1.05	0.11	66718.58	2084.956
B83	33	1.15	0.1	61938.33	1876.919
B92	4	2.83	0.32	1387.73	346.9325
B95	9	1.33	0.19	6467.65	718.6278
B98	8	3.66	0.24	5449.4	681.175
B99	5	3.54	0.28	2504.84	500.968

B100	7	1.29	0.21	4072.18	581.74
B101	6	4.38	0.21	6511.45	1085.242
B102	3	1.19	0.27	1968.72	656.24
B103	5	3.12	0.22	4513.82	902.764
B104	3	1.75	0.32	1209.9	403.3
B107	4	1.1	0.27	1882.49	470.6225
B109	17	1.47	0.14	22659.33	1332.902
B112	9	1.01	0.17	21362.64	2373.627
B113	9	1.26	0.16	15506.64	1722.96
B114	11	1.76	0.23	6823.42	620.3109
B115	9	1.91	0.19	13443.65	1493.739
B116	9	1.46	0.22	6020.1	668.9
B118	10	1.28	0.23	7302.05	730.205
B119	14	2.84	0.18	10297.58	735.5414
B120	14	3.33	0.16	16330.09	1166.435
B123	9	1.46	0.31	3066.55	340.7278
B125	9	3.66	0.28	4732.02	525.78
B126	3	1.51	0.32	1091.59	363.8633
B128	9	1.55	0.21	5820.5	646.7222
B129	8	1.86	0.2	10456.62	1307.078
B130	9	2.39	0.17	19790.65	2198.961
B131	16	1.69	0.19	12536.1	783.5063
B132	2	1.61	0.42	519.89	259.945
B135	15	2.5	0.19	10624.28	708.2853
B136	9	1.41	0.18	9826.34	1091.816
B143	21	1	0.19	11597.68	552.2705
B144	8	2.07	0.15	13428.79	1678.599
B145	16	1.21	0.14	23138.21	1446.138
B146	21	1.26	0.11	40531.38	1930.066
B147	4	1.71	0.34	1065.96	266.49
B149	5	1.44	0.25	2591.44	518.288
B153	9	1.44	0.13	22778.58	2530.953
B156	11	1.59	0.16	26527.08	2411.553
B165	7	1.41	0.23	5935.25	847.8929
B166	9	4.31	0.18	24331.82	2703.536
B168	6	1.09	0.23	4370.43	728.405
B169	24	1.43	0.14	28740.1	1197.504
B171	8	4.38	0.23	13650.1	1706.263
B172	9	2.46	0.26	5360.62	595.6244
B173	12	2.33	0.24	7117.3	593.1083
B174	9	1.65	0.2	7936.1	881.7889
B175	9	1.18	0.24	5815.89	646.21
B176	7	1.47	0.26	5541.07	791.5814
B177	9	1.55	0.25	5041.15	560.1278
B179	26	1.16	0.11	46341.45	1782.363
B180	26	1.1	0.1	68179.68	2622.295
B182	33	1.23	0.13	56104.8	1700.145
B183	31	1.14	0.12	54058.55	1743.824
B185	7	4.8	0.28	8175.36	1167.909
B186	2	3.05	0.42	667.82	333.91

B187	9	4.26	0.13	31016.07	3446.23
B188	7	2.61	0.25	4771.84	681.6914
B189	9	3.04	0.21	10139.38	1126.598
B190	34	1.39	0.12	52325.96	1538.999
B192	18	1.06	0.15	21509.91	1194.995
B193	10	1.43	0.18	8867.3	886.73
B194	9	1.95	0.19	13124.18	1458.242
B195	9	2.14	0.28	6586.17	731.7967
B196	7	2.03	0.29	5215.89	745.1271
B197	9	2.08	0.19	13762.32	1529.147
B198	5	2.92	0.27	2555.4	511.08
B199	8	2.74	0.18	9956.33	1244.541
B202	3	2.31	0.35	1003.37	334.4567
B204	11	1.9	0.15	29039.75	2639.977
B207	3	1.25	0.32	1177.71	392.57
B208	5	1.16	0.21	4405.21	881.042
B223	14	1.19	0.14	20026.24	1430.446
B225	7	3.14	0.21	5896.56	842.3657
B227	2	1.21	0.45	400.09	200.045
B229	9	2.53	0.22	9089.5	1009.944
B236	10	2.11	0.18	14224.33	1422.433
B237	8	3.53	0.22	5640.3	705.0375
B238	4	1.06	0.36	1432.29	358.0725
B249	12	1.56	0.17	25876.23	2156.353
B252	11	1.54	0.2	6318.5	574.4091
B253	10	2.86	0.25	4337.05	433.705
B254	8	1.06	0.27	4194.52	524.315
B255	9	2.64	0.16	15514.85	1723.872
B256	9	3.09	0.19	9827.5	1091.944
B257	8	3.19	0.2	8649.19	1081.149
B258	5	1.53	0.44	595.93	119.186
B259	9	1.71	0.19	6476.91	719.6567
B260	12	2.17	0.27	3982.9	331.9083
B263	8	3.19	0.27	3407.33	425.9163
B264	24	1.09	0.13	32613.95	1358.915
B265	9	1.28	0.25	6622.1	735.7889
B266	7	2.37	0.26	2905.35	415.05
B268	12	1.89	0.2	7120.21	593.3508
B269	13	3.02	0.12	30792.39	2368.645
B271	9	1.21	0.14	21289.27	2365.474
B272	7	1.97	0.27	2489.74	355.6771
B273	10	3.18	0.19	9539.76	953.976
B274	32	2.2	0.1	96964.97	3030.155
B275	14	1	0.13	19251.37	1375.098
B276	15	1.05	0.13	21464.75	1430.983
B277	26	1.4	0.12	45849.53	1763.443
B278	15	1.28	0.15	15090.37	1006.025
B279	15	1.14	0.16	18748.39	1249.893
B280	9	2.65	0.14	16290.95	1810.106
B281	15	1.33	0.16	19731.47	1315.431

B282	12	1.13	0.25	10310.6	859.2167
B287	12	1.13	0.26	3557.26	296.4383
B288	12	1.86	0.25	5443.59	453.6325
B289	12	1.09	0.17	12468.91	1039.076
B291	6	2.3	0.25	3026.19	504.365
B292	7	1.36	0.24	3370.44	481.4914
B293	15	1.11	0.15	13860.44	924.0293
B294	15	1.1	0.15	14896.58	993.1053
B295	15	1.29	0.15	17131.81	1142.121
B296	14	1.07	0.16	11716.75	836.9107
B297	5	1.17	0.2	4272.37	854.474
B298	7	1.21	0.2	4973.8	710.5429
B301	12	2.23	0.13	22333.86	1861.155
B302	4	1.22	0.31	1510.82	377.705
B303	10	1.05	0.25	12895.31	1289.531
B304	10	4.02	0.21	7843.59	784.359
B307	7	2.8	0.27	2910.35	415.7643
B308	7	1.36	0.24	6501.95	928.85
B309	7	1.61	0.34	1418.5	202.6429
B310	7	1.28	0.37	1126.03	160.8614
B312	6	1.79	0.34	1274.62	212.4367
B313	2	2.62	0.38	873.69	436.845
B314	2	1.69	0.35	1447.64	723.82
B316	7	3.63	0.27	4120.39	588.6271
B317	7	2.42	0.27	2632.21	376.03
B318	7	3.1	0.21	6077.14	868.1629
B319	7	3.46	0.22	5294.55	756.3643
B320	7	2.8	0.27	5201.55	743.0786
B321	8	4.28	0.2	9485.66	1185.708
B322	9	1.92	0.22	7634.89	848.3211
B323	3	1.44	0.43	477.88	159.2933
B324	17	1.53	0.23	9188.68	540.5106
B326	8	7.63	0.18	17404.76	2175.595
B331	8	2.19	0.29	2504.03	313.0038
B333	9	1.63	0.28	3298.65	366.5167
B335	4	1.34	0.24	2647.89	661.9725
B336	8	2.89	0.24	4270.23	533.7788
B338	2	1.56	0.4	629.02	314.51
B342	8	1.06	0.18	10028.03	1253.504
B347	10	1.41	0.17	11986.61	1198.661
B352	8	1.6	0.23	5081.66	635.2075
B355	6	2.04	0.23	4594.02	765.67
B356	7	1.19	0.17	8045.97	1149.424
B358	7	1.23	0.22	5453.51	779.0729
B360	7	1.5	0.24	4768.67	681.2386
B362	4	2.11	0.23	6045.85	1511.463
B363	4	1	0.24	3025.16	756.29
B366	4	3.13	0.3	1848.33	462.0825
B367	14	2.03	0.15	27895.2	1992.514
B368	11	1.08	0.24	8498.05	772.55

B370	6	1.64	0.21	5457.45	909.575
B371	9	1.78	0.23	6931.38	770.1533
B372	9	5.43	0.2	12391.82	1376.869
B373	2	1.44	0.4	768.78	384.39
B374	11	1.92	0.16	10060.6	914.6
B375	11	1.05	0.22	6689.8	608.1636
B376	14	1.4	0.18	22464.29	1604.592
B377	13	1.3	0.15	33673.3	2590.254
B378	11	2.33	0.22	6680.03	607.2755
B379	8	1.33	0.18	9468.63	1183.579
B380	9	1.18	0.19	8737.93	970.8811
B381	4	1.47	0.28	1635.41	408.8525
B382	10	1.11	0.15	24968.66	2496.866
B384	9	1.47	0.21	8702.29	966.9211
B386	8	1.25	0.23	4592.58	574.0725
B387	9	2.05	0.19	11010.76	1223.418
B391	8	1.04	0.18	9613.94	1201.743
B392	8	1.98	0.15	17048.69	2131.086
B394	9	1.13	0.15	14774.47	1641.608
B396	9	2.28	0.19	6976.04	775.1156
B397	9	2.02	0.2	7264.58	807.1756
B400	9	1.43	0.14	14402.19	1600.243
B401	27	1.36	0.13	32136.23	1190.231
B403	19	2.83	0.16	25446.94	1339.313
B404	6	1.47	0.25	2821.41	470.235
B405	15	1.19	0.21	9089.43	605.962
B406	5	3	0.3	1976.57	395.314
B407	6	1.11	0.25	2984.44	497.4067
B408	27	1.04	0.12	57135.1	2116.115
B409	2	5.91	0.61	339.52	169.76
B411	2	1.09	0.38	1122.92	561.46
B413	6	1.42	0.19	6646.81	1107.802
B414	9	1.22	0.12	49358.75	5484.306
B415	6	2.03	0.3	2208.34	368.0567
B417	10	1.61	0.18	12759.88	1275.988
B418	11	1.28	0.16	11572.4	1052.036
B419	8	1.08	0.32	1847.62	230.9525
B421	32	1.01	0.16	21636.26	676.1331
B422	19	1.52	0.16	17237.78	907.2516
B423	19	1.18	0.15	25474.97	1340.788
B424	6	2.18	0.22	7081.59	1180.265
B425	9	1.37	0.23	9154.04	1017.116
B427	10	1.55	0.18	14180.86	1418.086
B428	6	2.75	0.17	10961.16	1826.86
B429	10	2.07	0.15	30661.01	3066.101
B430	2	1.94	0.35	1027.52	513.76
B431	3	1.52	0.39	682.13	227.3767
B432	3	2.15	0.25	2783.11	927.7033
B433	9	1.1	0.2	8923.81	991.5344
B435	4	1.17	0.27	3704.02	926.005

B436	4	2.27	0.29	1886.79	471.6975
B437	6	2.06	0.22	4665.71	777.6183
B439	9	1.3	0.14	13799.85	1533.317
B442	5	1.44	0.27	3508.95	701.79
B443	7	1.97	0.28	2098.08	299.7257
B444	6	1.26	0.2	10365.44	1727.573
B445	7	1.03	0.29	3082.82	440.4029
B446	6	1.16	0.24	4667.87	777.9783
B447	24	2.64	0.42	2989.88	124.5783
B449	2	3.35	0.37	1058.36	529.18
B451	4	1.11	0.21	4142.12	1035.53
B453	6	3.5	0.25	5989.24	998.2067
B455	2	1.69	0.58	204.58	102.29
B456	2	1.51	0.62	159.14	79.57
B457	2	1.63	0.57	205.18	102.59
B458	3	1.41	0.52	292.02	97.34
B459	3	2.47	0.45	1297.97	432.6567
B460	16	2.65	0.26	5438.56	339.91
B462	15	1.19	0.11	35457.75	2363.85
B463	10	1.52	0.27	5048.55	504.855
B464	10	2.22	0.14	17262.37	1726.237
B465	28	1.18	0.14	34770.83	1241.815
B468	16	1.37	0.14	30126	1882.875
B471	5	1.25	0.2	4343.25	868.65
B474	13	1.38	0.2	7414.53	570.3485
B475	8	1.12	0.19	6052.74	756.5925
B476	3	1	0.31	1838.18	612.7267
B479	16	3.37	0.14	25744.12	1609.008
B480	11	1.31	0.14	27323.28	2483.935
B481	11	3.56	0.19	10903.33	991.2118
B482	10	1.31	0.21	8960.87	896.087
B483	9	1.26	0.24	6213.87	690.43
B484	6	2.88	0.27	2836.23	472.705
B485	10	1.68	0.2	26055.99	2605.599
B486	10	1.4	0.2	13900.53	1390.053
B487	1	1.8	0.51	769.3	769.3
B488	8	1.56	0.18	10021.29	1252.661
B489	9	1.51	0.17	8957.04	995.2267
B494	12	1.56	0.15	12995.95	1082.996
B495	12	1.97	0.16	26603.17	2216.931
B498	12	1.27	0.14	19664.93	1638.744
B500	12	1.42	0.17	23870.04	1989.17
B502	7	4.89	0.22	6658.51	951.2157
B504	7	2.93	0.28	3126.65	446.6643
B505	13	2.86	0.15	22869.74	1759.211
B509	13	1.73	0.24	7383.33	567.9485
B510	13	1.78	0.16	11827.06	909.7738
B514	6	1.1	0.36	1066.1	177.6833
B515	15	3.7	0.13	52484.24	3498.949
B516	8	1.24	0.28	2370.86	296.3575

B517	11	3.97	0.28	6987.7	635.2455
B519	10	2.45	0.21	7279.07	727.907
B520	7	2.17	0.17	15900.73	2271.533
B523	6	1.83	0.3	3896.21	649.3683
B525	7	2.28	0.22	3995.9	570.8429
B526	2	2	0.34	1260.66	630.33
B527	7	1.36	0.28	4215.79	602.2557
B528	7	3.4	0.22	5287.51	755.3586
B531	9	1.84	0.17	11203.23	1244.803
B535	9	2.16	0.25	8386.83	931.87
B536	9	2.05	0.21	9002.95	1000.328
B543	9	2.05	0.38	1769.12	196.5689
B544	9	1.19	0.25	5100.93	566.77
B545	8	1.69	0.2	7309.56	913.695
B546	9	2.48	0.19	13066.92	1451.88
B552	10	1.98	0.16	10464.77	1046.477
B554	7	3.41	0.26	4113.9	587.7
B555	5	1.15	0.43	594.24	118.848
B557	39	1.17	0.13	64615.27	1656.802
B558	30	1.95	0.16	24351.71	811.7237
B559	25	1.26	0.13	40847.7	1633.908
B560	21	1.08	0.14	33680.67	1603.841
B564	3	1.23	0.19	11665.4	3888.467
B570	7	1.44	0.22	3871.67	553.0957
B571	7	3.33	0.22	5494.84	784.9771
B572	8	2.15	0.26	3027.79	378.4738
B573	6	2.64	0.25	3150.15	525.025
B574	8	2.85	0.25	3931.15	491.3938
B575	2	2.78	0.37	1040.88	520.44
B576	4	2.4	0.37	943.43	235.8575
B578	30	1.4	0.12	92948.32	3098.277